Science and Technology of Nuclear Installations

Nuclear Fuel Reprocessing Technologies and Commercialization

Guest Editors: Michael F. Simpson, Candido Pereira, and Jack D. Law

Nuclear Fuel Reprocessing Technologies and Commercialization

Science and Technology of Nuclear Installations

Nuclear Fuel Reprocessing Technologies and Commercialization

Guest Editors: Michael F. Simpson, Candido Pereira, and Jack D. Law

Editorial Board

Contents

Hindawi Publishing Corporation
Science and Technology of Nuclear Installations
Volume 2013, Article ID 815693, 2 pages
http://dx.doi.org/10.1155/2013/815693

Editorial

Nuclear Fuel Reprocessing Technologies and Commercialization

Michael F. Simpson

Department of Metallurgical Engineering, University of Utah, Salt Lake City, UT, USA

Correspondence should be addressed to Michael F. Simpson; michael.simpson@utah.edu

Received 22 August 2013; Accepted 22 August 2013

The subject of this special issue of Science and Technology of Nuclear Installations is considered to be a very timely subject given the current expansion of nuclear energy and the lack of broadly accepted long-term spent fuel management solutions. Resource sustainability is also a concern with most projections predicting less than 100 years of easily and therefore economically recoverable natural uranium resources left at current consumption rates. The United States and several other countries are spending tens of millions of dollars each year on nuclear fuel reprocessing research, but there must be a connection to the needs of the existing nuclear power industry. Research at the US national level currently targets the development of a fully sustainable nuclear power infrastructure that maximizes resource utilization and power production, while managing wastes effectively and minimizing the risk of proliferation. Many technologies have been developed over the past half-century that address these areas, but a well-coordinated program is needed to assure efficient implementation. The utilities desire a process for managing the actinides in their used fuel stockpiles that does not impact their reactor operations. The Fukushima disaster has caused many nations to reevaluate how they currently manage spent nuclear fuel and their plans for future disposal or recycling. Given the existing infrastructure, it is unquestionably cheaper today to mine and enrich uranium. However, will significant expansion of nuclear power strain resources sufficiently to swing the pendulum toward reprocessing? Will the externalities associated with waste disposal soon have an impact on the cost of newly mined fuel and provide economic benefit to industry using reprocessed fuel? Can we manage the risks associated with nuclear fuel reprocessing to reap the benefits of better resource utilization and long-term waste management? These were some of the questions posed to the world's experts on nuclear fuel reprocessing. The papers that were received addressed both aqueous and pyrochemical reprocessing. And they touched upon three important issues that span all technologies—safeguards, economics, and waste management.

The concept of safeguards is undoubtedly a critical issue for the commercialization of nuclear fuel reprocessing, given the potential for separating or concentrating plutonium in the various processes being considered. Three papers are included that address this issue. M. Suzuki and N. Terao from Japan Atomic Energy Agency evaluated aqueous solution monitoring as a safeguards approach to reprocessing. This is an example of how the concept of safeguards by design can be implemented. The authors demonstrated via proliferation risk analysis the potential utility of this approach but noted that it is not immune to operator falsification. Meanwhile, T. Burr and colleagues from Los Alamos National Laboratory also addressed the issue of safeguards and utilization of process monitoring data. They studied alarm threshold estimation with the aim of minimizing the frequency of false alarms for nuclear material diversion. It was recommended to use process simulations to determine the optimal alarm thresholds. Not surprisingly, the more accurate the process simulation, the smaller the data sample size needed to establish appropriate alarm threshold levels. They also presented the application of process monitoring for near real-time accounting. In that case, they determined that data could be used as it is received rather than waiting for long periods of time to calculate cumulative material unaccounted for (MUF).

Economics was addressed by two of the papers—one by M. U. Mas et al. of Universidad Pontificia Comillas on a general comparison of open to closed fuel cycles and one by S. K. Kim et al. from Korea Atomic Energy Research Institute

on the sodium fast reactor and the associated pyrochemical reprocessing scheme. Interestingly, M. U. Mas et al. made the argument that the closed fuel cycle's costs can be reasonably estimated while much uncertainty remains with the long-term cost of the open fuel cycle. This argument largely hinges on the potential downside of unknown costs tied to long-term nuclear waste management. They also make the point that costs associated with deep geologic disposal likely increase as time passes and no action is taken, while reprocessing costs likely decrease due to the benefits of continued research and development. As time passes, it is argued that reprocessing becomes an increasingly compelling choice. A similar conclusion was drawn by S. K. Kim et al. who showed that the estimated cost for fabricating sodium fast reactor metallic fuel via a fuel cycle facility is currently quite close to the economic break-even point. Potential error in this analysis is acknowledged based on the lack of commercial sodium fast reactor fuel cycle facilities in the world, while also noting that costs are expected to come down as the technology is scaled up and widely implemented.

Finally, M. F. Simpson also contributed to this special issue in a paper on the projected salt waste from using the pyroprocessing approach to nuclear fuel reprocessing. This waste salt comes from the oxide reduction and/or electrorefining unit operations and is largely comprised of LiCl or LiCl-KCl. A significant range of salt waste generation rates was calculated based on various assumptions. The potential benefit from applying separation processes to recycle the LiCl or LiCl-KCl is quantified. And the trade-offs between disposing of the salt in a waste form and directly without treatment are given. While pyroprocessing has often been touted as having waste management benefits, it is clear that challenges exist in this area and process options must be carefully considered for overall fuel cycle optimization.

Collectively, it appears that nuclear fuel reprocessing does have great potential for commercialization. But there is much work to be done to derive optimal solutions to problems such as safeguards, economics, and waste management. It is, thus, expected that nations will wisely continue to invest in this very important research area.

Michael F. Simpson

Hindawi Publishing Corporation
Science and Technology of Nuclear Installations
Volume 2013, Article ID 702496, 12 pages
http://dx.doi.org/10.1155/2013/702496

Research Article

Radioactive Iodine and Krypton Control for Nuclear Fuel Reprocessing Facilities

Nick R. Soelberg,[1] Troy G. Garn,[1] Mitchell R. Greenhalgh,[1] Jack D. Law,[1] Robert Jubin,[2] Denis M. Strachan,[3] and Praveen K. Thallapally[3]

[1] *Idaho National Laboratory, Idaho Falls, ID 83415, USA*
[2] *Oak Ridge National Laboratory, Oak Ridge, TN 37831, USA*
[3] *Pacific Northwest National Laboratory, Richland, WA 99252, USA*

Correspondence should be addressed to Nick R. Soelberg; nick.soelberg@inl.gov

Received 4 March 2013; Accepted 22 July 2013

Academic Editor: Candido Pereira

The removal of volatile radionuclides generated during used nuclear fuel reprocessing in the US is almost certain to be necessary for the licensing of a reprocessing facility in the US. Various control technologies have been developed, tested, or used over the past 50 years for control of volatile radionuclide emissions from used fuel reprocessing plants. The US DOE has sponsored, since 2009, an Off-gas Sigma Team to perform research and development focused on the most pressing volatile radionuclide control and immobilization problems. In this paper, we focus on the control requirements and methodologies for ^{85}Kr and ^{129}I. Numerous candidate technologies have been studied and developed at laboratory and pilot-plant scales in an effort to meet the need for high iodine control efficiency and to advance alternatives to cryogenic separations for krypton control. Several of these show promising results. Iodine decontamination factors as high as 10^5, iodine loading capacities, and other adsorption parameters including adsorption rates have been demonstrated under some conditions for both silver zeolite (AgZ) and Ag-functionalized aerogel. Sorbents, including an engineered form of AgZ and selected metal organic framework materials (MOFs), have been successfully demonstrated to capture Kr and Xe without the need for separations at cryogenic temperatures.

1. Introduction

Nuclear fission results in fission products and activation products, some of which are volatile under the conditions of used nuclear fuel (UNF) reprocessing. The radionuclides that have been identified as "volatile radionuclides" are noble gases (most notably isotopes of Kr and Xe), ^{3}H, ^{14}C, and ^{129}I.

Radionuclides that tend to form volatile species evolve into reprocessing facility off-gas systems and are more challenging to be efficiently controlled compared to radionuclides that remain with the solids or liquids during fuel reprocessing. Unless otherwise managed, these radionuclides would be released to the environment. It is nearly certain that for any future used nuclear fuel (UNF) reprocessing facilities to meet licensing requirements in the United States, efficient capture of some volatile radionuclides from the plant off-gas streams will be needed.

In aqueous reprocessing, these radionuclides are most commonly expected to evolve into off-gas streams as tritiated water (^{3}HHO or $^{3}H_2O$), radioactive CO_2 ($^{14}CO_2$), noble gases (mainly ^{85}Kr), and iodine ($H^{129}I$, $^{129}I_2$, or organic iodides). The fate and speciation of these radionuclides from a nonaqueous fuel reprocessing facility are less well known at this time, especially with respect to organoiodide species, but active investigations are in progress.

An Off-Gas Sigma Team was formed in late fiscal year (FY) 2009 to integrate and coordinate the Department of Energy (DOE) Fuel Cycle Research and Development (FCR&D) activities directed towards the capture and sequestration of the these volatile radionuclides [1]. The Sigma Team concept was instituted in an effort to bring together multidisciplinary teams from across the DOE complex that would work collaboratively to solve the technical challenges and to develop the scientific basis for the capture and

immobilization technologies. The laboratories currently participating in this effort are Idaho National Laboratory (INL), Oak Ridge National Laboratory (ORNL), Pacific Northwest National Laboratory (PNNL), and Sandia National Laboratories (SNL).

In this paper, we focus on the control of ^{129}I and ^{85}Kr emissions from aqueous reprocessing of UNF. Most of the work by the Off-gas Sigma Team has focused primarily on the capture and sequestration of ^{129}I, ^{85}Kr, and ^{3}H, mainly because, as discussed below, control of ^{129}I can require high efficiencies to meet regulatory requirements; removal of ^{85}Kr with a cryogenic process, which has been the technology demonstrated to date, can add considerably to the construction and operating costs of a reprocessing facility; and tritium capture, while in theory relatively simple, is in practice quite complicated owing to the problems associated with its evolution prior the fuel dissolver, dilution with process water (liquid and vapor), and coadsorption with other species.

2. Regulatory Requirements for Iodine and Krypton Capture

Volatile radionuclide emissions from a nuclear fuel recycle facility are addressed in several regulations as summarized in Table 1.

2.1. The US Code of Federal Regulations (CFR) Title 40, Part 190: Environmental Radiation Protection Standards for Nuclear Power Operations. The United States (US) Environmental Protection Agency (EPA) has established, through 40 CFR 190 [2], annual dose limits for nuclear fuel cycle facilities in the commercial sector. In 40 CFR 190.10(a), dose limits to any member of the public are specified (25 mrem/y (0.25 mSv/y) to the whole body, 75 mrem/y (0.75 mSv/y) to the thyroid, and 25 mrem/y (0.25 mSv/y)) as a result of planned discharges of radioactive materials. Also in 40 CFR 190.10(b), release limits are specified for ^{85}Kr, ^{129}I, and ^{239}Pu and other alpha-emitting transuranic radionuclides with half-lives greater than one year in curies (Ci) released per gigawatt-year (GWy) of electric power produced (50 000 Ci (1.85×10^6 GBq) of ^{85}Kr, 5 mCi (0.185 GBq) of ^{129}I, and 0.5 mCi (0.0185 GBq) composed of ^{239}Pu and other alpha-emitting transuranic radionuclides with half-lives greater than one year).

According to 40 CFR 190, emissions of both ^{129}I and ^{85}Kr need to be limited to meet the lower value of (a) their specific fuel-cycle-based emission limit and (b) the value needed to limit the combined dose equivalent (from all radioactive material discharges) to any member of the public.

2.2. 10 CFR 20: Standards for Protection against Radiation. The US Nuclear Regulatory Commission (NRC) provides dose limits from facilities licensed by the NRC for workers and individual members of the public in 10 CFR 20 [3].

Section 10 CFR 20.1101(b) states that "*the licensee shall use, to the extent practicable, procedures and engineering controls based upon sound radiation protection principles to achieve occupational doses and doses to members of the public that are as low as is reasonably achievable (ALARA).*" Section 10 CFR 20.1301 specifies dose limits for individual members of the public (0.1 rem (1 mSv) per year and 0.002 rem (0.02 mSv) in any one hour). This section also states that "*a licensee subject to the provisions of EPA's generally applicable environmental radiation standards in 40 CFR Part 190 shall comply with those standards.*"

Section 10 CFR 20.1302 describes how to comply with the dose limits in 10 CFR 20.1301. Two options are to either demonstrate that the annual dose limit is not exceeded, or demonstrate that (a) "*the annual average concentrations of radioactive material released in gaseous and liquid effluents at the boundary of the unrestricted area do not exceed the values specified in Table 2 of Appendix B to Part 20,*" and (b) "*if an individual were continuously present in an unrestricted area, the dose from external sources would not exceed 0.002 rem (0.02 mSv) in an hour and 0.05 rem (0.5 mSv) in a year.*"

For the purposes of used fuel reprocessing facility research and development, planning, and preliminary design, the following considerations apply.

(i) Emissions of volatile radionuclides are assumed to be constant over a year—so the short-term limit of 0.002 rem (0.02 mSv) in 20.1302(b)(2)(ii) is not considered, since the lower annual limit is more restrictive than this hourly limit when annualized.

(ii) The dose limit from 10 CFR 20.1301 is 0.1 rem (1 mSv) per year, but the demonstration of compliance level in 10 CFR 20.1302 is one-half of that, at 0.05 rem (0.5 mSv) per year.

(iii) Table 2 of 10 CFR 20 (Appendix *B*) defines limits for annual average concentrations of radioactive material released in gaseous and liquid effluents at the boundary of an unrestricted area (the "fence line" that would surround a UNF reprocessing facility). These limits are based on an annual dose limit to an individual member of the public in the unrestricted area (just outside the fence line) of 0.05 rem (0.5 mSv). For conservatism and simplicity in this study, we consider only these annual average concentrations because they are more conservatively restrictive than analyses in which the derived air concentrations (DACs) are used to assess worker annual limits on intake (ALIs) and analyses in which the basis is the short-duration 1 h exposure limits to the public.

(iv) Since the annual limit of 0.05 rem (0.5 mSv) in 10 CFR 20.1302(b)(2)(ii) is higher than the annual limit of 25 mrem/y (0.25 mSv) from 40 CFR 190, we consider that volatile radionuclide control efficiencies that provide compliance to 40 CFR 190 will also provide compliance to 10 CFR 20.

(v) According to Regulatory Guide 8.37 [4], a dose limit to a member of the public of 10 mrem/y (0.1 mSv/y) should be achievable based on NRC-licensed facilities that have been surveyed. So the NRC may consider a 10 mrem/y [0.1 mSv/y] limit to be ALARA even though the limit in 10 CFR 20.1302(b)(2)(ii) is higher,

Table 1: The US radionuclide air emission regulations.

Regulation	Dose equivalent to public, mrem/y (mSv/y)	Max fuel cycle emissions per GWy electric energy
Nuclear fuel cycle (40 CFR 190.10) [2]	25 (0.25) to whole body; 75 (0.75) to thyroid; 25 (0.25) to any other organ	^{85}Kr: <50 000 Ci (<1.85E6 GBq); ^{129}I: <5 mCi (<0.185 gBq)
NRC licensees (10 CFR 20.1101, .1301, .1302, App. B) [3]	Dose limit: 100 (1) Compliance demonstration limit: 50 (0.5) ALARA limit: 10 (0.1)	—
DOE facilities (40 CFR 61.92) [4]	10 (0.1)	—

Table 2: Estimated DFs required for the volatile radionuclides for different selected types of used fuels and burn-ups.

Nuclide	Assumed dose limit for the volatile radionuclides = 25 mrem/y and 75 mrem/y to thyroid (40 CFR 190)			Assumed dose limit = 2.5 mrem/y and 7.5 mrem/y to thyroid (10% of the 40 CFR 190 limits)		
	PWR/UOX, BU = 60 GWd/tIHM	PWR/MOX, BU = 100 GWd/tIHM	AHTGR BU = 100 GWd/tIHM	PWR/UOX, BU = 60 GWd/tIHM	PWR/MOX, BU = 100 GWd/tIHM	AHTGR BU = 100 GWd/tIHM
^{3}H	25 (1 after 57 y cooling)	160 (1 after 90 y cooling)	42 (1 after 66 y cooling)	600 (1 after 110 y cooling)	720 (1 after 120 r cooling)	590 (1 after 110 y cooling)
^{14}C	1	1	4	10	15	30
^{85}Kr	9 (1 after 34 y cooling)	4.2 (1 after 22 y cooling)	9.2 (1 after 34 y cooling)	18 (1 after 45 y cooling)	13 (1 after 40 y cooling)	62 (1 after 64 y cooling)
^{129}I	380	630	650	3800	8000	6600

(1) PWR: pressurized water reactor.
(2) UOX: used uranium oxide fuel.
(3) MOX: mixed U and Pu oxide fuel.
(4) GWd/tIHM: Gigawatt-day per tonne initial heavy metal.
(5) AHTGR: advanced high temperature gas reactor.
(6) BU: fuel burn-up. The ^{3}H and ^{14}C DFs are based on the whole body dose limits—the doses to the organs are less restrictive. The ^{85}Kr DFs are based on the fuel cycle emission limit and the whole body dose limits—the doses to the organs are less restrictive. The iodine DFs are based on control efficiencies needed to meet the fuel cycle emission limit and the thyroid dose limit—the whole body dose is less restrictive.
(7) These DF values have been rounded to not more than two significant figures.

at 50 mrem/y (0.5 mSv/y). In that case, the 25 mrem/y limit in 40 CFR 190 is not the bounding case. In part for this reason, calculations of volatile radionuclide control efficiencies in this paper are based on dose limits between 2.5 and 25 mrem/y (0.025 to 0.25 mSv/y).

2.3. 40 CFR 61: National Emission Standards for Hazardous Air Pollutants, Subpart H—National Emission Standards for Emissions of Radionuclides Other Than Radon from Department of Energy Facilities, 61.92. This part applies to radionuclide emissions other than ^{222}Rn and ^{220}Rn from DOE facilities, except that this part does not apply to disposal at facilities subject to 40 CFR Part 191 Subpart B or 40 CFR Part 192 [5]: "*emissions of radionuclides to the ambient air from Department of Energy facilities shall not exceed those amounts that would cause any member of the public to receive in any year an effective dose equivalent of* 10 *mrem/yr*." This dose limit for DOE facilities equals the ALARA-based limit from 10 CFR 20 and is in the range of dose limits between 2.5 and 25 mrem/y (0.025 to 0.25 mSv/y) used in this paper.

3. Control Efficiency Requirements

A question that has persisted for years is how efficiently must the volatile radionuclides be captured to ensure that a reprocessing facility in the US will comply with air emission regulations? Such a simple question, in the case of volatile radionuclides, has a complicated answer—or at least an answer or range of answers—that must be accompanied by a list of assumptions. Control efficiencies needed for compliance to the fuel cycle isotope-specific limits specified in of 40 CFR 190 for ^{129}I and ^{85}Kr per GWy of electrical energy produced in the fuel cycle can be estimated from the following.

(i) The amount of ^{129}I and ^{85}Kr in UNF. The amount of these nuclides in UNF depends mainly on the fuel burn-up, reactor conditions during burn-up, and aging (cooling) time after reactor discharge.

(ii) The proportions of these nuclides released in process liquid or other streams, and the proportions released to reprocessing facility off-gas streams (and would be released to the atmosphere if not captured).

(iii) The thermal efficiency of the nuclear reactor.

(iv) The estimated values for any release of ^{129}I and ^{85}Kr in other parts of the fuel cycle besides the reprocessing facility.

Estimating dose-based removal efficiencies needed to ensure compliance to regulatory dose limits in 40 CFR 60.190, 40 CFR 61.92, or 10 CFR 20 is more complex and requires additional site-specific information. In addition to the bullets listed above, the following factors must be considered or assumed.

(i) Volatile radionuclide mass emission rates from the stack and mass emission rates of all other radionuclides from the stack. These rates depend on the amount of the volatile and other nuclides in the UNF, the reprocessing facility throughput, and the portions of these nuclides that are released to off-gas streams during reprocessing. Since all emitted radionuclides contribute to the total dose, the amount of the dose from any single radionuclide must be reduced to the extent needed to ensure that the cumulative dose from all the radionuclides is within the regulatory limit.

(ii) Many air dispersion and dose parameters, the most important of which are.

  (a) Stack gas parameters—stack gas flow rate, exit gas momentum (a function of the gas exit velocity and density).
  (b) Speciation of the volatile radionuclides.
  (c) Site-specific meteorological parameters.
  (d) Site-specific agricultural parameters.
  (e) Other site-specific parameters including distance from the stack (or stacks) to the access-controlled boundary (fence-line) up to which the public can approach and theoretically live and subsist). A person at this distance, in the direction of the highest average plume concentration from the stack(s), is termed the maximally exposed individual (MEI).
  (f) The air dispersion model used to calculate dispersal of the plume out to the location of the MEI.
  (g) Dose conversion factors used in the dose model.

Estimated volatile radionuclide control efficiencies needed to meet regulatory compliance in the US have been provided in previous studies [6–8]. The most recent and, in our view, comprehensive study of volatile radionuclide control efficiencies is reported by Jubin et al. [9].

Estimated decontamination factors (DFs) from Jubin et al. [9] to meet the regulations are shown in Table 2. The DF is the amount of a nuclide in the off-gas stream(s) divided by the amount in the off-gas stream downstream of the off-gas control system. In other terms, the DF = 1/(1 − (control efficiency%/100)). The DF values in this table have been used to provide direction and scope for volatile radionuclide control research and development, but they depend on the following assumptions.

(i) The fuel burn-ups shown here represent the maximum currently reasonable burn-up ranges for these fuel and reactor combinations; fuels with lower burn-ups would have lower DFs (down to DF = 1) and, for the shorter-lived ^{3}H and ^{85}Kr compared to ^{3}H and ^{129}I, shorter cooling times until when no control is needed.

(ii) Of the volatile radionuclides in the UNF, 100% is assumed to evolve into the reprocessing facility off-gas; no emissions of these volatile radionuclides are assumed to be released in other parts of the nuclear fuel cycle, that is, fuel production, reactor operation, and so forth, and no migration is assumed, for example, ^{3}H migration into and retention in the Zircaloy cladding, which would result in a decrease in the calculated radionuclide inventory.

(iii) Reprocessing facility throughput: 1000 tIHM/y (tonnes (metric tons) of initial heavy metal per year). Smaller reprocessing plants could have smaller DFs (down to DF = 1) and shorter cooling times until DF = 1 for ^{3}H and ^{85}Kr. Larger reprocessing plants will need larger DFs and longer cooling times until DF = 1 for ^{3}H and ^{85}Kr.

(iv) No engineering safety factors are assumed.

(v) The DF calculations are based on control efficiencies needed to comply with the fuel cycle emission limits for ^{129}I and ^{85}Kr and whole body, thyroid, and other organ dose calculations to the MEI.

(vi) Doses to the MEI are calculated with the US EPA Clean Air Act Assessment Package (CAP88-PC Version 3.0) computer model CAP88 [10, 11]. This model is a set of computer programs, databases, and associated utility programs used to estimate dose and risk to members of the public from radionuclide emissions in the air. Version 3.0 of CAP88 incorporates dose and risk factors from the Federal Guidance Report 13 [12] that are based on the methods of the International Commission on Radiological Protection [13].

(vii) The reprocessing facility site boundary is assumed to be the location of the MEI and is the distance from and in the direction of the maximum plume concentrations as determined with the CAP88 code. This can result in dose-based DF estimates that are conservatively high relative to the dose-based DFs for other site boundary and locations that are not at the location of the MEI.

(viii) With the dose limit of 25 mrem/y (0.25 mSv/y) from 40 CFR 190, no allowance is assumed for any other nuclide emissions besides these four volatile radionuclides and the presumed ALARA level of 10 mrem/y (0.1 mSv/y) from 10 CFR 20 is not considered. The dose limit of 2.5 mrem/y (0.025 mSv/y) bounds the presumed ALARA level of 10 mrem/y (0.1 mSv/y)

from 10 CFR 20 and reserves from 75% to 90% of the total allowable dose for the potential emissions of other dose contributors (75% in the case of the 10 mrem/y (0.1 mSv/y) ALARA value; and 90% in the case of the 25 mrem/y (0.25 mSv/y) 40 CFR 190 limit).

The amount of the volatile radionuclides in UNF varies depending on assumptions (Figure 1). The control efficiencies needed for the volatile radionuclides to meet the assumed dose limits are generally proportional to the amounts of volatile radionuclides and the UNF reprocessing rates, down to a DF = 1. The amounts of volatile radionuclides in UNF were calculated with the Oak Ridge Isotope Generation and Depletion (ORIGEN) code Automatic Rapid Processing (ARP) simulations [9]. The concentrations of chemical impurities in the starting UO_2 and PuO_2 materials are assumed to be one-half of the maximum values shown in the standard specifications by the American Society for Testing and Materials (ASTM) [14, 15].

About 80% of the ^{14}C in UOX UNF is from activation of the impurity ^{14}N, and most of the remainder is from the activation of ^{17}O, which has a natural abundance of 0.038 mol%. Most of the ^{14}C in the used tristructural isotropic (TRISO) fuel from an advanced high-temperature gas reactor (AHTGR) is from the activation of (a) ^{13}C (with a natural abundance of 1.1 mol%) in the carbon in the assumed TRISO fuel pebble, (b) ^{14}N, an impurity assumed in the uranium oxycarbide fuel core of TRISO kernels, and (c) ^{17}O isotope in the uranium oxycarbide. Different assumptions for impurity levels, fuel compositions, and fuel configurations result in different levels of volatile radionuclides in the used fuels.

Assumptions in addition to those shown above for UNF, reprocessing facility size, and CAP88 model were included in sensitivity studies [9]. Sensitivity studies of the site-specific parameters in the CAP88 model indicate the following.

(i) Increasing the emissions stack height by a factor of 4 (from 37 m to 150 m) resulted in a factor of ~16 reduction in the dose to the MEI.

(ii) Changing the speciation of ^{129}I from 100% particulate that was used in the calculations of this study to 30% to 70% particulate (a range consistent with measurements from the Karlsruhe Reprocessing Plant [16]) would reduce the ^{129}I dose to 30% to 70% of the 100% particulate value.

(iii) Changing the stack gas velocity and temperature can affect the dose to the MEI by up to a factor of 2, depending on the character of the plume (momentum or buoyancy dominated).

(iv) Site-specific meteorological parameters can (a) cause the ^{3}H dose to vary by a factor of 2 depending on the humidity, (b) increase the dose from ^{14}C and ^{129}I by more than 10% in areas with higher precipitation, and (c) cause the dose from any of the volatile radionuclides to vary by more than 20% for different wind velocities.

(v) Site-specific agricultural parameters, which vary for different locations in the US, affect dose from ingestion. Changing from the rural food scenario to an urban food scenario decreases the doses from those volatile radionuclides that play a role in the food cycle (^{3}H, ^{14}C, and ^{129}I) by 30–40%. The dose from ^{85}Kr is unchanged because it does not play a role in the food cycle.

4. History of Iodine and Krypton Capture

Both iodine and krypton capture have been used in various UNF reprocessing facilities worldwide. In addition, technologies for scrubbing iodine and other halogen gases and for separating noble gases, including Kr and Xe, are commercially available and used in industrial, nonradioactive processes.

4.1. Iodine Capture. Two types of technologies that have been developed and used for capturing gaseous ^{129}I-bearing components from reprocessing facility off-gas streams are caustic or acidic scrubbing solutions and chemisorption on silver-coated or -impregnated adsorbents. (During reprocessing, ^{131}I is generated from the fission of ^{244}Cm. We have not considered this source of iodine, because with the short half-life, it is unlikely to have any impact on the results discussed here). These processes are not selective to just iodine, but they also capture other halogen-bearing components that could be present in the off-gas streams. Some of these technologies have an affinity for other volatile radionuclides, such as ^{14}C, ^{3}H, and ^{85}Kr, thereby complicating later disposal.

Some specialized iodine wet scrubber concepts have been developed or used for gaseous iodine control, including caustic scrubbing, Iodox, and Mercurex [17, 18]. Caustic scrubbing for iodine capture is a relatively mature process; it is included in the dissolver off-gas control system at the La Hague Reprocessing Facility in France, the Windscale and the Thermal Oxide Reprocessing Plant (THORP) facilities in the United Kingdom [18], and the Rokkasho Reprocessing Plant in Japan. Past testing has shown that moderately high iodine DFs of 50–150 are possible with caustic scrubbing [17, 19], but it may not efficiently capture organic iodides.

The Iodox process was developed to capture ^{131}I released when reprocessing liquid metal fast breeder reactor (LMFBR) fuel [18], when the fuel is only cooled 180 days after reactor discharge. High concentrations of HNO_3 are used in this process. In nonradioactive engineering tests, DFs up to 10^6 were achieved. While both elemental and organic forms of iodine may be captured with this method, it requires several peripheral processes including the ability to concentrate the HNO_3, recycle the acid, and treat the waste stream.

Like the Iodox process, the Mercurex process was also developed for the treatment of the dissolver off-gas evolved during the processing of very short cooled fuels where very high DFs are required [18]. In this process, a $Hg(NO_3)_2$–HNO_3 solution is used in a wet scrubber. Gaseous iodine is absorbed in solution to form mercury iodate and iodide complexes. Mercurex was used at Dounreay, Scotland, and Nuclear Fuel Services at West Valley, New York, with reported

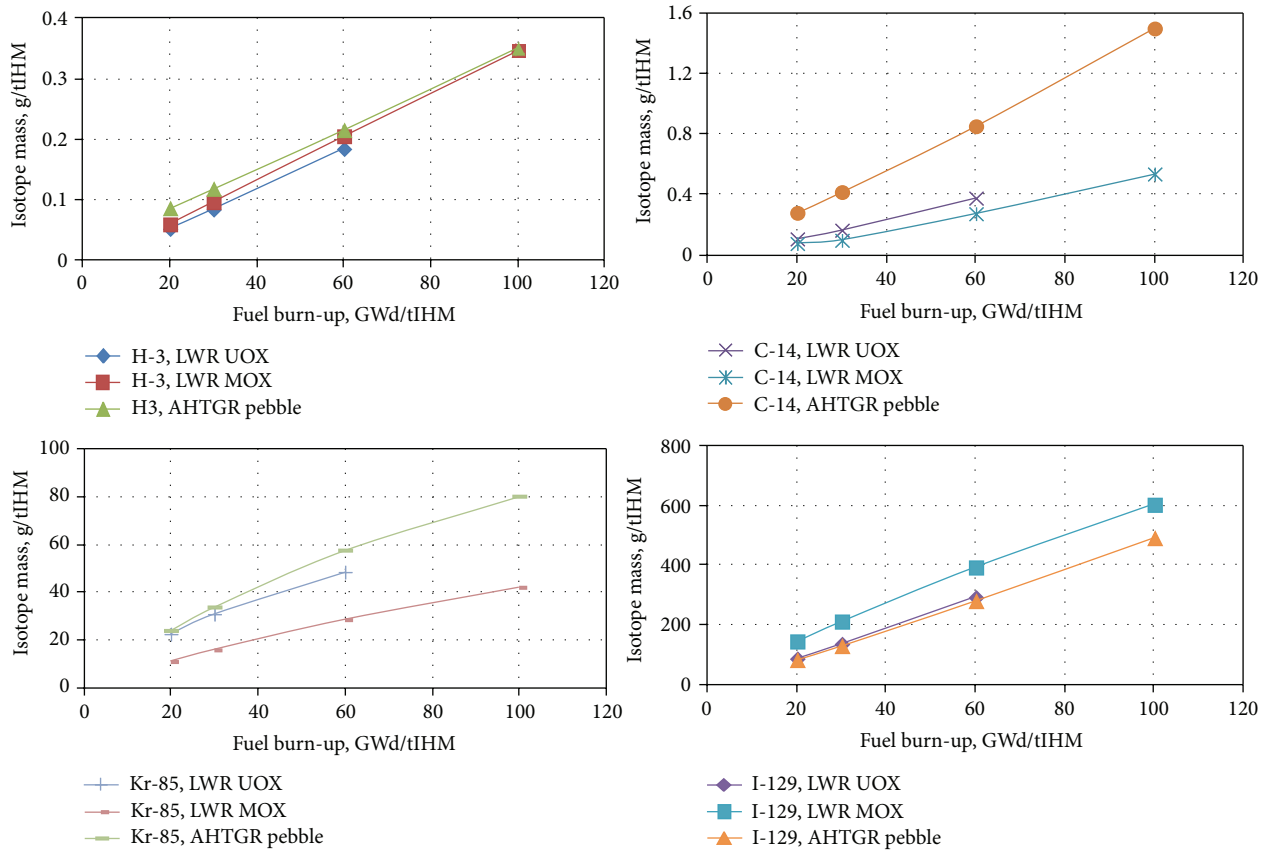

Figure 1: Amounts of volatile radionuclides in selected UNFs at the time of discharge (no cooling time), calculated with ORIGIN-ARP [9].

DFs of 150 and 32, respectively [15]. Mercurex was considered for use in the British Nuclear Fuels Limited reprocessing plant (BNFL) and Eurochemic in Belgium. Decontamination factors of 10–75 were claimed [18].

Adsorption of iodine on solid sorbents coated or impregnated with a metal, such as silver, has been studied and used in a few applications for decades. The presence of a metal, such as Ag, provides for chemical reaction of the gaseous iodine to form the metal halide. Chemisorption converts the sorbed form of iodine into a much less volatile material than the incoming gaseous form (expectedly I_2, but also possibly HI and organic iodides, such as CH_3I).

Silver nitrate-coated ceramic saddles were used at the Hanford Purex Plant and the Savannah River Plant to remove ^{131}I from off-gas streams [16]. The process involved passing the dissolver off-gas through a bed of heated ceramic saddles glazed with silver nitrate with which the iodine components of the off-gas would react to form AgI. Silver reactors have demonstrated DFs of 10 to 10^4 for ^{131}I recovery [16].

Silver nitrate-impregnated alumina (AgA) has been studied for capturing ^{131}I from off-gas streams and developed for treating off-gas streams at the Tokai Reprocessing Plant in Japan [19–22]. Silver nitrate-impregnated alumina with 10 and 24 mass% Ag is reported to have iodine adsorption capacities of about 0.12 Mg/m^3 and about 0.35 Mg/m^3, respectively [23]. Decontamination factors over 1000 were achieved [23].

The use of silver-exchanged zeolite (AgZ) sorbent is the leading approach in the US for capturing radioactive gaseous byproducts, such as I_2, during nuclear fuel reprocessing. This is because of expected high control efficiencies based on the solid sorbent mass transfer zone concept and the acid resistance of the zeolite compared to other substrates such as faujasite (AgX). Published studies surveyed by Thomas et al. [24] indicate I_2 loadings on silver-exchanged faujasite or AgZ ranged from 80 to 200 mg/g while maintaining decontamination factors in the range of 100 to 10 000 for I_2. Methyl iodide loadings of 140 to 180 mg/g are reported from tests on simulated dissolver off-gas streams [25, 26].

Indeed, for many decades, AgZ has been a benchmark for radiological I_2 capture [18, 22, 27]. Generally, AgZ is believed to benefit from high-efficiency adsorption, a high Si-to-Al ratio that enhances stability in acidic off-gas streams, relatively high Ag contents, and no flammability.

The base material used in the studies conducted in the 1970s and 1980s was a binderless synthetic mordenite (Zeolon 900) produced by Norton (Akron, OH, USA). The sodium form of Zeolon 900 was ion exchanged with silver from a silver nitrate solution. After exchange, the silver content in the AgZ was ~18 mass%. This material is no longer available commercially, so recent AgZ studies have to address the

quality of and differences between currently available natural and synthetic mordenites. The iodine capacities for different AgZ sorbents varied, introducing some uncertainty in the ability to achieve the DF values reported in the 1970s and 1980s.

Aerogels are being considered for capturing iodine compounds in the reprocessing plant off-gas. Aerogels start as a gel from which the solvent(s) is removed, typically with supercritical CO_2. This results in materials with very high porosity and surface area. Two aerogel materials are being considered: functionalized silica aerogels and chalcogels. Silica aerogels are available commercially. A functional group is tied to the silica surface inside the aerogel pores with an organic moiety that has silica-binding functionality on one end of the molecule and a Ag-specific functionality on the other. After functionalizing the pore surface, aqueous Ag^+ is added and subsequently reduced to Ag^0.

A key advantage of a silica aerogel sorbent is that, after loading with iodine, it can be consolidated into a dense and leach-resistant waste form. The density of the SiO_2 aerogel is about 1.9 kg/m^3. The density of iodine loaded silver functionalized aerogel is about 26 kg/m^3. Because of this low density, a granular form of Ag-functionalized aerogel is needed. The density of the iodine-laden aerogel after collapsing can be as high as 4000 kg/m^3.

Chalcogel is made from S-, Se-, or Te-bearing starting materials that are caused to crosslink in the presence of certain metal ions, such as Pt and Cu [28]. Chalcogels also have very high surface areas and porosities but do not need to be functionalized. In the case of chalcogel, the iodine compounds are soluble in the matrix of the material. Because of this, adsorption on chalcogel can be quite high, 100 to 200 mass%, relative to the starting material and 25 to 50 mass%, relative to the end product. The chalcogel density is about 3000 kg/m^3. When fully loaded with iodine, the density is about 4300 kg/m^3. These materials are not available commercially. As with the silica aerogel, a granular form is needed.

Metal-organic framework structures (MOFs) are viewed by many as the next generation of porous materials with promising applications in many areas [29, 30]. Gas sorption is the main focus of many MOF studies [31, 32] because of their high adsorptive capacity associated with very large surface areas and porosity [33, 34] and the ability to "tune" the organic moiety for specificity. At the same time, studies of gas separation are also becoming more widespread given that MOF structures are highly tunable towards specific applications [35].

4.2. Krypton Capture. The capture of noble gases can be achieved either by the use of cryogenic methods or by physical adsorption on solid matrices (e.g., molecular sieves, metal-organic frameworks, or porous organic polymers). Numerous candidate technologies have been investigated for the capture of Kr and Xe from UNF reprocessing off-gas streams. Here, we provide a short description of each technology.

4.2.1. Cryogenic Distillation. Of all noble gas separation technologies, cryogenic distillation is considered to be the most mature. Cryogenic separation of Kr and Xe from air is done commercially at air separations plants and provides 99.999% pure Kr and Xe. The principle operating basis is to utilize the differences in boiling points between the gases targeted for separation.

Cryogenic distillation units have been used at nuclear fuel reprocessing plants for several decades in the US and more recently in Japan [36–38]. Krypton decontamination factors of 100–1000 have been reported that would meet anticipated regulatory ^{85}Kr emission requirements [39]. Although these processes did not always achieve optimum ^{85}Kr decontamination, the successful operation did confirm the feasibility of the technology.

Some reprocessing facility off-gas pretreatment is necessary prior to cryogenic treatment. Nitrogen dioxide and other impurities are removed with a caustic scrubber. The scrubbed effluent contains mostly air, much reduced amounts of NO_x, small amounts of hydrogen, and rare gases. This effluent gas is stored in tanks. The stored gases are then processed through a rhodium catalyst bed at 540–650°C (813–923 K), in which the NO_x is reduced to nitrogen and the small amount of hydrogen reacts with oxygen to form water. The effluent from the catalytic reduction is then cooled, demisted, and dried before being sent to the cryogenic distillation process. The distillation process consists of heat exchangers, distillation column, and a batch still. The pretreated gas is cooled with heat exchangers and then sent to the cryogenic column where the O_2, Kr, Xe, and Ar are absorbed into countercurrent stream of liquid nitrogen. The uncondensed gases are released to the atmosphere. The absorbed gases are continuously concentrated and then collected in a batch still where the absorbed gases are selectively distilled.

The technology has certain drawbacks, one of which is the radiolytic formation of concentrated ozone that can be an explosion hazard. This hazard is minimized by complete removal of oxygen from the process gas or intermittent flushing to remove the ozone.

4.2.2. Fluorocarbon Absorption. A selective absorption process in which dichlorodifluoromethane (CCl_2F_2, also known as Freon-12 or R-12) is used was developed and tested at Oak Ridge National Laboratory and the Karlsruhe Research Center (formerly Forschungszentrum Karlsruhe) in Germany [40, 41]. This process is very similar to the cryogenic distillation process, but operated at higher temperatures and pressures.

The basis for this process lies within the solubility differences between the gas components in the solvent. Gas components can be removed from upper, middle, and lower sections of a single column. However, solvent carryover in product streams is a problem. The process gas stream is compressed and then cooled before it is injected into a column where it is bubbled through the freon. The Kr and Xe are absorbed into the freon and captured in the middle region of the column. Relatively pure Kr and Xe (with some solvent)

are removed from the column. Krypton removal efficiencies of 99% have been achieved with these systems.

Capital equipment and operating costs are similar to the cryogenic process. The absorption process is operated around −30°C (243 K) resulting in reduced refrigeration costs; however, higher operating pressures of 2.8 MPa (400 psig) can result in product losses from potential process gas leaks. Solvent costs are relatively low, but process leakage, volatilization, and radiolysis degradation combine to increase the costs.

Explosion hazards from ozone or Xe-tetrafluoride are reduced with the absorption process. This process has never been tested at plant scale.

4.2.3. Carbon Dioxide Absorption. This process is very similar to the fluorocarbon absorption process in terms of capital equipment and operating costs. The primary difference is the use of CO_2 as the solvent. The process is considered a potential candidate for use with gas streams rich in CO_2, such as could occur in the reprocessing of graphite fuels [42–44]. While CO_2 is readily available, the process is limited to only those gas streams with high CO_2 concentrations. Explosion hazards and radiolytic degradation have not been experienced in limited scoping studies. The scoping studies were mainly to evaluate basic absorption data for CO_2, so decontamination factor results were limited.

4.2.4. Selective Physical Adsorption. This technology is considered the simplest to operate of the off-gas treatment processes. Within a single temperature or pressure setting, Kr and Xe can be physically adsorbed into the pores of a selective sorbent material in the column. These operating conditions are commonly referred to as temperature swing adsorption (TSA) or pressure swing adsorption (PSA), where lower temperatures or higher pressures, respectively, result in greater sorbent capacities. The Kr and Xe can then be desorbed from the pores at increased temperature or decreased pressure [45].

Activated charcoal is well known as a material for the capture of Kr and Xe at reduced temperatures. The primary drawback of charcoal is the potential for fires during the thermal desorption stage because of the NO_x in the gas stream. Both natural and synthetic zeolites are known to have the proper cage structure and frameworks that result in high surface areas and a pore size conducive for Kr and Xe capture and are considered to be a suitable substitute to activated charcoal.

Zeolites have been studied for Kr recovery [18]. Xenon can be captured at ambient temperatures with AgZ. The "Xe free" gas is then chilled and passed through hydrogen mordenite (HZ) operated on which the Kr is adsorbed at ~80°C (~190 K). The HZ bed is bypassed and heated to ~60°C (~330 K) to desorb the Kr and regenerate the HZ; the desorbed Kr is captured on a second, offline HZ bed from which it is recovered with a temperature swing to a cold trap [46]. The Xe bed is regenerated at 200 to 250°C (473 to 523 K). Laboratory tests have shown DFs of 400 for Kr and 4000 for Xe [47].

The sorbent bed volumes associated with physisorption can be significantly reduced by the use of cryogenic temperatures, incurring the higher costs associated with refrigeration. The potential for enhanced safety coupled with reduced capital and operating costs supports further development as a viable process option.

5. Recent Advances in Iodine and Krypton Capture

Estimated required ^{129}I DFs exceed 1000 [9]. Estimated required ^{85}Kr DFs exceed 10, although, as UNF ages, the required DF decreases and no ^{85}Kr control would be needed after what may be just a few years up to perhaps 60 years decay time, depending on the UNF and other assumptions [9].

5.1. Recent Advances in Iodine Capture. The challenges for iodine capture include (a) sufficiently high control efficiency and selectivity to enable a reprocessing facility to meet US air emission regulations and (b) development of a process that can result in an acceptable waste form. While processes including caustic scrubbing and Ag-impregnated aluminas, silicas, and mordenites have been tested decades earlier and used in reprocessing facilities for iodine capture, it is unclear if these processes could meet current regulations. Research and development has focused on developing, evaluating, optimizing sorbents for iodine capture, and determining iodine adsorption rates, efficiency, capacity, and waste form development.

Recent results of iodine sorbent research and development are summarized from many separate Off-Gas Sigma Team reports in [1]. Experimental capabilities have been designed, built, and used for iodine adsorption testing. These include thin-bed and deep-bed iodine adsorption test systems. Many experiments have been performed with these experimental facilities including the following.

(i) Extended aging studies of reduced AgZ [1]: reduced iodine capture efficiency was measured with increasing air exposure. A more rapid reduction in iodine capture efficiency was measured with increasing air and moisture exposure. The sorbent capacity can be at least partially regenerated by re-reducing the silver, depending on how long the sorbent is exposed to moist air.

(ii) Measurement of iodine adsorption on tritium capture media and of water (tritiated water) on iodine capture media [48, 49].

(iii) Measurement of the adsorption capacity of AgZ: in thin-bed tests capacities ranged from about 3 to 6 mass% for gaseous I_2 concentrations ranging from 2.5 100 ppmv [1]. In deep-bed tests, capacities ranged from 3 to 17 mass% for I_2 concentrations ranging from 2 to 50 ppmv [48].

(iv) Measurement of iodine sorption efficiencies: DFs up to 1000–10 000 were measured, high enough to comply with air emission regulations [50].

(v) Estimation of mass transfer zone depths: mass transfer zone depths for I_2 adsorption ranged from 12 to 50 mm (0.5–2 inches) for low inlet I_2 concentrations (~2 ppmv) up to 50 to 100 mm (2–4 inches) for higher I_2 concentrations (~35 ppmv) [50].

(vi) Identification of a detailed mechanism for silver reduction and migration in and out of mordenite pores. The reduction and aging of silver on the zeolite affect the iodine loading. Iodine loadings increased from 1 to 3.4 mass% for increasing levels of silver reduction.

Silver-functionalized aerogels were developed as alternates to the silver-loaded zeolites [1]. These have high specificity, can be easily consolidated into a final waste form, and have low sorption of water. Iodine adsorption efficiencies of 99.9–99.99% (DFs up to 1000–10 000), and capacities between 32 to 41 mass% were measured for functionalized aerogel and 6-month aged functionalized aerogel, respectively [1, 50]. Aerogel capacities for I_2 of 20–46 mass% were demonstrated in deep-bed aerogel tests [50]. Aging tests indicated a decrease in iodine capacity of 9% after aging in a dry air stream for six months [51].

Metal-organic framework materials were also evaluated for iodine sorption [1]. These MOFs were pelletized into engineered forms for adsorption bed applications. A detailed crystallographic identification was done for I_2 sorption on ZIF-8 (zeolitic imidazolate framework 8). The capacity of an engineered MOF for iodine was measured at 2.6–3.4 mass%. Aqueous iodine capture and storage with Bi–I–O layered oxides was also studied.

5.2. Recent Advances in Krypton Capture. Recent investigations into alternative materials, such as inorganic synthetic titanosilicates and MOFs for physisorption, have resulted in a broadened field of new materials for the capture of Kr [52–57]. Test results for hydrogen mordenite and silver mordenite have shown good capacities and selectivities for Kr and Xe, indicating that they may be suitable substitutes for activated charcoal thereby eliminating the fire hazard [53, 58, 59]. Although Xe consists of stable isotopes after about 1 y of UNF aging (about 10 half-lives) and, thus, would not contribute to the regulated radionuclide release, it is present in process off-gas streams at about 10 times the Kr concentrations. Thus, the presence of Xe detrimentally impacts the capture of Kr in that it competes for the same sites on the sorption media as Kr and increases waste volume. The high commercial economic value and potential reduction in waste volume may drive the separation of Xe from Kr.

Recent Kr and Xe capture testing at the INL has included investigations of hydrogen and silver mordenites [60]. Synthetic mordenite powders are available commercially in hydrogen, sodium, and ammonia forms. The dimensions of the mordenite pores can be tuned for Kr and Xe specificity by removing a significant fraction of the aluminum from the framework with acid leaching without loss of crystalline structure. Engineered forms of the mordenites are commercially available in limited supply, but typically the pelletization process restricts the available porosity reducing sorbent capacities. The use of powders eliminates the reduced porosity but causes processing problems such as high differential pressures across a plant-sized fixed adsorption bed.

Recent results of Kr and Xe adsorption research and development at the INL include development of a custom cryostat for sorption tests, preparation of an engineered form of H-mordenite, and preparation of a Ag-exchanged mordenite for Kr and Xe sorption [61]. The need for an engineered form with good surface area and available micropores to maximize adsorption capacity led to the development of a novel engineered sorbent form at the INL [60]. An engineered sorbent form was prepared from hydrogen mordenite bound in a selected macroporous polymer. The resultant material was analyzed for surface area and microporosity with results indicating good retention of porosity. Krypton capacities of 0.1 mmol/g for the sorbent were obtained at 191 K, comparing well with experimental data obtained by Munakata et al. [58]. This sorbent form performed well for multiple adsorption and desorption cycles [60].

An engineered form of a silver-exchanged mordenite bound in a macroporous polymer was prepared and evaluated for Kr and Xe capacity [61]. The Kr capacity was found to be 0.057 mmol/g for the sorbent at 220 K. The Xe capacity was found to be 0.46 mmol/g for the sorbent at 220 K. These capacities compare well with the Kr and Xe capacities obtained by Munakata et al., on silver mordenite at 273 K [59].

Advances have been made recently at PNNL in the separation of Xe and Kr from air with MOFs. The research team synthesized three MOFs (nickel coordinated dioxobenzenedicarboxylic acid (NiDOBDC); copper coordinated with benzene-tri-carboxylic acid (CuBTC), called HKUST-1; and a partially fluorinated metal organic framework (FMOFCu)) [56, 62, 63]. These MOFs have different pore geometries and functionalities to remove the Xe and Kr from air at near room temperature. All of these MOFs were shown to have high capacities for adsorbing Xe and Kr at room temperature and 100 kPa (1 bar). The NiDOBDC MOF demonstrated the highest adsorption capacity for Xe. The uniform cylindrical pores in the NiDOBDC are believed to maximize Xe and Kr selectivity.

The NiDOBDC and HKUST-1 can selectively adsorb Xe and Kr at ppm concentrations from air. The NiDOBDC has a Xe capacity of 9.3 mmol/kg when the concentration of Xe is 1000 ppmv in air. Xenon separation selectivity from Kr of 7.3 was demonstrated for air containing 400 ppmv Xe, 40 ppmv Kr, 0.9 volume% Ar, and 0.03 volume% CO_2. Test results show that the FMOFCu can also selectively partition Kr from Kr and Xe mixtures at moderate temperatures below ambient.

In comparison with other sorbents, MOFs were shown to have high adsorption capacities, high surface areas (~4x higher), uniform porosity, and high diffusivity. Similarly, the ability to tune the properties of MOFs by replacing nickel with another transition metal or functionalizing the organic building blocks is also advantageous compared to other sorbents. These results show that NiDOBDC is a promising MOF for the separation of Xe from a mixture of Xe and Kr at room temperature. Because of the synthetic flexibility, additional MOFs can be synthesized to further enhance both

capacity and selectivity. It has been shown that MOFs can be used to separate Xe and Kr from air and Xe from Kr at near ambient conditions.

6. Conclusions

The removal of some volatile radionuclides generated during UNF reprocessing in the US is nearly certain to be necessary for the licensing of a future reprocessing plant in the US and to meet regulatory emission limits.

Various control technologies have been developed, tested, or used over the past 50 years to control volatile radionuclide emissions from UNF reprocessing plants. Some of these control technologies have been used in the past and some are in use today. Caustic scrubbing and adsorption on Ag-impregnated or -coated alumina for capturing iodine are in use today in reprocessing plants in France, the United Kingdom, and Japan. Cryogenic distillation has been used for krypton capture at UNF reprocessing plants.

The US DOE has sponsored, since 2009, an Off-Gas Sigma Team to perform research and development focused on the most pressing volatile radionuclide control and immobilization needs. This team has focused mainly on the control and immobilization of ^{85}Kr, and ^{129}I, because (a) US regulations drive the capture of both ^{129}I and ^{85}Kr based on both a fuel cycle emission rate limit and a dose limit, (b) high control efficiency requirements are expected to drive the development and demonstration of iodine control technologies, and (c) while estimated ^{85}Kr control efficiencies are not as high as control efficiencies estimated for ^{129}I or ^{3}H, the cost estimates based on cryogenic noble gas separations technology indicate that considerable cost savings might be possible if alternative krypton capture technologies were available.

Numerous candidate technologies have been researched and developed at laboratory and pilot-plant scales to meet the need for high iodine control efficiency and to advance alternatives to cryogenic separations for krypton control. Some of these show promising results as following.

(i) Iodine decontamination factors as high as 10^5, iodine loading capacities, and other adsorption parameters including adsorption rates have been demonstrated under some conditions for both AgZ and Ag-functionalized aerogel. Studies to convert the spent sorbents into acceptable waste forms are also underway.

(ii) Sorbents including engineered forms of HZ, AgZ, and selected MOFs have been successfully demonstrated to capture Kr and Xe at temperatures close to ambient.

References

[1] R. T. Jubin, "Summary of FY-12 off-gas sigma team activities," Report No. FCR&D-SWF-2012-000331, Oak Ridge National Laboratory, 2012.

[2] EPA, *Protection of Environment: Chapter I—Environmental Protection Agency (Continued), Part 190 Environmental Radiation Protection Standards for Nuclear Power Operations*, 40CFR190.10, US Environmental Protection Agency, Washington, DC, USA, 2010.

[3] NRC, *Energy: Part 20—Standards for Protection against Radiation*, 10CFR20, chapter 10, US Nuclear Regulatory Commission, Washington, DC, USA, 2012.

[4] NRC, *Regulatory Guide 8.37—ALARA Levels for Effluents from Materials Facilities*, Nuclear Regulatory Commission, Washington, DC, USA, 1993.

[5] EPA, *Environmental Protection Agency: Part 61—National Emission Standards for Hazardous Air Pollutants. Subpart H-National Emission Standards for Emissions of Radionuclides Other than Radon from Department of Energy Facilities*, 92—Standard, 40CFR61. 92, chapter 40, US Environmental Protection Agency, Washington, DC, USA, 2010.

[6] R. T. Jubin, B. B. Spencer, and R. M. Counce, "Review of off-gas treatment technology relevant to spent nuclear fuel reprocessing," in *Proceedings of the Advanced Nuclear Fuel Cycles and Systems International Conference (Global '07)*, September 2007.

[7] N. Soelberg, M. Abbott, D. Haefner, and R. T. Jubin, "Gaseous fission product emissions control during spent nuclear fuel recycling," in *Proceedings of the 235th American Chemical Society National Meeting and Exposition*, New Orleans, La, USA, April 2008.

[8] J. E. Kelly, *Assessment of the Technical Basis of 40CFR190*, Briefing, Sandia National Laboratory, 2009.

[9] R. T. Jubin, N. R. Soelberg, D. M. Strachan, and G. Ilas, "Fuel age impacts on gaseous fission product capture during separations," Report No. FCRD-SWF-2012-000089, Oak Ridge National Laboratory, 2012.

[10] R. Rosnick, *CAP-88 (Clean Air Act Assessment Package-1988)*, US Environmental Protection Agency, Washington, DC, USA, 1992.

[11] R. Rosnick, *CAP88-PC Version 3.0 User Guide*, Environmental Protection Agency, Washington, DC, USA, 2007.

[12] EPA, "Cancer risk coefficients for environmental exposure to radionuclides," Report No. EPA 402-R-99-001, Environmental Protection Agency, Washington, DC, USA, 1999.

[13] ICRP, "Age-dependent doses to the members of the public from intake of radionuclides—part 5 compilation of ingestion and inhalation coefficients," Report No. ICRP Publication 72, International Commission on Radiological Protection, Ottawa, Canada, 1995.

[14] ASTM, *ASTM C833-01, Standard Specification for Sintered Uranium-Plutonium Dioxide Pellets*, American Society for Testing and Materials, West Conshohocken, Pa, USA, 2008.

[15] ASTM, *ASTM C776-06, Standard Specification for Sintered Uranium Dioxide Pellets*, American Society for Testing and Materials, West Conshohocken, Pa, USA, 2011.

[16] H. Wershofen and D. C. Aumann, "Iodine-129 in the environment of a nuclear fuel reprocessing plant: VII. Concentrations and chemical forms of ^{129}I and ^{127}I in the atmosphere," *Journal of Environmental Radioactivity*, vol. 10, no. 2, pp. 141–156, 1989.

[17] W. Hebel and G. Cottone, "Management modes for iodine-129," in *Proceedings of the Commission of the European Communities Meeting*, Commission of the European Communities, Brussels, Belgium, 1982.

[18] D. Gombert, R. Counce, A. Cozzi et al., "Global nuclear energy partnership integrated waste management strategy waste treatment baseline study, volume I," Report No. GNEP-WAST-AI-RT-2007-000324, Idaho National Laboratory, Idaho Falls, Idaho, USA, 2007.

[19] IAEA, "Treatment, conditioning and disposal of iodine-129," Report No. Series 276, International Atomic Energy Agency, Vienna, Austria, 1987.

[20] T. Fukusawa, K. Funabashi, and Y. Kondo, "Influences of impurities on iodine removal efficiency of silver alumina adsorbent," in *Proceedings of the 24th DOE/NRC Nuclear Air Cleaning and Treatment Conference*, CONF-960715, Harvard Air Cleaning Laboratory, Boston, Mass, USA, 1996.

[21] M. Kikuchi, T. Yoshida, M. Matsuda, and H. Kanai, "Developing technologies for nuclear fuel cycles—radioactive waste treatment and spent fuel storage," *Hitachi Review*, vol. 48, no. 5, pp. 277–284, 1999.

[22] D. R. Haefner and T. J. Tranter, "Methods of gas phase capture of iodine from fuel reprocessing off-gas: a literature survey," Report No. INL/EXT-07-12299, Idaho National Laboratory, Idaho Falls, Idaho, USA, 2007.

[23] K. Funabashi, T. Fukasawa, M. Kikuchi, F. Kawamura, and Y. Kondo, "Development of silver impregnated alumina for iodine separation from off-gas streams," in *Proceedings of the 23rd DOE/NRC Nuclear Air Cleaning Conference*, CONF-940738, pp. 352–363, Harvard Air Cleaning Laboratory, Boston, Mass, USA, 1994.

[24] T. R. Thomas, B. A. Staples, and L. P. Murphy, "The development of Ag°Z for bulk ^{129}I removal from nuclear fuel reprocessing plants and PbX for ^{129}I storage," in *Proceedings of the 15th DOE Nuclear Air Cleaning Conference*, CONF-780819, p. 394, US Department of Energy, Washington, DC, USA, 1978.

[25] R. T. Jubin, "Organic iodine removal from simulated dissolver off-gas systems using partially exchanged silver mordenite," in *Proceedings of the 17th DOE Nuclear Air Cleaning Conference*, CONF-820833, pp. 183–196, The Harvard Air Cleaning Laboratory, Boston, Mass, USA, 1982.

[26] R. D. Scheele and L. L. Burger, "Selection of a carbon-14 fixation form," Report No. PNL-4447, Pacific Northwest Laboratory, Richland, Wash, USA, 1982.

[27] K. D. Kok, Ed., *Nuclear Engineering Handbook*, CRC Press, Boca Raton, Fla, USA, 2009.

[28] M. G. Kanatzidis and S. Bag, "Semiconducting aerogels from chalcogenide clusters wtih broad applications," US Patent No. 2008/0241050 A1, 2008.

[29] J. Lee, O. K. Farha, J. Roberts, K. A. Scheidt, S. T. Nguyen, and J. T. Hupp, "Metal-organic framework materials as catalysts," *Chemical Society Reviews*, vol. 38, no. 5, pp. 1450–1459, 2009.

[30] J. R. Long and O. M. Yaghi, "The pervasive chemistry of metal-organic frameworks," *Chemical Society Reviews*, vol. 38, no. 5, pp. 1213–1214, 2009.

[31] G. Férey, C. Serre, T. Devic et al., "Why hybrid porous solids capture greenhouse gases?" *Chemical Society Reviews*, vol. 40, no. 2, pp. 550–562, 2011.

[32] D. Zhao, D. Q. Yuan, and H. C. Zhou, "The current status of hydrogen storage in metal-organic frameworks," *Energy and Environmental Science*, vol. 1, no. 2, pp. 222–235, 2008.

[33] H. Furukawa, N. Ko, Y. B. Go et al., "Ultrahigh porosity in metal-organic frameworks," *Science*, vol. 329, no. 5990, pp. 424–428, 2010.

[34] K. Koh, A. G. Wong-Foy, and A. J. Matzger, "A porous coordination copolymer with over 5000 m^2/g BET surface area," *Journal of the American Chemical Society*, vol. 131, no. 12, pp. 4184–4185, 2009.

[35] J. R. Li, R. J. Kuppler, and H. C. Zhou, "Selective gas adsorption and separation in metal-organic frameworks," *Chemical Society Reviews*, vol. 38, no. 5, pp. 1477–1504, 2009.

[36] G. F. Offutt and C. L. Bendixen, "Rare gas recovery facility at the Idaho chemical processing plant," Report No. IN-1221, Idaho Nuclear Corporation, Idaho Falls, Idaho, USA, 1969.

[37] D. T. Pence, "Critical review of noble gas treatment systems," in *Proceedings of the 16th DOE Nuclear Air Cleaning Conference*, vol. 2 of *CONF-80138*, pp. 989–1013, The Harvard Air Cleaning Laboratory, Boston, Mass, USA, 1980.

[38] H. Yusa, M. Kikuchi, H. Tsuchiya, O. Kawaguchi, and T. Segawa, "Application of cryogenic distillation to Krypton-85 recovery," *Nuclear Engineering and Design*, vol. 41, no. 3, pp. 437–441, 1977.

[39] "Treatment of gaseous effluents at nuclear facilities," in *Radioactive Waste Management Handbook*, W. R. A. Goossens, G. G. Eichholz, and D. W. Tedder, Eds., vol. 2, Harwood Academic Publishers, 1991.

[40] D. K. Little, "Noble gas removal and concentration by combining fluorocarbon absorption and adsorption techniques," in *Proceedings of the 17th DOE Nuclear Air Cleaning Conference*, CONF-820833, pp. 694–716, US Department of Energy, The Harvard Air Cleaning Laboratory, 1983.

[41] IAEA, "Separation, storage and disposal krypton-85," Technical Report Series No. 199, International Atomic Energy Agency, Vienna, Austria, 1980.

[42] R. W. Glass, P. A. Haas, R. S. Lowrie, and M. E. Whatley, "HTGR head-end processing: a preliminary evaluation of processes for decontaminating burner off-gas," Report No. ORNL-TM-3527, Oak Ridge National Laboratory, Oak Ridge, Tenn, USA, 1972.

[43] R. W. Glass, A. B. Meservey, P. A. Haas et al., "Removal of krypton from the HTGR fuel reprocessing off-gases," *ANS Transactions*, vol. 15, no. 1, p. 95, 1972.

[44] M. F. Wheatley, "Calculations on the performance of the KALC process," Report No. ORNL-4859, Oak Ridge National Laboratory, Oak Ridge, Tenn, USA, 1973.

[45] D. M. Ruthven, *Principles of Adsorption & Adsorption Processes*, John Wiley & Sons, New York, NY, USA, 1984.

[46] L. E. Trevorrow, G. F. Vandegrift, V. M. Kolba, and M. J. Steindler, "Compatibility of technologies with regulations in the waste management of H-3, I-129, C-14, and Kr-85. Part I. Initial information base," Report No. ANL-83-57, Argonne National Laboratory, Argonne, Ill, USA, 1983.

[47] D. T. Pence, "Critical review of noble gas recovery and treatment systems," *Nuclear Safety*, vol. 22, no. 6, 1981.

[48] S. H. Bruffey, "Evaluation of iodine and tritium co-adsorption on silver mordenite using neutron scattering," Report No. FCRD-SWF-2012-000257, Oak Ridge National Laboratory, Oak Ridge, Tenn, USA, 2012.

[49] B. B. Spencer, R. T. Jubin, S. H. Bruffey, K. K. Anderson, and J. F. Walker Jr., "Assessment of tritium (water)/iodine co-adsorption on AgZ," Report No. FCRD-SWF-2012-000210, Oak Ridge National Laboratory, Oak Ridge, Tenn, USA, 2012.

[50] N. Soelberg and T. Watson, "Iodine sorbent performance in FY, 2012 deep bed tests," Report No. FCRD-SWF-2012-000278, INL/EXT-12-EXT-12-27075, Idaho National Laboratory, Idaho Falls, Idaho, USA, 2012.

[51] S. H. Bruffey, K. K. Anderson, R. T. Jubin, and J. F. Walker Jr., "Aging and iodine loading of silver-functionalized aerogels," Report No. FCRD-SWF-2012-000256, Oak Ridge National Laboratory, Oak Ridge, Tenn, USA, 2012.

[52] S. M. Kuznicki, V. A. Bell, S. Nair et al., "A titanosilicate molecular sieve with adjustable pores for size-selective adsorption of molecules," *Nature*, vol. 412, no. 6848, pp. 720–724, 2001.

[53] D. Ianovski, K. Munakata, S. Kanjo et al., "Adsorption of noble gases on H-mordenite," *Journal of Nuclear Science and Technology*, vol. 39, no. 11, pp. 1213–1218, 2002.

[54] A. Ansón, S. M. Kuznicki, T. Kuznicki et al., "Adsorption of argon, oxygen, and nitrogen on silver exchanged ETS-10 molecular sieve," *Microporous and Mesoporous Materials*, vol. 109, no. 1–3, pp. 577–580, 2008.

[55] C. A. Fernandez, S. K. Nune, R. K. Motkuri et al., "Synthesis, characterization, and application of metal organic framework nanostructures," *Langmuir*, vol. 26, no. 24, pp. 18591–18594, 2010.

[56] J. Liu, P. K. Thallapally, and D. M. Strachan, "Metal-organic frameworks for removal of Xe and Kr from nuclear fuel reprocessing plants," *Langmuir*, vol. 28, no. 31, pp. 11584–11589, 2012.

[57] D. W. Breck, *Zeolite Molecular Sieves*, John Wiley & Sons, New York, NY, USA, 1974.

[58] K. Munakata, S. Yamatsuki, K. Tanaka, and T. Fukumatsu, "Screening test of adsorbents for recovery of krypton," *Journal of Nuclear Science and Technology*, vol. 37, no. 1, pp. 84–89, 2000.

[59] K. Munakata, S. Kanjo, S. Yamatsuki, A. Koga, and D. Ianovski, "Adsorption of noble gases on silver-mordenite," *Journal of Nuclear Science and Technology*, vol. 40, no. 9, pp. 695–697, 2003.

[60] T. G. Garn, J. D. Law, M. R. Greenhalgh, and T. J. Tranter, "A composite media for fluid stream processing, a method of forming the composite media, and a related method of processing a fluid stream," US Patent Application 2939-10703 BA-590, 2012.

[61] T. G. Garn, J. D. Law, and M. R. Greenhalgh, "FY-12 INL krypton capture activities supporting the off-gas sigma team," Report No. FCR&D-SWF-2012-000252, Idaho National Laboratory, Idaho Falls, Idaho, USA, 2012.

[62] P. K. Thallapally, J. W. Grate, and R. K. Motkuri, "Facile xenon capture and release at room temperature using a metal-organic framework: a comparison with activated charcoal," *Chemical Communications*, vol. 48, no. 3, pp. 347–349, 2012.

[63] C. A. Fernandez, J. Liu, P. K. Thallapally, and D. M. Strachan, "Switching Kr/Xe selectivity with temperature in a metal-organic framework," *Journal of the American Chemical Society*, vol. 134, no. 22, pp. 9046–9049, 2012.

Hindawi Publishing Corporation
Science and Technology of Nuclear Installations
Volume 2013, Article ID 417048, 7 pages
http://dx.doi.org/10.1155/2013/417048

Review Article

Recycling versus Long-Term Storage of Nuclear Fuel: Economic Factors

B. Yolanda Moratilla Soria, Maria Uris Mas, Mathilde Estadieu, Ainhoa Villar Lejarreta, and David Echevarria-López

Universidad P. Comillas, ETSI (ICAI), Cátedra Rafael Mariño de Nuevas Tecnologías Energéticas, C/ Alberto Aguilera 23, 28015 Madrid, Spain

Correspondence should be addressed to B. Yolanda Moratilla Soria; ymoratilla@upcomillas.es

Received 13 December 2012; Revised 4 June 2013; Accepted 4 June 2013

Academic Editor: Candido Pereira

The objective of the present study is to compare the associated costs of long-term storage of spent nuclear fuel—open cycle strategy—with the associated cost of reprocessing and recycling strategy of spent fuel—closed cycle strategy—based on the current international studies. The analysis presents cost trends for both strategies. Also, to point out the fact that the total cost of spent nuclear fuel management (open cycle) is impossible to establish at present, while the related costs of the closed cycle are stable and known, averting uncertainties.

1. Introduction

1.1. State-of-the-Art. The current demand of resources and the increasing and intensive energy consumption per capita have motivated development policies of efficient forms of energy in the electric generation area. Nuclear and renewable energies play an important role in our energy future, helping to meet increasing electricity demand while at the same time decreasing carbon dioxide emissions [1]. As a nation develops its nuclear strategies, it must consider various aspects of nuclear energy such as sustainability, environmental friendliness, proliferation resistance, economics, and technologies and evaluate all the possible nuclear fuel cycle options [2–5].

Over the last decade, numerous assessments [6–14] have been developed in order to compare the two main spent fuel strategies: strategy one which is the disposal of spent nuclear fuel generated by nuclear power plants operating in a "once-through" fuel cycle in a deep geologic repository and strategy two which is closing the fuel cycle by reprocessing and recycling the spent nuclear fuel. One of the latest economic analyses carried out by Ko and Gao [15] shows that the difference in the fuel cycle costs between recycling strategy and "once-through" strategy is negligible. Therefore, other factors such as the intangible asset play important roles in determining the future nuclear fuel cycle options. De Roo and Parsons [16] have developed the first methodology to calculate the levelized cost of electricity extended to the reprocessing strategy.

Högselius [17] gives an explanation of why the world's nuclear power countries differ from each other with respect to their spent nuclear fuel (SNF) policies according to the five main broad explanatory factors: military ambitions and nonproliferation, technological culture, political culture and civil society, geological conditions, and energy policy.

The UK's nuclear energy landscape assessment [18] also considers the long-term strategy for storage, reprocessing or disposal of UK's current and future nuclear fuel and waste stockpiles.

Studies developed in US will need to compare each of the fuel cycle options regarding sustainability, proliferation risk, commercial viability, waste management, and energy security in order to define the future of nuclear power [19–21]. Recktenwald and Deinert [22] present a probabilistic analysis of the costs to build, operate, and decommission the facilities that would be required to reprocess all US spent nuclear fuel generated over a one-hundred-year time frame, showing

discounting results in life-cycle costs decreasing as recycling is delayed.

Although China's nuclear power industry is relatively young and the management of its spent nuclear fuel is not yet a concern, China's commitment to nuclear energy and its rapid pace of development require detailed analyses of its future spent fuel management policies. Zhou [23, 24] in his studies concluded that China can and should maintain a reprocessing operation to meet its R&D activities before its fast reactor program is further developed.

Suchitra [25], in his paper, assesses the economics of reprocessing in India and the cost of producing plutonium for the fast breeder reactor program, suggesting a cost of reprocessing approximately $600/kg HM with assumptions favorable to reprocessing and close to $675/kg HM under other assumptions.

The purpose of this report is to analyze and compare the results obtained from studies conducted by the Nuclear Energy Agency (NEA) for the Organization for Economic Co-operation and Development (OECD) in 1985 [6] subsequently updated in 1991, by the Massachusetts Institute of Technology (MIT) in 2003 [9], by the Boston Consulting Group (BCG) in 2006 [11], by De Roo and Parsons in 2011 [16], and by the Electric Power Research Institute (EPRI) in 2010 [12].

1.2. Used Fuel Management: General Aspects. Currently, the production of electricity from nuclear sources is based on the "fission" of U_{235} and, in lesser proportions, Pu_{239}. In order to better understand this process, we will review some of the concepts and milestones regarding this technology, albeit in a very simplified manner, as this paper focuses on economic aspects of management.

1.2.1. What Is Used Fuel? In light water reactor nuclear power plants such as those found in Western countries, fission is produced in the previously mentioned atoms. This fission generates energy which is then used to heat water from a cooling cycle which evaporates and enters into a steam generator, thereby producing electricity. With this "nuclear fuel fission" reaction, new isotopes, products of the fission, are created in the nuclear reactor. At the same time, transuranic elements are transmuted by neutron capture into actinides which are capable of fission and energy generation.

As the U-235 nuclei continue the fission process, the amount of fissile material decreases while the fission and actinide products increase until reaching the point in which the chain reaction is no longer maintained in the reactor. To prevent this, fuel elements must be substituted for the other nonirradiated elements.

The used fuel found in the light water reactors consists of uranium oxide enriched in isotope 235 by a variable percentage of approximately 5%. As previously indicated, some reactors use a mixture of enriched uranium and Pu-239, which is produced in the reactor. Natural uranium, which is extracted from mines, only contains roughly 0.7% of U-235. The natural uranium is concentrated and converted into uranium hexafluoride. This compound is enriched by the necessary quantity of U-235 in order to reach the required percentage for the reactor.

After its use in the reactor, the fuel is then discharged. The exact composition of the used fuel depends on the amount of time it was in the reactor as well as on the neutron flux levels to which it was subjected. In schematic terms, nuclear fuel evolution can be represented as shown in Figure 1. Initially, it consists of U-235 (fissile) and U-238 (fertile, as it can be transmuted to Pu-239). Once the fuels are removed from the reactor, a fraction of the initial U-235 remains and another fissile element has formed, Pu-239. *Both of these elements can be reused*. In some countries, and for several years now, mixed uranium and plutonium fuels have been used, made from already used and reprocessed fuels *(MOX fuels through mixed oxides), as well as* Enriched Reprocessed Uranium *(ERU) fuels, made of depleted uranium, the result of reprocessing (RepU—(Reprocessed Uranium))*.

The evolution of fuel during irradiation in a reactor can be simplified in the following manner.

(i) The content of U-235, initially at 4%, is reduced to 1%.

(ii) The 3% of U-235 is converted into fission products (FP).

(iii) The 3% of U-238 is converted principally into Pu and, in lesser amounts, into other transuranic elements, minor actinides (MA).

(iv) A portion of the Pu has fissioned, increasing the quantity of fission products.

When the fuel elements are removed from the reactor, they are deposited into specially prepared pools which are located in the nuclear plant complex in order to release any residual thermal energy and to reduce their level of radioactivity for later treatment, be it in the final waste deposit site or in reprocessing for subsequent recycling.

1.2.2. Long-Term Used Fuel Management Options. For very long-term management of these elements, transmutation or fission technologies in accelerator-assisted systems or Generation IV fast reactors are considered. In this way, the radiotoxicity of the radioactive waste, in a period of one-hundred years, will be reduced to levels existing naturally, due to the naturally radioactive elements of which they are composed.

These technologies are still in a developmental phase and have yet to be applied to an industrial scale. As previously mentioned, there are two existing alternatives for the definitive management of used fuel elements in a final stage. The elements can be safely stored in stable deep geological repositories (*DGR*) so as to be contained and isolated from the environment and humans for centuries, while their radiotoxicity declines. This is the open cycle. Or, on the contrary, processes can be applied to allow for the uranium and plutonium to be removed and recycled, isolating the fission products and other minor actinides in a glass matrix. This, the closed cycle, in removing plutonium from the final waste product, results in a reasonable level of radiotoxicity. In both cases, the fuel elements are specially prepared and

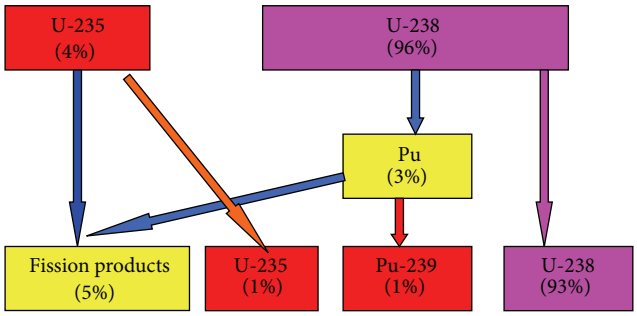

Figure 1: Evolution of fuel from a nuclear reactor during an operating cycle.

temporarily stored in an appropriately treated site until the final management phase is initiated.

Two countries, Sweden and Finland, have definitively adopted the open cycle and are in the preconstruction phase of the geological repositories for fuel element storage in copper capsules with granite subsoil.

One of the principles of any waste management policy in developed countries is that of reducing, recycling, and reusing waste products. The application of this principle to radioactive waste requires separating the unused and/or produced fissile material, reusing the material in new fuels, as previously described, and reducing the highly active waste to minor actinides—fission products that are obtained in a reactor by uranium transmutation.

In the closed cycle option, as it is currently practiced, after cooling the used fuel through chemical and mechanical processes, the recyclable uranium and plutonium materials are separated, so as to be used in the fabrication of new ERU fuels, and MOX fuels (Mixed Oxides with uranium and plutonium), which can be used in conventional reactors. This recycled fuel offers savings of up to 25% in natural uranium [9]. As stated in the MIT report, "recycle of the plutonium reduces uranium fuel demand by only 15% and recycle of the uranium reduces uranium fuel demand by only 10%." This is confirmed by AREVA's experience in the reprocessing of used fuel, where from 7 to 9 spent nuclear fuels (depending on the characteristics of spent UOx and burn up), 1 ERU and 1 MOX are fabricated. The nonreusable materials, both the fission products and the structural portions of the fuel element are the final waste products. When the fuel material is separated after the shearing, the metal parts become insoluble, so they can be compacted and the nuclear materials can be separated easier. The fission products and the minor actinides, making up some 90% of the radioactivity of the used fuel, are vitrified. The structural parts are crushed and compacted by a press, which enables to reduce its volume before being packed into stainless steel containers, so as to optimize their final management in the geological repositories. The companies that carry out this reprocessing confirm their ability to divide the volume of final waste by a factor of 5 and the toxicity by a factor of 10, since the final waste product is free of the highly radiotoxic plutonium [26].

Those countries with reprocessing facilities are France, Russia, the United Kingdom, Japan, India, Pakistan, and, most recently, China. However, many other countries reprocess or have reprocessed part of their used fuel, although they do not have their own facilities, and they recycle or have recycled in their reactors. This is the case in Holland, a country which has reprocessed the total amount of its used fuel and has a centralized storage facility where they store reprocessed vitrified waste instead of used fuel.

Today, some 90,000 tons of used fuels (of the 290,000 tons discharged) from commercial reactors have been reprocessed [27]. MOX fuel is currently used in various countries across the world, particularly in European countries such as France, Germany, and Switzerland, in order to feed their light water nuclear reactors. Some 5,500 elements from MOX and ERU fuels have been charged in reactors worldwide [28].

1.2.3. Closed or Open Cycle: A Choice Based on Energy Strategies, Both Worldwide and in Spain. It is noteworthy to mention that the large majority of countries [29] have delayed the decision regarding the direct deposit of fuel as waste or recycled material and currently choose to store the used fuel in a temporary manner, awaiting its final destination. Spain is among these countries. In the past, some of the used fuel was reprocessed in the Santa Maria de Garoña, José Cabrera and Vandellós I plants, but currently, as stated in the Radioactive waste management plan (VI General Radioactive Waste Plan, GRWP [30])—guidelines followed by ENRESA, the radioactive waste management organism in Spain—it is possible to partially reprocess abroad, which would be a "potential alternative scenario, even though this option cannot be considered to be exclusively a question of waste management, but rather, and depending on the quantity to be reprocessed, it is a policy issue of energy supply" [30]. Therefore, used fuel is currently considered to be highly active waste.

In Spain, some 2,000 tons of low- and medium-activity waste are produced annually along with some 160 tons of high activity waste. The eight operating nuclear reactors in Spain produced 21% of the electric energy that was consumed in Spain in 2011 and generated 95% of this waste.

The absence of a definitive decision regarding the final destination of the used fuel and the delay in the creation of programs for deep geological repositories (DGR) have created the need for temporary solutions: increased capacities of the used fuel pools in the plants, construction of temporary storage sites near the plants, and, key for Spanish used-fuel management: a project to create a temporary centralized storage facility.

On December 30, 2011, the Spanish Council of Ministers approved a resolution whereby the municipality of Villar de Cañas (Castilla-La Mancha) was chosen as site of the temporary centralized storage facility for highly active nuclear waste and used fuel generated by the Spanish nuclear energy industry. Planned for a total period of sixty years, this site will store all of the used fuel generated in the eight reactors in Spain for forty years—some 6,700 tons of used fuel.

2. Methodology

The methodology followed to evaluate the values presented in the analyzed reports consists of the comparison of three

concepts: the cost of uranium ore, the storage costs in deep geological repositories (DGR), and the cost of reprocessing the spent nuclear fuel. In order to work with comparable values, the criteria used for each cost has been as follows.

(i) Cost of uranium ore: over the past years, the uranium price has shown an increasing trend of \$36/lb. U_3O_8 reaching a maximum of almost \$45/lb U_3O_8 in 1975–1980, and a second maximum of \$136/lb U_3O_8 in 2007. This trend is shown in Figure 2.

(ii) DGR cost: the storage cost for spent nuclear fuel has been considered to be the cost per kilogram of heavy metal (kg HM) stored. Transport costs, combustible costs for transport, encapsulating costs, and uranium credits are not included.

(iii) Reprocessing cost: the cost of reprocessing the spent nuclear fuel includes reprocessing costs per se and the cost of vitrification.

In each study, a sensitivity analysis was carried out for the different variables, with the DGR costs as well as the reprocessing costs having nominal values within a range with upper and lower margins. The criterion used to determine the nominal value is described in detail in each report.

Table 1 shows the nominal values from each report, shown in dollars from the year of the study.

In order to make an appropriate cost comparison, the prices have been updated to the year 2011 using the following conversion equation:

$$\frac{C_2}{C_1} = \frac{I_2}{I_1}, \tag{1}$$

with C_2 and I_2 being, respectively, the cost and the cost index to be estimated at the current time and C_1 and I_1 being the cost of each study and the cost index of the corresponding year. For this purpose, the chemical engineering plant cost index (CEPI) has been used.

3. Results

3.1. Economic Values. Table 2 has been obtained updating the values from Table 1 in accordance with the CEPI price indexes, to the year 2011. Although the paper by De Roo was published in 2011, it was carried out with \$2007, so the costs have been updated also to 2011.

In order to analyze the values updated to the year 2011 for each report, a graphic evaluation of the DGR costs versus time has been created as shown in Figure 3.

The differences between the DGP costs trend published by the OCDE and BCG (growing trend) and the MIT and De Roo (decreasing trend) are remarkable. As stated in an OCDE study dedicated to geologic disposal, 1993, "Permanent geologic disposal of spent fuel and HLW has not been demonstrated, and approaches to waste disposal vary considerably from country to country, making cost estimates highly uncertain" [31]. And Sweden, quoted in a Harvard study of 2003, released, for example, a cost estimate in 1998 of \$300–\$350 kg HM [32]. It is noteworthy that all of the estimates show an increasing trend in time, including this last Swedish cost, except from the report of the MIT, which is significantly higher, although it should be more comparable with De Roo, since both reports use as a reference the Yucca Mountain storage for their DGR cost calculations.

A second analysis carried out to compare the trend for the reprocessing cost is presented in Figure 4.

The reprocessing costs show a decreasing trend since 1985 except in the MIT and De Roo study.

The decreasing trend could be explained by the technical and economic improvements of the reprocessing technology, which have turned it into a mature technology and consequently could have led to a cost decrease. This also will apply to the technology of the DGR, in a medium-long term, although this should not happen in the next years, due to the high level of uncertainties of estimates based on design studies, as stated in the OCDE study of 1993 [31].

3.1.1. Noneconomic Values. Other nonquantifiable economic factors should be considered to carry out a comparison between both spent fuel strategies; open cycle with direct disposal and closed cycle with reprocessing of the spent fuel. As stated in the OCDE study on the DGR of 1993, the disposal of spent fuel or reprocessing waste is expected to be a highly controversial political issue in most countries, and the social and political issues will inevitably affect the costs [31].

There, reprocessing and recycling of the spent fuel seems to be the most sustainable strategy mainly because of the reduction of total volume of final waste to dispose.

The nonquantifiable economic factors are the intangibles assets. The most noteworthy intangible assets are

(i) Reprocessing and recycling strategies save up to 25% uranium ore, as explained before, reducing the volume of nuclear waste to disposal by a factor of 5 as well as the thermal load.

(ii) The relative radiotoxicity and the radioactive decay are considered to be intangibles assets, difficult to evaluate quantitatively yet offering an undisputed added value compared to the open cycle, from a public opinion viewpoint. The relative radio toxicity level is reduced by a factor of 10, as can be observed in Figure 5.

(iii) The separation of plutonium 239 from spent nuclear fuel in the reprocessing phase and its later recycling into MOX avoids the nuclear proliferation. The plutonium of the spent MOX fuel is less appropriate for use in nuclear weapons.

(iv) The vitrified waste products, including the products obtained in the fission, are initially beta-gamma emitters, so the radioactive emission capacity is reduced in about some five-hundred years.

An opinion survey carried out in seven countries in 2010 showed that almost 80% of the respondents would advise their governments to begin recycling used nuclear fuel immediately, by using existing industrial solutions [33].

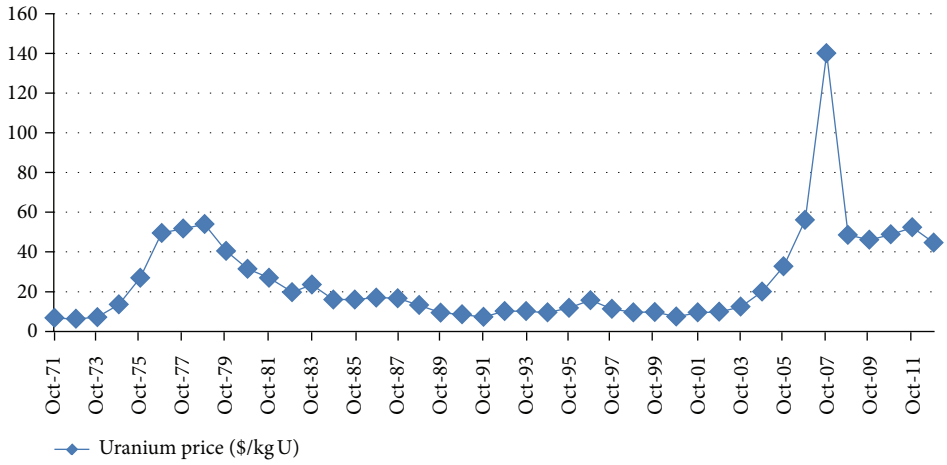

Figure 2: Uranium price chart.

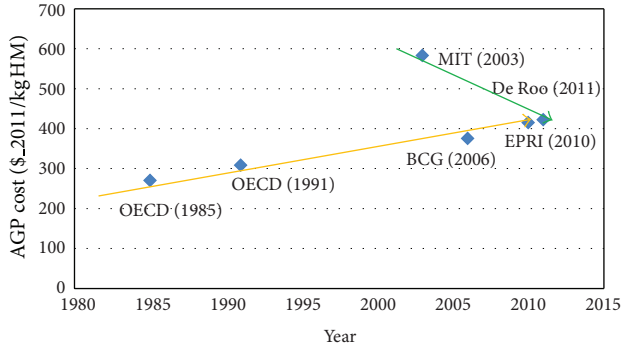

Figure 3: DGR costs trend.

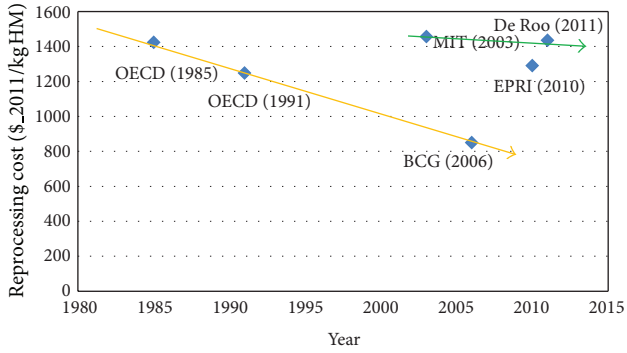

Figure 4: Reprocessing cost trend.

3.1.2. Spent Fuel Management Strategy in Spain. It is also necessary to consider the current instability of the Spanish legal landscape as exemplified by the draft bill on tax measures related to environmental and sustainable energy, placing new taxes on the value of electric energy generation, the production of spent nuclear fuel and the radioactive waste resulting from nuclear energy generation as well as on the storage of spent nuclear fuel, and radioactive waste in centralized interim storage facility (ATC).

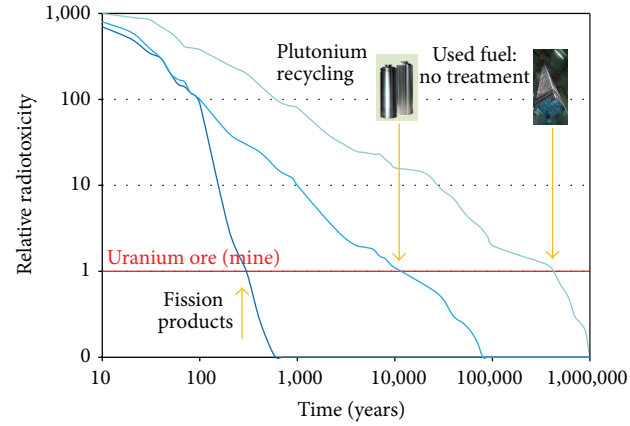

Figure 5: Radioactive decay. Source: adapted from Commissariat à l'énergie atomique 2013 [34].

Article 22 from Chapter III of the Spanish Bill on the Storage of High Level Waste and Spent Fuel distinguishes between spent fuel, whose taxable base is per kilogram of heavy metal, and other highly active waste, whose taxable base is per cubic meters.

(i) Spent nuclear fuel is taxed per kilogram of heavy metal stored, at a rate of 70€/kg HM.

(ii) Radioactive waste will be taxed per cubic meter, at a rate of 30,000€/m^3.

It should be noted that this distinction carries with it consequences for reprocessed Spanish used fuel: the tax applied to spent fuel will no longer be applied to the content of heavy metal in the stored fuel elements but rather, only to the 5th part: vitrified and compacted waste returned to Spain after being reprocessed-recycled, changing the taxable base and the applicable rate.

Also noteworthy is the fact that in the 6th GRWP, calculations for DGR cost have not been explicitly included as such. The base has been calculated up until 2070; however,

Table 1: Results from the studies.

	NEA-OECD (1985) [6]	NEA-OECD (1991) [6]	MIT (2003) [9]	BCG (2006) [11]	EPRI (2010) [12]	De Roo and Parsons (2011) [16]
Uranium price ($/kg U)	83.2	50	30	68.8	260	80
DGR cost ($/kg HM)	150	190	400	320	354	470
Reprocessing cost ($/kg HM)	790	770	1100	725	1100	1600

Table 2: Results obtained from studies updated to 2011.

	NEA-OECD (1985) [6]	NEA-OECD (1991) [6]	MIT (2003) [9]	BCG (2006) [11]	EPRI (2010) [12]	De Roo and Parsons (2011) [16]
Uranium price ($$_{2011}$$/kg U)	149.8	81	43.7	80.6	276.5	89
DGR cost ($$_{2011}$$/kg HM)	270.1	308.1	582.8	375.2	376.5	422
Reprocessing cost ($$_{2011}$$/kg HM)	1422.4	1248.3	1458	1602.6	1783.6	1169.7

many management and long-term costs for the construction of a DGR or for solutions such as transmutation have not been included while the implied costs for the DGR may have been underestimated, as can be deduced from the increase between the calculations of ENRESA between 1999 and 2006: the 6th GRWP acknowledged a 40% costs increase between the 2006 estimates and the last calculations made in 1999 for the interim storage [30]. ENRESA explains this increase by a better and more precise understanding of the design of the foreseen facility. This difference is most likely to be foreseen as well in the case of the DGR, taking in account to the previous observations. However, this increase could be minor in case of disposal of vitrified and compacted waste, as would be the case in the closed cycle: the management of a used fuel, 100-year old, from the time of its discharge to its ultimate storage for 60 years in a temporary centralized storage facility, requires various operations, perhaps complex ones, that would be unnecessary in the case of vitrified and compacted waste that was designated, from its production, to be stored for thousands of years.

4. Conclusions

When it comes to comparing global costs for the management of spent nuclear fuel, the studies analyzed in this report face considerable uncertainties due to two principle reasons: first, because this is a very long-term management issue, these theoretical and forward-looking studies must make several estimations based on the costs of certain processes that have yet to be fully developed and implemented, for a period of time in which costs could potentially change and be influenced by a variety of factors that are not currently known or quantifiable. Also, there are uncertainties related to these same characteristics of the potential management options: the overall cost of the open cycle as it is impacted by the estimated cost of certain solutions that have yet to be implemented on an industrial level, and in the closed cycle, as it deals with costs of commercial services that depend upon offers and are subjected to the policies of the service-providing company. As a consequence, the results of these comparative studies depend considerably upon the hypothesis which is chosen by the research team, explaining in great part why there are conflicting findings. However, we have determined that, in all of the studies, two factors decisively impact the overall cost of each option: the estimated cost of the deep geological repositories (DGR) in the open cycle and the reprocessing costs in the closed cycle. According to the information accumulated from all of the reports consulted, it was determined that while the costs associated with the DGR in the open cycle increase with time, due to the increasing uncertainties associated with the technology and its associated costs, the economic data related to the use of reprocessing decreases, precisely for the opposite reason, as this is a mature technology being consistently improved, with experience and R&D resulting in the lower prices. Controlled future back-end costs will significant decrease back-end's financial uncertainties going along recycling option thanks to mature industry. On the contrary, there is an important financial risk for used fuel disposal for which encapsulation is still under development and economic evaluation is usually revised upwards. Limitation of financial risk is related to final disposal along with recycling thanks to the volume, heat load, and radiotoxicity reduction and final waste conditioning in standard canisters.

This conclusion leads us to recall the advantage offered by the reprocessing-recycling option in the decrease of uncertainties, as it deals with known, stable and applied costs in a horizon that is closer to the production of used fuel.

It is also important to recall that the choice between direct deposal and recycling of spent nuclear fuel does not depend solely on a vision of industrial management responding to the criterion of economic profitability but also depends on a global energy policy. Thus, the decision must take into account logic behind environmental and social sustainability. Here, the intangible assets of reprocessing and subsequent recycling offer a more sustainable solution that greatly reduces the volume and toxicity of the final waste product that is to be stored—the legacy that is to be inherited by our future generations, and principal preoccupation of our fellow citizens.

References

[1] P. L. Joskow and J. E. Parsons, "The economic future of nuclear power," *Daedalus*, vol. 138, no. 4, pp. 45–59, 2009.

[2] B. H. Park, F. Gao, E.-H. Kwon, and W. I. Ko, "Comparative study of different nuclear fuel cycle options: quantitative analysis on material flow," *Energy Policy*, vol. 39, no. 11, pp. 6916–6924, 2011.

[3] R. Natarajan and B. Raj, "Fast reactor fuel reprocessing technology: successes and challenges," in *Proceedings of the 2nd International Conference on Asian Nuclear Prospects (ANUP '10)*, pp. 414–420, October 2010.

[4] L. Borges Silverio and W. D. Q. Lamas, "An analysis of development and research on spent nuclear fuel reprocessing," *Energy Policy*, vol. 39, no. 1, pp. 281–289, 2011.

[5] M. Kotschenreuther, P. Valanju, and S. Mahajan, "Reprocessing free nuclear fuel production via fusion fission hybrids," *Fusion Engineering and Design*, vol. 87, no. 4, pp. 303–317, 2012.

[6] OECD/NEA, *The Economics of the Nuclear Fuel Cycle*, OECD, Paris, France, 1994.

[7] F. N. Von Hippel, "Plutonium and reprocessing of spent nuclear fuel," *Science*, vol. 293, no. 5539, pp. 2397–2398, 2001.

[8] M. Bunn, S. Fetter, J. P. Holdren, and B. van der Zwaan, "The Economics of Reprocessing versus Direct Disposal of Spent Nuclear Fuel," Harvard Kennedy School. Project on Managing the Atom.

[9] *The Future of Nuclear Power, An Interdisciplinary MIT study*, Massachusetts Institute of Technology, 2003.

[10] T. P. Lagus, "Reprocessing of spent nuclear fuel: a policy analysis," *Journal of Engineering and Public Policy*, vol. 9, pp. 1–27, 2005.

[11] BCG, Economic Assessment of Used Nuclear Fuel Management in the United States, 2006.

[12] EPRI, "An Economic Analysis of Select Fuel Cycles Using the Steady-State Analysis Model for Advanced Fuel Cycles Schemes (SMAFS)," 1015387, Technical Update, EPRI Project Manager J. Hamel, 2007.

[13] Y. Du and J. E. Parsons, "Update on the Cost of Nuclear Power," Working Paper 09-004, Center for Energy and Environmental Policy Research, 2009.

[14] *The Future of Nuclear Power, An Interdisciplinary MIT study*, Massachusetts Institute of Technology, 2011.

[15] W. Ko and F. Gao, "Economic analysis of different nuclear fuel cycle options," *Science and Technology of Nuclear Installations*, vol. 2012, Article ID 293467, 10 pages, 2012.

[16] G. De Roo and J. E. Parsons, "A methodology for calculating the levelized cost of electricity in nuclear power systems with fuel recycling," *Energy Economics*, vol. 33, no. 5, pp. 826–839, 2011.

[17] P. Högselius, "Spent nuclear fuel policies in historical perspective: an international comparison," *Energy Policy*, vol. 37, no. 1, pp. 254–263, 2009.

[18] S. Widder, "Benefits and concerns of a closed nuclear fuel cycle," *Journal of Renewable and Sustainable Energy*, vol. 2, no. 6, Article ID 062801, 2010.

[19] "A low carbon nuclear future: economic assessment of nuclear materials and spent nuclear fuel management in the UK," Smith School of Enterprise and the Environment University of Oxford, 2011.

[20] W. M. Nutt, Z. Duncan, and T. Cotton, "Prioritization criteria for the selection of used nuclear fuel for recycling," in *Proceedings of the WM Conference*, Phoenix, Ariz, USA, 2011.

[21] E. A. Schneider, M. R. Deinert, and K. B. Cady, "Cost analysis of the US spent nuclear fuel reprocessing facility," *Energy Economics*, vol. 31, no. 5, pp. 627–634, 2009.

[22] G. D. Recktenwald and M. R. Deinert, "Cost probability analysis of reprocessing spent nuclear fuel in the US," *Energy Economics*, vol. 34, pp. 1873–1881, 2012.

[23] Y. Zhou, "Why is China going nuclear?" *Energy Policy*, vol. 38, no. 7, pp. 3755–3762, 2010.

[24] Y. Zhou, "China's spent nuclear fuel management: current practices and future strategies," *Energy Policy*, vol. 39, no. 7, pp. 4360–4369, 2011.

[25] M. V. Ramana and J. Y. Suchitra, "Costing plutonium: economics of reprocessing in India," *International Journal of Global Energy Issues*, vol. 27, no. 4, pp. 454–471, 2007.

[26] M. Chiguer, J.-L. Casabianca, and J.-P. Gros, "Recycling as an option of Used Nuclear Fuel Management Strategy for Europe".

[27] World nuclear Info, http://www.world-nuclear.org/info/inf69.html#R5.

[28] M. Chiguer, J.-L. Casabianca, and J.-P. Gros, "Recycling as an option of Used Nuclear Fuel Management Strategy for Europe".

[29] International Atomic Energy Agency, Country nuclear fuel profiles 2005.

[30] 6th GRWP;C.II.1.3 Strategic action lines.

[31] The Cost of High-Level Waste Disposal in Geological Repositories. An Analysis of Factors Affecting Cost Estimates. Nuclear Energy Agency. Organization for economic Co-Operation and Development, 1993.

[32] M. Bunn, J. P. Holdren, S. Fetter, and B. Van der Zwaan, "The economics of reprocessing versus direct disposal of spent nuclear fuel," Supported by the U.S. Department of Energy (DOE).

[33] http://www.tns-sofres.com/_assets/files/2010.02.22-areva.pdf.

[34] Monographies DEN: une monographie de la Direction de l'énergie nucléaire Commissariat à l'énergie atomique, L'énergie nucléaire du futur: quelles recherches pour quels objectifs? (2005).

Hindawi Publishing Corporation
Science and Technology of Nuclear Installations
Volume 2013, Article ID 705878, 18 pages
http://dx.doi.org/10.1155/2013/705878

Research Article

Estimating Alarm Thresholds for Process Monitoring Data under Different Assumptions about the Data Generating Mechanism

Tom Burr,[1] Michael S. Hamada,[1] John Howell,[2] Misha Skurikhin,[1] Larry Ticknor,[1] and Brian Weaver[1]

[1] *Statistical Sciences, Los Alamos National Laboratory, Los Alamos, NM 87545, USA*
[2] *Mechanical Engineering Department, University of Glasgow, Glasgow G12 8QQ, UK*

Correspondence should be addressed to Tom Burr; tburr@lanl.gov

Received 7 December 2012; Revised 10 May 2013; Accepted 15 May 2013

Academic Editor: Michael F. Simpson

Process monitoring (PM) for nuclear safeguards sometimes requires estimation of thresholds corresponding to small false alarm rates. Threshold estimation dates to the 1920s with the Shewhart control chart; however, because possible new roles for PM are being evaluated in nuclear safeguards, it is timely to consider modern model selection options in the context of threshold estimation. One of the possible new PM roles involves PM residuals, where a residual is defined as residual = data − prediction. This paper reviews alarm threshold estimation, introduces model selection options, and considers a range of assumptions regarding the data-generating mechanism for PM residuals. Two PM examples from nuclear safeguards are included to motivate the need for alarm threshold estimation. The first example involves mixtures of probability distributions that arise in solution monitoring, which is a common type of PM. The second example involves periodic partial cleanout of in-process inventory, leading to challenging structure in the time series of PM residuals.

1. Introduction

Nuclear material accounting (NMA) is a component of nuclear safeguards, which are designed to deter or detect diversion of special nuclear material (SNM) from the fuel cycle to a weapons program. NMA consists of periodic, low frequency, comparisons of measured SNM inputs to measured SNM outputs, with adjustments for measured changes in inventory. Specifically, the residuals in NMA are the material balances defined as $\mathrm{MB} = T_{\mathrm{in}} + I_{\mathrm{begin}} - T_{\mathrm{out}} - I_{\mathrm{end}}$, where T is a transfer and I is an inventory.

Process monitoring (PM) is a relatively recent safeguards component. Although usually collected very frequently, PM data are often only an indirect measurement of the SNM and are typically used as a qualitative measure to supplement NMA or to support indirect estimation of difficult-to-measure inventory for NMA [1–3]. However, possible new roles for PM are being evaluated in nuclear safeguards. One of the possible new PM roles involves PM residuals, where a residual is defined as residual = data − prediction. One challenge in combining NMA and PM data is that PM residuals often have a probability distribution that cannot be adequately modeled by a normal (Gaussian) distribution but instead have an unknown distribution that must be inferred from training data.

We assume throughout that typical behavior of PM residuals, as defined by the probability distribution of the PM residuals, must be estimated using training data that is assumed to be free of loss (by diversion or innocent loss). Because of this assumption, it is helpful to consider settings with many applications other than safeguards that arise in standard statistical process control. In standard statistical process control settings, a quantitative attribute such as a manufactured part's dimension is measured and monitored.

For part i, let the true part dimension be T_i and let the measured part dimension be $M_i = T_i + R_i$, where R_i is a random measurement error. Assuming the manufacturing process is "in control," Phase I of statistical process control refers to the training period on anomaly-free data that is used to characterize the distribution of M_i, which varies because both T_i and R_i vary among parts. Phase I is followed by Phase II which refers to ongoing testing or monitoring for departure from Phase I behavior that has been statistically characterized.

A common test for departure from Phase I behavior is to estimate an alarm threshold such as is done in the basic Shewhart control chart [4], where continuous data is often assumed to have approximately a normal distribution and pass-fail data is assumed to follow a homogeneous Bernoulli distribution. Although threshold estimation with the Shewhart control chart (which alarms if the maximum observed data value exceeds the alarm limit) dates back to the 1920s, it is timely to consider modern model selection options in the context of threshold estimation. This paper reviews alarm threshold estimation, introduces model selection options to support threshold estimation, and considers a range of assumptions regarding the data-generation mechanism. Two examples from nuclear safeguards are included to motivate the need for alarm threshold estimation. The first example involves mixtures of probability distributions that arise in solution monitoring, which is a common type of PM. The second example involves periodic partial cleanout of in-process inventory, leading to challenging structure in the time series of PM residuals.

The paper is organized as follows. Section 2 provides additional background and a brief literature review. Section 3 describes the specific cases considered and gives numerical examples. The cases are defined by assumptions made about the data-generating mechanism for the monitored quantities, which in our context are the PM residuals. Section 4 gives the two PM examples from safeguards. Section 5 is a summary.

2. Background and Literature Review

Phase I training as used in many quality control applications often has the luxury of very large sample size, such as 10^6 or more observations from a manufacturing step [4–9]. In the context of monitoring PM residuals, we seek to require as little Phase I training data as possible before monitoring for typical behavior begins. Therefore, the quality control literature that is most relevant for PM needs is that concerned with Phase I training data size requirements [4–27]. As one example, [7] considers the effect on estimated tail probabilities of estimation error in estimated parameters of assumed data distributions. As another example, [20] considers extreme tail probability estimation while making minimal assumptions about the distributional form of the tail behavior. References [4–27] are among relatively few quality control publications that have investigated the amount of Phase I training data required for accurate estimation of alarm limits to achieve a desired low false alarm probability α in Shewhart or other control charts. Estimation error can be expressed as error in the alarm limit or as error in the estimated false alarm probability.

Often in safeguards it is necessary to control the per-period false alarm rate. For example, if there are $n = 100$ observations per year and the application requires a false alarm probability of $\alpha = 0.01$ per year, then the Shewhart alarm rule considers the distribution of the maximum of x_1, $x_2, \ldots, x_n$. However, for simplicity here, we consider the alarm rate per data point rather than per period (see Section 3.1.3).

This paper focuses on the error in the estimated false alarm probability for several types of assumed data generating mechanisms, including single-family parametric models such as the normal and log-normal and mixtures of single-family parametric models. Specifically, we start by assuming that the individual data points $x_1, x_2, \ldots, x_n$ are independently and identically (iid) distributed as $N(\mu, \sigma^2)$, the normal distribution with mean μ and variance σ^2. Then the only inference task is to estimate μ and σ in order to estimate the alarm threshold T so that the probability of a data point being at or above T is some small false alarm probability α such as 0.01. That is, we want to estimate T so that $p = P(x_i \geq T) = \alpha$. We use the symbol α when a small probability p refers to the false alarm probability during Phase II monitoring. Alternatively, to estimate T, we might assume almost nothing about the distribution of the data points x_i and use a nonparametric alternative such as a weighted average of the sorted data values which are also known as the sample quantiles. For other assumptions about the data, the inference task will change, as we demonstrate in Section 3.

One conclusion of this paper is that a rough guide for the required training data size n for accurate quantile estimation is that $n \geq 100$. Suppose $n = 100$ and we want to estimate the 0.999 quantile, so $\alpha = 0.001$. Let $x_{(1)}, x_{(2)}, \ldots, x_{(100)}$ denote the sorted values. A reasonable estimate is some type of weighted average $a_1 x_{(99)} + a_2 x_{(100)}$ of the two largest values, where $a_1 + a_2 = 1$. There must be some type of modeling to select the weights a_1 and a_2. One type of modeling is described in paragraph three of this section, in which a parametric form $N(\mu, \sigma^2)$ for x_i is assumed. Other types of modeling are described in Section 3.

3. Cases Considered Regarding the Data-Generation Mechanism

This section examines the amount of training data required for accurate estimation of alarm limits for a range of assumptions regarding the data generation mechanism. The main question that we address is as follows: what is the behavior of the estimation error (relative and absolute) in $\hat{p}$, the estimate of the probability of a data point being above the threshold T as a function of sample size n under various assumptions about the data generation mechanism and under various estimation approaches.

For this question regarding estimation error in $\hat{p}$, we consider the following Cases (a)–(f). In each case we estimate a threshold T for a desired α. We summarize the behavior of $\hat{p}$ as an estimate of p in terms of root mean squared error

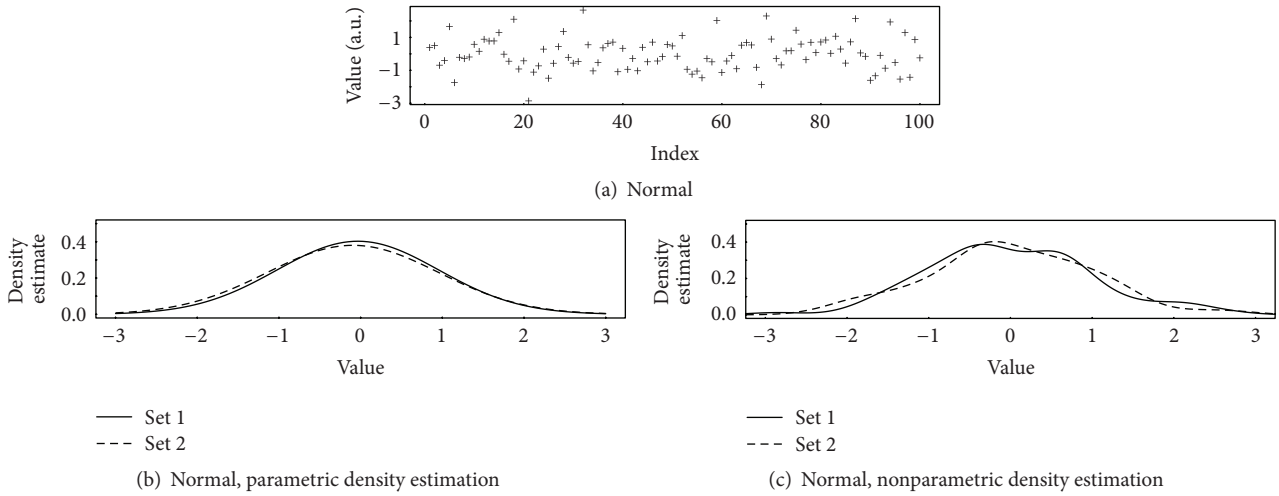

(a) Normal

(b) Normal, parametric density estimation

(c) Normal, nonparametric density estimation

FIGURE 1: (a) 100 transformed observations $y_i = (x_i - \overline{x})/\widehat{\sigma}$, in arbitrary units (au), with x_i simulated as $x_i \sim$ iid $N(\mu, \sigma^2)$; (b) the estimated probability density using parametric density estimation from two sets of 100 simulated and transformed observations as in (a); (c) same as (b) but using nonparametric density estimation.

(RMSE), with MSE = $E\{(\widehat{p} - p)^2\}$, where E denotes expected value with respect to the distribution of the x_i, and RMSE = $\sqrt{E\{(\widehat{p} - p)^2\}}$.

(a) Assume the x_i are from a single parametric model. First, the x_i are generated from a $N(\mu, \sigma^2)$ distribution, and we assume the x_i are iid $N(\mu, \sigma^2)$ and estimate μ and σ^2. Next, we generate the x_i as iid from distributions other than the normal, but we incorrectly assume normality and estimate the parameters of the assumed distribution in order to calculate T for a desired α. If instead we assume (correctly) the same distribution as that used to generate the data, then we use the correct distribution to calculate an estimate of T with estimated parameters and then estimate p.

(b) Assume the x_i are a mixture of a known number of normals and we estimate the mixture means and variances and relative frequencies as a way to estimate p.

(c) Assume the x_i are a mixture of an unknown number of normals, and as in (b) we estimate the mixture means and variances and relative frequencies as a way to estimate p.

(d) Assume the x_i are a mixture of an unknown number of unknown distributions.

(e) Assume the x_i are iid from some known distribution to be discovered using model selection.

(f) Assume nothing about the distribution of x_i. Evaluate density estimation [28] and nonparametric quantile estimation [29].

3.1. Case (a): Parametric Modeling

3.1.1. Normal Data. Figure 1(a) plots a time series of $n = 100$ transformed observations $y_i = (x_i - \overline{x})/\widehat{\sigma}$. Here, x_i is simulated as $x_i \sim$ iid $N(\mu, \sigma^2)$, $\overline{x} = \widehat{\mu}$ is the usual sample mean, and $\widehat{\sigma} = \sqrt{\sum_{i=1}^{n}((x_i - \overline{x})^2/(n-1))}$ is the usual sample standard deviation. The "~" is standard notation for "is distributed as." Figures 1(b) and 1(c) plot the estimated probability distribution for the same 100 y_i values as in Figure 1(a), and also for a second set of 100 y_i values to check for consistency between two sets of 100 simulated values. Figure 1(b) uses parametric density estimation while Figure 1(c) uses nonparametric density estimation. In Figure 1(b), $\overline{x} = \widehat{\mu}$ to estimate μ and $\widehat{\sigma}$ is used to estimate σ, so the two sets of 100 y_i values lead to quite similar density estimates based on the normal probability density $N(\widehat{\mu}_1, \widehat{\sigma}_1^2)$ in set 1 and $N(\widehat{\mu}_2, \widehat{\sigma}_2^2)$ in set 2. In Figure 1(c) we use nonparametric density estimation which is a type of smoothed histogram that does not assume we know the true probability distribution, so the two sets of estimated densities are more different than in Figure 1(b) (see Section 3.6.1).

In short, if we know the true parametric model and only need to estimate its parameters, then the RMSE will be relatively small even for small sample size n. Of course, one rarely knows the true parametric model, which is why we consider Case (b) in Section 3.2–Case (f) in Section 3.6 but include Case (a) in Section 3.1 for comparison and for comparison to other literature such as [9].

3.1.2. Example of Nonnormal Data. As an example of nonnormal data, Figure 2 is the same as Figure 1, but is for $x_i \sim$ iid gamma (shape = 1, rate = 0.1). Notice that for $n = 100$ observations, there is nonnegligible estimation error in the nonparametric estimate of the probability distribution (Figures 1(c) and 2(c)). However, as we will show, a rough rule of thumb is that $n = 100$ observations is adequate for estimation needs in PM, such as reasonably small RMSE in $\widehat{p}$ as an estimate of p. The rule of thumb is motivated by finding in our examples that either: (a) there is a very slow decrease

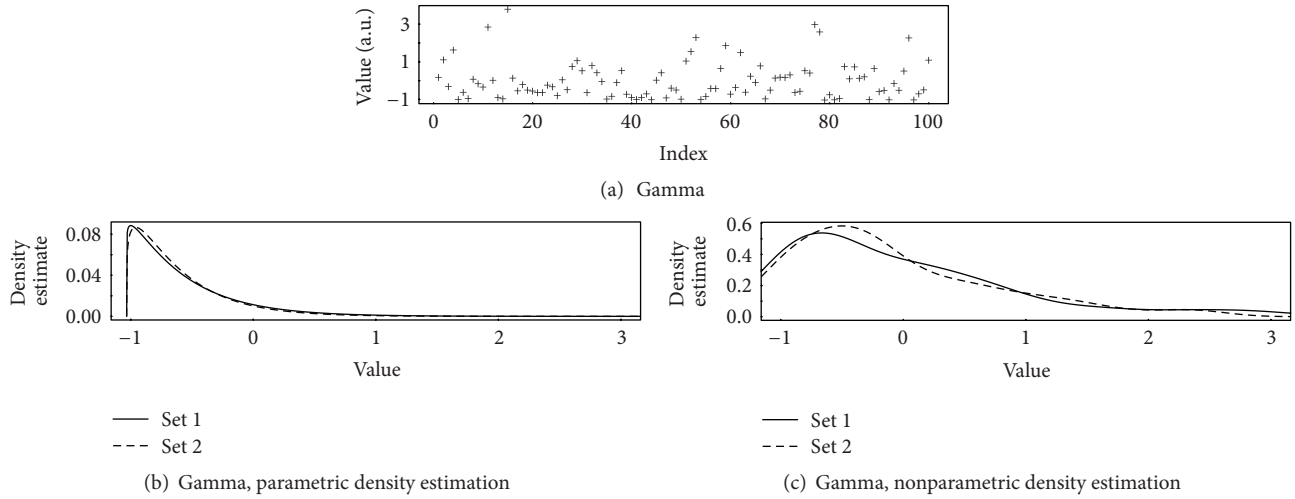

(a) Gamma

(b) Gamma, parametric density estimation

(c) Gamma, nonparametric density estimation

FIGURE 2: The same as Figure 1, but 100 transformed observations $y_i = (x_i - \overline{x})/\widehat{\sigma}$ from the gamma (shape = 1, rate = 0.1) distribution.

in the RMSE as n increases beyond 100, so increasing PM training data requirements beyond approximately $n = 100$ observations is probably not necessary, or (b) the RMSE is very small for some value of n near 100 or less.

3.1.3. The True Alarm Probability Compared to the Estimated Alarm Probability for Normal and Nonnormal Data. For normal data, Figure 3(a) plots the true alarm probability (see the next paragraph) versus the sample size using a nominal false alarm probability (FAP) of 0.001 to estimate the threshold T. We selected 0.001 as a small but reasonable FAP per PM data stream, anticipating that a per-year FAP over all NMA and PM streams should be 0.05 or less. In all our examples, we use either 0.001 or 0.025 as examples of small FAPs. As mentioned in Section 2, the desired FAP per PM stream will depend on the number of PM streams. And, the sampling frequency in a given PM stream will determine the FAP per sampling observation to maintain the desired per-year FAP. For example, if a PM stream has independent 10 samples per year, and a 0.01 FAP is allowed for that PM stream, then the per-sample FAP should be approximately 0.001.

Figure 3(a) was produced using simulation in R [30] as follows. As in Figure 1(a), generate data as $x_i \sim$ iid $N(\mu, \sigma^2)$. From these data estimate μ using $\widehat{\mu} = \overline{x}$ (the sample mean), and estimate σ^2 using $\widehat{\sigma}^2 = \sum_{i=1}^{n}((x_i - \overline{x})^2/(n-1))$ (the sample variance). Substitute $\widehat{\mu}$ for μ and $\widehat{\sigma}$ for σ in the normal probability cumulative distribution function to estimate the alarm threshold T corresponding to the 0.999 quantile. Specifically, $T_{0.001} = \mu + 3.09\sigma$ so $\widehat{T}_{0.001} = \widehat{\mu} + 3.09\widehat{\sigma}$. Notice in Figure 3(a) that the true alarm probability is considerably larger than the nominal (0.001) alarm probability marked by a horizontal line until approximately $n = 20$ or slightly larger. The "true" alarm probability was estimated with negligible estimation error by using 10^6 simulations. Throughout this paper we distinguish the true alarm probability (which is estimated with negligible estimation error by using many simulations) from the estimated alarm probability (whose estimation error is a key quantity that we study).

For nonnormal data in Figures 3(b)–3(d), x_i is generated as in Figure 3(a), but as iid from the lognormal, gamma and $t(2\text{df})$ distributions. In all four Figures 3(a)–3(d), we estimate the parameters of the normal distribution in order to estimate T for a desired α. That is, we assume (incorrectly for Figures 3(b)–3(d)) that the x_i are distributed as iid $N(\mu, \sigma^2)$ to illustrate the need for Case (b) in Section 3.2–Case (f) in Section 3.6. Therefore, we again use $\widehat{T}_{0.001} = \widehat{\mu} + 3.09\widehat{\sigma}$ in Figures 3(b)–3(d) for the lognormal generated from $\exp(x)$ with $x \sim N(\mu = 0, \sigma = 1)$ (so the mean of the lognormal is 1.65 and the variance is 4.67), the gamma (shape = 1, rate = 0.1), and the $t(2)$ distributions, respectively. Notice that for all three distributions, the true alarm rate goes below the nominal rate of 0.001 for large sample sizes. In other cases not shown (e.g., for the gamma (shape = 1, rate = 2) distribution), the true alarm rate is larger than the nominal rate for all sample sizes. If instead we correctly assume the same distribution as that used to generate the data, then we estimate parameters from the correct distribution to estimate p. For comparison, we return to this ideal situation in which we know the correct distribution in Section 3.4.

In addition to the true alarm probability, the estimation error in the alarm rate as measured, for example, by the RMSE is also of interest. The RMSE combines both bias (defined as the difference between the true alarm probability and the long-run average of the estimated probability) and variance in the well-known expression RMSE = bias^2 + variance [28].

Figure 4 plots the RMSE versus sample size for the same four distributions as in Figure 3(a), again assuming the true distribution is normal as described above, which is incorrect except for in Figure 4(a). The RMSE_{sim} was calculated across $n_{\text{sim}} = 10^4$ simulations using $\text{RMSE}_{\text{sim}} = \sqrt{\sum_{i=1}^{n_{\text{sim}}}(\widehat{p} - p)^2}$, where p is the true tail probability and $\widehat{p}$ is defined by using, for example, $\widehat{T} = \widehat{\mu} + 3.09\widehat{\sigma}$ as in Figure 3. Note that RMSE_{sim} approaches 0 as n increases (Figures 3(a) and 4(a)) as one

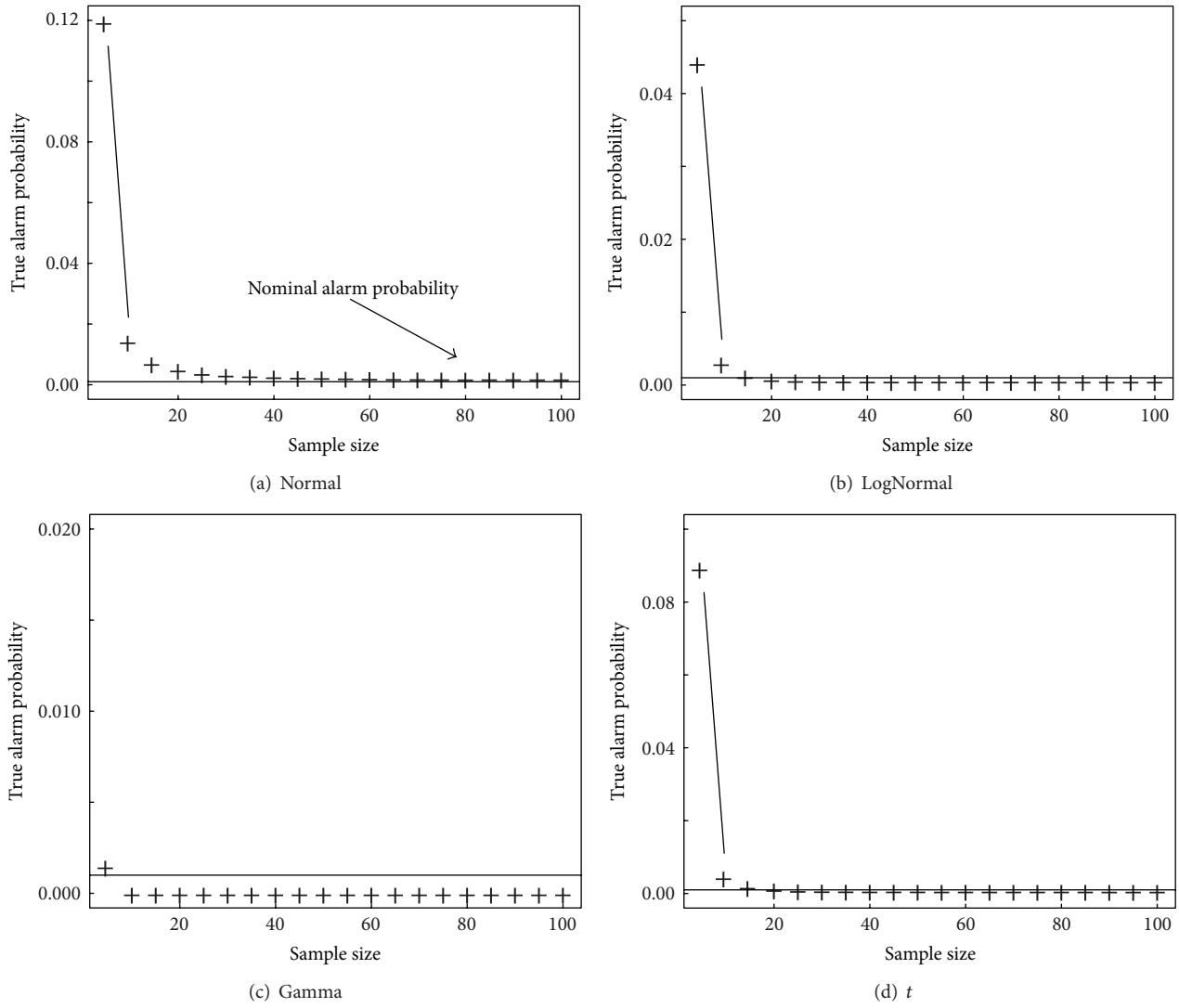

FIGURE 3: True alarm probability versus sample size (nominal alarm probability is 0.001) for (a) normal, (b) lognormal, (c) gamma (1, 0.1), and (d) $t(2)$. The true alarm probabilities were estimated by simulation of 10^4 observations in R, and results are repeatable to within ±0.0001.

would expect. Figure 4 includes a horizontal line at 10% of 0.001 (0.0001) for visual comparison.

Notice in Figure 4 that the RMSE does decrease as n increases, even when we incorrectly assume a normal distribution (Cases (b), (c), and (d)). Future work will investigate the tradeoff between estimator bias and variance in the RMSE in the context of assuming slightly wrong underlying distributions. That is, the RMSE could be acceptably low in Figures 4(b)–4(d) despite wrongly assuming that the true distribution is normal. However, the obvious bias in $\widehat{p}$ as an estimate of p does not vanish as n increases (see Figure 3), so it is unlikely to be acceptable to blindly assume PM data streams have a normal distribution. Therefore, we also consider Case (b) in Section 3.2–Case (f) in Section 3.6.

3.2. Case (b): Assume the x_i Are a Mixture of a Known Number of Normal Distributions and Estimate the Mixture Means and Variances and Relative Frequencies as a Way to Estimate p. In Case (b) we assume the x_i are a mixture of a known number of normal distributions, but we must infer which x_i belong to which mixture component. One tool to infer group membership is model based clustering as implemented in the `Mclust` function in R [30, 31]. Using `Mclust` to infer group membership, we estimated the RMSE versus sample size for a nominal alarm probability of $p = 0.001$ for the case of overlapping groups (see Figure 5(a)) and two well-separated groups (see Figure 5(b)). Figure 5 was generated by applying density estimation using the density function in R to 10^4 simulated values from the overlapping-group case and from the well-separated group case. Figure 6 shows the RMSE in the case of well-separated and overlapping groups. For comparison, notice from Figure 6 that the RMSE is smaller using `Mclust` than using a nonparametric option (based on the sample quantiles as described in Section 3.7), and that the RMSE is nearly the same whether the groups are overlapping or well separated.

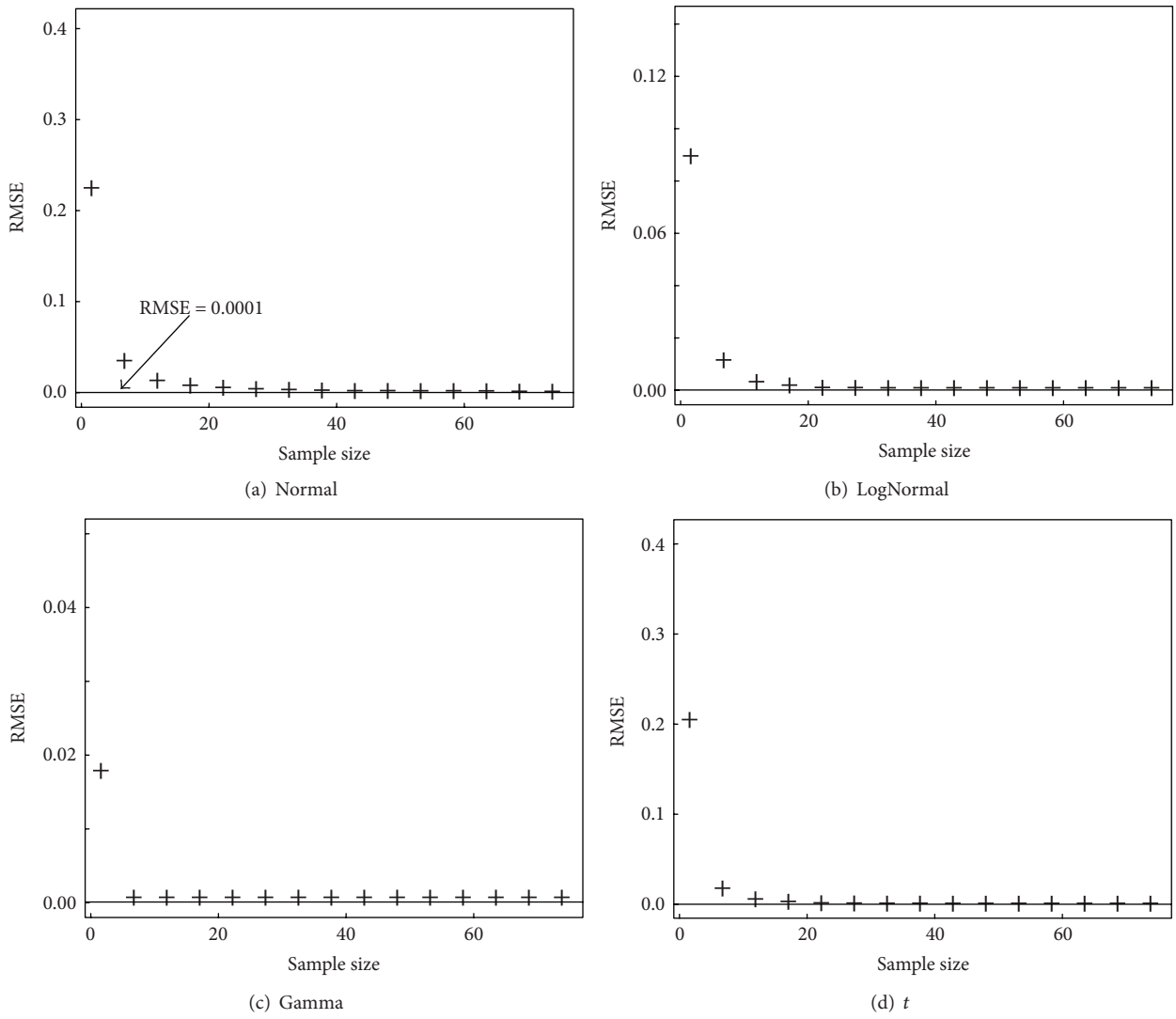

Figure 4: log (RMSE) versus sample size (nominal alarm probability is 0.001) for (a) normal, (b) lognormal, (c) gamma (1, 0.01), and (d) $t(2)$ for two estimation options labeled 1 and 2, respectively. The true RMSEs were estimated by simulation of 10^4 observations in R, and results are repeatable to within ±0.0001.

To explain our approach for estimating alarm thresholds using `Mclust`, we can simply consider the case where the means μ_i differ among components, but the standard deviations σ_i are the same in each component, denoted σ. The mean and standard deviation of the mixture are then $\mu_{\text{mix}} = \sum_{i=1}^{N_{\text{comp}}} \pi_i \mu_i$ and $\sigma^2_{\text{mix}} = \sigma^2 + \sum_{i=1}^{N_{\text{comp}}} \pi_i(\mu_i^2 - \mu^2_{\text{mix}})$, where π_i is the relative frequency of component i. Our main interest is in the probabilities of exceeding specified thresholds, such as a multiple k of the standard deviation, where k is usually in the range of approximately 2 to 4. It can be shown by straightforward calculation that when x_i are iid from a mixture of normal distributions, when testing only for large positive outliers as we do in all our examples, then $P(x - \mu_{\text{mix}} > k\sigma_{\text{mix}}) = \sum_{i=1}^{N_{\text{comp}}} \pi_{\text{i}}(1 - \varphi((\mu_{\text{mix}} - \mu_{\text{i}})/\sigma + k(\sigma_{\text{mix}}/\sigma)))$, where φ is the standard normal density. This expression for $P(x - \mu_{\text{mix}} > k\sigma_{\text{mix}})$ is used to estimate the threshold T using N_{comp} and using estimates provided by `Mclust` of the relative frequency π_i, the means μ_i, and standard deviations σ_i of each component.

For many mixtures, these tail probabilities are smaller than those of the corresponding reference distribution, which is a single-component normal having the same standard deviation as the mixture, σ_{mix}. Therefore, higher probabilities of mean-centered values exceeding $k\sigma$ are not necessarily expected. However, for other mixtures, particularly those having very unequal π_i, the tails are fatter (giving larger probabilities to extreme values) than the reference normal. For example, consider the random variable x arising from a mixture consisting of three components with $\pi_1 = 0.0833$, $\pi_2 = 0.833$, and $\pi_3 = 0.0833$; $\mu_1 = -3$, $\mu_2 = 0$, and $\mu_3 = 5$; $\sigma = 1$. For this random variable x we have $P(x - \mu_{\text{mix}} > k\sigma_{\text{mix}}) = 0.088$, 0.013, and 0.0001 for $k = 2, 3$, and 4, respectively. The corresponding probabilities for the single-component reference normal are 0.046, 0.003, and 0.00006, which are

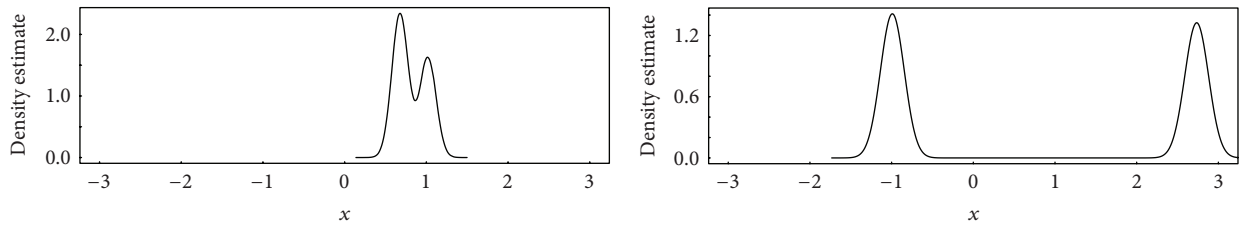

(a) Overlapping groups (b) Well-separated groups

Figure 5: Overlapping (a) and well-separated (b) groups.

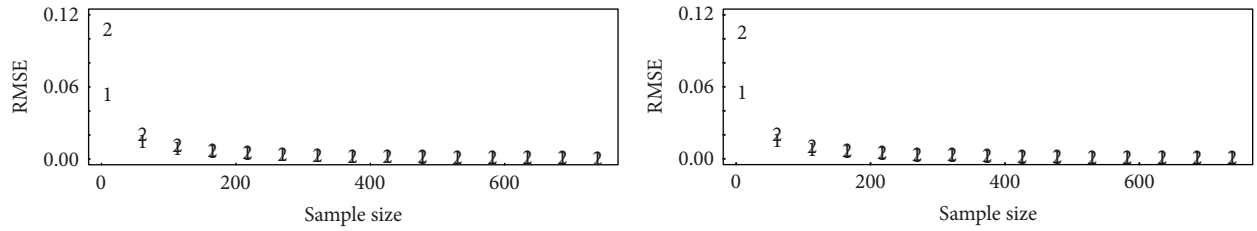

(1) Fit mixture
(2) Nonparametric

(a) Overlapping groups (b) Well-separated groups

Figure 6: The RMSE versus sample size for (a) overlapping groups and (b) well-separated groups for a known number of normals using the "fit mixture" option and using the quantile-based nonparametric option described in Section 3.7.

significantly smaller, indicating that this particular mixture has fatter-than-normal tails. On the other hand, consider the random variable X arising from a symmetric mixture consisting of three components having $\pi_1 = 0.25$, $\pi_2 = 0.5$, and $\pi_3 = 0.25$ and $\mu_1 = -3$, $\mu_2 = 0$, and $\mu_3 = 3$ with $\sigma = 1$. Then $P(x - \mu_{\text{mix}} > k\sigma_{\text{mix}}) = 0.023$, 0.000014, and 4.4×10^{-11} for $k = 2, 3$, and 4, respectively, indicating that this mixture has thinner-than-normal tails.

3.3. Case (c): Assume the x_i Are a Mixture of an Unknown Number of Normal Distributions, and as in (b), Estimate the Mixture Means and Variances and Relative Frequencies as a Way to Estimate p . In Case (c) we must estimate the number of components, unlike Case (b). We assume the x_i are a mixture of an unknown number of normal distributions, so we must infer which x_i belong to which mixture component and how many mixture components are present. As mentioned in Section 3.2, one tool to infer group membership is model-based clustering as implemented in the `Mclust` function in `R` [31]. As in Case (b), using `Mclust`, we estimated the RMSE versus sample size for a nominal alarm probability of $p = 0.001$.

As in Figures 6 and 7 plots the RMSE versus sample size for overlapping (Figure 7(a)) and well-separated (Figure 7(b)) groups. Using the Bayesian information criterion option in `Mclust` to choose the number of groups, the estimated probability of inferring the correct number of groups (2) when the candidate number of groups is any number from 1 to 10 is small to moderate (0.3 to 0.5) for overlapping groups and large (0.8 or higher) for well-separated groups. In comparing Figures 6 to 7, we note that for the examples considered, the RMSE is approximately the same whether we know there are 2 groups (Figure 6) or whether we estimate the number of groups (Figure 7).

3.4. Case (d): Assume the x_i Are iid from an Unknown Distribution (not a Mixture but a Single-Component Distribution) to Be Discovered Using Model Selection. First, assume we know the correct distribution and use the same four distributions (normal, lognormal, gamma (1,.1), $t(2)$) as in Figure 3. In this case, using `fitdistr` in `R` (which uses maximum likelihood fitting) to estimate the parameters of the known distribution, the bias $\widehat{p}$ is negligible for any of the four distributions. That is, if we are fortunate enough to correctly estimate or know the true distribution rather than blindly assume a normal, then the bias and RMSE in $\widehat{p}$ are approximately the same as shown in the "generate normal, assume normal" case shown in Figures 3(a) and 4(a).

Next, and more relevant for applications, assume the generating distribution is unknown, but one could use features of the data to select a distribution. Data features to choose a distribution could be the observed sample quantiles, or a quantitative assessment of a quantile-quantile plot that plots expected quantiles assuming a candidate data distribution versus the observed quantiles, or the raw data using model selection options such as the Bayesian information criterion (BIC). Here the BIC is defined as BIC $= 2\log(\text{ML}) - k\ln(n)$, [28, 31] where ML is the maximum value of the likelihood, k is the number of model parameters, and n is the sample size. Models having large BIC values are preferred. We note that

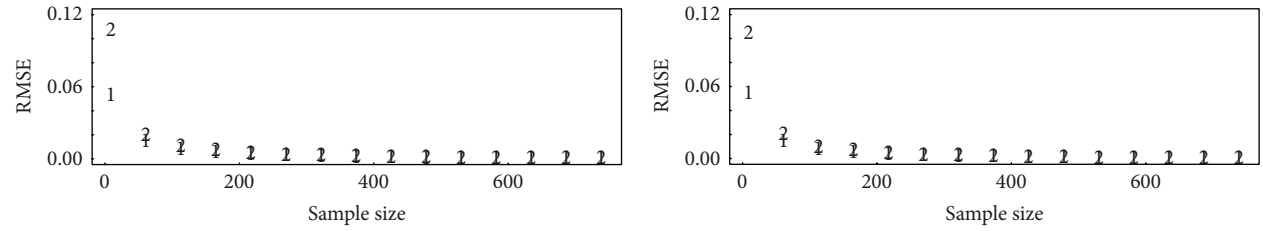

(1) Fit mixture
(2) Nonparametric

(a) Overlapping groups

(b) Well-separated groups

Figure 7: The RMSE versus sample size for (a) well-separated and (b) overlapping groups for a mixture of an unknown number of normals (same case as Figure 6, except the number of groups is unknown so it must be estimated).

the BIC is sometimes defined as −1 times the BIC definition we use, in which case models having small BIC values are preferred. We used the BIC as provided by `Mclust` in Case (c), and we use the BIC in the next example and in other examples to follow.

Figure 8 plots the RMSE versus sample size for the following experiment. For each of 1000 simulations, let the true likelihood be randomly selected with equal probability to be normal, t, lognormal, or gamma. Use the BIC to infer the likelihood and use estimated parameters of the chosen (inferred) likelihood to estimate, for example, the 0.0975 quantile, corresponding to a $p = 0.025$ tail area probability. Figure 8 shows that in this small experiment, large sample sizes are required in order for BIC-based model selection to outperform option 2, which blindly assumes the normal likelihood, or option 3 which blindly assumes a t distribution.

A second set of 1000 simulations shows that these RMSE results are repeatable to within 10% relative. In addition, it is of interest to assess how often the BIC approach leads to correct model selection in 1000 simulations, which is illustrated in Table 1. The three entries in each cell are the estimated probabilities of inferring the indicated distribution in the column when the true distribution is given in the row. The three cell entries correspond to sample sizes of $n = 25, 50$, and 1000, respectively. For example, when the true likelihood is the normal distribution, there is high probability, 0.86, 0.90, and 0.99, of correctly inferring the normal distribution for $n = 25$, 50, and 1000, respectively.

The RMSE results in Figure 8 are for the specific small experiment described. If a different collection of candidate likelihoods are used, we suggest using simulation to assess whether the BIC-based approach to choose a distribution is likely to lead to smaller RMSE than blindly assuming a particular likelihood such as the normal or t.

3.5. Case (e): Assume the x_i Are a Mixture of an Unknown Number of Unknown Distributions. In case (e) we assume the x_i are a mixture of an unknown number of unknown distributions, so we must infer which x_i belong to which mixture component and how many mixture components are present. One tool to infer group membership is model based clustering as implemented in the `mixtools` package in R [32].

Using `npEM` (nonparametric estimation maximization) in `mixtools`, we estimated the number of components in three cases (each case has 100 observations): a single-component normal, a mixture of two overlapping and equal proportion component (50 observations in each component) normal distributions as in Figure 6(b), and a mixture of two well-separated normal distributions (50 observations in each components) as in Figure 6(a). Figure 9 compares the BIC values from `npEM` (which does not assume a distributional form for the component) to the BIC values from `Mclust` (which assumes that each component has a normal distribution) for the three cases. Because the components are normal distributions in all three cases, we expect `Mclust` results to be better than `npEM` results. However, we also expected `npEM` results to do reasonably well even when the underlying distributions are all normal. Notice however in Figure 9(d) (for the case of two overlapping normal distributions) that `npEM` predicts 9 or 10 components rather than 2 components.

In repeated experiments such as this, `npEM` performs very erratically in the case of overlapping components. Apparently, using density estimation (see Section 3.6) in the manner that `npEM` does is not effective for the case of overlapping normal distributions. Of course `Mclust` is tuned to work best when the component distributions are normal, so we repeated the above experiment in which the true number of components is 1, 2 overlapping, and 2 well separated, but each component was lognormal. The estimated number of components was 2, 2, and 4, respectively for `npEM` and was 2, 3, and 9, respectively for Mclust, so neither `Mclust` nor `npEM` performed well, but `Mclust` did worse than `npEM`. The poor performance of `Mclust` is not surprising because of the lognormal distribution for each component, but `npEM` does not assume any particular distribution so its poor performance is disappointing. These experiments indicate that mixture fitting is difficult [33], and that `npEM` performs erratically for all sample sizes unless the groups are distinct and well separated.

Using either `npEM` or `Mclust` to infer the number of groups, we have a choice regarding how to estimate quantiles using the inferred groupings. For example, we could fit a distribution to each inferred component and follow options

Table 1: The estimated probability rounded to the nearest 0.01 of inferring the likelihood model using BIC. The inferred likelihood is in columns and the true likelihood is in rows, for sample sizes n = 25, 50, and 1000. The true likelihood is either normal, $t(2)$, lognormal, or gamma(1, 0.1) in the experiment.

True	Inferred			
	Normal	$t(2)$	Lognormal	Gamma(1, 0.1)
Normal	0.86, 0.90, 0.99	0.02, 0.07, 0	0, 0, 0	0.11, 0.03, 0
$t(2)$	0.81, 0.83, 0.98	0.06, 0.10, 0.02	0, 0, 0	0.13, 0.07, 0
Lognormal	0, 0, 0	0, 0, 0	0.64, 0.83, 1.0	0.36, 0.17, 0
Gamma(1, 0.1)	0, 0, 0	0, 0, 0	0.37, 0.24, 0.01	0.63, 0.76, 0.99

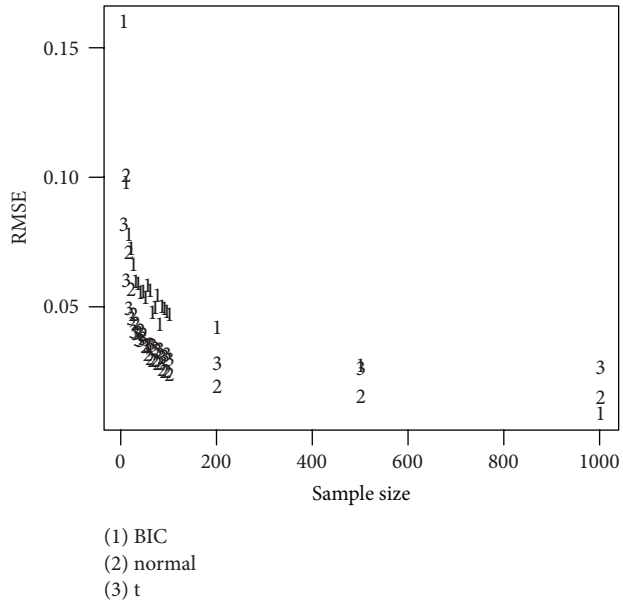

Figure 8: The RMSE versus sample size using the BIC to select the model, or blindly assuming the normal or t distribution.

described in Section 3.1.3 to estimate the tail behavior within each component. Because of the extremely slow run time and erratic performance of `npEM`, we do not experiment further with this option in this paper.

3.6. Case (f): Assume Almost Nothing about the Distribution of x_i Except That It Has Finite Moments of All Orders. In Case (f) we assume almost nothing about the distribution of x_i except that it has finite moments of all orders and consider a nonparametric ("distribution free") approach to quantile estimation. We note that the term "nonparametric," although well established in statistical literature, is somewhat misleading. The term "nonparametric" refers in this paper to the fact that the approach works for any distribution that has finite moments of all orders. All such distributions have parameters such as the mean and variance, but we follow convention and use the term "nonparametric."

Accurate nonparametric estimation of quantiles, particularly extreme quantiles, requires large n. Therefore, it is reasonable to consider whether there other options besides brute force nonparametric (sample quantiles) to estimate T. This subsection describes an option based on nonparametric density estimation and on empirical likelihood. A tail-behavior modeling option such as that in [20] will also be investigated in future work.

3.6.1. Density Estimation. The function `density` in `R` uses a kernel density estimation approach [28]. Most readers are familiar with histograms, which are crude density estimators. Improved density estimators essentially are smoothed histograms (as in Figures 1(c) and 2(c)). Typically, a density estimator at value x is given by $\widehat{f}(x) = (1/n)\sum_{i=1}^{n} K(x, x_i, h)$, where K is a symmetric "kernel" function such as the normal density function $K(x, \mu, \sigma) = (1/\sigma\sqrt{2\pi})\exp\{-(x-\mu)^2/2\sigma^2\}$ so $\widehat{f}(x) = (1/nh\sqrt{2\pi})\sum_{i=1}^{n}\exp\{-(x-x_i)^2/2h^2\}$. The estimate $\widehat{f}(x)$ can be used to estimate p for a candidate value of a quantile q simply by using $\widehat{p} = \int_{-\infty}^{q}\widehat{f}(x)dx$. The main technical challenge with kernel density estimation is choosing an effective bandwidth h [28] and cross validation as used in the function `density` in `R` is reasonably effective for bandwidth selection.

3.6.2. Empirical Likelihood. Empirical likelihood methods use likelihood methods but do not require a parametric family for the data. In the context of quantile estimation, smoothed versions of the empirical cumulative distribution function (which puts probability $1/n$ on each of n observations) are used with or without the sorted data $x_{(1)}, x_{(2)}, \ldots, x_{(n)}$. The versions that use the sorted data are extensions of the options available in the `quantile` function in `R`. We found that all 9 options in the `quantile` function give very similar RMSE results, and that all 9 options use weighted averages of the sample quantiles as described briefly in Section 2 and also in Section 3.7.

Motivated by empirical likelihood, we added a 10th option for nonparametric quantile estimate that uses a weighted average of all of $x_{(1)}, x_{(2)}, \ldots, x_{(n)}$ rather than a weighted average of the two sorted values $x_{(i)}, x_{(i+1)}$ that bracket the desired pth quantile such that $x_{(i)}/n \le p \le (x_{(i+1)}/n)x_{(i)}$. All 10 options give very similar results; however, if there is interest in providing a confidence interval for $\widehat{p}$, then [29] claims good accuracy (the nominal confidence interval behavior is close to the actual confidence interval behavior) with empirical likelihood [29].

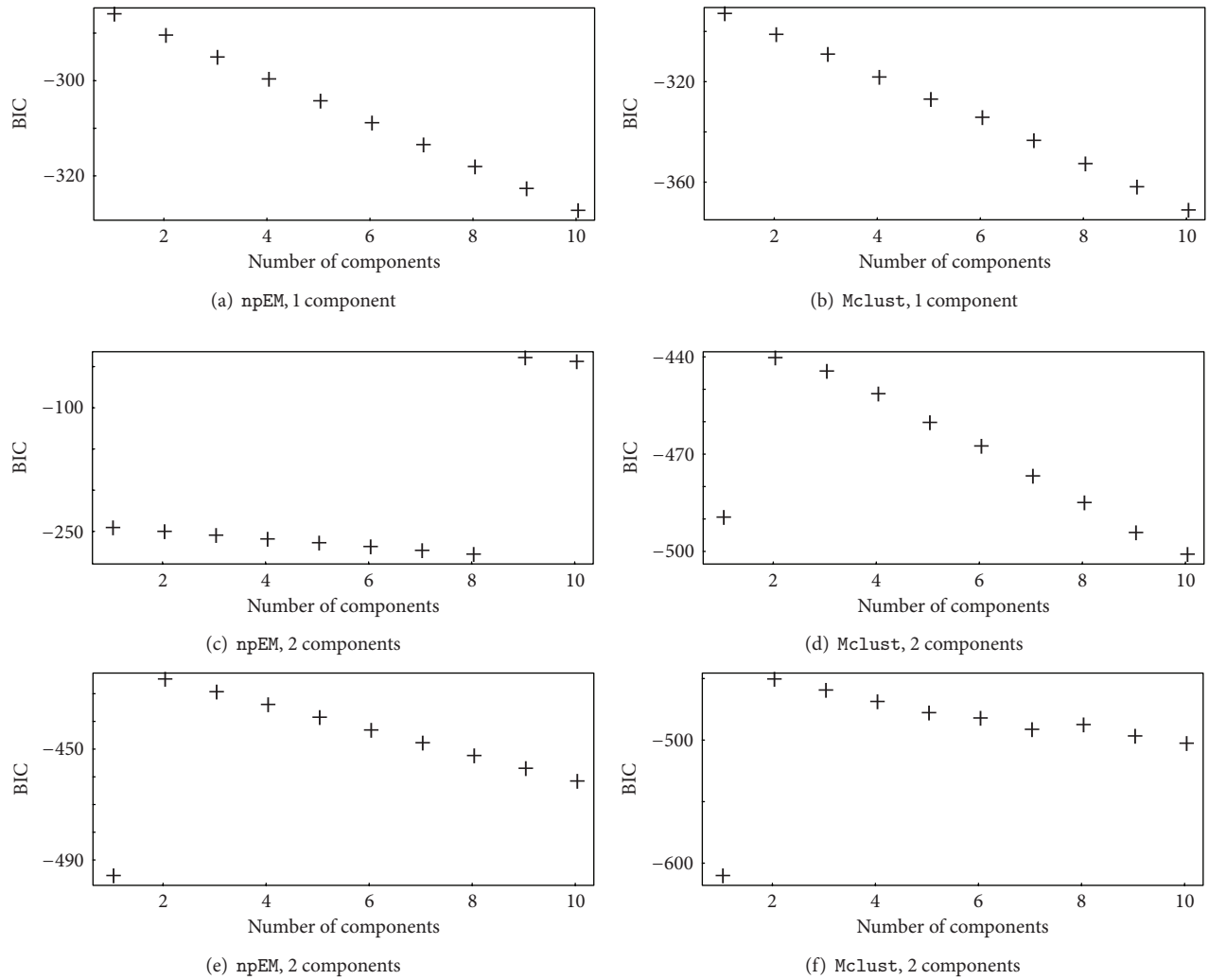

Figure 9: Comparison of `npEM` to `Mclust` for fitting: (a) single-component normal; (b) mixture of two overlapping normals as in Figure 6(b); (c) mixture of two well-separated normals as in Figure 6(a). In the application of both `npEM` and `Mclust`, the BIC is used to select the number of components, with the maximum BIC value corresponding to the chosen number of components.

3.7. Comparing Three Quantile Estimation Options for the 0.95, 0.99, 0.995, and 0.999 Quantiles. In this section we compare three of the presented quantile estimation options for four small false alarm probabilities (0.05, 0.01, 0.005, and 0.001). The three options are as follows: (1) assume a single-component normal (Section 3.1), (2) use a weighted average of the sample quantiles (Section 3.7.1 below), and (3) use density estimation (Section 3.6.1). For the sake of brevity here, we omit other options such as mixture fitting.

3.7.1. Using the Sample Quantiles. Section 2 described a nonparametric approach that uses the sample quantiles, which is robust to distributional assumptions but less efficient than option 1 if the true distribution is normal. To estimate the RMSE of $\widehat{p}$ for option 2 we used the `quantile` function to estimate the 0.999 quantile of the original simulated data. To estimate the true p corresponding to $\widehat{T}$, which is how often a data value would be above the estimated 0.999 quantile, we simulated 10^6 observations and tallied the number of times the simulated data exceeded the estimated quantile. Alternatively, to estimate p we could use the known true distribution in cases such as the $N(\mu, \sigma^2)$ for which integration is simple. The RMSE was then estimated as before, using 10^4 simulations for each evaluated sample size. There are many ways to estimate the 0.999 quantile and the `quantile` function in `R` implements the nine options described in [21] to estimate quantiles from data without explicitly assuming a parametric distribution. We experimented with all nine options available in the `quantile` function. In addition [29] considers weighted averages of the sample quantiles (see Section 3.6.2).

For option 2, we found almost no difference in average RMSE values among the nine `quantile` function options we tried (such as ordinary sample quantiles or linearly interpolating between sample quantiles) and report results here for option 4 in `quantile`, which linearly interpolates between sample quantiles.

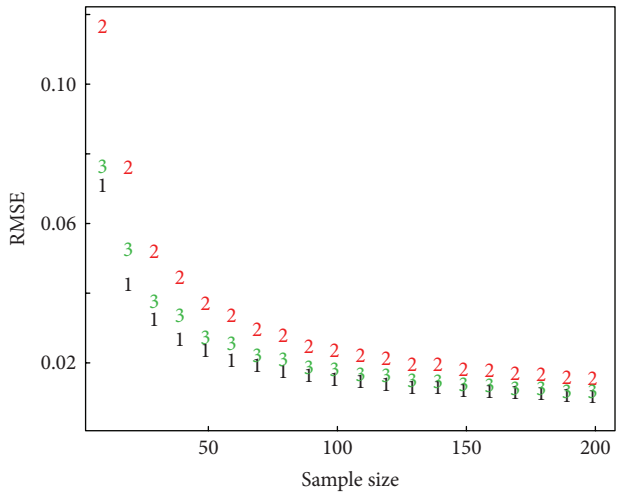

(1) Assume normal
(2) Quantile function
(3) Density estimation

(a) Estimate the 0.95 quantile

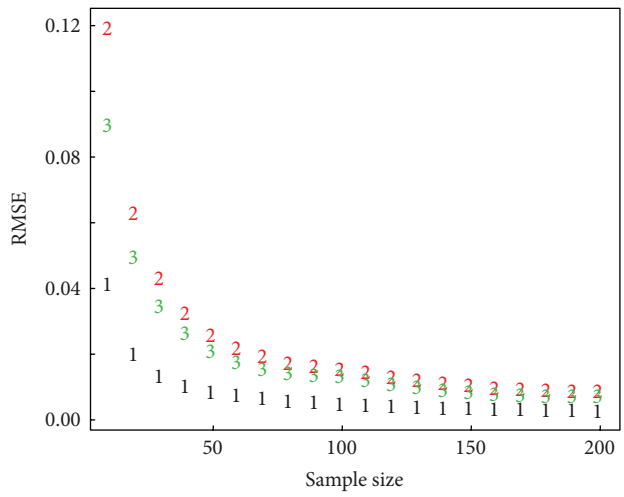

(1) Assume normal
(2) Quantile function
(3) Density estimation

(b) Estimate the 0.99 quantile

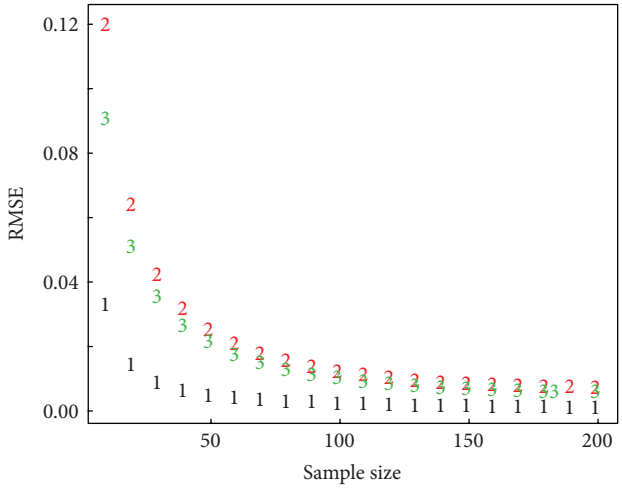

(1) Assume normal
(2) Quantile function
(3) Density estimation

(c) Estimate the 0.995 quantile

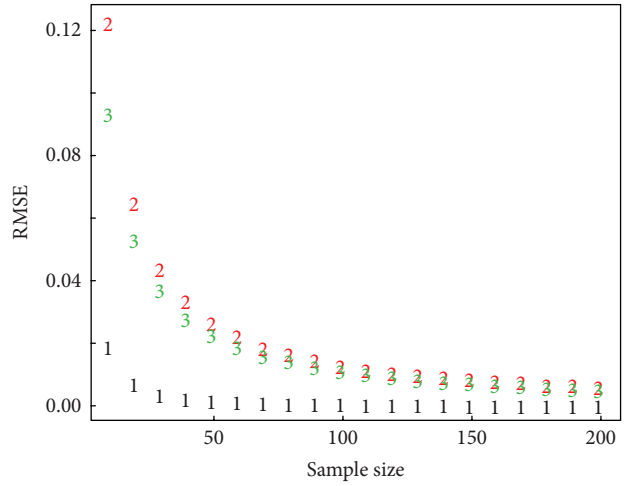

(1) Assume normal
(2) Quantile function
(3) Density estimation

(d) Estimate the 0.999 quantile

FIGURE 10: RMSE versus sample size assuming a normal distribution for three estimation options labeled 1–3. The true RMSEs were estimated by simulation of 10^4 observations in R, and results are repeatable to within ±0.001. Option 1 correctly assumes a normal distribution. Option 2 uses the `quantile` function in R. Option 3 is density estimation as discussed in Section 3.6.1.

3.7.2. RMSE Results for Options 1–3 in This Section. Figure 10 plots the RMSE in 10^4 realizations for sample sizes ranging from 5 to 200 for the case in which the true distribution is a single-component normal for false alarm probabilities of (a) 0.05, (b), 0.01, (c) 0.005, and (d) 0.001. We know that the "assume a single-component normal" is the best possible method, and we know that density estimation is nonparametric and therefore performs fairly well for a wide range of underlying true distributions. Therefore, for the case in Figure 10, we expect the RMSE for most other methods to lie between the RMSE of option 1 and option 3.

Figure 11 is the same as Figure 10, except the true distribution is a $t(2)$ distribution, so option 1 would not perform well, so we assumed (correctly) that the true distribution was known to be a $t(2)$ distribution. Notice in Figure 11 that we did not attempt to use the BIC to select a distribution (but see Case (d) in Section 3.4 where it appears that selecting a single-component distribution can be reasonably effective).

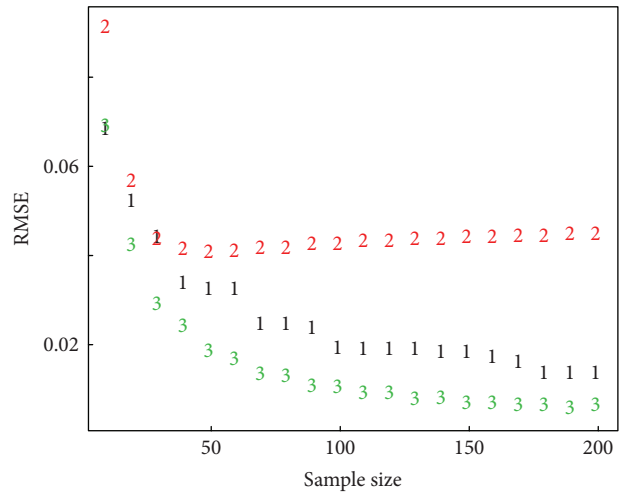

(1) Assume t
(2) Quantile function
(3) Density estimation

(a) Estimate the 0.95 quantile

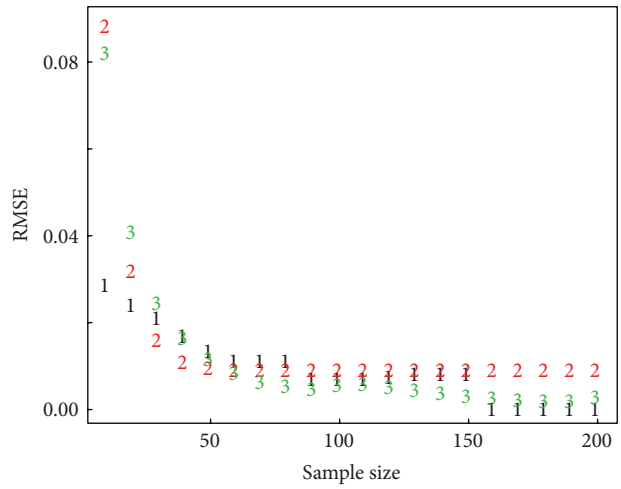

(1) Assume t
(2) Quantile function
(3) Density estimation

(b) Estimate the 0.99 quantile

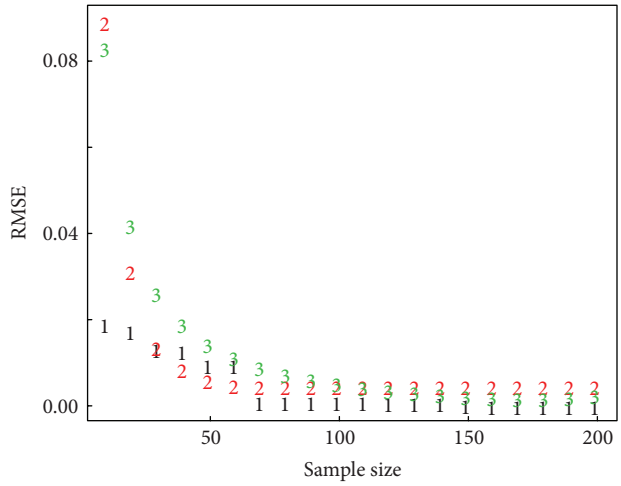

(1) Assume t
(2) Quantile function
(3) Density estimation

(c) Estimate the 0.995 quantile

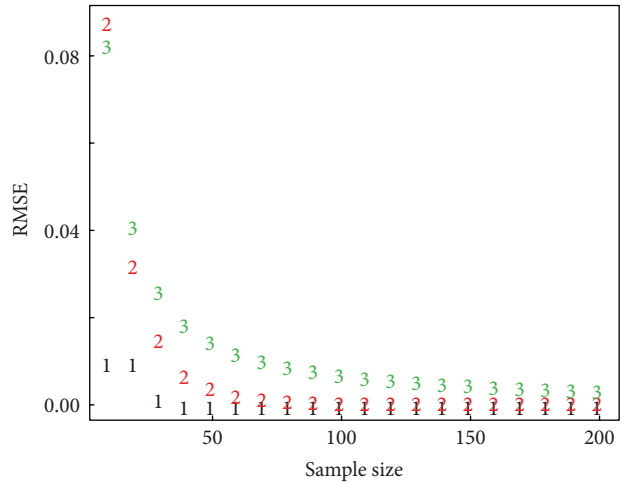

(1) Assume t
(2) Quantile function
(3) Density estimation

(d) Estimate the 0.999 quantile

FIGURE 11: RMSE versus sample size assuming a normal distribution for three estimation options labeled 1–3. The true RMSEs were estimated by simulation of 10^4 observations in R, and results are repeatable to within ±0.001. Option 1 correctly assumes a $t(2)$ distribution. Option 2 uses the `quantile` function in R. Option 3 is density estimation as discussed in Section 3.6.1. This is the same as Figure 10, but for a $t(2)$ distribution rather than a normal distribution.

3.8. Extensions. Extensions needed beyond those previously discussed include (1) evaluate our ability to estimate alarm limits for non-iid data such as Page's statistic (which could be applied to iid data, but would still not be iid due to the sequential nature of Page's statistic), (2) extend (1) to the multivariate setting, and (3) consider nonstationary data or "concept drift."

Regarding extension (1), Page's test [3, 27] is defined as $P_t = \max(0, P_{t-1}+x_t-k)$. In monitoring PM and/or NMA data streams, Page's test has been found to be simple and effective, and Page's test alarms if $P_t > h$ at any time t during the evaluation for some threshold h. Reference [34] and others in quality control outside of safeguards advocate the use of two Page's tests (one test for abrupt, one test for protracted). For good abrupt loss or diversion detection, use large k and very small h. For good protracted loss or diversion detection, use smaller k and larger h [34].

Regarding extension (2), note that we have considered only scalar data x, but multivariate versions of Page's test have been applied in safeguards [3]. Estimating multivariate

quantiles is more challenging, but we anticipate that multivariate density estimation is a feasible candidate for up to 5 or 10 dimensions.

Regarding extension (3), a real concern with some PM residual streams is that their behavior could change over time. In the sparse literature on such nonstationary behavior, "concept drift," includes the time lag from the past to the current observation and works with blocks of near-stationary residuals.

4. Case Studies from Nuclear Safeguards

In traditional safeguards, periodic nuclear materials accounting (NMA) measurements confirm the presence of special nuclear material (SNM) in accountability units to within relatively small measurement error. Process monitoring (PM) is used to confirm the absence of undeclared flows that could divert SNM for illicit use. Despite occasional attempts to quantify the diversion detection capability of PM, nearly all quantified statements regarding safeguards effectiveness involve NMA, with PM used as a added qualitative measure or to support very frequent NMA, which is called near real time accounting (NRTA).

To assess the extent to which PM can provide quantitative assessment in effectiveness evaluation is one of ten technical challenges in the anticipated increased use of PM data that were discussed during the "2011 Consultancy Meeting on Proliferation Resistance Aspects of Process Management and Process Monitoring/Operating Data" held at the International Atomic Energy Agency. This paper describes traditional roles for PM in support of NRTA and also describes possible front-line roles for PM. If PM data is to be used more quantitatively than it currently is, then historical training data is required in order to estimate PM data behavior under normal operating conditions. Normal operating conditions typically exhibit process variation, so PM data analysis can require relatively long periods of diversion-free training data.

The goal of this case study is to support the goal of using PM data in a more quantitative manner than it currently is. One obstacle to quantitative use of PM data is the need to estimate alarm limits using training data that is free from facility misuse.

In the context of nuclear safeguards, [3] describes how both traditional nuclear material accounting (NMA) data and process monitoring (PM) data analyses lead to time series of residuals that can be monitored, as in statistical process control settings. Unlike standard statistical process control, NMA and PM residuals are usually on different time scales, are serially and cross-datastream correlated, and exhibit departure from standard statistical distributions such as the normal distribution [3]. By "cross-datastream," we mean, for example, that a time series of NMA residuals could be cross correlated with a time series of PM residuals. An example is a waste stream measurement that is used as part of the material balance in NMA and is also used in PM [1–3].

In the context of quantitatively combining PM and NMA subsystems for an improved overall system, some PM data streams [1–3] and/or NMA data streams could be recorded at very high frequency, requiring a very low false alarm rate (extreme quantile) such as 0.0001. For comparison to nonparametric quantile estimation in cases having a few tens or hundreds of observations, we also consider more moderate false alarm rates such as 0.05 or 0.025.

In most applications of PM, some type of training period during which we assume there are no diversions is required in order to learn normal behavior. The goal is to assess training data needs for various PM data types. This section considers two examples. These two case studies examine the amount of training data required for accurate estimation of alarm limits for a range of assumptions regarding the data generation mechanism.

4.1. Example 1: Mixture Fitting for Solution Monitoring Data. Initial studies on solution monitoring data indicate various nonnormal behavior in residuals that arise from monitoring tanks during nontransfer ("wait") modes and also during transfer modes [33, 35, 36]. And, one study considers the impact of nonnormal behavior on loss detection probabilities [37].

Figure 12 plots the estimated probability density (a smoothed histogram) for residuals during 73 wait modes for U storage tank named B3-1 and during 74 tank wait modes for storage tank named 17-2 at Savannah River National Laboratory. The residual is the tank level at the end of the wait mode minus the tank level at the beginning of the wait mode. There is qualitative evidence for mixture behavior and Figure 13 provides quantitative assessment using the BIC as in Section 3 [34, 35, 38, 39]. The normal probability plots in Figure 12 provide additional qualitative evidence for nonnormal behavior. For most mixtures [33] found that approximately 100 training observations are required for adequate estimation of mixture components.

To illustrate the impact of modeling assumptions on estimated tail probabilities, we scale the 73 residuals from tank B3-1 by dividing by the observed standard deviation and estimate the probability the scaled residual exceeds the sample mean by 2. For a standard normal random variable, the estimate is 0.023. If we fit a mixture with 3 components as suggested by the BIC in Figure 13 (differences in BIC of 10 or more are strong evidence for favoring one model over another), the mixture-based estimate is 0.0065, which is considerably smaller than 0.023. Similarly, we scale the 74 residuals from tank 17-3 by dividing by the observed standard deviation deviation and estimate the probability the scaled residual exceeds the sample mean by 2. If we fit a mixture with 2 components (the BIC in Figure 13 suggests that 1 component is adequate so this calculation is purely for illustration), the mixture-based estimate is 0.04, which is considerably larger than 0.023.

Examples with mixtures in Section 3 and in [33] suggest that approximately 100 or more observations are required in order to have a reasonably high probability of inferring the correct number of components. In solution monitoring, each component has a physical explanation, such as a period of

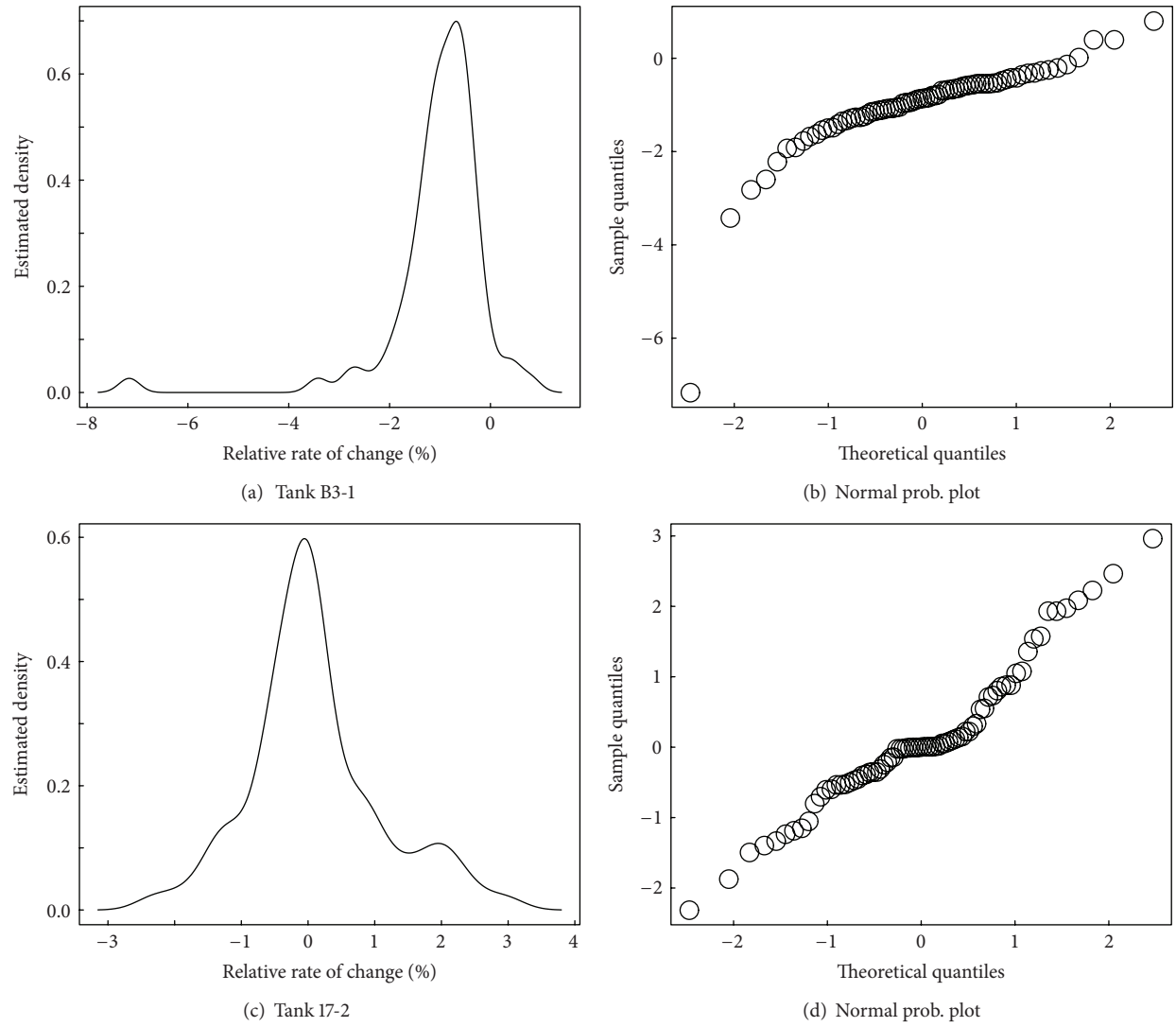

(a) Tank B3-1 (b) Normal prob. plot

(c) Tank 17-2 (d) Normal prob. plot

Figure 12: Qualitative evidence of mixtures during (a) 73 (from tank B3-1) and (c) 74 (from tank 17-2) tank wait modes.

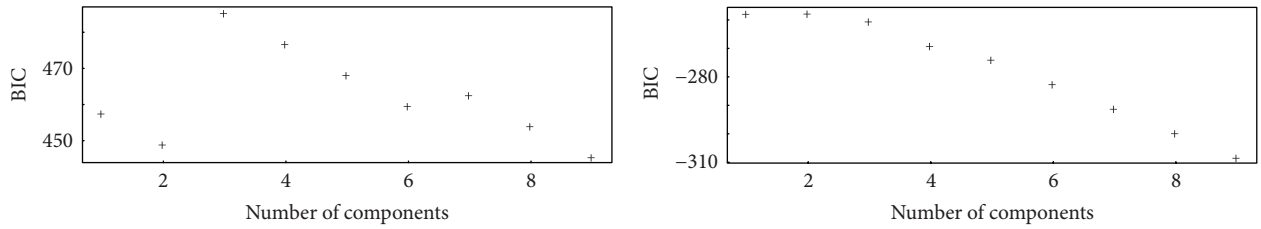

(a) Tank B3-1 (b) Tank 17-2

Figure 13: The BIC values versus candidate number of components for the 73 wait mode residuals in tank B3-1 and the 74 wait-mode residuals in tank 17-2.

evaporation leading to slight loss during the "wait" mode or condensation leading to slight gain during the "wait" mode.

4.2. Example 2. As an example of batch-to-batch cross talk, in a Pu oxide powder-handling facility, it is common to weigh each can of oxide as it enters [40] and exits a glove box operation. Waste generated during the glove box operation is periodically recovered using a partial or full cleanout [40], and the material not recovered there is distinguished as either "hidden" inventory and "holdup." Hidden inventory remains

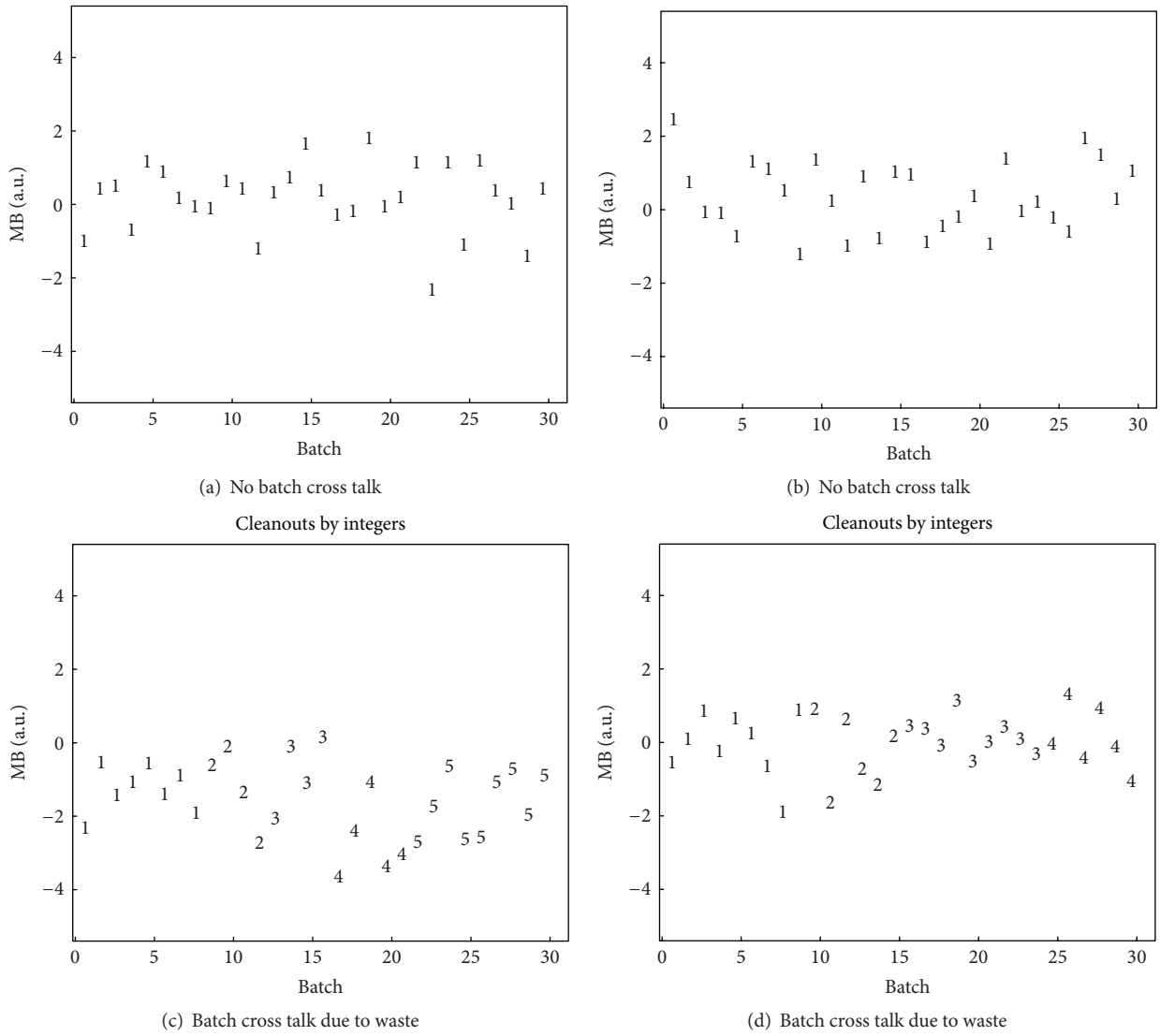

FIGURE 14: Simulated examples of MB sequences in arbitrary units (a.u.). In (a) and (b) there is no batch-to-batch cross talk and in (c) and (d) there is batch-to-batch cross talk. Plots (c) and (d) have batch-to-batch cross talk due to periodic cleanout of glove box waste.

even after thorough cleanout and is not accessible even to indirect measurement while holdup can partly remain after cleanout but is accessible to indirect measurement.

In this example, the periodically recovered Pu powder is allocated to an estimate of holdup for each batch occurring during the period between glove box cleanouts. For example, suppose 100 mg of Pu powder is recovered after 3 batches of processing Pu oxide cans in a glove box. Then 100/3 = 33.3 mg of Pu powder is reassigned to each of batch 1, batch 2, and batch 3. Figure 14 is an example, with two realizations in a situation with zero holdup, and two realizations in a situation as just described, but with some variation in how many batches of cans are processed before the glove box is cleaned out, with batch-to-batch cross talk arising from periodic cleanout of holdup.

Section 3 described quantile estimation for desired small tail probabilities for several cases, including assuming the data x is normally distributed and assuming the distribution of x is a mixture of distributions. Process variation arising from varying amounts of waste generated per batch will generally lead to batch MBs having an unknown distribution. Therefore, either mixture fitting (because mixtures of normal distributions are known to provide an effective approximation to many distributions) or BIC-based likelihood selection can be considered as a way to estimate desired quantiles.

The residuals in nuclear material accounting (NMA) are the material balances defined as $\mathrm{MB} = T_{\mathrm{in}} + I_{\mathrm{begin}} - T_{\mathrm{out}} - I_{\mathrm{end}}$, where T is a transfer and I is an inventory. In the absence of process variation such as irregular amounts of SNM deposited to holdup per period, and periodic cleanout of the holdup, then the MB will have approximately a normal distribution (because of the central limit effect that arises from combining many measurements in the MB calculation). However, facilities have sometimes observed nonnormal

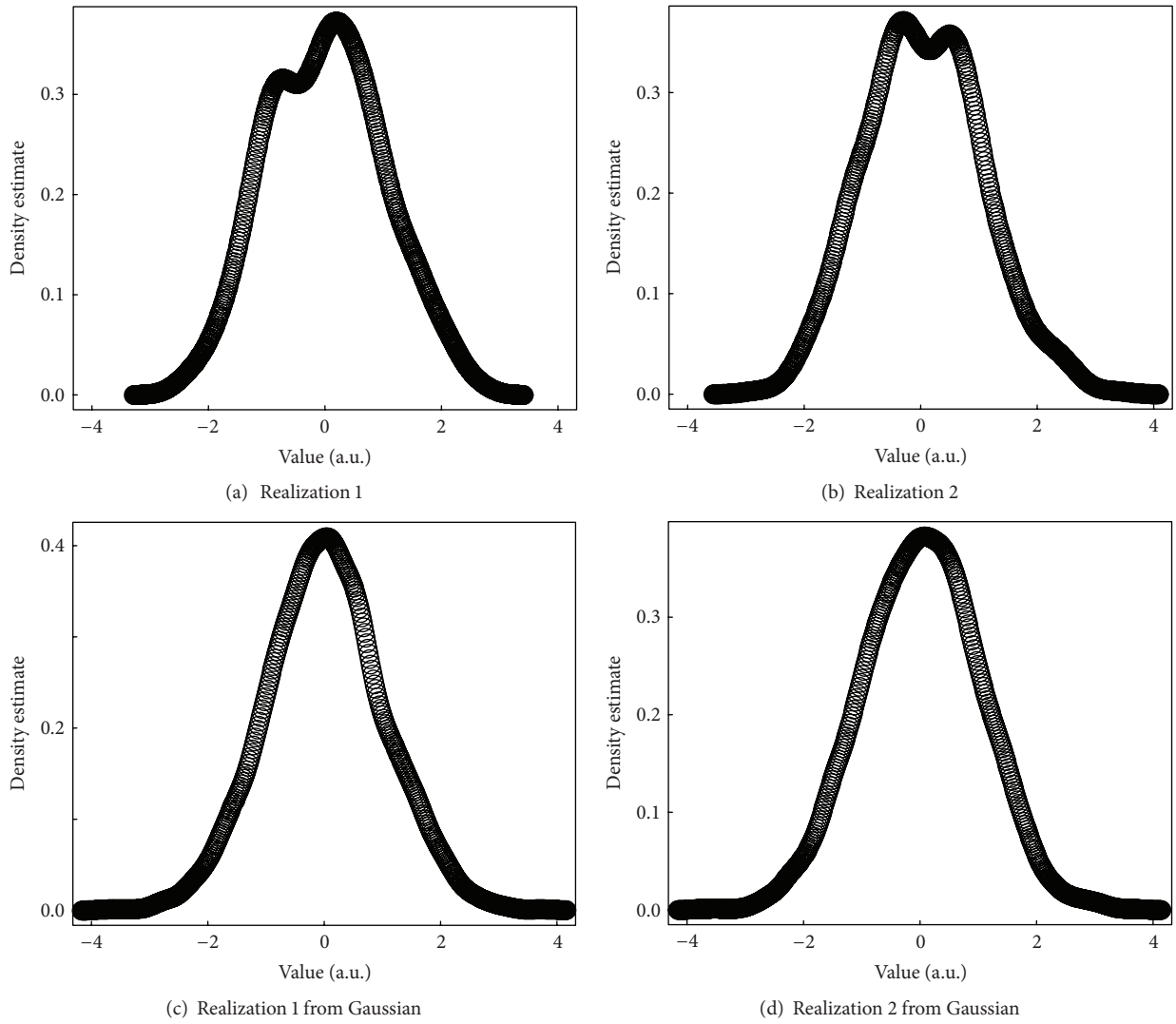

FIGURE 15: Realizations of 600 values in arbitrary units (a.u.). In (a) there are 600 MBs with cleanout between every batch of 3 MBs, with the amount to holdup each period having a normal distribution. Subplot (b) is the same as (a), but with the amount to holdup each period having a uniform distribution. Subplots (c) and (d) are for 600 realizations from a normal distribution for comparison.

MBs, particularly if holdup can fluctuate wildly, as assumed in Example 2.

Figure 15 plots nonparametric density estimates from 600 simulated batches, with cleanout between every set of 3 batches, so there are 200 cleanouts. In Figure 15, the assumed throughput is 100 units, inventory is 100 units, and amount deposited to the glove box is 5 units per batch. The assumed measurement error standard deviations are 0.5% relative random and systematic, with 10% process variation in the average amount deposited to holdup of 5 units. The recovered powder is measured with 1% relative random and systematic error standard deviation. Figure 15(a) assumes the amount deposited to holdup each batch is $H \sim N(5,.5)$. Figure 15(b) assumes the amount deposited to holdup each batch is $H \sim$ Uniform with a mean of 5 and width corresponding to a standard deviation of 0.5. For comparison, Figures 15(c) and 15(d) are each for 600 simulated normal random variables. There is evidence for mixture behavior in Figures 15(a) and 15(b) and also evidence for thinner-than-normal tails in Figures 15(a) and 15(b).

For a more quantitative assessment of whether the resulting distribution of the 600 MBs is approximately normally distributed, one can estimate the 0.025 and 0.975 quantiles for a normal distribution by using $\widehat{\mu} \pm 1.96\widehat{\sigma}$, where $\widehat{\mu}$ is the sample mean and $\widehat{\sigma}$ is the sample standard deviation. Alternatively, one can simply use the observed quantiles of the 600 observations to estimate the 0.025 and 0.975 quantiles (or use any of the options described in Section 3). For Figure 15(b), the (0.025, 0.975) quantiles are estimated as (−3.72, 6.04) using the observed quanttiles or (−3.44, 5.82) using $\widehat{\mu} \pm 1.96\widehat{\sigma}$. The differences $-3.44 - (-3.72) = 0.28$ and $(6.04 - 5.82) = 0.22$ are both much too large to occur by chance (which we confirmed by simulation in R), so there is strong evidence that it is not adequate to assume a normal

distribution. For Figure 15(b), the (0.025, 0.975) quantiles are estimated as (−2.43, 3.06) using the observed quantiles and (−2.46, 3.16) using $\widehat{\mu} \pm 1.96\widehat{\sigma}$. In this case, the differences $-2.46 - (-2.43) = -0.03$ and $3.16 - 3.06 = 0.10$ are not too large to have occurred by chance; however, the differences are in the direction of evidence for a thinner-than-normal distribution.

This batch-to-batch cross talk illustrates the possibility of nonnormal MBs when MBs are computed for each batch. Batch MBs are currently regarded as PM residuals rather than NMA residuals. In either case, sequences of batch MBs are very likely to require cautious analyses, with attention to alarm threshold estimation as in Section 3.

To end this Examples section, we mention that although pyro-reprocessing options are only in the development stages, similar batch-to-batch cross talk is expected, for example, to arise from partial cleanouts of the electrorefiner (ER) [40–47]. PM residual streams associated with the ER are therefore likely to exhibit batch-to-batch "cross-talk" that complicates safeguards, largely due to Uranium and U/TRU (transUranium) behavior in the ER and other process equipment. That is, apparent losses in one batch can appear as a gain in another batch as in our example above.

5. Summary

We presented options to estimate an alarm threshold corresponding to a small false alarm probability p for a range of assumptions regarding the data-generating mechanism. Because analytical evaluation is very difficult, depending on the case, we recommend simulation studies such as presented here to estimate the root-mean-squared estimation error in $\widehat{p}$ to estimate a false alarm probability for candidate threshold estimation options.

In some cases, parametric distributions such as the normal or lognormal or a mixture of normals can provide a reasonable approximation upon which to base alarm threshold estimation. Not surprisingly, the more one correctly assumes about the underlying data-generation mechanism, the smaller the required sample size for accurate estimate of p. As a rough rule of thumb, approximately 100 observations are required for reasonably effective estimation of p. The rule of thumb is motivated by finding in our examples that either (a) there is a very slow decrease in the RMSE as n increases beyond 100, so increasing PM training data requirements beyond approximately $n = 100$ observations is probably not necessary, or (b) the RMSE is very small for some value of n near 100 or less. Of course there are exceptions to any such rule. For example, we considered mixture distributions for which none of the components was extremely rare. If one or more mixture components is rare (such as less than 5% of the overall distribution), then larger sample sizes are needed.

Two process monitoring case studies from nuclear safeguards were presented. The case studies support a safeguards systems option that combines PM and NMA residuals on equal footing [31]. The option requires estimating quantiles in PM residuals corresponding to user-specified small tail probabilities per residual stream, such as 0.001 or 0.025, in order to maintain a small (such as 0.05) per-year system-wide false alarm probability.

Acknowledgments

The authors thank the US National Nuclear Security Administration, office NA22 and the Materials Protection, Control and Accounting (MPACT) program under Nuclear Energy programs.

References

[1] T. Burr, A. Bakel, S. Bryan et al., "Roles for process monitoring in nuclear safeguards at aqueous reprocessing plants," *Journal of Nuclear Materials Management*, vol. 40, no. 2, pp. 42–53, 2012.

[2] T. Burr, M. S. Hamada, J. Howell, M. Skurikhin, L. Ticknor, and B. Weaver, "Data requirements for learning alarm rules for process monitoring," in *Proceedings of the 9th ANS/INMM conference on facilities operation and safeguards interface*, Savannah, Ga, USA, 2012.

[3] T. Burr, M. S. Hamada, M. Skurikhin, and B. Weaver, "Pattern recognition options to combine process monitoring and material accounting data in nuclear safeguards," *Statistics Research Letters*, vol. 1, no. 1, 2012.

[4] C. Roes, *Shewhart-Type Charts in Statistical Process Control [Ph.D. thesis]*, University of Amsterdam, 1995.

[5] W. Albers and W. C. M. Kallenberg, "Self-adapting control charts," *Statistica Neerlandica*, vol. 60, no. 3, pp. 292–308, 2006.

[6] W. Albers and W. Kallenberg, "Alternative Shewhart-type charts for grouped observations," *Metron*, vol. 64, pp. 357–375, 2006.

[7] W. Albers and W. C. M. Kallenberg, "New corrections for old control charts," *Quality Engineering*, vol. 17, no. 3, pp. 467–473, 2005.

[8] W. Albers and W. Kallenberg, "Improved data driven control charts," *International Journal Pure and Applied Mathematics*, vol. 37, pp. 423–439, 2005.

[9] W. Albers, W. C. M. Kallenberg, and S. Nurdiati, "Parametric control charts," *Journal of Statistical Planning and Inference*, vol. 124, no. 1, pp. 159–184, 2004.

[10] W. Albers and W. Kallenberg, "Are estimated control charts in control?" Technical Report 1569, Faculty of Mathematical Sciences, 2001.

[11] W. Albers, W. Kallenberg, and S. Nurdiati, "Parametric control charts," Technical Report 1623, Faculty of Mathematical Sciences, University of Twente, 2002.

[12] W. Albers and W. Kallenberg, "Estimation in Shewhart control charts," Memorandum 1559, University of Twente, 2000.

[13] S. Chakraborti, "Run length, average run length and false alarm rate of shewhart X-bar chart: exact derivations by conditioning," *Communications Statistics in Simulation and Computation*, vol. 29, no. 1, pp. 61–81, 2000.

[14] L. K. Chan, K. P. Hapuarachchi, and B. D. Macpherson, "Robustness of XQ and R charts," *IEEE Transactions on Reliability*, vol. 37, no. 1, pp. 117–123, 1988.

[15] G. Chen, "The mean and standard deviation of the run length distribution of X-charts when control limits are estimated," *Statistica Sinica*, vol. 7, no. 3, pp. 789–798, 1997.

[16] B. Colosimo and E. Castillo, *Bayesian Process Monitoring, Control, and Optimization*, Chapman and Hall, Boca Raton, Florida, USA, 2007.

[17] L. de Haan and A. K. Sinha, "Estimating the probability of a rare event," *Annals of Statistics*, vol. 27, no. 2, pp. 732–759, 1999.

[18] A. Dekkers and L. de Haan, "On the estimation of the extreme-value index and large quantile estimation," *Annals of Statistics*, vol. 17, pp. 1795–1832, 1989.

[19] B. Ghosh, M. Reynolds Jr., and Y. Hui, "Shewhart XQ-charts with estimated process variance," *Communications in Statistics*, vol. 10, pp. 1797–1822, 1981.

[20] P. Hall and I. Weissman, "On the estimation of extreme tail probabilities," *Annals of Statistics*, vol. 25, no. 3, pp. 1311–1326, 1997.

[21] R. J. Hyndman and Y. Fan, "Sample quantiles in statistical packages," *The American Statistician*, vol. 50, no. 4, pp. 361–365, 1996.

[22] W. A. Jensen, J. B. Birch, and W. H. Woodall, "High breakdown estimation methods for phase I multivariate control charts," *Quality and Reliability Engineering International*, vol. 23, no. 5, pp. 615–629, 2007.

[23] G. R. Mercado, M. D. Conerly, and M. B. Perry, "Phase I control chart based on a kernel estimator of the quantile function," *Quality and Reliability Engineering International*, vol. 27, no. 8, pp. 1131–1144, 2011.

[24] G. Nedumaran and J. J. Pignatiello Jr., "On estimating Xčontrol chart limits," *Journal of Quality Technology*, vol. 33, no. 2, pp. 206–212, 2001.

[25] E. A. Pappanastos and B. M. Adams, "Alternative designs of the Hodges-Lehmann control chart," *Journal of Quality Technology*, vol. 28, no. 2, pp. 213–223, 1996.

[26] C. Quesenberry, "The effect of sample size on estimated limits for XQ and X control charts," *Journal of Quality Technology*, vol. 25, pp. 237–247, 1993.

[27] W. H. Woodall and D. C. Montgomery, "Research issues and ideas in statistical process control," *Journal of Quality Technology*, vol. 31, no. 4, pp. 376–386, 1999.

[28] T. Hastie, R. Tibshirini, and J. Friedman, *The Elements of Statistical Learning*, Springer, New York, NY, USA, 2001.

[29] W. Zhou and B.-Y. Jing, "Adjusted empirical likelihood method for quantiles," *Annals of the Institute of Statistical Mathematics*, vol. 55, no. 4, pp. 689–703, 2003.

[30] R Development Core Team. R: a Language and Environment for Statistical Computing. R Foundation for Statistical Computing, 2004, http://www.r-project.org/ .

[31] C. Fraley and A. E. Raftery, "Model-based clustering, discriminant analysis, and density estimation," *Journal of the American Statistical Association*, vol. 97, no. 458, pp. 611–631, 2002.

[32] T. Benaglia, D. Chauveau, D. R. Hunter, and D. S. Young, "Mixtools: an R package for analyzing finite mixture models," *Journal of Statistical Software*, vol. 32, no. 6, pp. 1–29, 2009.

[33] T. Burr and M. S. Hamada, "Estimating alarm thresholds and the number of components in mixture distributions," *Nuclear Instruments and Methods in Physics Research A*, vol. 685, pp. 55–61, 2012.

[34] B. Jones and J. Wark, "Near real time materials accountancy system for THORP, ESARDA Bulletin," 1991, http://esarda2.jrc.it/db_proceeding/mfile/P_1991_avignon_117.

[35] T. Burr, M. Suzuki, J. Howell, M. S. Hamada, and C. E. Longo, "Signal estimation and change detection in tank data for nuclear safeguards," *Nuclear Instruments and Methods in Physics Research A*, vol. 640, no. 1, pp. 200–212, 2011.

[36] M. Suzuki, M. Hori, S. Nagaoka, and T. Kimura, "Study on loss detection algorithms using tank monitoring data," *Journal of Nuclear Science and Technology*, vol. 46, no. 2, pp. 184–192, 2009.

[37] T. Burr, M. S. Hamada, J. Howell, and M. Suzuki, "Loss detection results on simulated tank data modified by realistic effects," *Journal of Nuclear Science and Technology*, vol. 49, no. 2, pp. 209–221, 2012.

[38] J. L. Wadsworth and J. A. Tawn, "Likelihood-based procedures for threshold diagnostics and uncertainty in extreme value modelling," *Journal of the Royal Statistical Society B*, vol. 74, no. 3, pp. 543–567, 2012.

[39] M. Black and R. Hickey, "Maintaining the performance of a learned classifier under concept drift," *Intelligent Data Analysis*, vol. 3, pp. 453–474, 1999.

[40] C. Xerri, J. Beckers, M. Boella et al., "Control of nuclear material holdup in MOX fuel fabrication plants in Europe," *ESARDA Bulletin*, vol. 31, pp. 69–75, 2002.

[41] R. O. Hoover, S. Phongikaroon, M. F. Simpson, S. X. Li, and T.-S. Yoo, "Development of computational models for the mark-IV electrorefiner-Effect of uranium, plutonium, and zirconium dissolution at the fuel basket-salt interface," *Nuclear Technology*, vol. 171, no. 3, pp. 276–284, 2010.

[42] M. Simpson and S. Herrmann, "Modeling the pyrochemical reduction of spent UO_2 fuel in a pilot-scale reactor," Tech. Rep. INL/CON-06-11597, 2006.

[43] M. A. Williamson and J. L. Willit, "Pyroprocessing flowsheets for recycling used nuclear fuel," *Nuclear Engineering and Technology*, vol. 43, no. 4, pp. 329–334, 2011.

[44] D. Vaden, R. Benedict, K. Goff, R. Bucher, and A. Yacout, "Material accountancy in an electrochemical fuel conditioning facilty, Argonne National Laboratory report-9606116," 1996, http://www.iaea.org/inis/collection/NCLCollectionStore/_Pub-lic/27/063/27063600.pdf .

[45] J. Zhang, "EChem modeling: a kinetic model for electrorefining based on diffusion control," Los Alamos National Laboratory Report, 2011.

[46] D. Vaden, "Fuel conditioning facility electrorefiner process model," *Separation Science and Technology*, vol. 41, no. 10, pp. 1985–2001, 2006.

[47] G. Cowell, J. Howell, and T. Burr, "Some implications of applying NRTA to a MOX facility with significant temporary stores," in *Proceedings of the 51st Annual Meeting of the Institute of Nuclear Materials Management*, 2010.

Hindawi Publishing Corporation
Science and Technology of Nuclear Installations
Volume 2013, Article ID 945858, 8 pages
http://dx.doi.org/10.1155/2013/945858

Research Article

Projected Salt Waste Production from a Commercial Pyroprocessing Facility

Michael F. Simpson

Idaho National Laboratory, P.O. Box 1625, Idaho Falls, ID 83415, USA

Correspondence should be addressed to Michael F. Simpson; michael.simpson@inl.gov

Received 20 February 2013; Accepted 24 April 2013

Academic Editor: Candido Pereira

Pyroprocessing of used nuclear fuel inevitably produces salt waste from electrorefining and/or oxide reduction unit operations. Various process design characteristics can affect the actual mass of such waste produced. This paper examines both oxide and metal fuel treatment, estimates the amount of salt waste generated, and assesses potential benefit of process options to mitigate the generation of salt waste. For reference purposes, a facility is considered in which 100 MT/year of fuel is processed. Salt waste estimates range from 8 to 20 MT/year from considering numerous scenarios. It appears that some benefit may be derived from advanced processes for separating fission products from molten salt waste, but the degree of improvement is limited. Waste form production is also considered but appears to be economically unfavorable. Direct disposal of salt into a salt basin type repository is found to be the most promising with respect to minimizing the impact of waste generation on the economic feasibility and sustainability of pyroprocessing.

1. Introduction

Pyroprocessing is currently being developed by several nations (including but not limited to the USA, Republic of Korea, Russia, and India) for potential implementation in a large-scale, commercial fuel cycle. In most cases, this is driven by the process' deemed compatibility with a fast reactor. There is also a nonproliferation element to its attractiveness. Japan is the only nuclear nonproliferation Treaty (NPT) nonnuclear weapons state that possesses full-scale nuclear fuel reprocessing facilities. They use a PUREX-based process to coextract uranium and plutonium from their spent fuel. Due to the potential to adapt this process to extract weapons-grade plutonium, Japan's use of the technology has come under widespread international criticism. In an effort to avoid such controversy, the Republic of Korea has been developing pyroprocessing since 1997 for the purpose of closing the fuel cycle and managing their used fuel stockpiles [1]. Pyroprocessing has been viewed as being significantly less versatile with respect to producing weapons-grade materials. Another attractive feature is that the process can be designed into compact facilities colocated on reactor sites to minimize the risk of transporting used nuclear fuel on public transportation routes. In the Republic of Korea (South Korea), pyroprocessing is the only used fuel management technology option currently being considered because of the diplomatic situation on the Korean peninsula.

The pyroprocessing flowsheet is conceptually simple with a limited number of unit operations. A sample flowsheet that could be used for treating either oxide or metal fuel is shown in Figure 1. Unit operations are included for selectively removing fission products from electrorefiner salt (zeolite columns), producing waste forms (ceramic waste furnace and metal waste furnace), and distilling salt from actinide products (cathode processor).

One potential application for this process would be to treat used oxide fuel from wet storage facilities at commercial light water reactor sites. Processing this fuel would be considered an alternative to continued on-site dry storage or permanent disposal in a geologic repository. As laid out in Figure 1, the process generates one product (actinide metals) and has two waste streams (high-level ceramic waste and high-level metal waste). The actinide metals could be used to fabricate fresh fuel for a fast reactor. The waste products are designated as high-level waste by the US legal definition. Until recently,

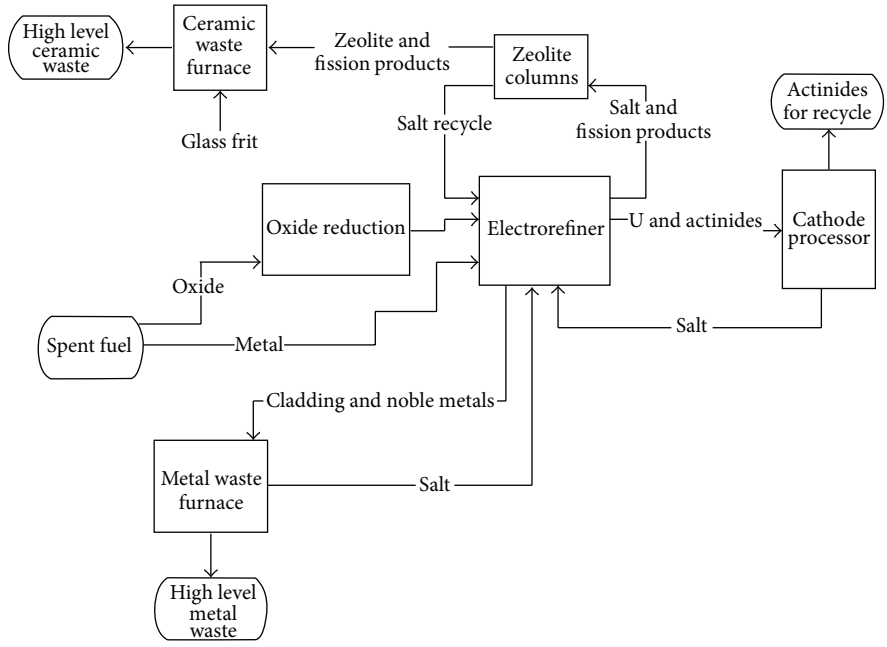

Figure 1: Sample flowsheet for pyroprocessing.

high-level radioactive waste (HLW) was intended to be disposed of in a permanent geologic repository in Yucca Mountain (Nevada). At this time, the U.S. DOE has cancelled the Yucca Mountain nuclear waste repository project, and there is currently no path for permanent disposal of used nuclear fuel or byproducts of nuclear fuel reprocessing (HLW).

The HLW ceramic from Figure 1 can for all practical purposes be referred to as the salt waste. During the development of the Integral Fast Reactor (IFR) and later the EBR-II Spent Fuel Treatment (SFT) process, it was established that the salt waste could be stabilized in zeolite followed by conversion to glass bonded sodalite [2–4]. In the IFR-based pyroprocessing flowsheet, electrorefiners use molten LiCl-KCl in a eutectic composition as their electrolyte. Uranium trichloride is another essential component in this salt. When the used fuel is immersed into the salt, UCl_3 oxidizes active metals in the fuel—including metallic sodium used to bond the fuel to the cladding, rare earth fission products, minor actinides including plutonium, and Group I/II fission products. All of these elements are converted to chloride salt and partition into the molten LiCl-KCl salt pool. When it is necessary to remove some of the salt and prepare it for waste disposal, it is first milled to a powder or fine particulate. It is then blended with dehydrated zeolite-4A at 500°C, which immobilizes the salt into the zeolite's microscopic pores. The salt-loaded zeolite is cold-blended with glass frit powder followed by thermally induced consolidation at a temperature up to 950°C [5]. The zeolite-4A converts to sodalite during the consolidation. This glass-bonded sodalite is designated as *ceramic waste*, given that the waste forms are monolithic ceramic in consistency. Ceramic waste form samples were generated during the EBR-II SFT demonstration project and shown to be more corrosion resistant than a reference glass waste form that had been developed for immobilizing reprocessing wastes at the Savannah River Site [6]. The ceramic waste form and other waste form options will be further discussed in a later section of this paper.

In addition to the electrorefiner, the oxide reduction unit operation can also be the source of salt waste in a pyroprocessing facility. If oxide fuel is being used as the process feed, it must be reduced to metallic form prior to loading into the electrorefiner. Such reduction is accomplished either via reaction of a reducing metal or via electrolytic reduction—both in a molten chloride salt pool [7, 8]. Currently, the electrolytic process is generally favored. It utilizes an LiCl-Li_2O salt operating at 650°C. Certain fission products in the used fuel (Cs, Sr, and Ba most notably) partition into the salt phase during electrolytic reduction of the used fuel [8]. When the concentration of those fission products exceeds the operating limit for the process, it is necessary to bleed out some of the used salt and replace it with clean LiCl-Li_2O, thus reducing the concentration of the fission products. This salt waste has been considered to be particularly problematic to researchers developing pyroprocessing, due to the relatively high melting point of the LiCl-based oxide reduction salt. Occlusion of this salt by the zeolite is considered to be more challenging than the LiCl-KCl-based salt used in electrorefiners because of its higher melting point (610°C versus 350°C for eutectic LiCl-KCl). Another likely problem with making ceramic waste from the oxide reduction salt is the high generation of radioactive decay heat from Cs-137 and Sr-90. Ceramic waste forms can be considered to be thermal insulators and thus can be prone to excessive heat buildup when loaded with Cs and Sr unless the waste forms are kept relatively small.

Table 1: Major contaminants of the electrorefiner and oxide reducer.

Electrorefiner	Oxide reducer [8]
Na	Cs
Rare earths (Ce, Pr, Sm, Pm, Nd, Eu, Gd)	Sr
Group I (Cs, Rb)	Ba
Group II (Sr, Ba)	Te
Group III (La, Y)	

Table 2: Nominal composition of sodium-bonded metal used fuel.

Component	Mass fraction
Pu	0.01
Na (bonding)	0.02
Active metal fission products (includes Group I/II/III and rare earths)	0.04
U	0.93

2. Analysis of Salt Waste Production

In this section, the primary objective is to provide estimates under a variety of scenarios for the mass of salt waste that would be generated from a large-scale, commercial pyroprocessing facility. Both electrorefiner salt waste and oxide reduction salt waste is considered. To the extent possible, generic processes are considered. The point of this analysis is not to make precise predictions based on current technology, but rather it is to provide an estimate of the limiting conditions and to quantify the potential benefit from specific technology improvements.

2.1. Limiting Factors. There are a number of factors that can dictate the need to remove and dispose of salt from an electrorefiner or an oxide reducer. These include total mass or volume of the salt, heat generation from the fission product decay, fission product concentration, and plutonium inventory. There are important differences between the electrorefining and oxide reduction processes, including the elements that partition into their salt phases. Table 1 summarizes the behavior of key elements in each of these systems. Salt inventory limits would be based on the number of units in a facility and maximum volume per unit. For this analysis, it is assumed that the facility operates in start-up mode for some period of time before one or more of the limits are reached. The duration of this startup period is not important, and the ultimate decommissioning of the pyroprocessing facility is not considered.

2.2. Metal Fuel Processing. First, consider metallic fuel processing. This only requires operation of the electrorefiner (ER). The oxide reduction (OR) system is not needed in this case. Practically speaking, plutonium inventory should not be considered a limiting factor in an ER, since a commercial facility would almost certainly recover plutonium for fuel fabrication. The rate of the plutonium recovery could match the rate of it being fed into the ER. Since fission product decay heat and fission product concentration are directly related, there are essentially two factors to consider for the ER—total mass of salt and total concentration of fission products in the salt.

Consider the point when all of the electrorefiners in a pyroprocessing facility reach their salt limit—whether defined based on total mass or concentration of fission products (FPs). From that point onward, an amount of salt proportional to the processing rate of fuel will need to be pulled out of the ER. Salt waste can be directly correlated with fuel processed. Mass in the salt phase increases due to accumulation of minor actinides, sodium, and fission products. The chloride ions in the salt molecules must also be counted. Those chloride ions come from UCl_3 which is added to the ER salt. The UCl_3 would likely be produced within the facility and be mixed with LiCl-KCl. Nominally, it can be assumed that the UCl_3 would be contained in an LiCl-KCl-UCl_3 mixture consisting of 75 wt% UCl_3. Thus, with every batch of fuel added to the ER it is necessary to calculate the mass of LiCl-KCl-UCl_3 added as well as the mass of fission product, sodium, and transuranic chlorides that would form. The mass of U from the LiCl-KCl-UCl_3 can be neglected, since it is reduced to metal during the process of oxidizing active metals from the fuel and is subsequently electrochemically recovered from the ER. The following formula can be generally applied:

$$M_{\text{salt waste}} = M_{\text{NaCl}} + M_{\text{FP salts}} + M_{\text{TRU salts}} + M_{\text{oxidant salt}} - M_{\text{U oxidant}}. \quad (1)$$

Calculations require detailed fuel composition, which cannot be bracketed for all potential scenarios. For illustrative purposes, however, consider the nominal composition given in Table 2.

Two demonstrated processes can be used to minimize the mass of salt waste generated—U/TRU recovery and sodium distillation. U/TRU recovery can be accomplished via deposition on a liquid cadmium cathode (LCC) or via drawdown using a reducing metal [9–11]. Ideally using such processes, all of the Pu and other minor actinides in the used fuel could be kept out of the salt waste stream and recovered for use in fabricating new fuel elements. Sodium distillation could be performed after fuel chopping but prior to electrorefining and would result in the majority of the sodium metal being removed from the fuel. For high burnup fuel, a fraction of the sodium has been found to be inseparable via distillation. Table 3 gives the salt waste calculations for the nominal fuel given in Table 2 under the four possible scenarios involving Pu and Na. For a facility that processes 100 MT of used sodium bonded fuel per year, the mass of salt waste generated is estimated to range from 12.3 to 21.7 MT. For this exercise, the glass-bonded sodalite is assumed to be the waste form of choice. Salt content in the sodalite waste form is approximately 7.5 wt%. It can thus be calculated that the ceramic waste mass per year would range from 164 to 289 MT. Clearly, sodium removal should be pursued as a technically simple process with a substantial waste minimization benefit. While Pu should be recycled for the sake of fabricating new fuel elements, its removal results in a relatively insignificant reduction in waste. However, if

Table 3: Salt waste calculations based on nominal composition and total mass limit.

Case	Pu recycle	Sodium removal	Mass of salt waste per mass of fuel	Mass of ceramic waste per mass of fuel
1	No	No	0.217	2.89
2	No	Yes	0.133	1.77
3	Yes	No	0.207	2.76
4	Yes	Yes	0.123	1.64

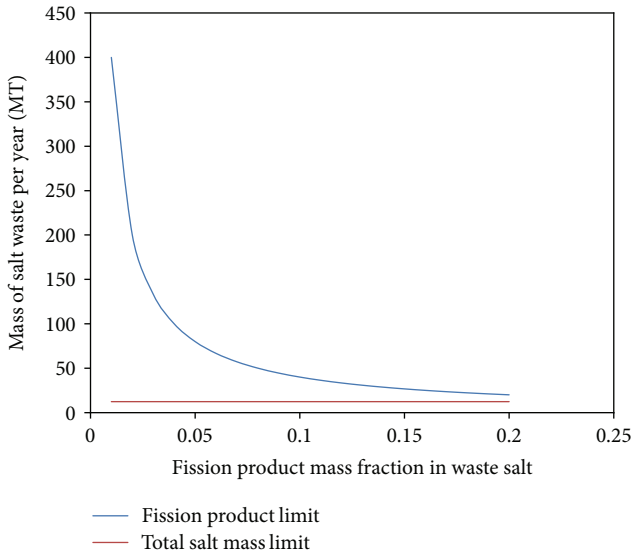

Figure 2: Estimated ER salt waste mass per year for a 100 MT/year used metal fuel pyroprocessing facility considering cases where the ER is fission product limited or total salt mass limited and only salt throw-away is pursued.

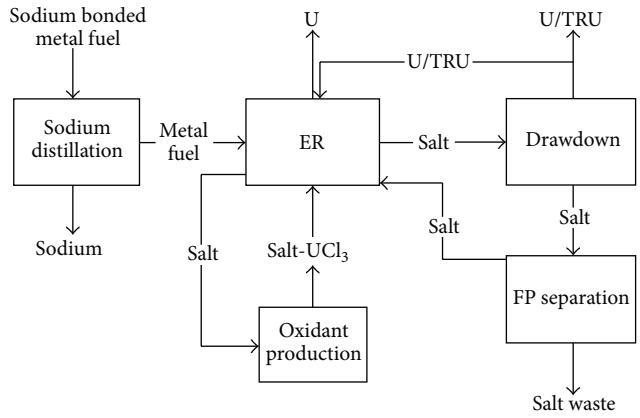

Figure 3: Used metal fuel pyroprocessing flowsheet involving selective separation of actinides and fission products from electrorefiner Salt.

the Pu was not recovered, its limiting concentration could dictate a higher rate of salt removal from the ER. Case 4 in Table 3 should be considered the ideal situation—a true minimum with respect to waste production based on the fuel composition given in Table 2.

Alternatively, consider the case where fission product concentration in the ER salt may be the limiting factor. This could be based upon melting point of the salt, fission product decay heat, or contamination of actinide deposits. If this analysis indicates less salt waste production than 12.3 MT per 100 MT of fuel, then the minimum would revert to that level. If a higher salt waste production rate were identified based on fission product removal, then that higher rate would be established as the new minimum.

The key variable for assessing the salt waste mass production due to fission product removal is what the maximum fission product concentration is for the salt. This would likely range between 5 and 20 wt%. As previously mentioned, this could be based upon the liquidus temperature of the salt, heat from decay, or contamination of actinide products. Detailed consideration of these factors is not in the scope of this paper, as it requires extensive and costly experimentation. For any commercial facility being designed, salt limit tests would be an important prerequisite for completion of the design. Rather the entire range was considered and included in the plot shown in Figure 2. As can readily be seen from this plot, the fission product removal dictates a higher rate of salt waste generation unless the salt can be allowed to run at contamination levels in excess of 20 wt% fission products.

The previous analysis considers only disposal of salt as an option for dealing with ER salt processing limits. What if selective chemical separations processes are employed? Could the amount of waste generated from pyroprocessing of used nuclear fuel be substantially reduced? In particular, consider two types of processes—actinide drawdown and fission product removal. The former is used to virtually eliminate the U/TRU chlorides from the salt with a variety of approaches feasible (electrolysis, reaction with reducing metal, oxidation induced precipitation, and molten liquid extraction). The latter is then employed to extract fission product chlorides from the salt. Again, a number of processes have been developed for that purpose, including zeolite ion exchange, oxygen sparging, and phosphate precipitation [12–14]. To model the potential impact of these two separations processes, the flowsheet shown in Figure 3 was considered.

In modeling the flowsheet shown in Figure 3, it was assumed that the sodium distillation and drawdown processes are both 100% efficient. In order to consider a wide range of fission product separation processes, a generic unit operation was modeled in which the efficiency is defined based on the amount of LiCl-KCl that is effectively carried along with the fission products:

$$\chi = \frac{M_{\text{LiCl-KCl waste}}}{M_{\text{FP chlorides}}}. \quad (2)$$

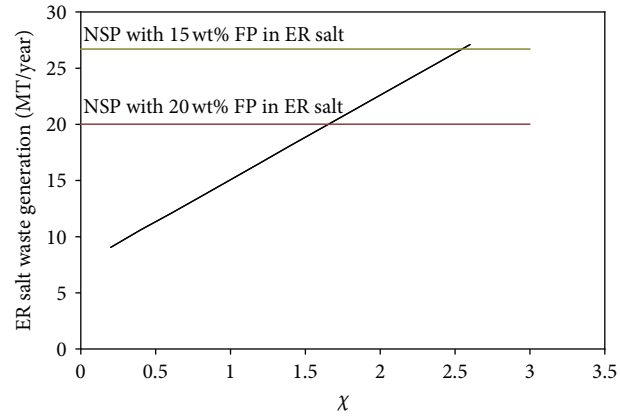

Figure 4: Comparison of ER salt waste generation rates for a 100 MT/year facility using selective process (black curve) versus nonselective process (NSP) with two different levels of fission product accumulation in the electrorefiner for used metal fuel processing.

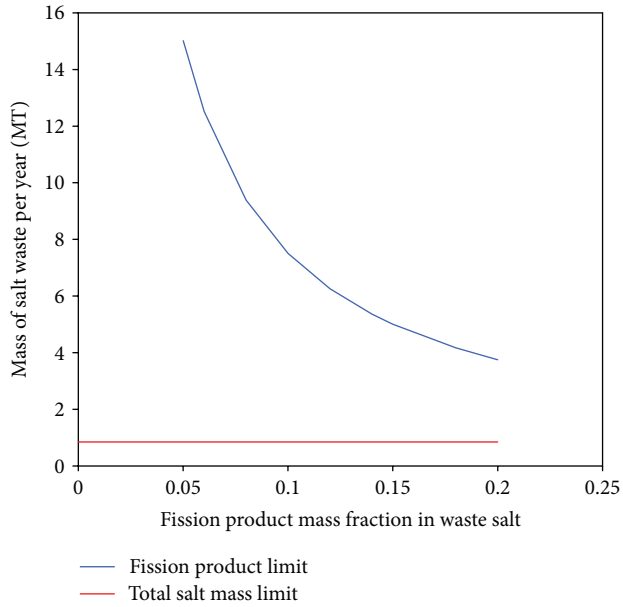

Figure 5: Estimated OR salt waste mass per year for a 100 MTHM/year pyroprocessing facility considering cases where the OR is fission product limited or total salt mass limited and only salt throw-away is pursued.

The mass of waste salt was calculated for various values of this ratio and plotted in Figure 4. A comparison between the selective process and the nonselective process (NSP) is shown in this plot. If the NSP can be run with the ER fission product concentration of 20 wt%, then the χ value must be about 1.6 or less to show an improvement. If the NSP can be run at 15 wt% fission products in the ER, then the χ value would need to be 2.6 or less. This can also be viewed in terms of the effective concentration of the fission product stream coming out of the selective process. The key to waste minimization is to minimize the amount of LiCl-KCl discarded during the waste process. For an ideal separation process, only about 7.5 MT of salt waste (all fission product chlorides) would be generated per 100 MT of metallic fuel. Bracketing the other end of the spectrum with nonselective processes, up to 20–27 MT of salt waste would be generated for the same amount of fuel. This clearly motivates the development and implementation of selective fission product separation processes.

Table 4: Nominal composition of oxide used fuel. Mass fraction calculated on metal basis (oxygen neglected). Composition based on ORIGIN calculation of 33 MWd/kg burn-up, 10-year decayed fuel.

Component	Mass fraction
U	0.974
TRU	0.010
Cs	0.0023
Sr	0.00080
Ba	0.0020
Other active metal fission products*	0.011

*Rare earths, Group III, and Rb.

2.3. Oxide Fuel Processing. Oxide fuel must first be converted to metallic form using an oxide reduction (OR) unit operation before it is fed into an electrorefiner. In contrast to metallic fuel, there would be no metal sodium to remove from the fuel prior to processing. The used fuel would essentially be uranium oxide (UO_2) with a variable amount of TRU and fission products mostly in oxide form. Actual TRU and fission product concentrations vary based on burn-up level of the fuel as well as cooling time after removal from the reactor. While the oxide reduction process is designed to simply convert oxide compounds to metals and leave all used fuel components in the fuel basket, some of the fission products have been found to partition into the molten LiCl-Li_2O electrolyte [8]. Most notably, this includes cesium, strontium, and barium. It is assumed that the following reactions occur during this process:

$$\begin{aligned} \frac{1}{2}Cs_2O + LiCl &\longrightarrow CsCl + \frac{1}{2}Li_2O \\ SrO + 2LiCl &\longrightarrow SrCl_2 + Li_2O \\ BaO + 2LiCl &\longrightarrow BaCl_2 + Li_2O \end{aligned} \quad (3)$$

Assume the used oxide fuel nominally has the composition given in Table 4.

Similar to the ER, the salt processing limit for the OR would be dictated either by total mass of the salt or fission product concentration. In this case, only Cs, Sr, and Ba are considered to be fission products of interest. For a facility in which 100 MTHM (metric tons heavy metal) is processed each year, the plot in Figure 5 shows the amount of salt that would need to be disposed from the OR unit based on either the total salt mass limit or the fission product limit. The x-axis represents the maximum allowable mass fraction of fission product chlorides in the salt. The curve for the fission product limit case was calculated based on all of the cesium, strontium, and barium partitioning into the salt phase. The total salt mass limit curve is a constant based on the total

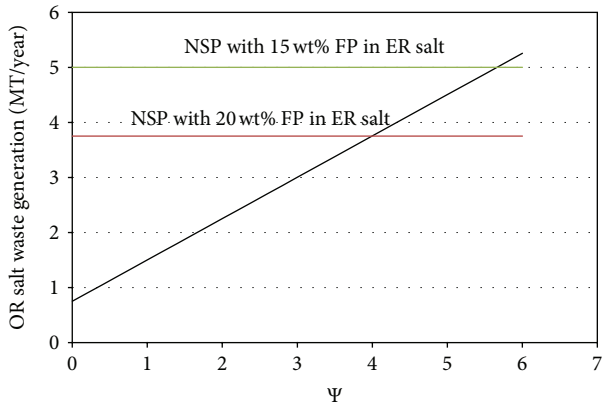

Figure 6: Comparison of OR salt waste generation rates for 100 MTHM/year facility for selective process (black curve) to non-selective process (NSP) with two different levels of fission product accumulation in the OR.

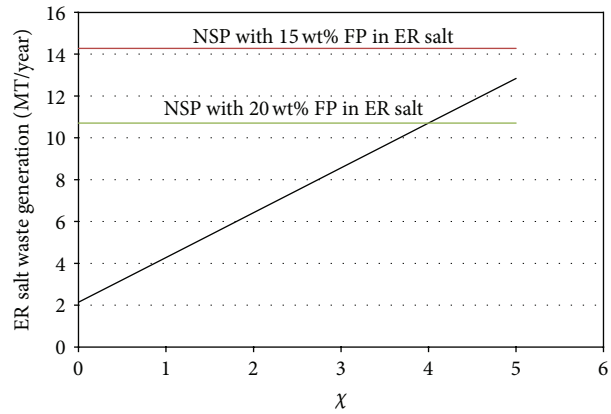

Figure 7: Comparison of ER salt waste generation rates for 100 MTHM/year facility for selective process (black curve) to non-selective process (NSP) with two different levels of fission product accumulation in the ER.

mass added to the salt for 100 MTHM of spent fuel. Under achievable contamination levels in the OR salt, the fission product limit is more restrictive than the total salt mass limit.

As with the case of the ER salt disposal, there are selective separation processes that can be considered for removing Cs, Sr, and Ba from the OR salt without carrying as much other salt (LiCl and Li_2O in this case) with it. These generally are based on the mechanisms of selective precipitation, ion exchange, intercalation, surface complexation, or melt crystallization [15]. The flowsheet for oxide fuel treatment with selective salt separation would be nearly identical to that shown in Figure 3 but with the oxide reduction unit preceding the ER. Salt adhered to the reduced fuel from the OR could be distilled and returned to the OR. As with the analysis of selective separation processes for ER salt, it is simplest to characterize the selective separation process by a mass ratio rather than delve into the details of each processing option:

$$\Psi = \frac{M_{\text{LiCl-Li}_2\text{O}}}{\left(M_{\text{CsCl}} + M_{\text{SrCl}_2} + M_{\text{BaCl}_2}\right)}. \quad (4)$$

As can be seen in Figure 6, there is a large improvement in OR salt waste generation that can be achieved with only moderately selective fission product separation processes. The best possible salt waste generation rate for a very high 20 wt% FP in the OR salt would be 3.75 MT/year, while an ideal selective process would only generate 0.75 MT of OR salt waste per year (all based on 100 MTHM fuel input per year). Selective processes with Ψ values of less than 4 should be considered attractive for waste minimization.

There would also be ER salt waste generated from processing of oxide fuel. The OR only removes Cs, Sr, and Ba from the fission product inventory. The remaining fission products which are primarily in the rare earth family would partition into the ER salt. Applying the same selective process model as used for ER treatment of sodium bonded metal fuel, the plot in Figure 7 was generated. Interestingly, the removal of Cs, Sr, and Ba from the used fuel results in a much more favorable situation with respect to ER salt waste. Even without using a selective process, waste generation rates are cut in half. And there is a substantially greater improvement that can be attained by using a selective FP removal process. The removal process does not need to be as selective as with the metal fuel in order to improve upon the salt bleed process.

Combining the OR and ER salt waste from oxide fuel yields 14.4 MT of salt waste per 100 MTHM fuel treated for the case where the fission product limits are set at 20 wt% and non-selective processing is employed. From examining Figures 6 and 7, it is reasonable to expect that this could be reduced to about 8 MT/year via use of selective fission product separation. While these are estimates based on nominal fuel compositions and idealized processing assumptions, it does provide a basis for assessing the cost/benefit ratio of implementing FP separation technology. Conventional assumptions in this area have been that selective salt processing would have a much greater impact on salt disposal and perhaps lead to a near-zero waste facility. Based on these calculations, this does not appear to be a reasonable assumption.

3. Waste Disposal

The previous analysis calculates the mass of waste salt generated under various scenarios. But it does not consider the actual waste form of this salt that will be disposed. If the waste is truly in the form of chloride salt, consider three possible alternatives—glass bonded sodalite (GBS), glass, and direct disposal. The GBS waste form (also known as *ceramic waste*) was developed initially at Argonne National Laboratory for the Integral Fast Reactor (IFR) process [2–6]. It is produced by occluding the salt into zeolite-A, blending in glass frit, and thermally converting the glass/zeolite to glass-bonded sodalite. The process equipment and operating conditions are well understood for the ceramic waste process. But the drawback is that only about 7.5 wt% salt can be incorporated into the GBS. That would equate to as much as 187 MT of ceramic waste per 100 MTHM of used oxide fuel.

Alternatively, the salt could be incorporated into a pure glass waste form. Limited research has been performed on using tellurite glass to immobilize electrorefiner salt [16]. In this case, the glass can hold up to about 10 wt% salt—equating to a still considerable mass of waste (140 MT of glass waste for 100 MTHM of used oxide fuel).

For a nuclear fuel cycle to be considered appealing to the general public, it would seem that the mass of waste produced should be less than the mass of used fuel processed. This directs one to consider the most radical case of simply disposing of the salt without any added components or waste form processing. This is the direct disposal/no waste form option. Intuitively, this would seem like a nonstarter of an idea due to the extremely hygroscopic nature of the chloride salts. These salts will pick up substantial quantities of water by simply being in contact with humid air. They have a high solubility in water. It would seem that they would be considered completely inappropriate for direct disposal. But what if they could be essentially stabilized by the geologic environment? Consider a repository such as the Waste Isolation Pilot Plant (WIPP), which was constructed within a salt basin. Brines in such a salt repository are fully saturated with K- and Na-bearing chloride salt minerals in the salt formation, and the salt waste (except LiCl components if present in substantial amounts) would be considered thermodynamically compatible to the geochemical conditions in the repository. Salt creep and deformation in such a repository are greatly positive attributes and will have significantly favorable impacts on safe long-term waste isolation. Over thousands of years, the salt waste may become essentially encapsulated by the geologic salt formations and stabilized with no loss of radioactive materials outside of the repository boundary [17]. Currently, an investigation into such a disposal configuration is being carried out jointly by the INL and Sandia National Laboratory (SNL). Generic salt repositories are being considered, since it is unlikely that WIPP would be open long enough to accept salt waste from a pyroprocessing facility. The soonest that this concept could actually be tested would be in the next 10 years or so with salt currently being used to treat used EBR-II fuel at INL. Total waste salt from EBR-II fuel processing is expected to be about 2 MT, which would occupy a volume of only 1 m^3. Even a 100 MTHM per year pyroprocessing facility would generate a relatively small amount (7 m^3) of salt waste per year.

4. Conclusions

An analysis of salt waste generation for both metallic and oxide used fuel in a pyroprocessing facility has been performed. Interesting insight into this problem has been obtained from relatively simple models and generalized treatment of processes. Fission product limits in the molten salt electrolyte of both the electrorefiner and oxide reduction unit appear to be the most restrictive—assuming that TRU elements would be recovered for new fuel fabrication. For the metallic fuel, first removing any bond sodium before the fuel is electrorefined is the key to reducing the amount of salt waste generated. Then the amount of salt waste generated would be dictated by the fission product concentration limit in the ER. Even at very high fission product chloride concentrations (20 wt%), it is apparent that selective fission product separations processes can further reduce the amount of salt waste. Efficiency is defined as how much useful salt is carried along with the fission products into the waste stream. This efficiency must be higher for the metal fuel case compared to the oxide fuel case to provide overall benefit. That is largely because some of the fission products from oxide fuel partition into the oxide reduction salt and lead to waste generation from that unit operation. For metal fuel treatment, it is estimated that total salt waste generation would vary from 15 to 20 MT/year (for a processing rate of 100 MT fuel per year). For oxide fuel treatment, it is estimated that the total salt waste generation would vary between 8 and 14 MT/year (100 MTHM fuel per year processing rate). Note that these fuels cannot be directly compared since the burnup and fission product content for each fuel type considered are different.

With respect to selective fission product separations processes, this paper presents both a motivation to design them into a pyroprocessing facility an indication to their limited benefit. Ultimately, a cost/benefit analysis would be needed for a specific pyroprocessing facility design to determine whether the salt should be disposed of in a non-selective or selective method. While there are durable ceramic and glass waste forms that can readily be produced with this waste salt, they increase the mass of waste by at least a factor of 10. Creating such waste forms would result in the total waste mass exceeding the mass of used fuel processed. Alternatively, it is suggested that direct disposal of the salt without a waste form in a salt repository may be the most logical path to pursue. A study is currently underway to assess the feasibility of direct disposal of salt waste in such an environment. If it appears to be sufficiently promising, the concept may be tested in the near term with waste salt from INL's electrorefiners. Ultimately, very compact waste disposal is possible by combining pyroprocessing with selective salt separations processes and direct disposal of the salt waste in a salt repository.

References

[1] K. C. Song, H. Lee, J. M. Hur, J. G. Kim, D. H. Ahn, and Y. Z. Cho, "Status of pyroprocessing technology development in Korea," *Nuclear Engineering and Technology*, vol. 42, no. 2, pp. 131–144, 2010.

[2] J. P. Ackerman, T. R. Johnson, L. S. H. Chow, E. L. Carls, W. H. Hannum, and J. J. Laidler, "Treatment of wastes in the ifr fuel cycle," *Progress in Nuclear Energy*, vol. 31, no. 1-2, pp. 141–154, 1997.

[3] L. J. Simpson and D. J. Wronkiewicz, "Evaluation of standard durability tests towards the qualification process for the glass-zeolite ceramic waste form," in *Proceedings of the 20th Scientific Basis for Nuclear Waste Management*, W. Gray and K. Knecht, Eds., vol. 465, pp. 441–448, Materials Research Society, 1997.

[4] C. Pereira, "Production of sodalite waste forms by addition of glass," *Ceramic Transactions*, vol. 61, p. 389, 1997.

[5] S. Priebe and K. Bateman, "The ceramic waste form process at Idaho National Laboratory," *Nuclear Technology*, vol. 162, no. 2, pp. 199–207, 2008.

[6] M. F. Simpson, K. M. Goff, S. G. Johnson et al., "A description of the ceramic waste form production process from the demonstration phase of the electrometallurgical treatment of EBR-II spent fuel," *Nuclear Technology*, vol. 134, no. 3, pp. 263–277, 2001.

[7] E. J. Karell, K. V. Gourishankar, J. L. Smith, L. S. Chow, and L. Redey, "Separation of actinides from LWR spent fuel using molten-salt-based electrochemical processes," *Nuclear Technology*, vol. 136, no. 3, pp. 342–353, 2001.

[8] S. D. Herrmann, S. X. Li, M. F. Simpson, and S. Phongikaroon, "Electrolytic reduction of spent nuclear oxide fuel as part of an integral process to separate and recover actinides from fission products," *Separation Science and Technology*, vol. 41, no. 10, pp. 1965–1983, 2006.

[9] S. X. Li, S. D. Herrmann, and M. F. Simpson, "Electrochemical analysis of actinides and rare earth constituents in liquid cadmium cathode product from spent fuel electrorefining," *Nuclear Technology*, vol. 171, no. 3, pp. 292–299, 2010.

[10] S. X. Li, S. D. Herrmann, K. M. Goff, M. F. Simpson, and R. W. Benedict, "Actinide recovery experiments with bench-scale liquid cadmium cathode in real fission product-laden molten salt," *Nuclear Technology*, vol. 165, no. 2, pp. 190–199, 2009.

[11] M. F. Simpson, T. S. Yoo, D. LaBrier, M. Lineberry, M. Shaltry, and S. Phongikaroon, "Selective reduction of active metal chlorides from molten LiCl-KCl using lithium drawdown," *Nuclear Engineering and Technology*, vol. 44, no. 7, pp. 767–772, 2012.

[12] C. Pereira, M. C. Hash, M. A. Lewis, M. K. Richmann, and J. Basco, "Incorporation of radionuclides from the electrometallurgical treatment of spent fuel into a ceramic waste form," *Materials Research Society Symposium Proceedings*, vol. 556, p. 115, 1999.

[13] Y. Z. Cho, H. C. Yang, H. C. Eun, E. H. Kim, and I. T. Kim, "Characteristics of oxidation reaction of rare-earth chlorides for precipitation in LiCl-KCl molten salt by oxygen sparging," *Journal of Nuclear Science and Technology*, vol. 43, no. 10, pp. 1280–1286, 2006.

[14] V. A. Volkovich, T. R. Griffiths, and R. C. Thied, "Treatment of molten salt wastes by phosphate precipitation: removal of fission product elements after pyrochemical reprocessing of spent nuclear fuels in chloride melts," *Journal of Nuclear Materials*, vol. 323, no. 1, pp. 49–56, 2003.

[15] Y. Z. Cho, G. H. O. Park, H. S. U. Lee, I. N. T. Kim, and D. S. Han, "Concentration of cesium and strontium elements involved in a LiCl waste salt by a melt crystallization process," *Nuclear Technology*, vol. 171, no. 3, pp. 325–334, 2010.

[16] B. J. Riley, B. T. Rieck, J. S. McCloy, J. V. Crum, S. K. Sundaram, and J. D. Vienna, "Tellurite glass as a waste form for mixed alkali-chloride waste streams: candidate materials selection and initial testing," *Journal of Nuclear Materials*, vol. 242, no. 1–3, pp. 29–37, 2012.

[17] Y. Wang, M. Simpson, J. Rath et al., "Closing the nuclear fuel cycle with salt," in *Proceedings of the 13th International High-Level Radioactive Waste Management Conference*, Albuquerque, NM, USA, 2011.

Hindawi Publishing Corporation
Science and Technology of Nuclear Installations
Volume 2013, Article ID 412349, 10 pages
http://dx.doi.org/10.1155/2013/412349

Research Article

Economic Viability of Metallic Sodium-Cooled Fast Reactor Fuel in Korea

S. K. Kim,[1] W. I. Ko,[1] and Yoon Hee Lee[2]

[1] *Korea Atomic Energy Research Institute, 1045 Daedeokdaero, Yuseung-Gu, Daejeon 305-353, Republic of Korea*
[2] *Department of Nuclear and Quantum Engineering, Korea Advanced Institute of Science and Technology, 291 Daehakro, Yuseong-Gu, Daejeon 305-353, Republic of Korea*

Correspondence should be addressed to S. K. Kim; sgkim1@kaeri.re.kr

Received 7 November 2012; Revised 18 February 2013; Accepted 19 February 2013

Academic Editor: Michael F. Simpson

This paper evaluates whether SFR metallic nuclear fuel can be economical. To make this determination, the cost of SFCF (SFR fuel cycle facilities) was estimated, and the break-even point of the manufacturing cost of SFR metallic nuclear fuel for direct disposal option was then calculated. As a result of the cost estimation, the levelized unit cost (LUC) for SFCF was calculated to be 5,311 $/kgHM, and the break-even point was calculated to be $5,267/kgHM. Therefore, the cost difference between LUC and the break-even point is not only small but is also within the relevant range of the uncertainty level of Class 3 in accordance with a generic cost estimate classification matrix of AACE (the Association for the Advancement of Cost Engineering). This means it is very difficult to judge the economical feasibility of SFR metallic nuclear fuel because as of today there are no commercial facilities in Korea or the world. The economic feasibility of SFR metallic nuclear fuel, however, will be enhanced if the mass production of SFCF becomes possible in the future.

1. Introduction

Since the accident in the nuclear power plant in Fukushima, Japan, occurred, some advanced countries are attempting to better manage their nuclear power generation and spent fuel. In addition, these countries are carrying forward the development of alternative energy such as solar heat and wind power; however, for now there is no appropriate alternative electric power production that can substitute for nuclear energy. For now, there are limitations for alternative energy to replace nuclear energy, and for the recycling of uranium the method of recycling spent fuel accumulated in nuclear power plants or in intermediate storage facilities in an SFR (sodium-cooled fast reactor) is judged to have sufficient investment value. To develop a sodium-cooled fast reactor (SFR), however, the part that should be reviewed priorly in the aspect of economic feasibility is to judge its economic feasibility and compare it with direct disposal. This is because direct disposal is known to be economical in the alternatives of nuclear fuel cycle. Therefore, it is necessary to calculate the break-even point by comparing the Pyro-SFR nuclear fuel cycle cost, which considers the manufacturing cost of the SFR metallic nuclear fuel, with the direct disposal cost.

Korea is presently operating 21 nuclear power plant units and has plans to continuously increase the capacity of nuclear power generation in the future. However, the operation of nuclear power plants inevitably causes the generation of spent fuel. In addition, the capacity of Korea's present temporary storage facilities for spent fuel will become lower than the required storage capacity in each nuclear power plant site and will reach the saturation condition in 2016.

According to the 2009 yearbook of Korea's nuclear energy, we have a plan to manage the spent fuel generated from nuclear power plants through the installation of a high density storage rack, the transferring between units, and the installation of a dry storage facility at each nuclear power plant site. Therefore, for a continuous increase in nuclear energy, we should fundamentally solve the problem of spent fuel presently accumulated in nuclear power plants. The selection of a site, however, for interim storage or a repository for spent fuel is recognized as a big obstacle. Therefore, to solve the problem of a shortage of natural uranium and

to decrease the scale of a high-level waste repository, the recycling of spent fuel is inevitable. In addition, to increase the efficiency of uranium use, the development of an SFR and SFR fuel cycle facilities (SFCF) is necessary.

Pyroprocess, which is a dry reprocessing method, converts the spent fuel into metal in high-temperature molten salt phase and decreases the volume of the spent fuel to increase its economic feasibility of disposal innovatively [1].

Namely, the technology of the Pyro-SFR nuclear fuel cycle is one of the alternatives that can fundamentally solve the problem of spent fuel management and is known to be an advanced technology with high proliferation resistance [2].

Some experts, however, still have doubt whether Pyro-SFR nuclear cycle technology is feasible in terms of technology know-how and economics. Therefore, to introduce facilities related to the SFR nuclear cycle, not only continuous research on the manufacture process of SFR metallic nuclear fuel but also the review of the economic feasibility of the pyroprocess for SFR spent fuel is required.

This paper defines the design requirements of SFR nuclear fuel manufacturing facilities and calculates the manufacturing cost of SFR nuclear fuel using the engineering cost estimation method. In addition, by comparing the direct disposal cost with the Pyro-SFR nuclear fuel cycle cost, the break-even point of the SFR metallic nuclear fuel manufacture cost was elicited. This is because the manufacturing cost of SFR metallic nuclear fuel is a major cost driver of the Pyro-SFR nuclear fuel cycle cost.

2. Conceptual Design of SFR Facility

To calculate the break-even point of the manufacturing cost of SFR metallic nuclear fuel, we should first calculate the Pyro-SFR nuclear cycle cost based on Figures 1 and 2, and to do this we should estimate the cost of the manufacture facilities of the SFR nuclear fuel. Therefore, a conceptual design of SFR facilities as shown in Figure 1 is necessary. The engineering cost estimation method using a conceptual design is for now a realistic method with high reliability [3] and can calculate the cost of SFR nuclear fuel in manufacturing facilities.

We can calculate the cost of investment in the facilities used for SFR nuclear fuel manufacturing, as well as the operation and maintenance cost (O&M) and decontamination and decommissioning (D&D) cost from the bottom up. The cost calculation of SFR metallic nuclear fuel manufacturing is shown in Figure 3.

2.1. Major Function of SFR Fuel Cycle Facility (SFCF). The SFR fuel cycle facility (SFCF) recycles the spent fuel discharged from the SFR of 6 units of a 600 MWe as shown Figure 2.

In the main manufacture facility, after going through the head-end processes such as inspection, dissolution, cutting, and removing sodium of the spent fuel, uranium is collected through the electrorefining process [4], and by collecting the remaining uranium and TRU (transuranium) through the electrowinning process [5].

Table 1: Design standard of SFR fuel cycle facilities.

Capacity	
Annual SFR SF	32.94 tHM/yr (9.12 tTRU/yr); SF of SFR 6 unit (600 MWe per unit)
Manufacturing of SFR new fuel	HM: 38.62 tHM/yr, TRU: 11.4 tTRU/yr, annual manufacturing of fuel rod: 327,139/yr, annual fuel assemblies: 1,207/yr
Plant function	Head-end process, pyroprocess, manufacturing of SFR nuclear fuel
Annual load factor	55%, 200 day/year
Design lifetime	60 year
Input material	U/TRU/RE metal ingot, SFR spent fuel
Output material	initial and make-up SFR new fuel, waste (ceramic, metal)
Fuel composition	
Fuel composition	U-20.6 wt.%, TRU-10 wt.%
MA composition	<5 wt.%
RE composition	<5 wt.%
Injection	Sodium

The collected uranium and U-TRU ingot are recycled as SFR nuclear fuel after going through the metallic nuclear fuel manufacture process [6].

In addition, in KAPF (Korea Advanced Pyroprocess Facility Plus), uranium metal (U metal, U/TRU metal) produced by treating light-water nuclear reactor (PWR) spent fuel in the pyroprocess is supplied to the SFR nuclear fuel manufacturing facility and used for the initial core and supplement.

2.2. Design Requirement and Criteria. The design standard of SFCF (SFR fuel cycle facility) is shown in Table 1.

2.3. Reference Spent Fuel of SFR. It is assumed that the reference SFR spent fuel is cooled in the storage tank for 5 years or longer after being taken out from the SFR, and the average burnup is 91,429 MWd/tHM. The composition of the major nuclear material before and after the burnup is shown in Table 2.

3. Material Flow of SFR Nuclear Fuel

To calculate the cost of the Pyro-SFR nuclear cycle, the nuclear material balance of each process was calculated. To do this, if we look at the flow of the manufacturing process, the core process of the SFR nuclear fuel manufacture facility is largely divided into the head-end process, the pyroprocess, and the SFR nuclear fuel manufacture process.

The flow of pyroprocess is as shown in Figure 4. The pyroprocess was done in an argon gas atmosphere with little air ($\leq$50 ppm O_2).

The SFR nuclear fuel manufacturing facility receives the SFR spent fuel of 32.94 tHM annually based on 200 days

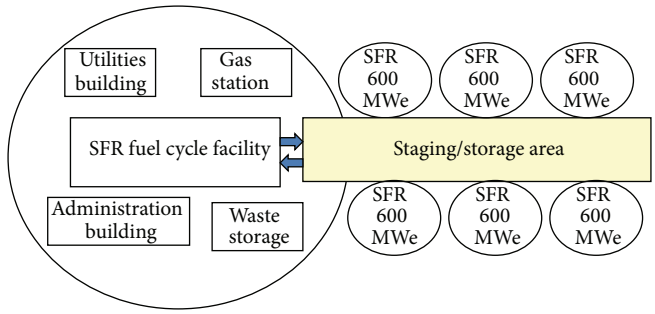

Figure 1: The sketch of SFR fuel cycle facility.

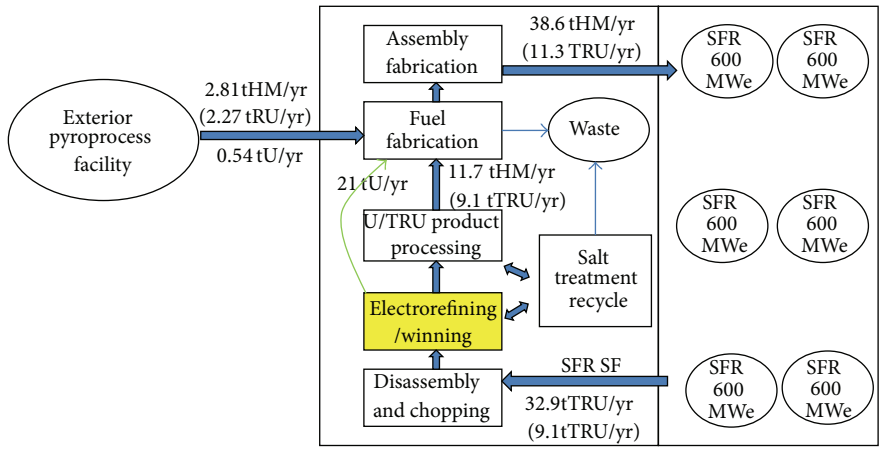

Figure 2: The mass flow diagram of SFR fuel cycle facility.

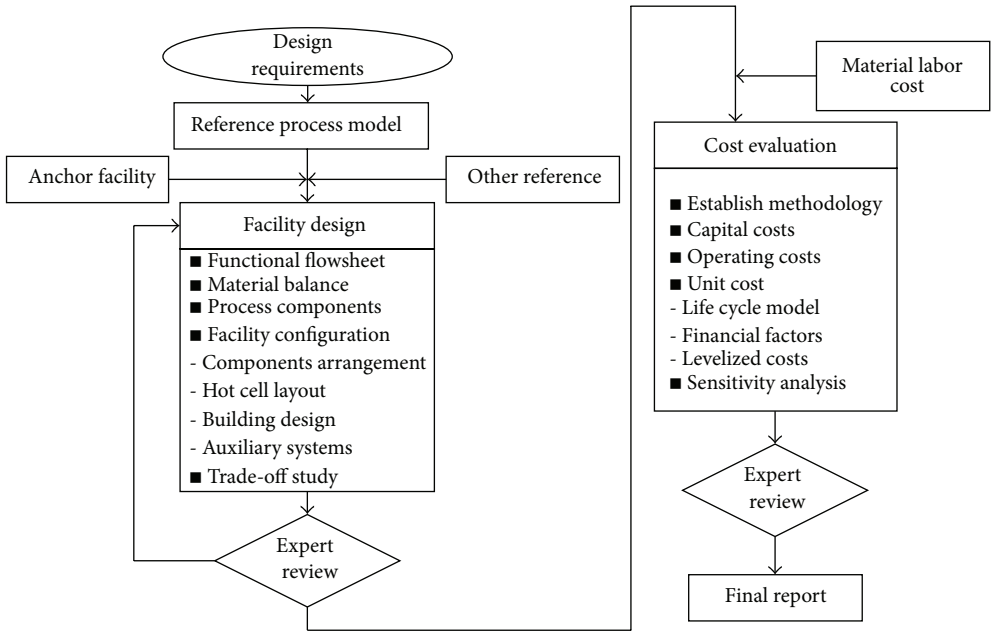

Figure 3: The calculation procedures of the manufacturing cost of SFR metallic nuclear fuel.

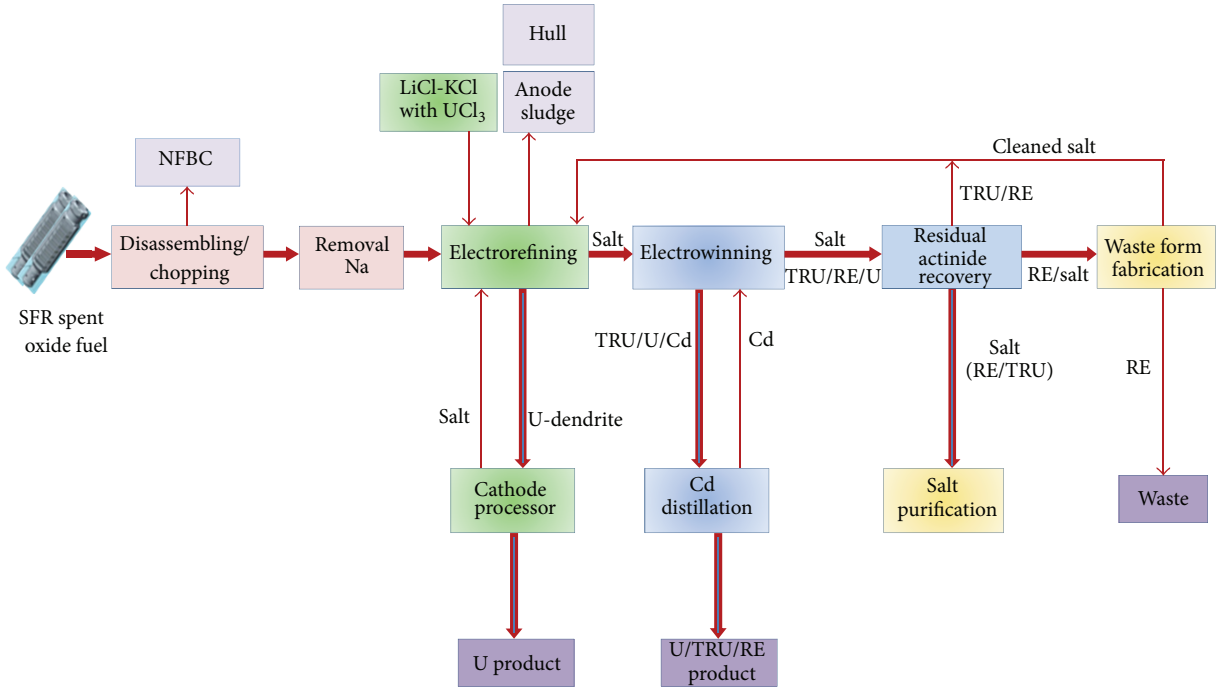

Figure 4: The process flow diagram of pyroprocess.

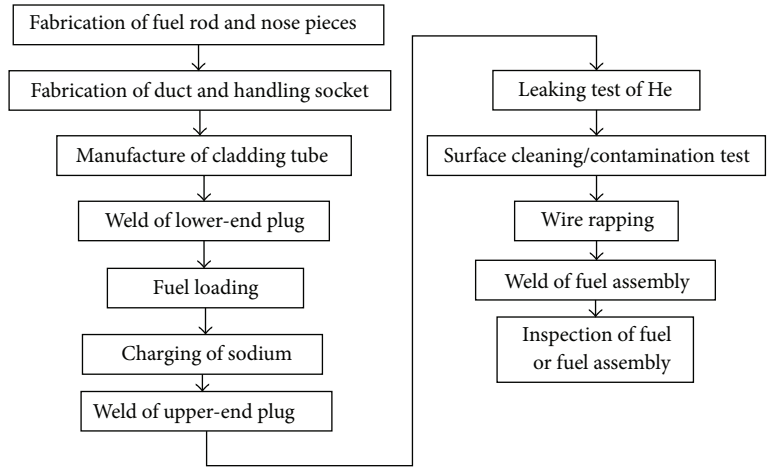

Figure 5: The manufacturing process of SFR nuclear fuel.

of work as shown in Table 1 and manufactures SFR metallic nuclear fuel of 38.62 tHM.

Uranium and transuranium (TRU) produced through the pyroprocess is transferred to the nuclear fuel manufacturing hot cell to manufacture the metallic nuclear fuel, and after carrying out the component adjustment (U/TRU/Zr) of the nuclear fuel fuel slug is manufactured using an injection cast method. The completely manufactured fuel slug is charged together with sodium to the fuel rod. A flowchart of the manufacturing process of SFR metallic nuclear fuel is shown in Figure 5.

The assumptions required for the pyroprocess of the SFR nuclear fuel manufacturing facility are shown in Table 3.

The SFR spent fuel is received, and in the SFR nuclear fuel manufacturing facility uranium ingot 21.1 tU/yr and U-TRU-RE ingot 11.75 tHM/yr are produced. In addition, off-gas waste is generated from the high-temperature oxidation volatilization process [8]. This waste will be disposed of in a deep geological repository.

4. Cost Estimation

4.1. Cost Structure

4.1.1. Investment Cost. The cost of investment in facilities is defined as the expense occurring from the time when the

Table 2: Characteristics of reference SFR spent fuel.

Nuclides	New fuel Annual input (g) (600 MW × 6)	Ratio (%)
^{234}U	$4.19E-02$	0.11
^{235}U	$2.05E-02$	0.05
^{236}U	$1.53E-02$	0.04
^{238}U	$2.73E+01$	70.35
U	$2.72E+01$	70.55
^{237}Np	$2.57E-01$	0.67
^{238}Pu	$3.20E-01$	0.83
^{239}Pu	$4.81E+00$	12.46
^{240}Pu	$3.46E+00$	8.97
^{241}Pu	$7.47E-01$	1.93
^{242}Pu	$7.65E-01$	1.98
Pu	$1.01E+01$	26.17
^{241}Am	$3.89E-01$	1.01
^{242}Am	$2.17E-02$	0.06
^{243}Am	$2.95E-01$	0.76
^{242}Cm	$3.77E-04$	0.00
^{243}Cm	$1.71E-03$	0.00
^{244}Cm	$2.00E-01$	0.52
^{245}Cm	$6.44E-02$	0.17
^{246}Cm	$3.69E-02$	0.10
MA	$1.27E+00$	3.28
TRU	$1.14E+01$	29.45
Total (HM)	$3.862E+01$	
Nuclides	Spent fuel Annual output (g) (600 MW × 6)	Ratio (%)
^{234}U	$3.72E-02$	0.11
^{235}U	$1.04E-02$	0.04
^{236}U	$1.68E-02$	0.05
^{237}U	$1.10E-04$	0.00
^{238}U	$2.37E+01$	72.07
^{239}U	$4.00E-05$	0.00
U	23.809	72.3
^{237}Np	$1.36E-01$	0.41
^{238}Np	$1.53E-04$	0.00
^{239}Np	$5.76E-03$	0.02
^{238}Pu	$3.09E-01$	0.92
^{239}Pu	$3.66E+00$	11.10
^{240}Pu	$3.00E+00$	9.09
^{241}Pu	$5.05E-01$	1.53
^{242}Pu	$6.84E-01$	2.08
Pu	$8.15E+00$	24.72
^{241}Am	$2.69E-01$	0.82
^{242M}Am	$3.25E-03$	0.01
^{242}Am	$1.06E-04$	0.00
^{243}Am	$2.37E-01$	0.72
^{244}Am	$5.43E-05$	0.00
^{242}Cm	$2.07E-02$	0.06
^{243}Cm	$1.90E-03$	0.01
^{244}Cm	$2.05E-01$	0.62
^{245}Cm	$6.29E-02$	0.19
^{246}Cm	$3.67E-02$	0.11
^{247}Cm	$2.18E-03$	0.01
^{248}Cm	$1.70E-04$	0.00
MA	$9.81E-01$	2.98
TRU	$9.13E+00$	27.72
Total (HM)	$3.294E+01$	

Burnup: 91,429 MWd/tHM, cooling: 5 years, calculation code: Origen 2.1, conversion ratio: 0.60.

Table 3: Main constraints of prime process.

Category of process	Assumption
Head-end cell	Annual assemblies treated in head-end cell: 930
	Recovery factor of fuel: 99.99%
	Removal rate for Na, Cs, Sr, Ba, I: 99%
Electrorefining	Annual throughput: 32.94 tHM
	Throughput per batch: 45.75 kgHM/batch
	Volume of molten salt: 2,900 kg LiCl-KCl/batch—1unit
	Initial UCl_3 concentration: 9 wt%
	Recovery factor of uranium in electrorefining: 99.67%
Electrowinning	Composition in molten salt: Pu/U > 3
	U coefficient: U_{salt}/U_{cd} = 1.13
	Recovery factor of TRU in RAR (residual actinide recovery): 0.99
Salt waste treatment	Annual solidification volume of nuclides and concentrated salt: 3,895 kg
	Annual solidification volume of RE/TRU oxide: 870 kg

owner decides on the construction of the facilities to the time when the facilities are commercially operated, which includes the costs of obtaining the land, the design, the infrastructure, the construction, the equipment, and the interest accrual during the construction period.

To estimate the cost, the conversion factor considering the complication, size, and degree of development of the technology was reflected, and the inflation rate was reflected to estimate the construction cost based on the end of 2009. The exchange rate of won-dollar assumed is 1 USD = 1,100 won. The investment costs of the SFR nuclear fuel manufacture facilities are estimated as shown in Table 4.

Table 4: Investment costs of SFR fuel cycle facilities.

Capital cost	Estimated cost (kUSD)	Ratio (%)
Direct cost		
Site preparation	9,445	
Process systems	199,194	
Main processing building	238,668	
Site support facilities	15,266	
Sub total	462,573	50
Indirect cost		
Conceptual/final design (14%)	64,760	
Licenses (7%)	32,380	
General and administrative costs (5%)	23,129	
Engineering and construction management (10%)	46,257	
Startup and testing (20%)	92,515	
Initial training (3%)	13,877	
Subtotal	272,918	30
Contingency (25%)	183,873	20
Total	919,364	100

4.1.2. Operation Cost. The operation cost is defined as all necessary annual expenses related to the use of the facilities and includes the labor cost, maintenance cost, and service costs (water, electricity, etc.).

The estimated annual operation cost of the SFR nuclear fuel manufacturing facilities is shown in Table 5.

4.1.3. Decommissioning Cost. For the decommissioning cost of the SFR nuclear fuel manufacture facilities,it is assumed that 1% of the direct investment cost is accumulated every year for a lifespan period of 60 years in consideration of the scale of the facilities based on expert judgment [9]. Generally, the decommissioning cost of a nuclear facility is calculated to be 10–20% of the direct investment cost. This cost includes the cost of the disposal of equipment. The accumulated annual decommissioning cost is 4,626,000 USD, and the total decommissioning cost is estimated to be 277,544,000 USD.

4.2. Cost Estimation Method. The general cost estimation methods are analogy cost estimation, parametric cost estimation, and engineering cost estimation.

The analogous cost estimation method selects the similar cost object. The parameter cost estimation method assumes the total cost as a dependent variable and sets the characteristics (facility scale, production quantity of nuclear fuel, etc.) of the prime cost as an independent variable. Therefore, the parameter estimation method can be expressed as a regression model.

The engineering cost estimation method carries out a detailed estimation from the low phase, which is a component of the prime cost object and accumulates up to the highest phase to calculate the total cost [10]. Therefore, we need to first conduct a conceptual design for the cost object.

Table 5: Annual operation costs of SFR fuel cycle facilities.

Description	Estimated cost (kUSD)	Ratio (%)
O & M cost		
Staff	18,184	12
Materials	92,601	62
Equipment replacement	28,456	19
Utilities	9,530	7
Total	148,771	100

Other cost estimation methods include expert estimations and the earned value management system (EVMS) method. In the expert estimation method, a one-to-one interview with an expert is conducted, or multiple experts are gathered in one place to conduct a group decision making.

The earned value management system (EVMS) method integrates the schedule and cost of the business. Therefore, the EVMS can be classified into plan elements, measurement elements, and analysis elements. The plan elements are the work breakdown structure, control account, and performance measurement baseline, while the measurement elements are composed of the actual cost and earned value. The earned value means the budgeted cost for work performed. In addition, the analysis elements are the scheduled variance, cost variance, and schedule performance index. The purpose of an EVMS is to accurately evaluate the quantitative performance and is a method that can be used to measure the efficiency of the investment cost.

In addition, the levelized unit cost, which is used a lot in the engineering cost estimation method, was used. The levelized unit cost (LUC) can be expressed as in (1) using the continuous discount rate R if it is assumed that the electric power production is continued [11]:

$$\mathrm{LUC} = \frac{\mathrm{PV}}{\mathrm{PB}} \frac{\int_{\mathrm{time}} \exp(-Rt)\, C_i dt}{\int_{\mathrm{time}} \exp(-Rt)\, Q_i dt}. \quad (1)$$

Here LUC is levelized unit cost, PV is present value, PB is present benefits, C_i is costs for the year, Q_i is benefits of the year such as processing volume of uranium or electricity generation, $R = \ln(1 + r)$, and r is discount rate.

4.3. Cash Flow. Figure 6 shows a graph expression of the annual cost trends as overnight costs of investment, O&M, and D&D using (1) based on the end of 2009 on the assumption that the time of initiating the operation of the SFR nuclear fuel manufacturing facilities is 2051, the construction period is 7 years, and the lifespan period is 60 years.

The present cost at the end of the year 2009 needed for the SFR nuclear fuel manufacture facilities was calculated to be about 531,779 k$, and the present treatment quantity is estimated to be about 96.5 tHM. If the total cost needed for the SFR nuclear fuel manufacturing facilities is subdivided,

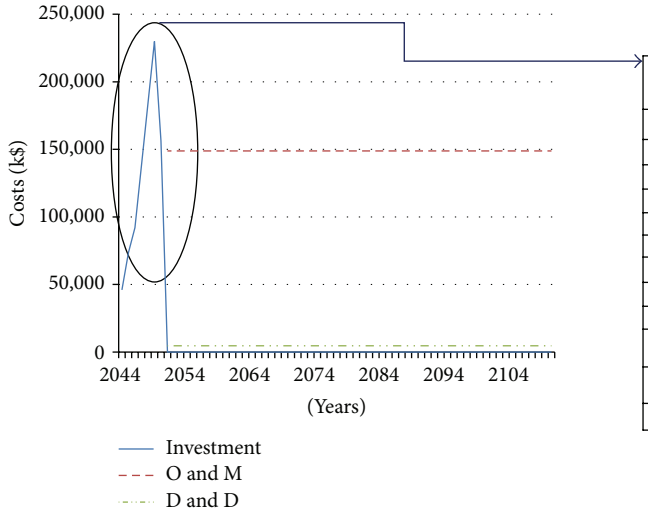

Years	Costs (k$)		
	Investment	O and M	D and D
2044	45,968		
2045	73,549		
2046	91,936		
2047	137,905		
2048	183,873		
2049	229,841		
2050	156,292		
2051	0	148,771	4,626
2052	〃	〃	〃
∫	∫	∫	∫
2110	0	148,771	4,626
Total	919,364	8,926,282	277,544

Figure 6: Cost trends of SFR facilities.

it is composed of the investment cost of 138,962 k$ (26%), the operation and maintenance cost of 380,971 k$ (72%), and the decontamination and decommissioning cost of 11,845 k$ (2%). These three main costs (investment cost, O&M cost, and D&D cost) were discounted by 5% using (2) with the annual cost from 2044 to 2110 as shown in Figure 6:

$$\mathrm{NPV} = \sum_{t} \frac{\mathrm{AC}(t)}{(1+r)^{Y_c - Y_b}}. \tag{2}$$

Here NPV is net present value, AC is annual cost, r is discount rate, Y_c is current year, and Y_b is base year.

As the result of dividing the total present value of the SFR nuclear fuel manufacturing facilities by the total present treatment quantity as a benefit, the levelized unit cost (LUC) for SFR nuclear fuel manufacturing facilities was calculated to be 5,311 $/kgHM.

5. The Break-Even Point Analysis

Generally, the break-even point is the point where total revenue equals total cost (i.e., the point of zero profit). Therefore, in this paper, only the SFR nuclear fuel manufacture cost is changed, and fixed values for all other costs were used to define the SFR nuclear fuel manufacturing cost in which the direct disposal is equal to the Pyro-SFR nuclear fuel cycle cost as the break-even point, as in (3) [12].

The direct disposal is considered applicable to vertical disposal in 500 m underground granitic rocks. The objects of disposal cost are limited to the deep geological repository with disposal capacity covering PWR spent fuel (20,000 tons) on the assumption that the PWR's initial enrichment is 4.5% and its burnup is 55 GWD/MtU. In addition, the cooling time is assumed to last for 10 years [13]:

$$\begin{aligned}&\mathrm{BEP}_{\text{SFR Fuel Manufacturing}}\\ &= \mathrm{TC}_D - \left(\mathrm{MC} + \mathrm{CC} + \mathrm{EC} + \mathrm{ISC} + \mathrm{RC}_{\text{Pyro}} + \mathrm{DC}_{\text{Pyro Waste}}\right)\\ &= 0.\end{aligned} \tag{3}$$

Here $\mathrm{BEP}_{\text{SFR Fuel Manufacturing}}$ is a breakeven point of the manufacturing cost of metallic SFR fuel for the direct disposal option, TC_D is the total cost of direct disposal option, MC is the raw material cost, CC is the conversion cost, EC is the enrichment cost, ISC is the interim storage cost, $\mathrm{RC}_{\text{Pyro}}$ is the pyroprocess cost, and $\mathrm{DC}_{\text{Pyro Waste}}$ is the disposal cost of the pyrowaste.

Additionally, if the break-even point is expressed in cost accounting, it could be expressed as [14]

$$\mathrm{BEP}_{\text{Accounting}} = \frac{\mathrm{FC}}{\mathrm{UCM}}. \tag{4}$$

Here FC is the fixed cost and UCM is the unit contribution margin.

In (4), the fixed cost is the investment cost of the SFR nuclear fuel manufacturing facilities, and the unit contribution margin is the value calculated by dividing the value of the subtraction of the variable cost from the total revenue by the output [14]:

$$\mathrm{UCM} = \frac{\mathrm{TR} - \mathrm{VC}}{\mathrm{Q}}. \tag{5}$$

Here TR is the total revenue, VC is the variable cost, and Q is the output.

In (5), the total revenue can be calculated as the fuel sales, and the variable cost can use the operation cost change

Table 6: Input data for economic assessment of SFR fuel.

Category	Unit	Reference	Minimum	Maximum
Uranium	\$/kgU	150	53	318
Conversion*	\$/kgU	6	3	9
Enrichment*	\$/SWU	165	84	210
Reprocessing cost				
UO_2 pyroprocess (reduction/refining)	\$/kgHM	781	373	1,866
SFR metal fuel pyroprocess	\$/kgHM	2,000	1,000	2,500
Fabrication cost				
UO_2 fuel*	\$/kgHM	256	206	307
SFR metal fuel	\$/kgHM	3,000	1,000	4,000
Storage cost*				
UO_2 S/F dry storage	\$/kgHM	180	78	392
UO_2 pyroprocess, HLW dry storage	\$/m^3	120,000	80,000	200,000
SFR pyroprocess, HLW dry storage	\$/m^3	120,000	80,000	200,000
Disposal cost				
LILW (long lived)*	\$/m^3	6,000	4,000	8,000
Packing (PWR SF)*	\$/kgHM	350	250	500
HLW (underground cost)	\$/m^3	1,200	600	2,000

*OECD/NEA, advanced nuclear fuel cycles and radioactive waste management, 2006 [7].

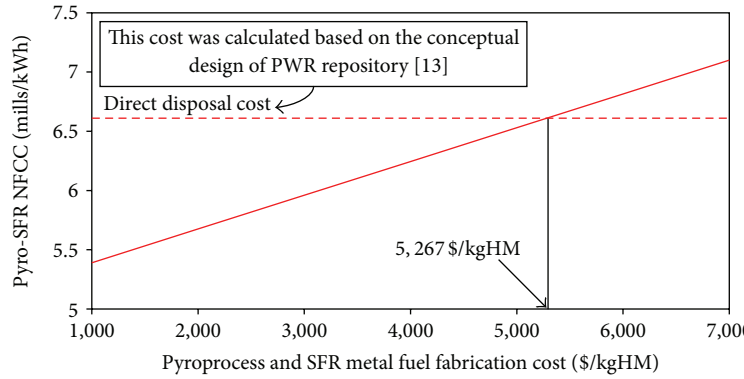

Figure 7: The break-even point of the manufacturing cost of SFR metallic nuclear fuel.

according to the output of the nuclear fuel of the SFR nuclear fuel manufacturing facilities. The output can also use the quantity of manufacturing of SFR nuclear fuel. Therefore, the break-even point obtained with the method of accounting means the quantity of the manufacturing of the SFR nuclear fuel, which makes the revenue equal to the cost. However, in this paper, through an analysis of the comparative cost of the direct disposal and Pyro-SFR nuclear fuel cycle, as in (3), rather than using the method of cost accounting, the break-even point of the SFR nuclear fuel manufacture cost was calculated. This is because the method of calculating the break-even point in the accounting method should use the past actual cost to make the reliability of the cost calculation results. Therefore, calculating the break-even point using the engineering cost estimation method, which uses the nuclear fuel cycle cost, can be regarded as a valid method whose accuracy is somewhat higher [15].

5.1. Input Data. The input data used to calculate the nuclear cycle cost can be largely divided into the economic data and technical data. In particular, the unit cost should be adjusted to the cost at which the inflation index is reflected in case a constant price is not used. Namely, it is necessary to calculate the cost fitting for a certain standard year. The input data is shown in Table 6. In addition, it is assumed that the cost of construction of the SFR is about 20% higher than that of light-water reactor [7].

5.2. The Break-Even Point Calculation Result. As a result of calculating the cost of the nuclear fuel cycle using the reference value in Table 6, the direct disposal cost was calculated to be 6.71 mills/kWh, and the Pyro-SFR fuel cycle cost was calculated to be 6.60 mills/kWh using (1).

In addition, as a result of calculating the break-even point of the manufacture cost of SFR metallic nuclear fuel for direct

Table 7: Equations for the direct disposal cost.

Recharge interval	$R_i = \frac{C_s}{N_b} \times \frac{\text{BU}}{\text{MWt} \times C_f \times 365}$ (Unit: year)
Generation cost	$C = F_c + V_c = \frac{C_{\text{uc}} \cdot R}{T \cdot U_r \cdot (1 - I_c)} + \text{NFCC}$
Quantity of fabrication	$\text{Qf}(t) = \frac{C_s}{N_b},\ t = \text{batch}$
Quantity of enrichment	$\text{Qe}(t) = \left[V(\text{EL}) + \left(\frac{\text{EL} - T_a}{\text{NAT} - T_a} - 1\right) \cdot V(T_a) - \frac{\text{EL} - T_a}{\text{NAT} - T_a} V(\text{NAT})\right] \text{Qf}(t)(1 + \text{LF})$
Quantity of conversion	$\text{Qc}(t) = \frac{\text{EL} - T_a}{\text{NAT} - T_a} \text{Qf}(t)(1 + \text{LF})$
Quantity of uranium	$\text{Qu}(t) = \text{Qc}(t)(1 + \text{LF})$
Spent fuel generation	$\text{Qsf}(t) = \frac{P365C_f}{\varepsilon \text{BU}}$
Cost of uranium	$\text{Cu} = \sum_t \frac{\text{Qu}(t) \cdot \text{UCu} \cdot (1 + E_{\text{U}})^{L(t) - \text{LEDu} - \text{YRc}}}{(1 + D)^{L(t) - \text{LEDu} - \text{YRp}}}$
Cost of conversion	$\text{Cc} = \sum_t \frac{\text{Qc}(t) \cdot \text{UCc} \cdot (1 + E_c)^{L(t) - \text{LEDc} - \text{YRc}}}{(1 + D)^{L(t) - \text{LEDc} - \text{YRp}}}$
Cost of enrichment	$\text{Ce} = \sum_t \frac{\text{Qe}(t) \cdot \text{UCe} \cdot (1 + E_e)^{L(t) - \text{LEDe} - \text{YRc}}}{(1 + D)^{L(t) - \text{LEDe} - \text{YRp}}}$
Cost of fabrication	$\text{Cf} = \sum_t \frac{\text{Qf}(t) \cdot \text{UCf} \cdot (1 + E_f)^{L(t) - \text{LEDf} - \text{YRc}}}{(1 + D)^{L(t) - \text{LEDf} - \text{YRp}}}$
Cost of transportation; applied LAG time	$\text{Ct} = \sum_t \frac{\text{Qsf}(t) \cdot \text{UCt} \cdot (1 + E_t)^{D(t) + \text{LAGt} - \text{YRc}}}{(1 + D)^{D(t) + \text{LAGt} - \text{YRp}}}$
Cost of storage	$\text{Cs} = \sum_t \frac{\text{Qsf}(t) \cdot \text{UCs} \cdot (1 + E_s)^{D(t) + \text{LAGs} - \text{YRc}}}{(1 + D)^{D(t) + \text{LAGs} - \text{YRp}}}$
Cost of disposal	$\text{Cd} = \sum_t \frac{\text{Qsf}(t) \cdot \text{UCd} \cdot (1 + E_d)^{D(t) + \text{LAGd} - \text{YRc}}}{(1 + D)^{D(t) + \text{LAGd} - \text{YRp}}}$
Total cost of direct disposal option	$\text{TC}_D = \text{Cu}(t) + \text{Cc}(t) + \text{Ce}(t) + \text{Cf}(t) + \text{Ct}(t) + \text{Cs}(t) + \text{Cd}(t)$

R_i: recharge interval, C_s: core size, N_b: total number of batches, BU: burn up, MWt: thermal power, C_f: load (Capacity) factor, $L(t)$: loading time, $D(t)$: discharging time, LED: lead times, LAG: lag times, F_c: fixed unit cost, V_c: variable unit cost, C_{uc}: construction unit cost (\$/kW), R: fixed charge rate, T: 8760 (=365 days × 24 hours), I_c: consumption rate in power plant, NFCC: nuclear fuel cycle cost, EL: enrichment of equilibrium core, NAT: enrichment of natural uranium, T_a: tail assay, LF: loss rate factor, $V(x) = (2x-1)\ln(x/(1-x))$, Cu: cost of uranium, Qu(t): quantity of uranium, P: capacity (MWe), ε: thermodynamic efficiency (MWe/MWt), UC: unit cost, UCu: unit cost of uranium, Eu: escalation rate of uranium, D: discount rate, YRt: base year, Qsf(t): quantity of spent fuel, $\text{TC}_D(t)$: total cost of direct disposal option, Cu(t): uranium cost, Cc(t): conversion cost, Ce(t): enrichment cost, Cf(t): fabrication cost, Ct(t): transportation cost, Cs(t): storage cost, Cd(t): disposal cost, t: years.

disposal using the equations in Table 7, the break-even point was calculated to be \$5,267/kgHM, as shown in Figure 7.

Therefore, the pyroprocess cost and the SFR metallic nuclear fuel manufacture cost, \$5,272/kgHM, exceeds the break-even point of \$5,267/kgHM slightly. Here, an inflation rate of 2.3% is applied because the inflation rate was specified as 2.3% in the Korea Radioactive Waste Management Law [16].

In addition, the cost difference between the break-even point and estimated cost of SFCF is within the relevant range of the uncertainty level of Class 3 in accordance with the general cost estimate classification matrix of AACE (the Association for the Advancement of Cost Engineering). It is expected that the calculated break-even point will be used as a valuable clue for estimating the economic feasibility of the SFR metallic nuclear fuel in the future.

6. Conclusions

The break-even point of the manufacturing cost of the SFR nuclear fuel using the nuclear fuel cycle cost was calculated to be \$5,267/kgHM. Namely, if the manufacturing cost of SFR metallic nuclear fuel including the pyroprocess cost is less than \$5,267/kgHM, we can say that the economic feasibility of the SFR metallic nuclear fuel in the Pyro-SFR nuclear cycle exists. In other words, if the SFCF cost excluding the pyroprocess cost of \$2,000/kgHM announced in the report of the OECD/NEA in 2006 is less than \$3,267, it can be judged that the economic feasibility of SFR metallic nuclear fuel exists.

In this paper, the investment cost of the manufacturing facilities of SFR nuclear fuel was estimated to be about 919 MUSD, the annual operation cost was about 149 MUSD,

and the decontamination and decommissioning cost was about 5 MUSD based on the price at the end of 2009. In addition, the levelized unit cost of the manufacturing of SFR metallic nuclear fuel including the pyroprocess cost was calculated to be 5,311 \$/kgHM, and it exceeded the break-even point \$5,267/kgHM. Therefore, based on the manufacturing cost of the metallic nuclear fuel the cost difference between the break-even point and the estimated cost of SFCF is not only small but also within the relevant range of the uncertainty level of Class 3 AACE estimate.

Manufacturing facilities of SFR nuclear fuel are presently in the stage of research and development, and no commercial scale processing equipment and facilities exist.

To reduce this uncertainty, therefore, is difficult to judge the economic feasibility. However, if the technology developments of a mass production pyroprocess system and SFR metallic nuclear fuel manufacturing facilities are enhanced, the economics of SFR metallic nuclear fuel are expected to be better.

Acknowledgment

This work was supported financially by the Ministry of Education, Science and Technology under the Mid- and Long-Term Nuclear R & D Project, and the authors express their sincere gratitude for supporting this important work.

References

[1] D. C. Wade and R. N. Hill, "The design rationale of the IFR," *Progress in Nuclear Energy*, vol. 31, no. 1-2, pp. 13–42, 1997.

[2] H. Ohmura, K. Mizuguchi, S. Kanamura et al., "Development of hybrid reprocessing technology based on solvent extraction and pyro-chemical electrolysis," *Progress in Nuclear Energy*, vol. 53, pp. 940–943, 2011.

[3] K. sungjin, *The Theory of Cost Estimation*, Dunam Press, Seoul, Republic of Korea, 2010.

[4] J. J. Laidler, L. Burris, E. D. Collins et al., "Chemical partitioning technologies for an ATW system," *Progress in Nuclear Energy*, vol. 38, no. 1-2, pp. 65–79, 2001.

[5] KAERI, "Development of Head-end Pyrochemical Reduction Process for Advanced Oxide Fuels," KAERI/RR-2939, 2007.

[6] C. E. Boardman, M. Thompson, C. E. Walter, and C. S. Ehrman, "The separations technology and transmutation systems (STATS) report -implications for nuclear power growth and energy sufficiency," *Progress in Nuclear Energy*, vol. 32, no. 3-4, pp. 411–419, 1998.

[7] OECD/NEA, *Advanced Nuclear Fuel Cycles and Radioactive Waste Management*, OECD Publishing, 2006, Appendix L.

[8] C. E. Till, Y. I. Chang, and W. H. Hannum, "The integral fast reactor-an overview," *Progress in Nuclear Energy*, vol. 31, no. 1-2, pp. 3–11, 1997.

[9] KAERI, "Preliminary Conceptual Design and Cost Estimation for SFR fuel cycle facility," KAERI/CM-1383, 2010.

[10] D. E. Shropshire, K. A. Williams, W. B. Boore et al., *Advanced Fuel Cycle Cost Basis*, Idaho National Laboratory, Idaho Falls, Idaho, USA, 2008.

[11] OECD/NEA, "The Economics of the Nuclear Fuel Cycle," Tech. Rep. NEA/EFC/DOC(93), 1993.

[12] KAERI, "Development of System Engineering Technology for Nuclear Fuel Cycle," KAERI/RR-3426, 2011.

[13] KAERI, "KAERI's spent fuel repository design evaluation and cost estimation," R&D Report 2003-02, 2003.

[14] M. Maryanne Mowen, R. don Hansen, and L. dan Heitger, *Managerial Accounting*, South-Western Press, 4th edition, 2012.

[15] S. K. Kim, W. I. Ko, H. D. Kim, S. T. Revankar, W. Zhou, and D. Jo, "Cost-benefit analysis of BeO-UO_2 nuclear fuel," *Progress in Nuclear Energy*, vol. 52, no. 8, pp. 813–821, 2010.

[16] "Ministry of Knowledge Economy," Radioactive Waste Management Law, Article 15, Section 1, 2009.

Hindawi Publishing Corporation
Science and Technology of Nuclear Installations
Volume 2013, Article ID 961360, 15 pages
http://dx.doi.org/10.1155/2013/961360

Research Article

Revisiting Statistical Aspects of Nuclear Material Accounting

T. Burr and M. S. Hamada

Los Alamos National Laboratory, Statistical Sciences Group, NM 87545, USA

Correspondence should be addressed to T. Burr; tburr@lanl.gov

Received 4 December 2012; Accepted 18 February 2013

Academic Editor: Michael F. Simpson

Nuclear material accounting (NMA) is the only safeguards system whose benefits are routinely quantified. Process monitoring (PM) is another safeguards system that is increasingly used, and one challenge is how to quantify its benefit. This paper considers PM in the role of enabling frequent NMA, which is referred to as near-real-time accounting (NRTA). We quantify NRTA benefits using period-driven and data-driven testing. Period-driven testing makes a decision to alarm or not at fixed periods. Data-driven testing decides as the data arrives whether to alarm or continue testing. The difference between period-driven and datad-riven viewpoints is illustrated by using one-year and two-year periods. For both one-year and two-year periods, period-driven NMA using once-per-year cumulative material unaccounted for (CUMUF) testing is compared to more frequent Shewhart and joint sequential cusum testing using either MUF or standardized, independently transformed MUF (SITMUF) data. We show that the data-driven viewpoint is appropriate for NRTA and that it can be used to compare safeguards effectiveness. In addition to providing period-driven and data-driven viewpoints, new features include assessing the impact of uncertainty in the estimated covariance matrix of the MUF sequence and the impact of both random and systematic measurement errors.

1. Introduction

One challenge in modern safeguards at declared facilities that process special nuclear material (SNM) is how to quantify the benefit of process monitoring (PM) [1–4]. There are many examples of PM data used in safeguards, such as neutron-based counting of a waste stream (the "hulls") exiting the dissolver in an aqueous reprocessing facility, or in-tank bulk mass measurements of solutions in tanks. Although there is no standard definition of PM data, it is generally collected very frequently (in-line), is often an indirect measurement of SNM, and is often collected by the operator for process control. Recent efforts to quantify the benefits of PM data are described, for example, in Burr et al. [1, 2].

Because PM can have several roles, it is necessary to consider the quantitative benefits of each possible role. For example, PM can have a "front-line" role in monitoring for indicators of facility misuse, such as a shift in nitric acid concentration to direct excess Pu to a waste stream from a separations area in an aqueous reprocessing facility [5]. Alternatively, in the role this paper considers, PM can enable in-process inventory estimation by using empirical modeling and measurements of flows in and out of a separations area [4]. In a pyroreprocessing facility, several PM options are being studied, such as monitoring voltage and current in the electrorefiner, which holds most of the in-process inventory [6–9]. Electrorefiner voltage and current are among the measured quantities that can, using a model such as the one in Zhang [10], predict the SNM inventory in the electrorefiner in real time.

Traditionally, nuclear material accounting (NMA) consists of relatively infrequent material balance closures (such as once per year), with the material balance (MB) defined as $\mathrm{MB} = I_{\mathrm{begin}} + T - I_{\mathrm{end}}$, where I is an inventory and T is a transfer. And, assuming that the MB has approximately a normal distribution (the assumption is justified because many measurements enter an MB calculation, so the central limit theorem is in effect), the measurement error standard deviation of the MB, σ_{MB}, determines the probability to detect a specified amount of SNM for a given false alarm probability. Therefore, for a single balance period, σ_{MB} is the main quantitative measure of safeguards effectiveness, with PM in

a support role without a quantitative measure of effectiveness. Similarly, for multiple balance periods, the covariance matrix Σ is the main quantitative measure of safeguards effectiveness, with single-period variances on the diagonal and between-period covariances on the off-diagonal. Some studies such as Burr et al. [1, 2] have considered data from PM used in another role not considered here, where PM data are put on the same statistical footing as NMA data (the MB sequences).

Toward the goal of quantifying the benefits of PM data, this paper revisits statistical methods for NMA and for frequent NMA, called, near-real-time accounting (NRTA). Both NMA and NRTA have been discussed in two main literature reviews, Speed and Culpin [11] and Goldman et al., 1982 [12]. Speed and Culpin [11] described some of the sequential tests used for NMA and advocated a controversial Bayesian approach to testing for loss of SNM. The controversy arose for the usual reasons in Bayesian approaches: the need to specify costs of wrong decisions and the need to specify a prior probability of SNM loss. Goldman et al. [12] speculated that NRTA would replace conventional NMA and described the important possibility of data falsification by the operator in the context of international safeguards. Here we consider the operator's MB sequence, so most directly address domestic safeguards. However, the operator's MB sequence is also used within the framework of international safeguards, along with the inspector's "difference" statistic.

NRTA is made possible by PM in the support role of enabling frequent material balance closures. The statistical methods include Shewhart charts based on multiple material balances during a year on MB data (the International Atomic Energy Agency refers to the MB sequence as the material unaccounted for, MUF, sequence), SITMUF (standardized independent transformed MUF) data, and a once-per-year balance based on the MUF data, known as CUMUF. The SITMUF sequence is a transform of the MUF sequence X given by $\widetilde{X} = C^{-1}X$ (where C is the Cholesky decomposition of Σ so that $\Sigma = CC^T$) that is independently and identically distributed as a normal random variance with mean 0 and variance 1 [13]. Therefore, the SITMUF sequence has an identity matrix as its covariance matrix, while the MUF sequence has a positive definite but otherwise arbitrary covariance matrix Σ.

As is customary in safeguards, entries in Σ are estimated using metrology of individual measurement methods and variance propagation to combine measurement error effects from multiple measurements [12, 14, 15]. After sufficient operating history, production facilities can typically estimate Σ reasonably well, with much of the uncertainty in the estimated entries (variances and covariances) in Σ arising from in-process inventory measurements whose quality is not well known. For example, Yamaha et al. [4] used measurements of flows in and out of a pulsed column at the Rokkasho aqueous reprocessing facility to estimate the SNM (Pu) in the column. The quality of such indirect SNM measurements is assessed using very limited data, typically from measurements of SNM that is recovered from infrequent equipment washout. Section 3.5 considers the impact of estimation error in Σ on estimated alarm probabilities from sequential testing.

We also consider joint cumulative sum or cusum (also known as Page's test) methods [16] for the multiple balance MUF and SITMUF data. Shewhart and cusum methods are studied with several forms of Σ with and without systematic measurement error in addition to random measurement error.

We revisit NRTA as a quantitative component of safeguards at declared facilities to monitor for SNM loss using both period-driven and data-driven testing. A period-driven approach makes a statistical decision to alarm or not at the end of each fixed period. A data-driven approach (also known as sequential testing) does not use a set decision period but instead decides as the data arrives whether to alarm or continue testing.

The difference between period-driven and data-driven viewpoints is illustrated simply by using both one-year and two-year periods, with sequential testing using a two-year truncation period serving as a surrogate for data-driven testing. For both one-year and two-year periods, conventional (period-driven) NMA using a once-per-year cumulative MUF (CUMUF, cumulative material unaccounted for) testing is compared to Shewhart and joint sequential cusum testing using either MUF or SITMUF (standardized, independently transformed MUF) data.

In addition to providing period-driven and data-driven viewpoints, new features include assessing the impact of uncertainty in the estimated covariance matrix of the MUF sequence and the impact of both random and systematic measurement errors.

There is interest in comparing pyroreprocessing to aqueous (and comparing several variations of aqueous) reprocessing with regard to proliferation resistance [6, 7]. With PM in the role of enabling NRTA to be performed (mainly by assisting with in-process inventory estimates), NRTA effectiveness can be compared by comparing Σ at a pyrofacility to Σ at an aqueous facility, and using data-driven testing, which we show in Section 2, is more appropriate than period-driven testing for NRTA.

The paper is organized as follows. Section 2 reviews and then describes our extensions to previous period-driven NMA studies. Section 3 gives numerical results of our simulation study. Section 4 describes our two-year truncated sequential test that is a surrogate for full-blown sequential testing. Section 5 is a summary.

2. One-Year Study

Avenhaus and Jaech [17] and Jones [18–23] studied period-driven testing, making a statistical decision to alarm or not once per year.

Avenhaus and Jaech [17] compared the annual CUMUF test to more frequent Shewhart testing and used the Neyman-Pearson lemma from classical statistical hypothesis testing to prove that if the loss vector is proportional to the row sums of Σ, $L \propto \Sigma 1^T$, then the CUMUF test has the highest alarm probability (AP). Assuming a loss of one significant quantity (SQ) over one year, testing for loss only (not gain), and setting the false alarm probability (FAP) to 0.05, the AP

is 0.95, provided $\sigma_{\mathrm{MB}} \leq (\mathrm{SQ}/3.3)$. The factor of 3.3 arises from double use of the value 1.65, which corresponds to both the 0.05 FAP and the 0.95 AP [1, 2].

In period-driven (annual) testing, Burr et al. [1, 2] point out that an adversary could divert a significant quantity (SQ) over 12 months by diverting one half SQ during year one and the other half during year two (e.g., from months 7 to 18). In that case, assuming the same 0.05 annual FAP, the 0.95 AP decreases to 0.75, because the per-year AP decreases from 0.95 to 0.50 and two-year AP $= 1 - 0.5^2 = 0.75$, which follows because the probability of nondetection over the two years is $1 - 0.5^2$. This simple example illustrates why we endorse data-driven testing over period-driven testing. The more relevant AP is 0.75 rather than 0.95 because it is unrealistic to assume the adversary will divert the entire SQ during a specific 12-month period. Also, "front-line" roles for PM are under evaluation [1, 2] in which data-driven testing will almost certainly be used. Therefore, for a fair comparison of NMA alone to PM alone to combined NMA and PM systems, it is helpful to assume that the same type of testing (data-driven or period-driven) will be used on all candidate safeguards system options.

In response to the "worst-case" loss scenario given previously from Avenhaus and Jaech [17], Jones [18–23] evaluated a statistical test consisting of two sequential cusum tests. The cusum test at period t for an abrupt threat is calculated as $S_{t,A} = \max(S_{t-1,A} + Z_t - K_A, 0)$, where Z_t is the quantity being monitored, such as the MUF sequence or the SITMUF sequence, and K_A is a control parameter. For a protracted threat, the cusum test at period t is calculated as $S_{t,P} = \max(S_{t-1,P} + Z_t, 0)$. As in the Shewhart test, the cusum tests alarm on period t if $S_{t,A} > 0$ or $S_{t,P} > H_P$ for an alarm threshold H_P. In using two cusum tests, Jones [18–23] aimed for high AP against abrupt (single-period) loss while still having almost as high AP against the "worst-case" protracted loss as the single CUMUF test (which has the highest possible AP for the "worst-case" loss). Of course any number of cusum tests could be used, but limiting to two cusum tests, one best for abrupt loss and the other best for protracted loss, seems to provide reasonable AP for a wide range of loss scenarios.

Avenhaus and Jaech [17] and Jones [18–23] ignored the impact of systematic errors on Σ and ignored the effects of estimation error in Σ. Therefore, one contribution of this paper is to redo these studies while considering impact of systematic measurement error. In addition, modern computational methods (we use the package mvtnorm in R from the R Development Core Team [24]) allow us to easily provide exact critical values for an FAP of 0.05 under the null hypothesis of no loss. Although both "exact" and "approximate" critical values are given in Avenhaus and Jaech [17], even the "exact" critical values were based on approximate numerical techniques. However, our study confirms that the reported APs in Avenhaus and Jaech are correct for the cases considered. We calculated the AP under various loss scenarios using the multivariate normal cdf (pmvnorm function in the mvtnorm package for R) for Shewhart tests applied to the MUF and SITMUF data. We used simulated multivariate normal data (10^5 sequences) to accurately estimate the AP for the cusum test applied to the MUF and SITMUF data.

We consider the following setup motivated by Avenhaus and Jaech [17] and Jones [18–23]:

(i) 48, 36, 24, 12, 6, 4, 1 balances per year, n.

(ii) $\sigma_I = 1$ for inventory ($\sigma_I = 1$ is the absolute standard deviation of the inventory measurement).

(iii) $\sigma_T = 0.1, 0.5, 1$ for transfers with associated total amount lost $M = 4, 6, 10$ the total threat amount over one year. Note that the σ_I to σ_T ratio varies as 10, 2, 1. For comparison to other methods, the APs for CUMUF are 0.85 for all three cases defined by $\sigma_T = 0.1, 0.5, 1$ for Σ_1 (a tridiagonal covariance matrix) and total loss $M = 4, 6, 10$ (actually, $M = 3.90, 5.99, 10.03$, resp., when our exact calculations replace Avenhaus's approximate calculations and we fix the CUMUF AP at 0.85 for all three cases). See the next point regarding MUF covariance matrices.

(iv) MUF covariance matrix

(a) Σ_1 is tridiagonal with variances equal to $2 \times \sigma_I^2 + (12/n) \times \sigma_T^2$ and off-diagonals equal to $-\sigma_I^2$ for elements (i, j) with $|i - j| = 1$. Note that the base case is for $n = 12$ as in Avenhaus and Jaech [17]. The negative correlation at lag 1 results from the previous balance ending inventory being the next balance beginning inventory. Jones [18–23] assumed a facility cleanout after each balance, so his covariance matrix is slightly different. Note that for this covariance matrix the sum of its entries is the same for all n, so the CUMUF variance does not depend on n, the number of balances per year. Specifically, for the tth balance, $X_t = I_t + T_t - I_{t-1}$ where σ_I and σ_T are the standard deviations of I_t and T_t, respectively. Then $\sigma_X^2 = 2\sigma_I^2 + \sigma_T^2$ for all t and $\mathrm{Cov}(X_{t-1}, X_t) = \mathrm{Cov}(X_t, X_{t+1}) = -\sigma_I^2$.

(b) Avenhaus and Jaech [17] and Jones [18–23] considered only random errors. Here we also consider systematic errors in the measurement error modeling. For the tth balance, $X_t = I_t + T_t - I_{t-1}$ where $\sigma_{I,\mathrm{ran}}$ and $\sigma_{I,\mathrm{sys}}$ are the random and systematic error standard deviations of I_t and $\sigma_{T,\mathrm{ran}}$ and $\sigma_{T,\mathrm{sys}}$ are the random and systematic error standard deviations of T_t. Then we have

$$\begin{aligned} &\mathrm{Var}\left(I_t + T_t - I_{i-1}\right) \\ &\quad = 2\sigma_{I,\mathrm{ran}}^2 + \sigma_{T,\mathrm{ran}}^2 + \sigma_{T,\mathrm{sys}}^2, \\ &\mathrm{Cov}\left(I_t + T_t - I_{t-1}, I_{t+1} + T_t - I_t\right) \\ &\quad = -\sigma_{I,\mathrm{ran}}^2 + \sigma_{T,\mathrm{sys}}^2, \end{aligned} \tag{1}$$

and for $j \geq 2$,

$$\mathrm{Cov}\left(I_{t+j} + T_t - I_{t+j-1}, I_t + T_t - I_{t-1}\right) = \sigma_{T,\mathrm{sys}}^2. \tag{2}$$

We let $\sigma_I^2 = \sigma_{I,\text{ran}}^2 + \sigma_{I,\text{sys}}^2$ and $\sigma_T^2 = \sigma_{T,\text{ran}}^2 + \sigma_{T,\text{sys}}^2$ with $\sigma_{I,\text{ran}}/\sigma_{I,\text{sys}}$ and $\sigma_{T,\text{ran}}/\sigma_{T,\text{sys}}$ both equal to 2 and 1; these are denoted by Σ_2 and Σ_3, respectively.

(v) The methods we consider are

(a) MUF for n balances, $X_1, \ldots, X_n$ with covariance matrix Σ.

(b) SITMUF for n balances, $\widetilde{X}_1, \ldots, \widetilde{X}_n$ with identity covariance matrix.

(c) CUMUF—one balance per year so CUMUF $= \sum_{i=1}^{n} X_i$, alarm if CUMUF $> C_{\text{CUMUF}}$ for critical value C_{CUMUF}.

(d) MUF Shewhart—multiple balances—alarm if any $X_i/\sqrt{\Sigma_{i,i}} > C_{\text{MUF,Shewhart}}$ for common critical value $C_{\text{MUF,Shewhart}}$.

(e) SITMUF Shewhart—multiple balances—alarm if any $\widetilde{X}_i > C_{\text{SITMUF,Shewhart}}$ for common critical value $C_{\text{SITMUF,Shewhart}}$.

(f) MUF joint cusum—two cusum streams, one for abrupt $H_A = 0$, one for protracted $K_P = 0$, compute cusum streams on normalized MUF $X_i/\sqrt{\Sigma_{i,i}}$, $Z_0 = 0$, $Z_{i,A} = \max(0, Z_{i-1} + (X_i/\sqrt{\Sigma_{i,i}} - K_A))$ and $Z_{i,P} = \max(0, Z_{i-1} + (X_i/\sqrt{\Sigma_{i,i}} - K_P))$. Alarm if $\max_i\{Z_{i,A}\} > H_A$ or $\max_i\{Z_{i,P}\} > H_P$. Find K_A and H_P so that FAP using protracted stream is 0.04 and the joint FAP using both streams is 0.05 following Jones [21, 22].

(g) SITMUF joint cusum—two cusum streams, one for abrupt $H_A = 0$, one for protracted $K_P = 0$, compute cusum streams on SITMUF $\widetilde{X}_i = C^T X_i$, $S_0 = 0$, $S_{i,A} = \max(0, S_{i-1} + (\widetilde{X}_i - K_A))$ and $S_{i,P} = \max(0, S_{i-1} + (\widetilde{X}_i - K_P))$. Alarm if $\max_i\{S_{i,A}\} > H_A$ or $\max_i\{Z_{i,P}\} > H_P$. Find K_A and H_P so that FAP using protracted stream is 0.04 and the joint FAP using both streams is 0.05 following Jones [21, 22].

(vi) Our approach: critical values are found exactly or by simulation (10^5 simulations). The APs (powers) are found exactly or by simulation (10^5 simulations).

(vii) Our performance criteria are as follows.

(a) For protracted threat, AP over one year.

(b) For abrupt threat, timeliness AP, AP within 30 days; 90 and 60 days for n equals 4 and 6, respectively. Jones [21] introduced timeliness AP.

(c) For protracted threat (same loss per balance), AP and expected loss. The AP is over the entire year and expected loss EL is computed as

$$\text{EL} = \sum_{i=1}^{n} L_i \times p_i + M \times \left(1 - \sum_{i=1}^{n} p_i\right), \tag{3}$$

where $L_i = (M/n)i$ is the cumulative loss after ith balance and p_i is the probability of alarming in the ith balance. The expected loss for CUMUF is M. Jones [21] introduced expected loss.

3. Results

3.1. Protracted Threat, AP. From Figure 1 for ($\sigma_T = 0.1$, $M = 4$), we make the following observations. The CUMUF APs (dashed lines) are smallest to largest in the order Σ_1 to Σ_2 to Σ_3 for $n \leq 12$ but are smallest to largest in the opposite order Σ_3 to Σ_2 to Σ_1 for $n \geq 24$. The SITMUF Shewhart dominates MUF Shewhart for Σ_1, but for Σ_2 and Σ_3, SITMUF Shewhart is only somewhat better than MUF Shewhart especially for large n. The SITMUF joint cusum dominates MUF joint cusum for Σ_1 especially for large n. For Σ_3, SITMUF joint cusum is only somewhat better than MUF joint cusum especially for large n. Note for large n, the SITMUF joint cusum dominates CUMUF.

From Figure 2 for ($\sigma_T = 0.5$, $M = 6$), we see that the CUMUF AP (dashed lines) decreases from Σ_1–Σ_3 for all n. The performance of SITMUF Shewhart, MUF joint cusum and SITMUF joint cusum decreases substantially for Σ_2 and Σ_3 for large n so that all these methods are not much better than MUF Shewhart. We see that for Σ_2 and Σ_3 and large n, MUF joint cusum is slightly better than SITMUF joint cusum. For Σ_3 and $n = 4$, MUF Shewhart is slightly better than SITMUF Shewhart. Note that SITMUF joint cusum dominates CUMUF only for Σ_3.

For the ($\sigma_T = 1$, $M = 10$) case, there are similar patterns except that for Σ_2 and Σ_3, the MUF versions are better than the SITMUF versions of Shewhart (for small n) and joint cusum (for large n).

We emphasize that what is new here is that we have identified different covariance matrices than considered previously where the SITMUF version does not dominate (have uniformly higher APs than) the MUF version and the joint cusum versions do not dominate CUMUF in terms of the AP.

3.2. Protracted Threat, Expected Loss. For CUMUF, the expected loss EL $= M$. From Figure 3 for ($\sigma_T = 0.1$, $M = 4$), all methods outperform CUMUF. The SITMUF versions outperform the MUF versions. We see that as n increases the joint cusum methods outperform the Shewhart methods. The methods do better going from Σ_1 to Σ_3 for $n \leq 12$ and do worse going from Σ_1 to Σ_3 for $n \geq 24$. The SITMUF joint cusum EL is less than 70% of CUMUF's especially for Σ_1, slightly worse for Σ_2 and somewhat more worse for Σ_3 for $n \geq 12$.

For ($\sigma_T = 0.5$, $M = 6$), all methods outperform CUMUF but not substantially for Σ_2 and Σ_3. All methods are similar for Σ_2 and Σ_3. Only for Σ_1 and especially for large n do the SITMUF versions outperform the MUF versions and the joint cusum methods outperform the Shewhart methods. The SITMUF joint cusum EL is less than 70% of CUMUF's only for Σ_1 and $n \geq 24$.

For ($\sigma_T = 1$, $M = 10$), similar observations hold as those for ($\sigma_T = 0.5$, $M = 6$). Here the SITMUF versions are not much better than the MUF versions. The SITMUF

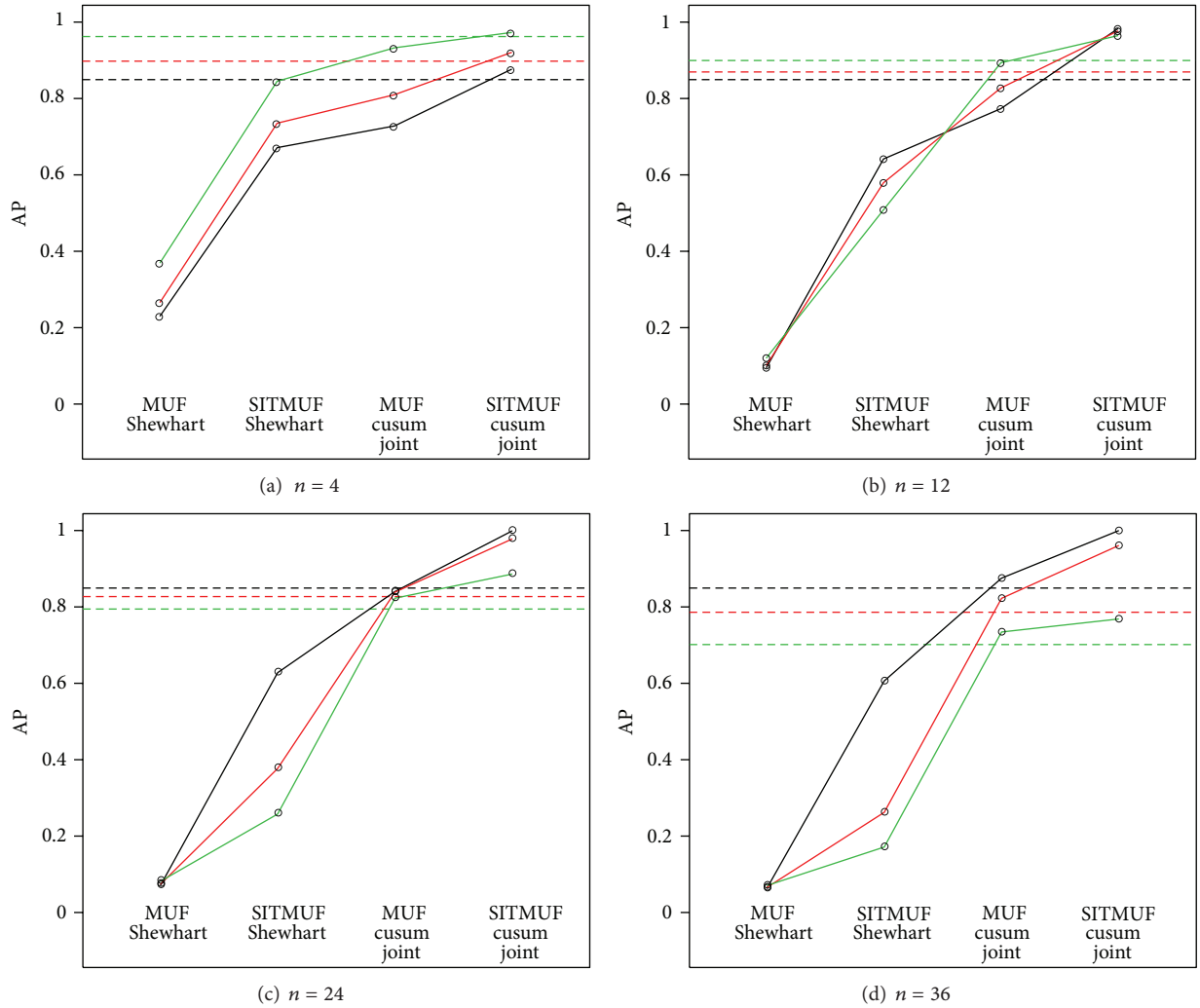

(a) $n = 4$ (b) $n = 12$

(c) $n = 24$ (d) $n = 36$

FIGURE 1: AP for protracted threat, $\sigma_T = 0.1$, $M = 4$. (Colors black, red, and green correspond to Σ_1–Σ_3. Dashed lines are for CUMUF.)

joint cusum EL is less than 75% of CUMUF's only for Σ_1 and $n \geq 24$.

3.3. Abrupt Threat, Timeliness AP. From Figure 4 for ($\sigma_T = 0.1$, $M = 4$), timeliness AP (TAP) improves going from Σ_1 to Σ_3 with the SITMUF Shewhart and joint cusum methods outperforming the MUF Shewhart method; the SITMUF Shewhart and joint cusum methods perform similarly.

For ($\sigma_T = 0.5$, $M = 6$), the performance is flat across all the methods and near 1.0 for all covariance matrices. Perhaps there is more differentiation for smaller M. The SITMUF joint cusum method is somewhat better than MUF joint cusum method for Σ_2 especially for larger n. Figures illustrating this case and other cases throughout the results sections are in Burr and Hamada [25], which is available upon request.

For ($\sigma_T = 1, M = 10$), the performance is flat across all the methods and near 1.0 for all covariance matrices. It is possible there would be differences in APs for smaller M.

3.4. Optimal Protracted Threat for CUMUF, AP. From Figure 5 we see that CUMUF outperforms the other methods for $\sigma_T = 0.5$, $M = 6$, as Avenhaus and Jaech [17] showed for MUF Shewhart under optimal protracted threat (MUF means are proportional to row sums of Σ). This holds for the other n values not shown here, and results are qualitatively similar for $\sigma_T = 0.1$, $M = 4$ and for $\sigma_T = 1$, $M = 10$.

3.5. SITMUF Joint Cusum. Here we consider the SITMUF joint cusum method performance as n varies in Figures 6–8. For protracted loss, Figure 6 shows that AP improves as n increases for Σ_1 but decreases as n increases for Σ_2 and Σ_3. Consequently, for Σ_2 and Σ_3, a small n is recommended. Note that the CUMUF AP plotted as dashed lines is a function of n and depends on the MUF covariance matrix.

From Figure 7(a) for protracted loss and ($\sigma_T = 0.1$, $M = 4$), EL improves as n increases for Σ_1 but first decreases and then increases as n increases for Σ_2 and Σ_3.

From Figures 7(b) and 7(c) for protracted loss and ($\sigma_T = 0.5$, $M = 6$) and ($\sigma_T = 1$, $M = 10$), EL decreases as n increases for Σ_1 but increases as n increases for Σ_2 and Σ_3.

From Figure 8 and abrupt loss, the timeliness AP (TAP) is quite high especially for $n \geq 24$. Note that in Figure 8, the

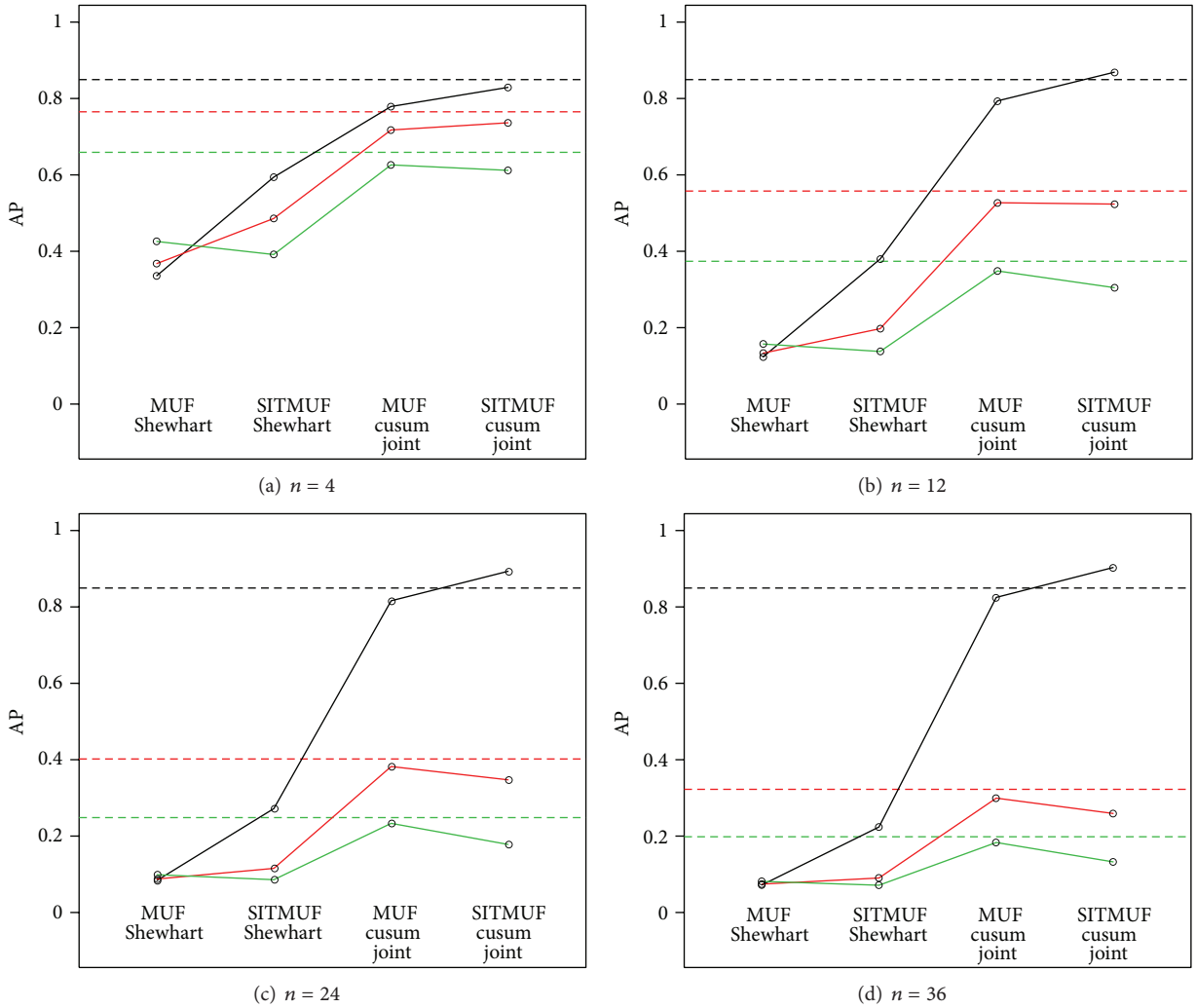

(a) $n = 4$ (b) $n = 12$

(c) $n = 24$ (d) $n = 36$

FIGURE 2: AP for protracted threat, $\sigma_T = 0.5$, $M = 6$. (Colors black, red, and green correspond to Σ_1–Σ_3. Dashed lines are for CUMUF.)

"30 Day AP" is actually "90 Day AP" and "60 day AP" for n equal to 4 and 6, respectively. We see that TAP increases from Σ_1 to Σ_3.

Jones [22] points out the serious drawback about the MUF joint cusum method; one needs to know the MUF covariance ahead of time in order to set up the method. Consequently, the SITMUF joint cusum method is preferred from this practical point of view. However, while the SITMUF joint cusum generally has higher AP over most of the situations considered here, we show in Section 3.7 that the MUF join cusum can have just as large an AP.

3.6. SITMUF Cusum or Joint Cusum Robustness to MUF Covariance Matrix. As mentioned in Section 1, production facilities with some operation history can reasonably expect to achieve approximately 15% relative estimation error in the entries in Σ. That is, we chose the 15% variation as being a typical amount by which estimated entries in Σ might vary from the respective true values. Recall that Σ is estimated using variance propagation applied to measurement control data collected from the same instruments as those making the NMA measurements.

As a convenient way to introduce measurement error in the MUF covariance matrix Σ, we use sample MUF covariance matrices based on 50 to 100 samples that produce samples variances and covariances that vary about 15% relative to the true values.

To study robustness to estimation error in $\widehat{\Sigma}$, previous analyses were repeated with estimated (rather than true) covariance matrices. For example, for the SITMUF cusum, using the MUF covariance matrix Σ_2 with $\sigma_I = 1$ and $\Sigma_T = 0.5$, with $\sigma_{I,\text{ran}} = \sigma_{I,\text{sys}}$, and $\sigma_{T,\text{ran}} = \sigma_{T,\text{sys}}$, for $n = 12$ balances per year, the nominal FAP of 0.05 varied from 0.04 to 0.06 across 1000 simulations when $\widehat{\Sigma}$ was fixed without error $\widehat{\Sigma} = \Sigma$. When $\widehat{\Sigma}$ was estimated using 100 samples, the FAP varied from 0.033 to 0.070 and when estimated using 200 samples, the FAP varied from 0.029 to 0.077. The alarm probabilities showed a similar sensitivity to estimation error in $\widehat{\Sigma}$. When the number of balance periods was increased to $n = 24$ per year, the FAP varied from 0.11 to 0.12 (using the

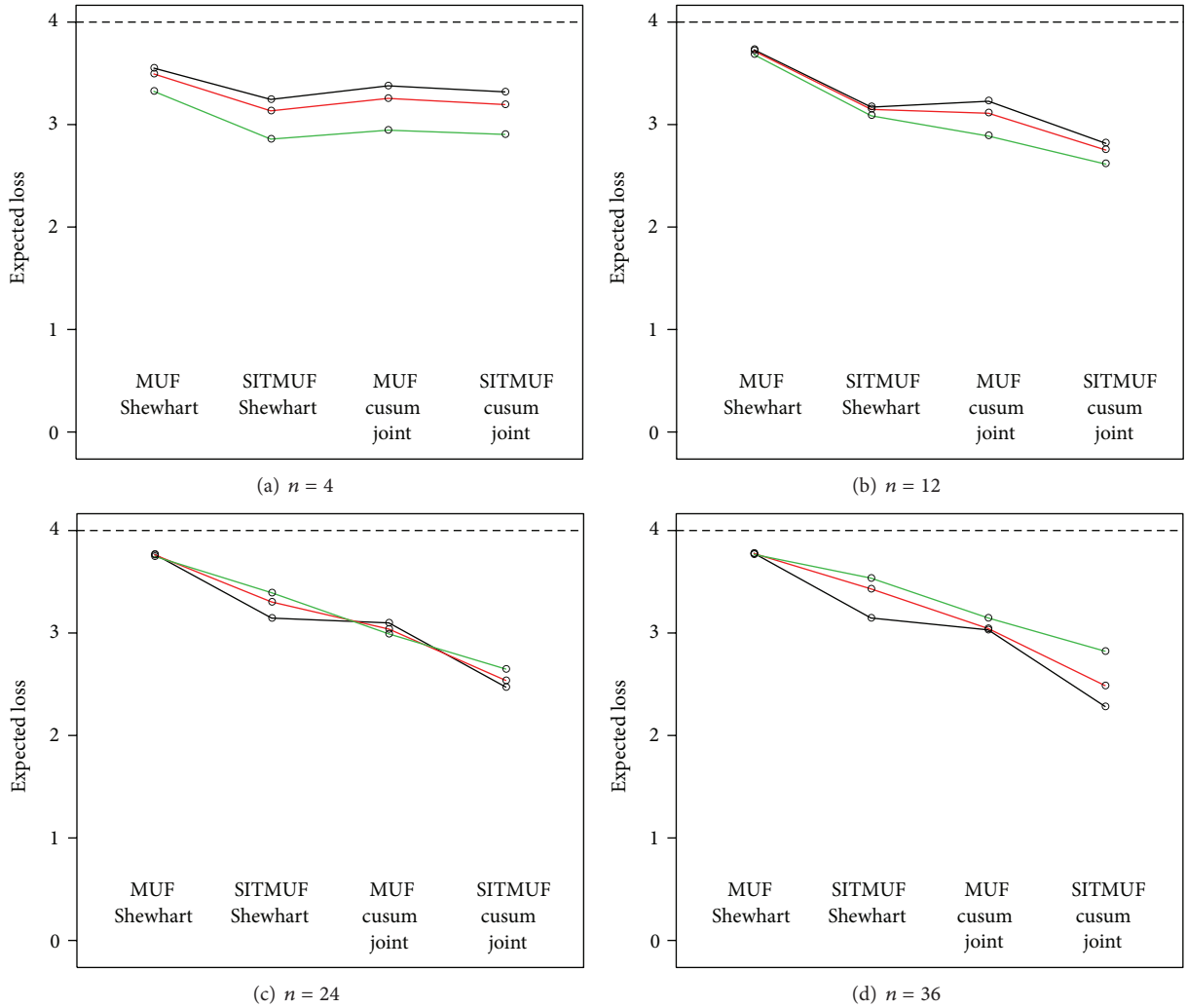

FIGURE 3: Expected loss for protracted threat, $\sigma_T = 0.1$, $M = 4$. (Colors black, red, and green correspond to Σ_1–Σ_3. Dashed lines are for CUMUF.)

same alarm threshold as in the $n = 12$ case) and from 0.09 to 0.14 when using 100 samples.

Similarly, for the SITMUF joint cusum, the critical values we used were based on the true MUF covariance matrix, and the FAP increases on average from 0.05 to 0.055 and the 0.05 and 0.95 quantiles across 1000 realizations of the estimated Σ are approximately 0.05 and 0.06, respectively (depending on the case, as defined by n_T, σ_I, and σ_T). The 0.05 and 0.95 quantiles in the APs across 1000 realizations of the estimated Σ are approximately 0.67 and 0.68, respectively (depending on the case).

These findings for the SITMUF cusum or joint cusum suggest robustness to 15% estimation error in Σ. Note for comparison that if only a single MUF value is considered and Σ is the scalar σ, then 15% estimation error in σ also increases the FAP on average from 0.05 to 0.055, but the 0.05 and 0.95 quantiles are 0.02 and 0.11, respectively, and are 0.34 and 0.66 for a mean shift of 2σ. So if only a single balance period is considered, then 15% measurement error in σ leads to large uncertainty in the true FAP and true AP. But when a matrix of, for example, 12-by-12 variances and covariances in a sequence of 12 MUFs has 15% estimation error in each entry, apparently there is friendly cancellation of effect, leading to small changes in the FAPs and APs.

We find that the estimated APs are robust by being nearly the same as in the situation of having zero error in Σ.

3.7. Threat Scenarios in Which MUF Outperforms SITMUF for the Joint Cusum Method. In a real facility, Σ is rarely known in advance of a processing campaign so it must be estimated at each balance period. For that reason, there is a logistic advantage in using tests based on the SITMUF sequence rather than the MUF sequence. The advantage is that the SITMUF sequence is iid $N(0, 1)$ if no loss has occurred, so it is relatively simple to control the FAP for any type of testing.

Regarding a possible performance advantage of SITMUF over MUF, this section shows that on average across random loss scenarios, the AP for SITMUF-based testing is the same as the AP for MUF-based testing. Note that because the SITMUF sequence $\widetilde{X}$ is a transform of the MUF sequence X

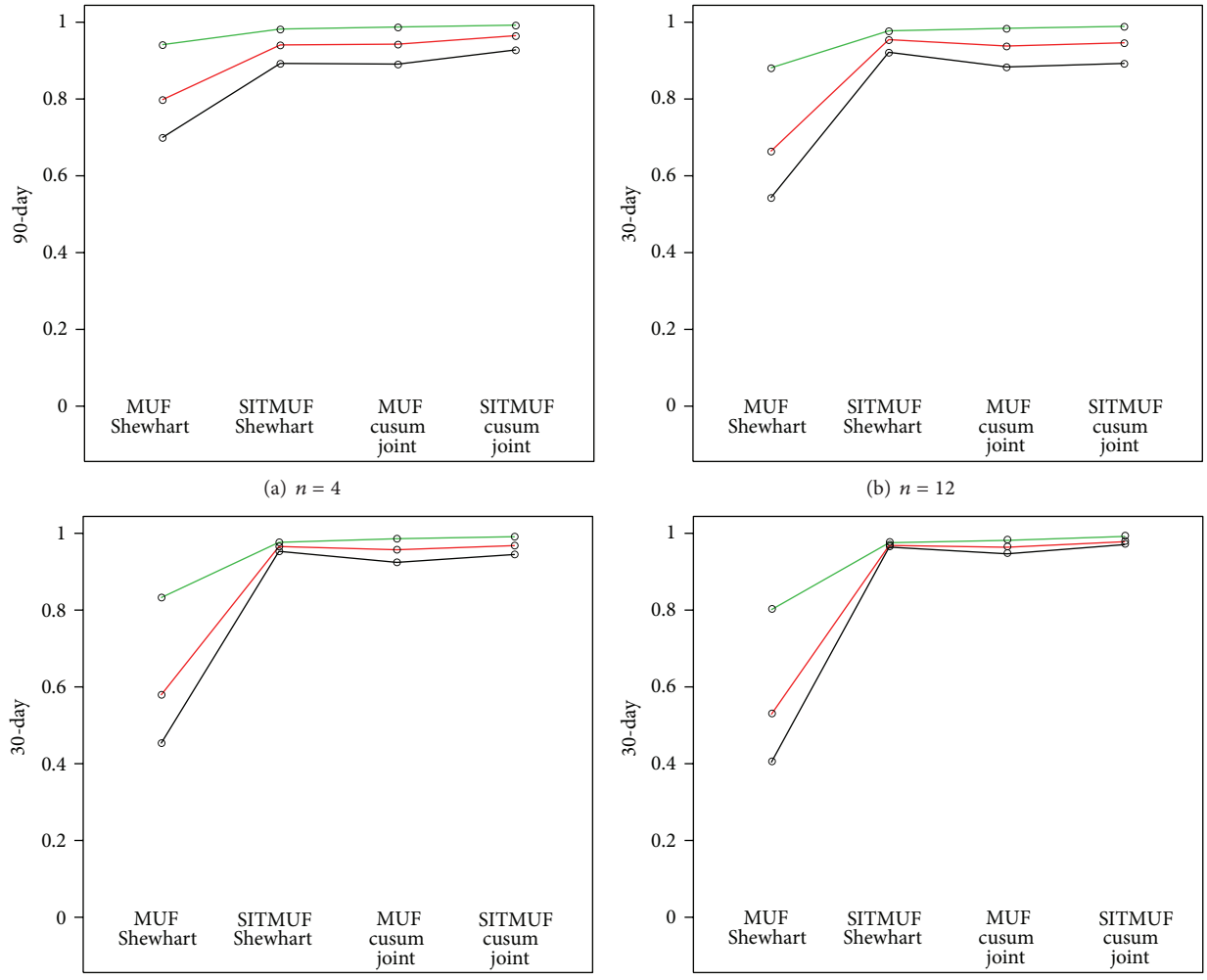

(a) $n = 4$ (b) $n = 12$

(c) $n = 24$ (d) $n = 36$

Figure 4: Timeliness AP for abrupt threat, $\sigma_T = 0.1$, $M = 4$. (Colors black, red, and green correspond to Σ_1–Σ_3.)

given by $\widetilde{X} = C^T X$ (where C is the Cholesky decomposition of Σ so that $\Sigma = CC^T$), a test based on SITMUF with loss $\widetilde{L} = CL$ will have statistically the same behavior as a test based on MUF with loss L. By "statistically the same behavior," we mean that the average AP across many realizations of the SITMUF sequence is the same for the SITMUF with loss $\widetilde{L} = CL$ as for the MUF with loss L (which we confirmed using simulation in R).

Burr and Hamada [25] evaluate the APs for MUF and for SITMUF for the study reported previously (MUF joint cusum AP minus SITMUF joint cusum AP so that a positive value means that the MUF-based method has higher AP).

Burr and Hamada [25] give results for cases 1–3 corresponding to Σ_1–Σ_3. Under each case, there are matrices for the three σ_T's (0.1, 0.5, 1). The matrices are 7 rows by 5 columns. The 7 rows correspond to n equal to 48, 40, 36, 24, 12, 6, and 4. The 5 columns correspond to threat scenarios: none, protracted with even loss each balance, protracted with even loss every other balance, abrupt loss at balance $(n/2) + 1$, and protracted loss that CUMUF is guaranteed to dominate according to Avenhaus and Jaech [17].

We also used a genetic algorithm (GA) to find scenarios which maximizes the MUF versus SITMUF difference. We considered 8 cases defined by $n = 12, 36$, MUF covariance matrices Σ_1, Σ_3, and $\sigma_T = 0.1, 1$ (and associated $M = 4, 10$). We ran the GA for 25 generations or stopped sooner if the best MUF versus SITMUF difference stopped changing. There is no guarantee that the GA found the scenario with the maximum difference but it does find several with positive differences that are too large to explain by chance.

4. Two-Year Study

To contrast period-driven (make a statistical decision to alarm or not once per year, e.g.,) from data-driven testing (make a statistical decision to alarm or not on the fly, as data arrives), we can mimic data-driven testing by comparing a two-year study with truncated sequential testing to a one-year period-driven study.

We consider five covariance matrices for two years. These correspond to (1) no cleanout, no systematic measurement error, and the other four have systematic measurement

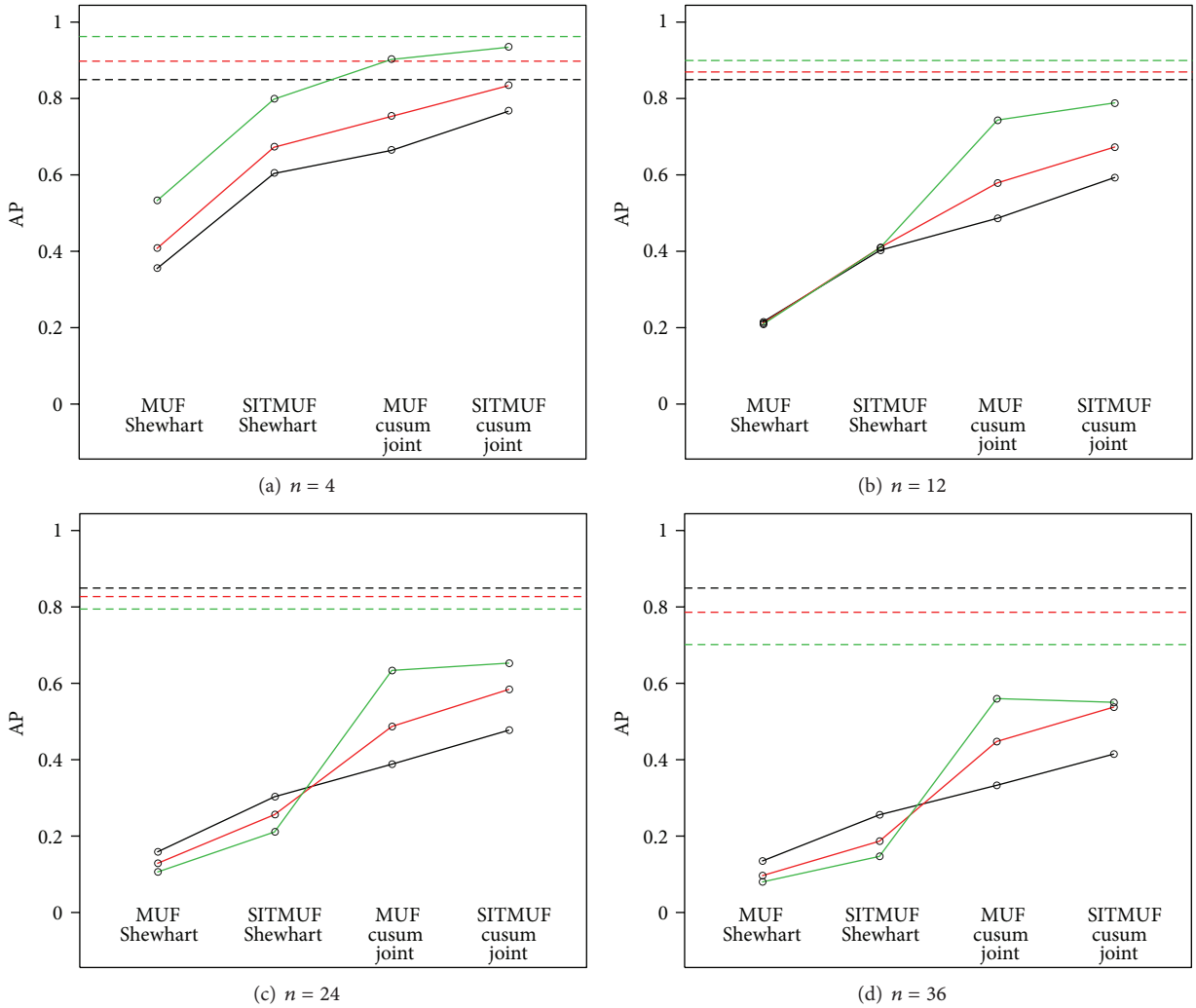

FIGURE 5: AP for optimal protracted threat for CUMUF, $\sigma_T = 0.1$, $M = 4$. (Colors black, red, and green correspond to Σ_1–Σ_3. Dashed lines are for CUMUF.)

error with (2) no cleanout, with measurement calibration, (3) no cleanout, without measurement calibration, (4) with cleanout, with measurement calibration, (5) with cleanout, with measurement calibration.

4.1. A&J/Jones Model. Avenhaus and Jaech [17] assume only random error components for I_t and T_t, inventory and transfer at the tth balance. There is no cleanout and no systematic measurement error. We have the tth balance, $X_t = I_t + T_t - I_{t-1}$ where σ_I and σ_T are standard deviations of I_t and T_t, respectively. Then $\sigma_X^2 = 2\sigma_I^2 + \sigma_T^2$ for all t and $\mathrm{Cov}(X_{t-1}, X_t) = \mathrm{Cov}(X_t, X_{t+1}) = -\sigma_I^2$. A&J use values $\sigma_I = 1$ and $\sigma_T = 0.5$ based on 12 balance periods per year. If there are n balance periods per year, then $\sigma_T^2 = (12/n)0.5^2$.

The scenarios in the remainder of this section have systematic measurement error.

4.2. Extended Model, No Cleanout, with Measurement Calibration. In the remaining sections we consider both random and systematic error components for I_t and T_t. Avenhaus and Jaech [17] and Jones [18] considered only random errors. We have the tth balance, $X_t = I_t + T_t - I_{t-1}$ where $\sigma_{I,\mathrm{ran}}$ and $\sigma_{I,\mathrm{sys}}$ are the random and systematic error standard deviations of I_t and $\sigma_{T,\mathrm{ran}}$ and $\sigma_{T,\mathrm{sys}}$ are the random and systematic error standard deviations of T_t. Then we have for the first year:

$$\begin{aligned} \mathrm{Var}\left(I_t + T_t - I_{i-1}\right) &= 2\sigma_{I,\mathrm{ran}}^2 + \sigma_{T,\mathrm{ran}}^2 + \sigma_{T,\mathrm{sys}}^2, \\ \mathrm{Cov}\left(I_t + T_t - I_{t-1}, I_{t+1} + T_{t+1} - I_t\right) &= -\sigma_{I,\mathrm{ran}}^2 + \sigma_{T,\mathrm{sys}}^2, \end{aligned} \tag{4}$$

and for $j \geq 2$,

$$\mathrm{Cov}\left(I_{t+j} + T_{t+j} - I_{t+j-1}, I_t + T_t - I_{t-1}\right) = \sigma_{T,\mathrm{sys}}^2. \tag{5}$$

For multiple years, the covariance matrix is block diagonal, except the last balance of one year and the first balance of the next year, where

$$\mathrm{Cov}\left(I_n + T_n - I_{n-1}, I_{n+1} + T_{n+1} - I_n\right) = -\sigma_{I,\mathrm{ran}}^2, \tag{6}$$

and for the first balance of one year and the first balance of the next year, where

$$\mathrm{Cov}\left(I_1 + T_n - I_1, I_0 + T_{n+1} - I_n\right) = -\sigma_{I,\mathrm{sys}}^2. \tag{7}$$

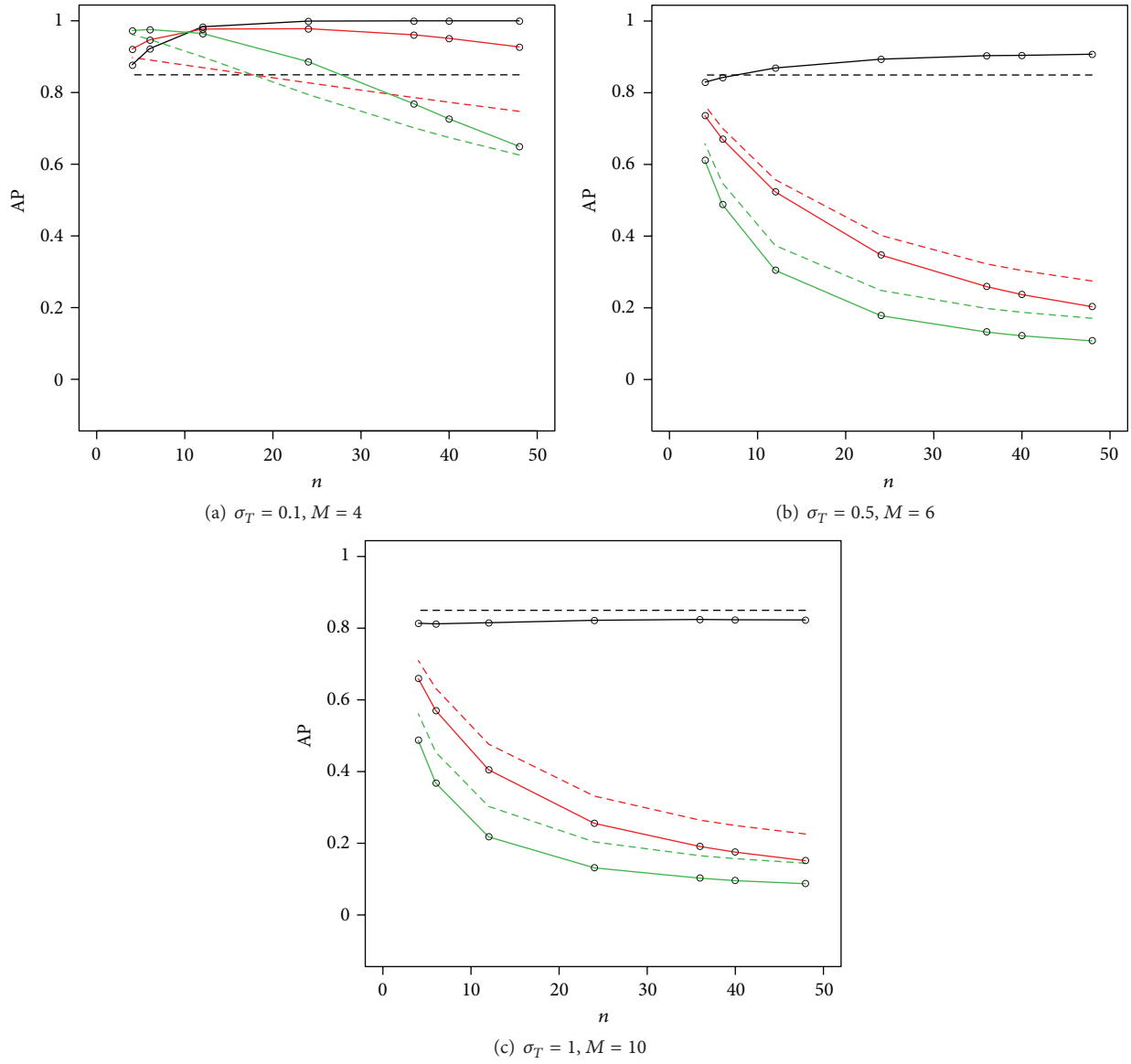

(a) $\sigma_T = 0.1$, $M = 4$

(b) $\sigma_T = 0.5$, $M = 6$

(c) $\sigma_T = 1$, $M = 10$

FIGURE 6: AP for protracted threat using SITMUF joint cusum for $n = 4, 6, 12, 24, 36, 40, 48$. (Colors black, red, and green correspond to Σ_1–Σ_3. Dashed lines are for CUMUF.)

4.3. Extended Model, No Cleanout, No Measurement Calibration. We have the tth balance, $X_t = I_t + T_t - I_{t-1}$ where $\sigma_{I,\text{ran}}$ and $\sigma_{I,\text{sys}}$ are the random and systematic error standard deviations of I_t and $\sigma_{T,\text{ran}}$ and $\sigma_{T,\text{sys}}$ are the random and systematic error standard deviations of T_t. Then we have

$$\begin{aligned} \text{Var}\left(I_t + T_t - I_{i-1}\right) &= 2\sigma_{I,\text{ran}}^2 + \sigma_{T,\text{ran}}^2 + \sigma_{T,\text{sys}}^2, \\ \text{Cov}\left(I_t + T_t - I_{t-1}, I_{t+1} + T_{t+1} - I_t\right) &= -\sigma_{I,\text{ran}}^2 + \sigma_{T,\text{sys}}^2, \end{aligned} \tag{8}$$

and for $j \geq 2$,

$$\text{Cov}\left(I_{t+j} + T_{t+j} - I_{t+j-1}, I_t + T_t - I_{t-1}\right) = \sigma_{T,\text{sys}}^2. \tag{9}$$

This holds for multiple years.

4.4. Extended Model, Cleanout, Measurement Calibration. We have the tth balance, $X_t = I_t + T_t - I_{t-1}$ where $\sigma_{I,\text{ran}}$ and $\sigma_{I,\text{sys}}$ are the random and systematic error standard deviations of I_t and $\sigma_{T,\text{ran}}$ and $\sigma_{T,\text{sys}}$ are the random and systematic error standard deviations of T_t. Because of cleanout, I_0 and I_n are zero with no associated measurement error. Then we have for the first year:

$$\begin{aligned} \text{Var}\left(I_1 + T_1\right) &= \sigma_{I,\text{ran}}^2 + \sigma_{I,\text{sys}}^2 + \sigma_{T,\text{ran}}^2 + \sigma_{T,\text{sys}}^2, \\ \text{Var}\left(T_n - I_{n-1}\right) &= \sigma_{I,\text{ran}}^2 + \sigma_{I,\text{sys}}^2 + \sigma_{T,\text{ran}}^2 + \sigma_{T,\text{sys}}^2, \\ \text{Var}\left(I_t + T_t - I_{t-1}\right) &= 2\sigma_{I,\text{ran}}^2 + \sigma_{T,\text{ran}}^2 + \sigma_{T,\text{sys}}^2, \\ \text{Cov}\left(I_1 + T_1, I_2 + T_2 - I_1\right) &= -\sigma_{I,\text{ran}}^2 + \sigma_{T,\text{sys}}^2. \end{aligned} \tag{10}$$

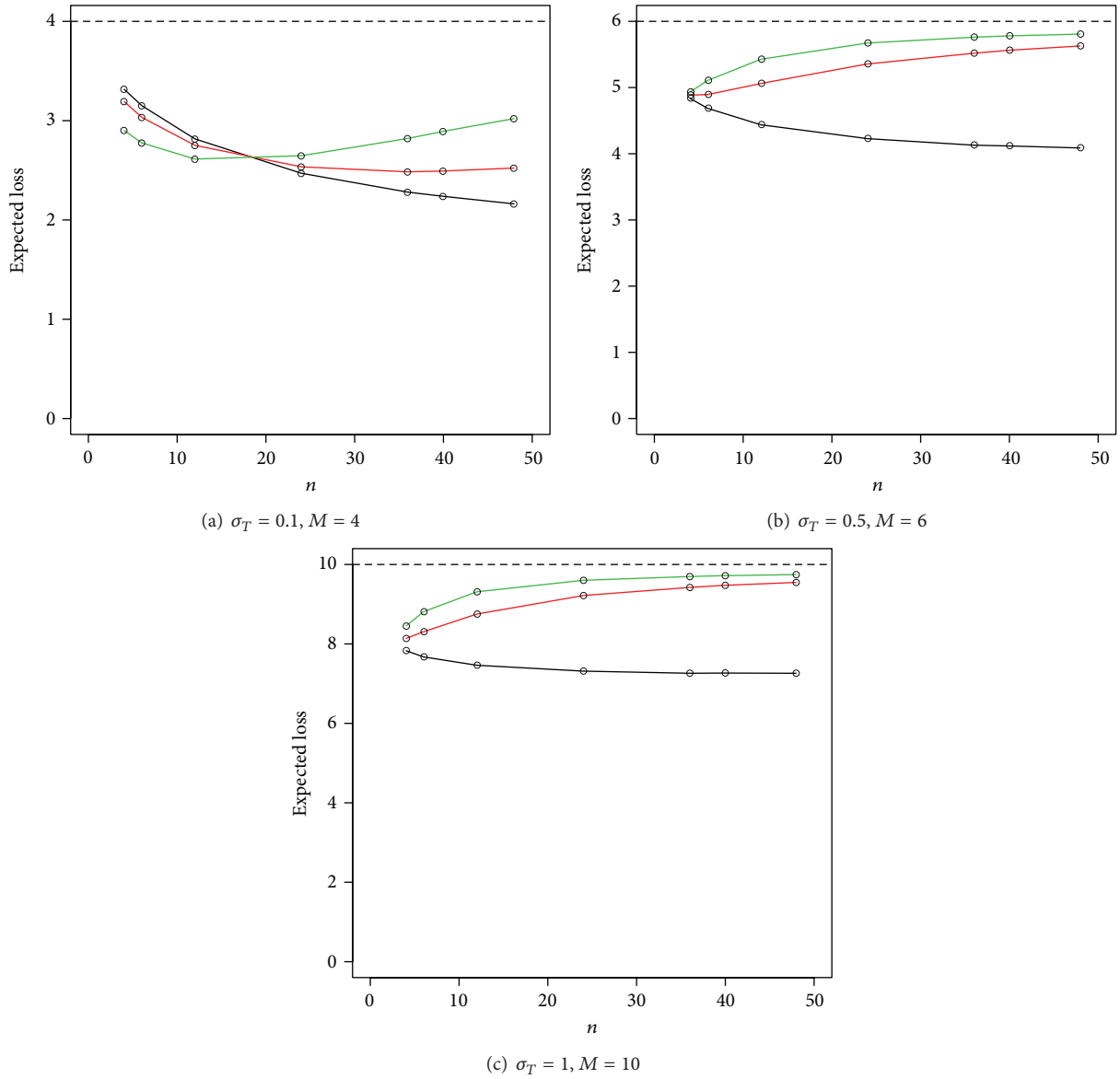

(a) $\sigma_T = 0.1, M = 4$

(b) $\sigma_T = 0.5, M = 6$

(c) $\sigma_T = 1, M = 10$

FIGURE 7: Expected loss for protracted threat using SITMUF joint cusum for $n = 4, 6, 12, 24, 36, 40, 48$. (Colors black, red, and green correspond to Σ_1–Σ_3. Dashed lines are for CUMUF.)

For $3 \le t \le n-1$,

$$\operatorname{Cov}\left(I_1 + T_1, I_t + T_t - I_{t-1}\right) = \sigma^2_{T,\text{sys}},$$

$$\operatorname{Cov}\left(I_1 + T_1, T_n - I_{n-1}\right) = -\sigma^2_{I,\text{sys}} + \sigma^2_{T,\text{sys}}, \tag{11}$$

$$\operatorname{Cov}\left(I_{n-1} + T_{n-1} - I_{n-2}, T_n - I_{n-1}\right) = -\sigma^2_{I,\text{ran}} + \sigma^2_{T,\text{sys}}.$$

For $2 \le t \le n-2$,

$$\operatorname{Cov}\left(I_t + T_t - I_{t-1}, T_n - I_{n-1}\right) = \sigma^2_{T,\text{sys}}. \tag{12}$$

For $2 \le t \le n-2$,

$$\operatorname{Cov}\left(I_t + T_t - I_{t-1}, I_{t+1} + T_{t+1} - I_t\right) = -\sigma^2_{I,\text{ran}} + \sigma^2_{T,\text{sys}}. \tag{13}$$

For $t \ge 2$, $j \ge 2$, and $t + j \le n - 1$,

$$\operatorname{Cov}\left(I_t + T_t - I_{t-1}, I_{t+j} + T_{t+j} - I_{t+j-1}\right) = \sigma^2_{T,\text{sys}}. \tag{14}$$

For multiple years, the covariance matrix is block diagonal.

4.5. Extended Model, Cleanout, No Measurement Calibration. We have the same covariances for balances within the same year as given in the preceding scenario. The Appendix gives what has to be added for years 1 and 2 which applies to all pairs of years.

4.6. Results. The FAP is set at $0.0975 = 1 - 0.95^2$ over two years. We compare the CUMUF and SITMUF joint cusum. The protracted loss cusum FAP is 0.08 and the joint cusum

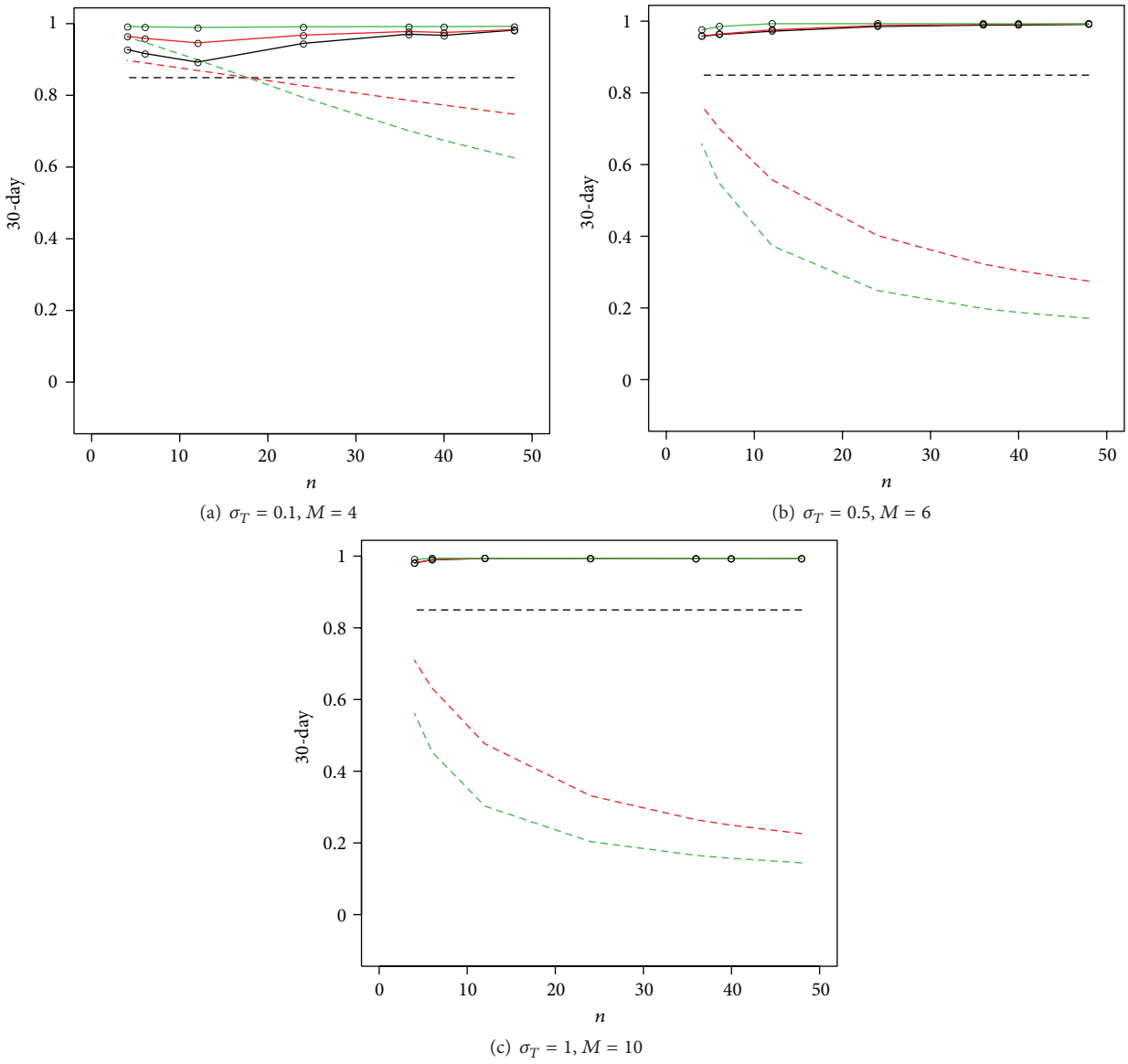

(a) $\sigma_T = 0.1$, $M = 4$

(b) $\sigma_T = 0.5$, $M = 6$

(c) $\sigma_T = 1$, $M = 10$

FIGURE 8: Timeliness AP for abrupt threat using SITMUF joint cusum for $n = 4, 6, 12, 24, 36, 40, 48$. (Colors black, red, and green correspond to Σ_1–Σ_3. Dashed lines are for 1-year CUMUF.)

FAP is 0.0975. We consider the loss scenario of even loss across the last half of the first year and the first half of the second year with total loss of M; the values of M used are the same as before that depend on σ_T.

First we compare the APs from Σ_1–Σ_5 in Figure 9.

The APs for loss over two years of $M/2$ and $M/4$ are qualitatively similar to those shown in Figure 9.

Next we compare SITMUF joint cusum with CUMUF for Σ_1, Σ_4, and Σ_5 in Figure 10. Results for a two-year loss of $M/2$ and $M/4$ are somewhat different than the results for a two-year loss of M as in Figure 10 [25].

5. Summary

We have considered process monitoring in the support role of enabling NRTA. In most facilities, frequent balance closure is made possible by process monitoring to aid in estimating in-process inventory. We have evaluated options for NRTA, extending results from the safeguards literature by presenting both data-driven and period-driven views, including the effects of systematic measurement errors in several distinct covariance matrices Σ for a sequence of material balances. The quantitative effect of estimation error in Σ was also evaluated.

Our main summary points are the following.

(i) In evaluating NRTA data, data-driven (sequential) testing is more appropriate than period-driven testing. However, the Neyman-Pearson lemma for fixed-period testing is convenient (as shown by [17]) for identifying the worst-case loss scenario and calculating the corresponding detection probability, provided

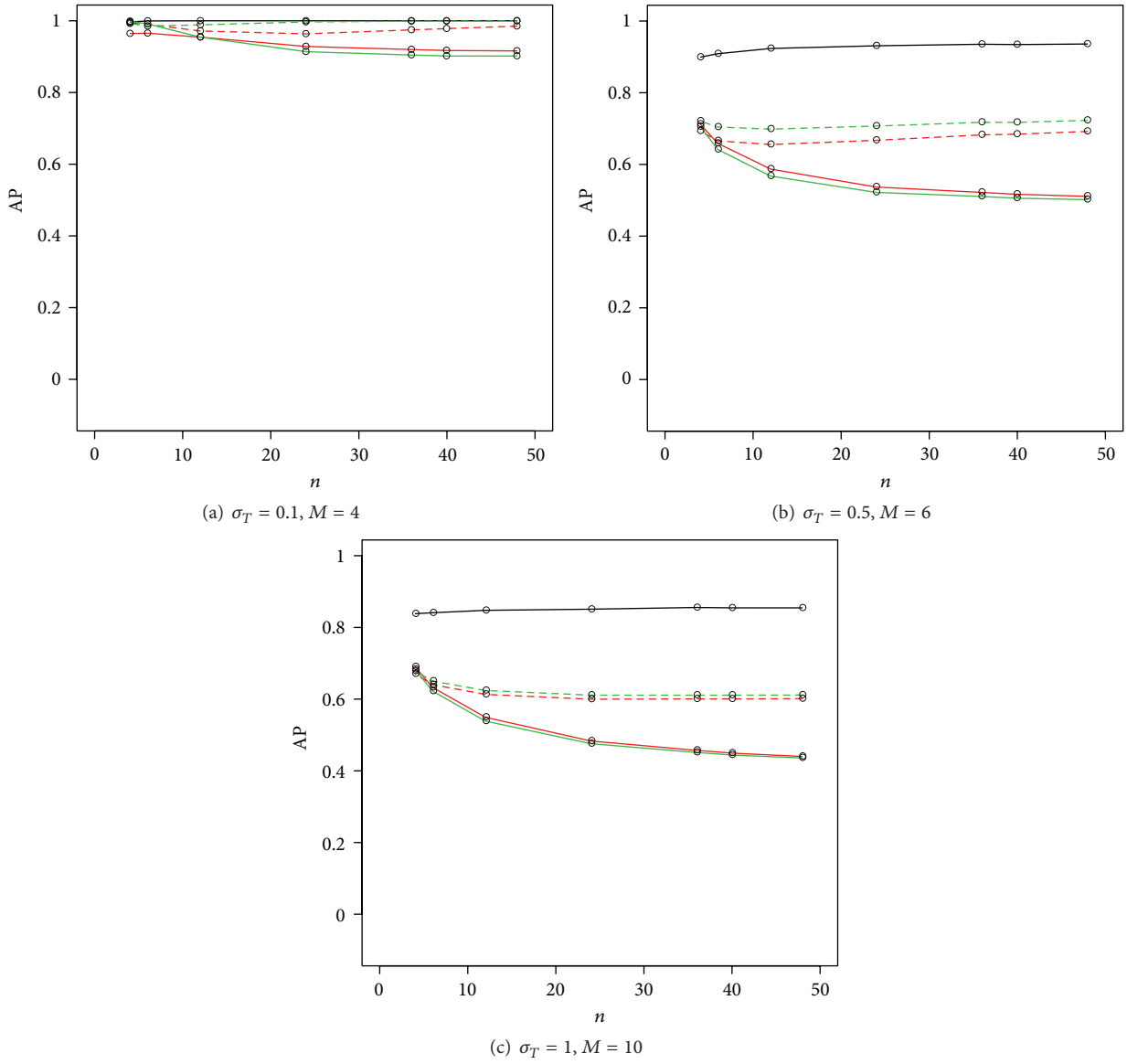

(a) $\sigma_T = 0.1, M = 4$

(b) $\sigma_T = 0.5, M = 6$

(c) $\sigma_T = 1, M = 10$

FIGURE 9: AP for protracted threat using SITMUF joint cusum for $n = 4, 6, 12, 24, 36, 40, 48$ (colors black Σ_1, solid red Σ_2, dashed red Σ_3, solid green Σ_4, dashed green Σ_5). Loss of two years is M.

one assumes that the loss occurs over the particular 12-month period being evaluated.

(ii) For system studies such as those presented in Sections 2–4, data-driven testing can be evaluated using period-driven (truncated) sequential testing over long periods. For example, the IAEA goal is to detect abrupt or protracted (over 1 year) diversion with high probability. To detect diversion over 1 year, it is adequate to consider a 2-year period truncated version of the cusum (Page's) sequential test.

(iii) In sequential testing, there is no analogue to the classic Neyman-Pearson lemma to identify the best test. However a joint cusum test as in Jones [18] is recommended as a good compromise that balances the competing goals of having large AP for abrupt loss and reasonably large AP for protracted loss. For logistic convenience in system studies and because entries in Σ become known at each balance period rather than in advance, it is best to apply the joint cusum to the SITMUF rather than to the MUF sequence. For suitably transformed loss vector, the AP is the same for the joint cusum applied to the SITMUF or to the MUF sequence; therefore, there is no performance advantage in using the SITMUF sequence rather than MUF sequence.

(iv) Our numerical study of robustness to estimation error in Σ suggests that at least 15% relative standard deviation in the entries in Σ can be present with quite small effects on the APs.

(v) Our inclusion of systematic errors in the measurements that are involved in estimating Σ clearly shows

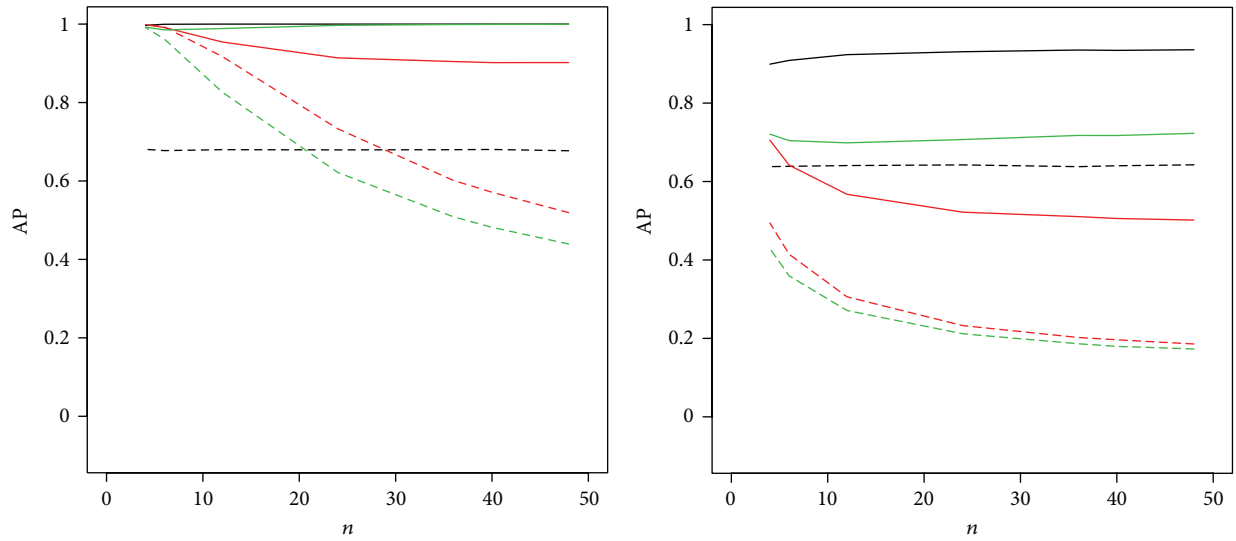

(a) $\sigma_T = 0.1$, $M = 4$

(b) $\sigma_T = 0.5$, $M = 6$

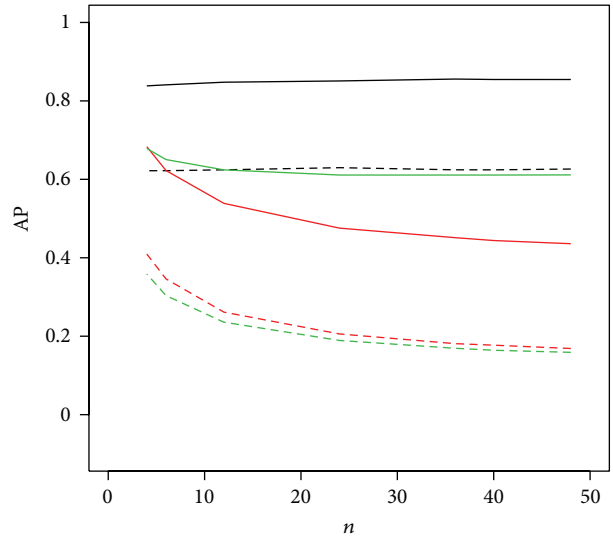

(c) $\sigma_T = 1$, $M = 10$

FIGURE 10: AP for protracted threat using SITMUF joint cusum versus CUMUF for $n = 4, 6, 12, 24, 36, 40, 48$. (Colors correspond to black Σ_1, red Σ_4, and green Σ_5. Solid is SITMUF joint cusum and dashed is CUMUF.) Loss of two years is M.

that systematic errors have an important impact on Σ and therefore also on APs.

(vi) We concur with Avenhaus and Jaech [17] and Jones [18] that NRTA is not a panacea, because NRTA does not increase APs for protracted loss, even in data-driven testing. That is, using PM to enable NRTA will not solve the known dilemma that protracted loss is difficult to detect. However, PM in other front-line roles could detect specified protracted loss for which the PM option is tuned to detect [1, 2].

There are other possible roles for PM in safeguards, so future work will quantify the benefit of PM in possible roles other than enabling NRTA.

Appendix

Section 4.5 Additional Results

This appendix gives what has to be added to Section 4.5 results for years 1 and 2 and applies to all pairs of years:

$$\begin{aligned} \mathrm{Cov}\left(I_1 + T_1, I_{n+1} + T_{n+1}\right) &= \sigma^2_{I,\mathrm{sys}} + \sigma^2_{T,\mathrm{sys}}, \\ \mathrm{Cov}\left(T_n - I_{n-1}, I_{n+1} + T_{n+1}\right) &= -\sigma^2_{I,\mathrm{sys}} + \sigma^2_{T,\mathrm{sys}}. \end{aligned} \tag{A.1}$$

For $n + 2 \le k \le 2n - 1$,

$$\begin{aligned} \mathrm{Cov}\left(I_1 + T_1, I_k + T_k - I_{k-1}\right) &= \sigma^2_{T,\mathrm{sys}}, \\ \mathrm{Cov}\left(I_1 + T_1, T_{2n} - I_{2n-1}\right) &= -\sigma^2_{I,\mathrm{sys}} + \sigma^2_{T,\mathrm{sys}}. \end{aligned} \tag{A.2}$$

For $2 \le j \le n-1$,

$$\begin{aligned} \mathrm{Cov}\left(I_j + T_j - I_{j-1}, T_{2n} - I_{2n-1}\right) &= \sigma^2_{T,\mathrm{sys}}, \\ \mathrm{Cov}\left(T_n - I_{n-1}, T_{2n} - I_{2n-1}\right) &= \sigma^2_{I,\mathrm{sys}} + \sigma^2_{T,\mathrm{sys}}. \end{aligned} \tag{A.3}$$

For $2 \le j \le n-1$ and $n+2 \le k \le 2n-1$,

$$\mathrm{Cov}\left(I_j + T_j - I_{j-1}, I_k + T_k - I_{k-1}\right) = \sigma^2_{T,\mathrm{sys}}. \tag{A.4}$$

For $2 \le j \le n-1$,

$$\mathrm{Cov}\left(I_j + T_j - I_{j-1}, I_{n+1} + T_{n+1}\right) = \sigma^2_{T,\mathrm{sys}}. \tag{A.5}$$

For $n+2 \le j \le 2n-1$,

$$\mathrm{Cov}\left(T_n - I_{n-1}, I_j + T_j - I_{j-1}\right) = \sigma^2_{T,\mathrm{sys}}. \tag{A.6}$$

Acknowledgments

The authors acknowledge support from the National Nuclear Security Administration Office of Nuclear Nonproliferation Research and Development (NA-22) and Nuclear Energy (NE) programs.

References

[1] T. Burr, A. Bakel, S. Bryan et al., "Roles for process monitoring in nuclear safeguards at aqueous reprocessing plants," *Journal of Nuclear Materials Management*, vol. 40, no. 2, pp. 42–53, 2012.

[2] T. Burr, M. S. Hamada, M. Skurikhin, and B. Weaver, "Pattern recognition options to combine process monitoring and material accounting data in nuclear safeguards," *Statistics Research Letters*, vol. 1, no. 1, pp. 6–31, 2012.

[3] M. Suzuki, M. Hori, S. Nagaoka, and T. Kimura, "Study on loss detection algorithms using tank monitoring data," *Journal of Nuclear Science and Technology*, vol. 46, no. 2, pp. 184–192, 2009.

[4] K. Yamaha, S. Nobuharu, T. Iseki, A. Kawai, and T. Iwamoto, "Plutonium inventory estimation of extraction cycles at Rokkasho reprocessing plant," in *Proceedings 50th Annual Meeting of the Institute of Nuclear Materials Management*, 2009.

[5] A. Bakel, T. Burr, S. Demuth et al., "A dissolver diversion scenario illustrating the value of process monitoring," in *Proceedings of the 52nd Annual Meeting of the Institute of Nuclear Materials Management*, 2011.

[6] T. Burr and M. Skurikhin, "Proliferation evaluation criteria in next-generation reprocessing options: combining process monitoring with nuclear material accounting for improved safeguards," Tech. Rep. LAUR 22504, Los Alamos National Laboratory, 2012.

[7] M. Fukushima, T. Nagai, H. Kofuji, H. Hirano, and M. Myochin, "Development of measurement techniques for density and liquid level of molten salt to assess an inventory in equipment of pyro-reprocessing," in *Proceedings of the 51st Annual Meeting of the Institute of Nuclear Materials Management*, 2010.

[8] R. O. Hoover, S. Phongikaroon, M. F. Simpson, S. X. Li, and T. S. Yoo, "Development of computational models for the mark-IV electrorefiner—effect of uranium, plutonium, and zirconium dissolution at the fuel basket-salt interface," *Nuclear Technology*, vol. 171, no. 3, pp. 276–284, 2010.

[9] M. Simpson and S. Hermann, "Modeling the pyrochemical reduction of spent UO_2 fuel in a pilot-scale reactor," INL/CON 06-11597, 2006.

[10] J. Zhang, "EChem modeling: a kinetic model for electrorefining based on diffusion control," Report, Los Alamos National Laboratory, 2011.

[11] T. Speed and D. Culpin, "The role of statistics in nuclear materials accounting: issues and problems," *Journal of the Royal Statistical Society B*, vol. 149, no. 4, pp. 281–313, 1986.

[12] A. Goldman, R. Picard, and J. Shipley, "Statistical methods for nuclear materials safeguards: an overview," *Technometrics*, vol. 24, no. 4, pp. 267–275, 1982.

[13] R. R. Picard, "Sequential analysis of materials balances," *Nuclear Materials Management*, vol. 15, no. 2, pp. 38–42, 1987.

[14] K. Zhao, M. Penkin, C. Norman et al., "International target values 2010 of measurement uncertainties in safeguarding nuclear materials," Technical Paper STR-368, International Atomic Energy Agency, 2010, http://www.inmm.org/.

[15] T. Burr, G. Hemphill, V. Longmire, and M. Smith, "The impact of combining nuclear material categories on uncertainty," *Nuclear Instruments and Methods in Physics Research, Section A*, vol. 505, no. 3, pp. 707–717, 2003.

[16] E. Page, "Continuous inspection scheme," *Biometrika*, vol. 41, pp. 100–115, 1954.

[17] R. Avenhaus and J. Jaech, "On subdividing material balances in time and/or space," *Nuclear Materials Management*, vol. 10, no. 3, pp. 24–33, 1981.

[18] B. Jones, "Calculation of diversion detection using the SITMUF sequence and page's test: application to evaluation of facility designs," in *Proceedings of the 7th ESARDA Symposium on Safeguards and Nuclear Material Management*, Liege, Belgium, 1985.

[19] B. Jones, "Calculation of diversion detection using the SITMUF sequence and page's test: response to abrupt and protracted diversion," in *Proceedings of the International Symposium on Nuclear Material Safeguards*, IAEA-SM-293/23, Vienna, Austria, 1986.

[20] B. Jones, "Comparison of near real time materials accountancy using SITMUF and page's test with conventional accountancy," in *Proceedings of the 9th ESARDA Symposium on Safeguards and Nuclear Material Management*, London, UK, 1987.

[21] B. Jones, "Near real time materials accountancy using SITMUF and a joint page's test: dependence of response on balance frequency," in *Proceedings of the 3rd International Conference on Facility Operations-Safeguards Interface*, San Dieg, Calif, USA, 1987.

[22] B. Jones, "Near real time materials accountancy using SITMUF and a joint page's test: comparison with MUF and CUMUF tests," *ESARDA Bulletin*, vol. 15, pp. 20–26, 1988.

[23] B. Jones, "Near real time materials accountancy using SITMUF and a joint page's test: improvement of the test," *ESARDA Bulletin*, vol. 16, pp. 13–19, 1989.

[24] R Development Core Team R, "A Language and Environment for Statistical Computing," R Foundation for Statistical Computing, Vienna, Austria, 2004, http://www.R-project.org/.

[25] T. Burr and M. S. Hamada, "Revising statistical aspects of nuclear material accounting," Report LAUR12-26303, Los Alamos National Laboratory, 2012.

Hindawi Publishing Corporation
Science and Technology of Nuclear Installations
Volume 2013, Article ID 590684, 10 pages
http://dx.doi.org/10.1155/2013/590684

Research Article

Solution Monitoring Evaluated by Proliferation Risk Assessment and Fuzzy Optimization Analysis for Safeguards in a Reprocessing Process

Mitsutoshi Suzuki and Norichika Terao

Department of Science and Technology for Nuclear Material Management, Japan Atomic Energy Agency, 2-4 Shirane, Shirakata, Tokai-mura, Naka-gun, Ibaraki-ken 319-1195, Japan

Correspondence should be addressed to Mitsutoshi Suzuki; suzuki.mitsutoshi@jaea.go.jp

Received 21 November 2012; Accepted 17 January 2013

Academic Editor: Jack D. Law

Solution monitoring (SM) has been used in a nuclear reprocessing plant as an additional measure to provide assurance that the plant is operated as declared. The inline volume and density monitoring equipment with dip tubes is important for safety and safeguards purposes and is a typical example of safeguards by design (SBD). Recently safety, safeguards, and security by design (3SBD) are proposed to promote an efficient and effective generation of nuclear energy. In 3SBD, proliferation risk assessment has the potential to consider likelihood of the incidence and proliferation risk in safeguards. In this study, risk assessment methodologies for safeguards and security are discussed and several mathematical methods are presented to investigate risk notion applied to intentional acts of facility misuse in an uncertainty environment. Proliferation risk analysis with the Markov model, deterrence effect with the game model, and SBD with fuzzy optimization are shown in feasibility studies to investigate the potential application of the risk and uncertainty analyses in safeguards. It is demonstrated that the SM is an effective measurement system using risk-informed and cost-effective SBD, even though there are inherent difficulties related to the possibility of operator's falsification.

1. Introduction

As a result of greenhouse warming and increased energy demand, a global trend to introduce nuclear power into emerging countries has been a growing and increasing concern from the international society about the consequent impact on safety, safeguards, and security (3S). Introducing 3S mechanisms in an efficient and effective manner will require not only a balance between economic utilization of energy resource and mandatory installment of 3S countermeasures, but also intercooperation between those practices and implementation. The 3S initiative was launched at the Hokkaido Toyako Summit of 2008 by G8 countries [1] and was partly driven by the fact that the emerging nuclear countries are struggling with lack of national legal and technical expertise. The goals of the 3S initiative are to ensure that countries planning to use nuclear energy are supported by strong national programs and to prove to the international audience that the programs are purely peaceful and that nuclear material is properly handled, accounted for, and protected.

A systematic approach to enhance the timely, efficient and cost-effective integration of safety objectives, material control and accountability, and physical protection into the overall initial planning phase for a nuclear fuel facility may be applied for the introduction of nuclear energy by the "3S by design (3SBD)" methodology in which 3S countermeasures are considered in the design stage of those nuclear facilities [2, 3]. In comparison with numerous safety installations, one of the well-known achievements in safeguards is the solution monitoring (SM) system that was installed into the Rokkasho reprocessing plant (RRP) in the initial design phase as an output of safeguards by design (SBD) activities. Although SM prior to the RRP was limited to the solution storage area in the Tokai reprocessing plant, SM in the RRP includes all tanks in the main process line, containing 12 authenticated and 80 unauthenticated SM instruments. In a modern large

reprocessing plant, the SM system plays an important role as an additional measure to provide assurance of the facility operation as declared and also measurement instrument for solution volume and density to verify in-process inventory.

In order to promote the designing work in a quantitative manner, the effective and time-consuming installment of countermeasures could be encouraged by risk assessment to enhance reliability, robustness, and transparency of nuclear facilities in an explicit and implicit manner. Probabilistic safety assessment (PSA) has been developed for several decades in safety and is noted again after the Fukushima accident to perform severe accident analysis. Although safeguards and security communities have different histories and encounter technical aspects due to the inherent nature of intentional and malicious acts, probabilistic risk approach (PRA) should be investigated to pursue cost-effective implementation. In the existing regulations of safeguards and security, it would be not so straightforward that the risk notion is applied to inherent threat and hazard recognition. In addition, the risk notion sometime leads to political and sociological concerns and has not been well discussed so far in an international community. However, in order to enhance the 3SBD methodologies, an integrated risk-informed approach is explored with attention to the scarcity of intentional acts in safeguards and the secrecy of actual incident data in security.

In this paper, we will show the SM system as an example of SBD and will investigate the risk assessment methodologies that could be applied to the integrated risk approach for 3S assessment. In feasibility studies SM will be shown as advanced measurement technologies to ensure an operational transparency and a full obedience of safeguards implementation.

2. Solution Monitoring

In international safeguards, quantitative and timely judgments regarding the location and movement of special nuclear material (SNM) are performed to ensure that there is no loss or unauthorized removal of SNM [4]. Nuclear material accounting (NMA) is used to confirm the quantity of SNM in all declared locations and measurement error uncertainty plays an essential role in NMA. Material balance (MB) closure is conducted after plant shutdown and cleanout measures to move material into measureable locations, so that the time-consuming procedure is conducted on annual basis as physical inventory verification (PIV). As increasing throughput of a reprocessing plant, NMA requires frequent MB with the concept of near-real-time accounting (NRTA) to meet the timeliness goals of international safeguards criteria without shutdown and flush-out as interim inventory verification (IIV). Because the timeliness goals are deterministic and are defined by the conversion time, more frequent inventory verification would become mandatory in a large reprocessing plant dealing with high-burnup fuels if the safeguards measures heavily rely on NMA alone.

Due to concerns about proliferation risk that have been recognized as an important aspect of 3S and about requirement of the timeliness goal of the IAEA safeguards, modern reprocessing facilities should be provided with SM to increase safeguardability [5] as well as to respond to the requirement. As SM in conventional PUREX facilities, the level, density, and temperature (LDT) measurements of tanks are performed in SM management system (SMMS) [6]. Because NMA is a component in the IAEA safeguards, IIV by measurement and/or estimation is mandatory verification in NRTA. SM has become a tool of international safeguards and provides additional assurance that the plant is operated as declared. In addition to this, SM is utilized for partial SNM accounting in which tank volume is measured by SM and the SNM concentration is estimated by an empirical formula that is a function of acidity. However, the frequent NMA is still costly and inefficient, so that an enhanced SM application has been investigated to reduce this burden.

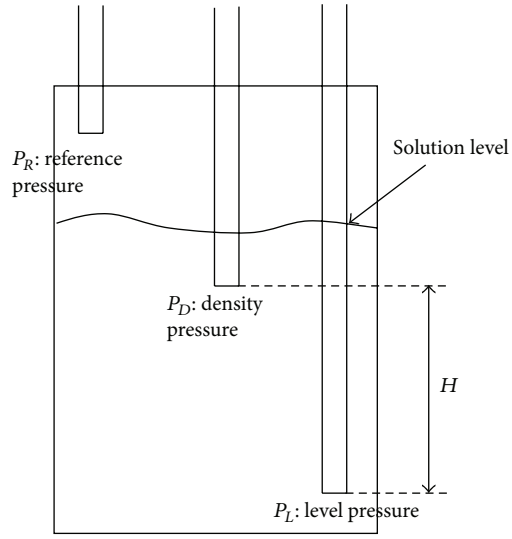

Figure 1: Schematics of SM composed of three dip tubes inserted into tank, each of which measures three pressures at different heights inside the tank. The calibration equation is decided as a function of the solution level and temperature beforehand.

In the SMMS, the LDT tank data is produced by three dip tubes installed into tanks. Each of the three tubes measures pressure at different heights inside the tank, such as the level (P_L), density (P_D), and reference pressure (P_R), as shown in Figure 1.

The three pressure values are used to calculate the density (ρ_L), level (L), and volume (V), using (1). The density is calculated from P_L and P_D with a separation height (H) between the density pressure and the level pressure dip tube. And the level is derived from P_L and P_R. The volume is obtained from the level and the temperature with a tank calibration equation (F). The three pressure values are measured by high precision pressure transducer connected with dip tubes and the temperature is by thermocouple:

$$\rho_L = \frac{P_L - P_D}{gH}, \qquad L = \frac{P_L - P_R}{\rho_L g}, \qquad V = F(L, T). \quad (1)$$

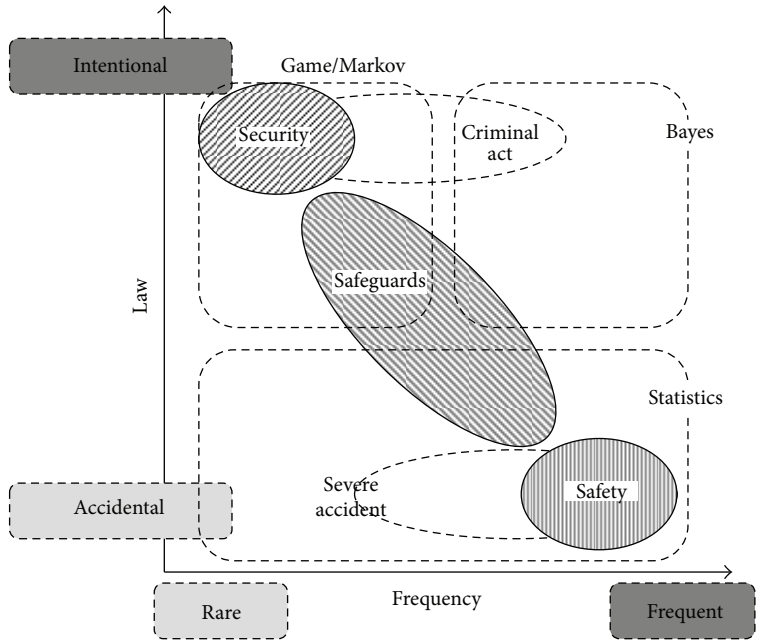

Figure 2: Mathematical models and assessment methodologies applied to safety, safeguards, and security (3S). The governing law and incidence frequency are selected to classify the inherent nature among the 3S incidences. The mapping of individual 3S region is drawn heuristically.

The SM application in the IAEA safeguards must rely on process data that are assured to be accurate and complete to draw safeguards conclusions and the data validity is checked using an authentication process. The authenticated equipment is owned and controlled by the IAEA, and when deployed for an unattended operation, it should be installed with tamper-indicated enclosure and seal system. However, in a large reprocessing facility, the number of SM instruments becomes large and it becomes expensive to install and maintain by the IAEA. Therefore, the IAEA, national safeguards authority, and operator can establish joint use equipment (JUE) resulting in ease of data collection, reduction of maintenance burden, and reduced cost of multiple parties. In case of SM at the RRP, that is, a typical example of JUE, the electric signal from the operator-owned SM is not strictly guaranteed to be secured, so the IAEA randomly selects the instrument for independent authentication in which the inspector can carry an agency-controlled instrument to check for proper operation of the operator equipment [6]. Instead of the authentication of individual instrument, reliability of authentication could be verified by the direct comparison of data collected from adjacent and connected tanks. The notion of self-authentication was proposed to make use of solution transfer between the authenticated and unauthenticated tanks [7]. The self-authentication notion in which falsification attempt of data from any one tank requires falsification of data from connected tanks has not been approved by the IAEA.

3. Risk Assessment Methodologies

One of the most promising synergies resulting from the integrated 3S consideration is the adoption of 3SBD approach for new nuclear facilities. An incorporation of 3S synergism into the conceptual design and system development phase increases regulatory effectiveness as well as operational efficiency and also reduces expensive and time-consuming retrofitting. Promoting 3SBD will require, among other technical and institutional issues, harmonization of the risk notion embedded in each of the "S" areas. The benefit of the 3SBD concept has been pointed out and discussed extensively in the international community. To assess the 3S risk, several mathematical tools are mapped according to incidence frequency and governing law as shown in Figure 2.

In safety, PSA has been developed by the long historical trials and discussions. This approach is to estimate the frequencies of accidents and failures from the historical data and to analyze the accident sequence with event trees and fault trees based on these parameters. Because of the recent concern about nuclear security, similar probabilistic assessment was extended for use in developing guidelines for protection of nuclear power plants against sabotage [8]. Although the conventional vulnerability assessment in physical security has been well developed on a deterministic and prescriptive basis, an inherent difficulty in determining the frequency of terrorist attacks by malicious acts is undertaken by the conservative estimate in which the initial probability is assumed to be unity as in the case of a postulated accident in safety. The risk formalization in security is expressed as follows [9]:

$$R = P_A \times \left(1 - P_E\right) \times C = P_A \times \left(1 - P_I \times P_N\right) \times C, \quad (2)$$

where (P_A) is the incidence probability, (P_E) the performance probability, (P_I) the interruption probability, (P_N)

the neutralization probability, and (C) the consequence, respectively. After assuming that the most upstream event is deterministic and the incidence probability is unity, the event sequence is analyzed probabilistically on a basis of the plant layout, system design, and structural robustness. Because of the difficulty of specifying the incidence probability, the security system is usually evaluated by the performance probability in which the timeline analysis is performed to identify the interruption probability and the security countermeasures; fence, sensor, camera, and so on are designed and installed into actual nuclear facilities. The neutralization probability is the unique feature of the security risk assessment and is determined by the performance of the response force. In addition to this, the deterrence effect can be estimated with a Bayesian method utilizing historical data, the game method assuming rational behaviour and payoff matrix, and others, and the incidence probability could be evaluated qualitatively as in the decision process [10].

Similarly, a major difficulty encountered in applying probabilistic methods to safeguards is to determine the incidence of diversion and misuse. Although the mathematical formalization for the international safeguards has been developed for several decades [11], the discussion of developing probabilistic methodology to address nonproliferation issues was done in a different perspective [12]. In safeguards, the diversion of nuclear material and the misuse of technology are initiated by the motivation of state and intentional act by facility operator, therefore the estimation of intentional act is generally very difficult. In addition to the incidence probability, there is another uncertainty related to measurement error in material accounting. This is the significant quantity (SQ) and timeliness goal that underlines the basis for NMA. Based on the prescriptive and deterministic logic, uncertainty of NMA should be controlled under this limit as a first priority in safeguards. The IAEA determined the threshold value for nuclear material losses for each type of facility and process. However, as an amount of nuclear material increases in large-scale facilities, uncertainty due to measurement error becomes large and likely exceeds the limit. Because it is important to control the mass measurement error within the absolute threshold of NMA, a probability distribution of the measurement error of NMA has to be considered in conjunction with the incidence probability as shown in Figure 3. The two-dimensional probability formalization is proposed as follows [13, 14]:

$$R = P \times C = P(t, m) \times C = P(t) \times P(m \mid t) \times C. \quad (3)$$

In (3), the measurement error probability is defined as $P(m)$ related to measurement error in material accounting. The measurement error probability is the probability density function and the accumulated distribution function is detection probability. On the other hand, the incidence probability is defined as a Poisson density function. It should be noted that both probabilities are not independent and those are closely correlated each other. This will be discussed later in the game theoretical study.

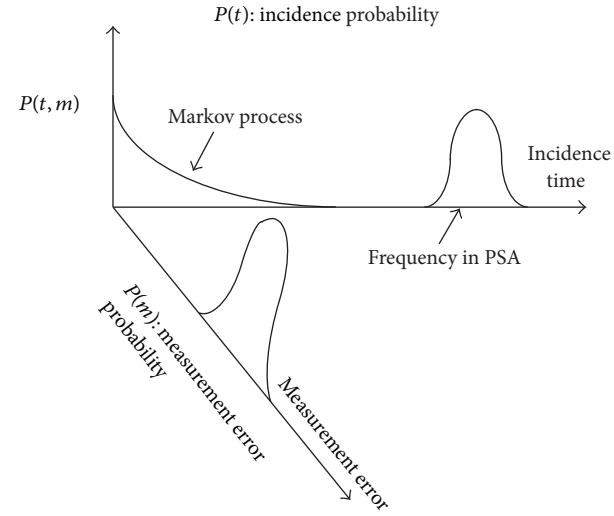

Figure 3: Two-dimensional probability for safeguards. The probability distribution composed of two random variables, the incidence time, and the measurement error is a characteristic feature of the proliferation risk.

4. Feasibility Studies in Safeguards

4.1. Proliferation Risk Analysis. Without showing an explicit description of proliferation risk, the risk notion has already been considered in the IAEA safeguards as the state-level evaluation, and the safeguards inspection is carried out according to risk analysis with an expert elicitation. However, using a mathematical formalization of proliferation risk probability one could demonstrate its advantage in an objective manner, and the quantitative representation is valuable in the 3SBD approach. The assessment method of the proliferation resistance (PR) of generation IV reactors was addressed by the proliferation resistance and physical protection working group (PRPPWG) of generation IV international forum (GIF) [15]. The method is intended to be used to evaluate the PR, defined as the degree to which a system can be put with proliferation acts even under international safeguards and those attributes are defined for its characterizations. The evaluation methodology has been clearly noted for the notion of proliferation risk with assuming the Markov process model for all extrinsic and intrinsic measures and the diversion probability directly indicates the vulnerable path instead of an expert elicitation. It should be noted that the measurement error probability shown in (3) is not considered in this model, so that only the incidence probability can be calculated through the Markov model. This is a clear difference from the conventional NMA in safeguards even if the results closely relate to the safeguards effectiveness.

In this study, an aqueous reprocessing model that is composed of the total 43 process steps from spent fuel pond to product storage is assumed as a typical PUREX process. As shown in the Figure 4, the Markov model is assumed for the entire PUREX process in which an initiation of diversion as well as a detection of the diversion is governed by random stochastic process with the characteristic time

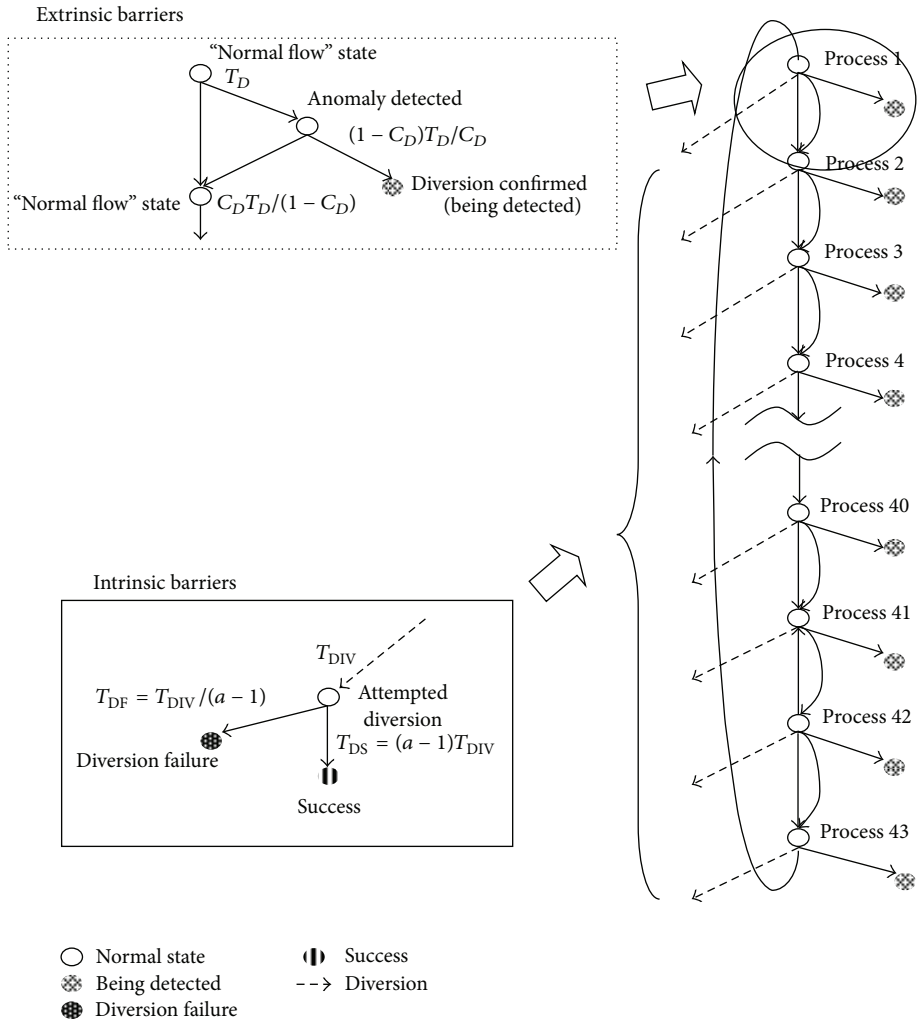

FIGURE 4: Markov model applied to estimation of the incidence probability. "T_D" is the time needed to detect an anomaly, "C_D" the confidence level of diversion confirmation, "T_{DIV}" the time of coupling diversion without any intrinsic barrier, "T_{DF}" the mean time to diversion failure, "T_{DS}" the mean time to diversion success, and "a" the time factor related to intrinsic barriers.

intervals. In addition to PIV and IIV, monitoring benefit of SMMS as an additional measure is considered in the extrinsic barriers in this model. Individual time intervals of these safeguards measures, characterized by "T_D", are assumed to be frequencies of the incidence of diversion and/or detection at each process and this random stochastic process can be modeled as a Poisson probability distribution. This is a special assumption used in the PRPPWG and is a well-known methodology for proliferation resistance evaluation. Intrinsic barriers with radiation exposure and heat generation from residual fission products (FPs) have to be overcome to proceed to weapon production from a diverter's point of view. However, no matter how much FPs remain in the product solution, the diverter could have a capability to lessen the barrier and to remove these radioactive materials using radiation protections, chemical reactions, and separation facilities. Therefore, the prolonged time to prepare an additional process to extract from radioactive solution to raw material for weapon production is modeled as a time factor representing the technical difficulty as "a."

While the SM can generate real-time LDT data of the tank inventory, the SM capability depends on not only software performance of pattern recognition but also noisy background by sampling, homogenization, evaporation, and so on. The confidence level of diversion confirmation, shown by "C_D" and related to the SM capability, is defined corresponding to the process steps with an assumption that the plutonium concentration determines the detection capability of the solution level change corresponding to a SQ (= 8 kg-Pu). And also the technical difficulties are assumed to be proportional to the decontamination factors in the entire process; the head end, the extraction and separation, the first and second purification, and concentration processes. Assuming typical PUREX process composed of 43 process steps and using these parameters, such as T_D, a, C_D, and processing times, at each process, the proliferation risk analysis with the Markov model is performed. After solving a

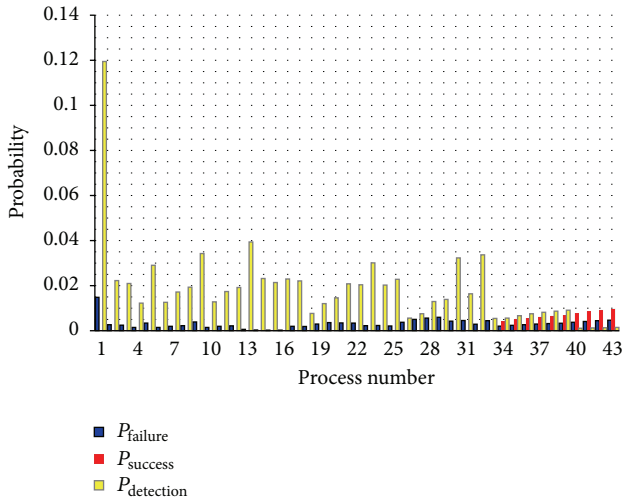

Figure 5: Proliferation risk analysis in the typical PUREX process composed of the total 43 process steps from the spent fuel pond to the product storage tank. The failure, success, and detection probabilities are expressed at the individual process step number.

set of 43 differential equations with the assumed parameters, one can estimate the relative likelihood of failure, success, and detection, as proliferation risk analysis. At each process step, the detection, failure and success probabilities are shown in Figure 5. The detection probability at step number 1, spent fuel pond, shows the largest probability due to the residence time of the fuel in the pond. The success probability, that means "success" form the diverter's point of view, can be seen after step number 34 and especially after the number 40. In the downstream from the second purification process and the concentrated solution from evaporator and in product tanks the process is assigned to have the low intrinsic factors because of low radioactivities and heat generation from FPs as well as high concentration of plutonium. It is clearly understood that the proliferation risk analysis is capable of showing the proliferation vulnerability in the entire process steps and the detection capability of SM plays an important role in this vulnerable region as effective safeguards measure.

4.2. Deterrence Effect. The relation between the measurement error and the incidence probability is correlated with each other. Although the proliferation risk analysis in the preceding section does not consider the measurement error probability, both probabilities are investigated as a deterrence effect in this section. The incidence probability is determined by the diverter's intention and the deterrence effect on the diverter should influence the initiation of the incidence and the possible deterrence effect is studied using a game theoretical model. Although a payoff matrix is not easily defined objectively to model the inspector-operator relation, a noncooperative two-person zero-sum game is assumed to investigate an effectiveness of the operator's restraint of falsification in the SM data that is an indication of the operator's diversion. The game theoretical model in safeguards

Table 1: Payoff matrix of two-person and zero-sum game for the D and MUF combined test problem. Mixed strategy is chosen to investigate for the inspector and operator deterrence effect and the quantitative relation between the individual payoffs are assumed as shown.

Inspector	Operator		
	Legal	D	MUF
D-alarm	$-a$	c	—
MUF-alarm	$-b$	—	d
non-detection	0	$-e$	$-f$

$0 < a < c < e$, $0 < b < d < f$.

verification has been developed in series of the reference papers and the challenge is continued in recent work in which the time dependency in the payoff matrix was discussed [16]. In this study, the time-varying and randomly distributed variables representing the SM performance related to the material unaccounted for (MUF) are considered with a stochastic game model to investigate the operator's choice of D-diversion, which is applied to falsifying data in an attempt to conceal diversion [17]. It should be noted that the MUF- and D-diversions are a traditional theme in the IAEA safeguards. The inspector trusts the measurement data taken by the operator but is not allowed to use them for the MUF verification without ensuring no data falsification in the D verification.

The stochastic game model is an integration of a Markov decision process and a matrix game and is utilized to consider the inspector-operator relation among multiple players and at multiple stages [18]. The payoff matrix of the game model is assumed as shown in Table 1. The MUF- and D-diversions in the operator's choices are specific cases in the international safeguards and those correspond to concealment of the diversion in the measurement uncertainty and data falsification to mask the diversion, respectively. And the legal choice means no-diversion attempt. A mixed strategy is chosen to investigate for the inspector and operator deterrence effect. Generally it can be assumed that a D-diversion should have an important influence and a first kind of error probability likely keeps large to avoid nondetection. Therefore, the relation between a,c, and e is assumed as $0 < a < c < e$. Similarly, the relation between b, d, and f is $0 < b < d < f$. The payoff parameters a and b are set constant values throughout the calculations. And the parameters of c and e are set the same value and those of d and f are set the same value but different from c. When the variance of MUF increases according to the frequency of MB closure, it leads to decrease of the SM performance and the detection probability. This results in an increase of average run length (ARL). Because this delay detection likely increases the chance of diversion, it can be modelled as increase of the payoff parameters of c and d in Table 1. Despite the increases of c and d, the probability of operator's choice in legal behaviour nearly approaches unity and the choices in MUF- and D-diversions are nearly zero as shown in Figure 6(a) as a result of the game theoretical calculation. This is clear evidence for the deterrence effect that the operator will likely tend to obey legal behaviour even

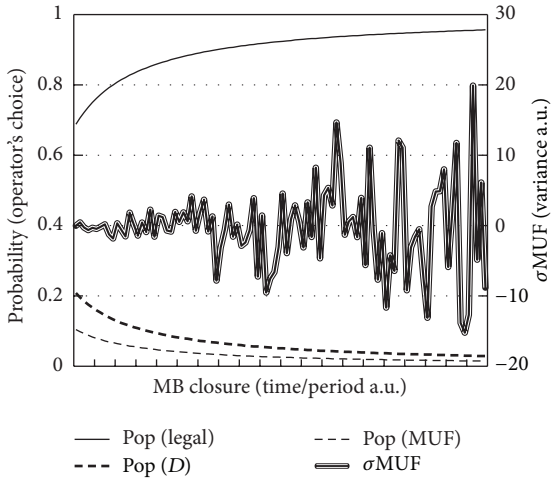

(a) Operator's choices as increasing MUF uncertainty

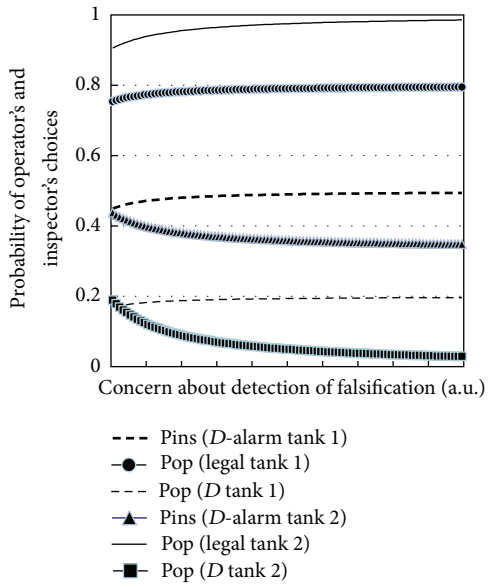

(b) Operator's and inspector's choices as increasing concern

Figure 6: Stochastic game calculation for the deterrence effect on the inspector and operator. In case (a), the increase of MUF variance due to the measurement error induces the increase of ARL, so that it is assumed as the increase of the payoff parameter of c and d in Table 1. In case (b), the operator's concern about the detection between tanks 1 and 2 is assumed as the increase of payoff parameter of c in Table 1.

if the payoff increases according to the decrease of the SM performance.

On the other hand, in case that the solution transferring from the unauthenticated tank 1 to the authenticated tank 2, tank 1 is shipper and tank 2 receiver, the operator likely has a concern about detection of the falsification during the transfer. Because the transferred solution is conserved between the two tanks and the downstream tank 2 is independently monitored by the inspector, any falsifications in the upstream tank 1 are likely detected. The increase of concern can be modeled to the increase of the payoff parameter of c. In case (b) in Figure 6, the differences between the inspector and the operator choices in tanks 1 and 2 are shown according to the increase of operator's concern. The probability of operator's legal choice in tank 2 is larger than that in tank 1. And the inspector's choice of D-alarm and the operator's choice of D-diversion in tank 1 are always larger than those in tank 2. These results mean that falsification in the unauthenticated tank more likely happens than that in the authenticated tank. Moreover, the probabilities of D-diversion or D-alarm in the unauthenticated tank do not increase much in spite of the increase of concern. The inspector's and operator's choices can be estimated in advance by the dependency of payoff parameters on the assumption that the inspector and operator behave rationally.

4.3. Fuzzy Optimization. In this section the safeguards performance by the SM and minimization of initial and running costs is investigated as an uncertainty analysis for multiple-objective problem. The multiple-objective problem can be solved by several mathematical methods. However, in this study a fuzzy optimization technique is applied to obtain multiple-goals solution by a well-known liner programming (LP) method. The fuzzy linear programming (FLP) has originally been proposed in the 1970's and the application for nuclear fuel cycle optimization has been investigated thereafter [21, 22]. The FLP is currently improved and the basic FLP using a linear membership function is employed as follows.

First, two ordinary linear optimizations are performed incorporating the objective functions of ERROR(X) and COST(X). Because the piecewise linear cases of ERROR(X) and COST(X) are reducible to a standard LP scheme, the optimization problem becomes the customary form with constraint conditions. The solution of these problems leads to Pareto optimal strategies, in which COST(C) is the lowest attainable cost and ERROR(C) the smallest measurement error, and COST(C) and ERROR(C) are utilized to find boundaries for the multiple-goals optimization. In the FLP, the two objective functions of COST(X) and ERROR(X) are transformed into their membership functions which are denoted by $\mu_C[\mathrm{COST}(X)]$ and $\mu_E[\mathrm{ERROR}(X)]$. The membership functions of the fuzzy sets characterizing the objective functions increase linearly from 0 to 1 at the highest achievable values. For example, the membership function of the cost objective can be expressed as

$$\mu_C\left[\mathrm{COST}\left(X\right)\right] = \begin{cases} \dfrac{\mathrm{CMAX} - \mathrm{COST}\left(X\right)}{\mathrm{CMAX} - \mathrm{COST}\left(C\right)} & \text{if } \mathrm{COST}\left(X\right) \le \mathrm{CMAX} \\ 0 & \text{if } \mathrm{COST}\left(X\right) \ge \mathrm{CMAX}, \end{cases} \quad (4)$$

where CMAX is the boundary value in the allowable region and the maximum value of μ_C is reached at $X = C$. The similar expression to (4) is defined for μ_E in an analogous way, with the constant EMAX. The objective for the multicriteria optimization is to maximize the compound membership function:

$$\mu\left(X\right) = \min\left(\mu_C\left[\mathrm{COST}\left(X\right)\right], \mu_E\left[\mathrm{ERROR}\left(X\right)\right]\right). \quad (5)$$

Table 2: Three schemes of safeguards measures for the advanced reprocessing process.

	Scheme A	Scheme B	Scheme C
Safeguards measures	SM + DA (IDMS)	SM + NDA (HKED)	FM + NCC (NDA)
Measurement error (random, systematic) %	(0.4. 0.3) % [19]	(0.7, 0.4) % [19]	5 %
Error scaling (N: throughput)	N	N	$N^{1/2}$ [20]
Cost	300 k$	600 k$	500 k$
(Initial (k$) + running (FTE))	+5FTEs + 10FTEs [19]	+3FTEs [19]	+3FTEs

SM: solution monitoring, DA: destructive analysis, IDMS: isotope dilution mass spectroscopy, NDA: nondestructive analysis, HKED: hybrid K-edge densitometry, NCC: neutron coincidence counting, N: throughput (au), and FTE: full-time equivalent years of personnel effort.

Due to the form of (5), the maximization of $\mu(X)$ corresponds to the problem as follows:

$$\begin{aligned} &\max \lambda \\ &\lambda \le \mu_C\,[\mathrm{COST}\,(X)] \\ &\lambda \le \mu_E\,[\mathrm{ERROR}\,(X)] \\ &AX \le b. \end{aligned} \tag{6}$$

Because of the linearity of the functions μ_C and μ_E, (6) is solved as a standard LP problem. The solution $X = M$ maximizes λ and consequently $\mu(X)$ as well. The value of λ reflects the deviation of the multi-criteria optimum M from the various single-criteria optima. If the solution of (6) yields $\lambda = 0$, no strategy can be found with all the objective function values within allowed limits. This possibility, however, should be normally excluded due to the symmetric balance.

In order to investigate the cost effectiveness of the safeguards system in an advanced reprocessing plant, the performance of several safeguards measures governed by the measurement error is compared. The optimization using the FLP is applied to pursue the optimal design with considering the tradeoff relation between the safeguards performance and the cost. One of the controversial points in safeguards measures is a tradeoff relation between destructive analysis (DA) and nondestructive analysis (NDA). NDA instruments are generally remotely operated, do not need much labor, do not produce contamination, and provide results more quickly than DA. In addition to this, DA increases cost for labor due to the huge amount of samples in a plant operation and this leads to a high operational cost. On the other hand, at the dissolution process of spent nuclear fuel and at the input accountability tank, NDA instruments are not supposed to be used in a high radiation field environment. Therefore, DA is the only method that could be used for elemental identification and conducting NMA for plutonium under harsh circumstances.

After taking into account the constraints, an optimum selection of DA or NDA is investigated using the single-objective functions. A fuzzy technique based on LP is applied to the optimization. The three schemes in the safeguards measures are examined for the typical three stages in an advanced reprocessing process. The three schemes are a combination of SM and isotope dilution mass spectroscopy (IDMS), that of SM and hybrid K-edge densitometry (HKED), and that of flow meter (FM) and other advanced NDA such as neutron coincidence counting (NCC). For the typical three stages in the reprocessing process, we select dissolution, solvent extraction, and concentration processes. In the dissolution process, there is the constrained condition for NDA due to harsh circumstances. As increasing of the throughput of nuclear material, both the measurement error and the cost estimation are modeled to change as a function of the throughput and as shown in Table 2. Random and systematic errors leading to the performance and initial investment and running cost of individual measurement scheme are shown. The error scaling of the FM and NCC is proportional to the square of throughput N due to the neutron counting statics. It should be noted that schemes A and B have been already developed and are currently applied to the reprocessing plant. But scheme C is under development and the parameters of scheme C are tentatively assumed.

The optimized selections of three schemes from stages 1 to 3 according to the increase of the throughput are shown in Figure 7 [23]. In a small throughput region, scheme A, SM and IDMS, is the optimum selection. These are indicated as a, b, and c in Figure 7 for all stages 1 to 3. In a medium throughput region, schemes A and B show intermediate values only in stage 1. This means that the two schemes are the possible selections for stage 1 and scheme A is still optimum for stages 2 and 3. However, in a large throughput region, the scheme C becomes the optimum selection in the stage 1, schemes B and C are in stage 2, and the scheme B in stage 3. This means that scheme C, combination of FM and NCC, becomes the better selection in a large throughput region based on the measurement error and the cost. It should be pointed out that the assumption on the measurement error and the cost of the individual scheme as a function of the throughput is a preliminary one. However, it is understood that the general characteristic of the competitive relation between DA and NDA is shown qualitatively and the FM scheme assists a cost-effective performance of the safeguards system in a large throughput plant.

5. Summary

PRA in safeguards and security has been evolving and applied to the promotion of 3SBD activities. However, the theoretical basis is diverse and the effectiveness of PRA in these areas has not been clearly demonstrated yet. SM with the LDT tank data has been widely used to implement the IAEA safeguards in the large reprocessing plant and has become an important measure to assure the credibility of no diversion and no misuse of SNM. Not only for an advanced instrument

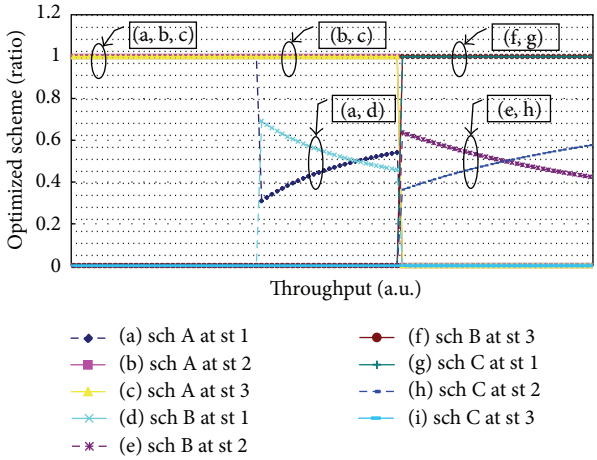

Figure 7: Fuzzy optimization for safeguards measures in the reprocessing process. The performance of safeguards measures and the initial and running cost for the safeguards measures are compared in the typical three stages; dissolution, solvent extraction, and concentration stages. As increasing the throughput in the horizontal axis, the optimal choice for the safeguards measures is changed according to the assumed dependency of the performance and cost on the throughput.

but also for risk-oriented installation, it is shown that SM is a good example of safeguards by design activities. The Markov model is applied to PRA with the PUREX model and it is clearly demonstrated that the vulnerable path in the PUREX process is safeguarded by the SMMS originally installed based on the expert elicitation. The game theoretical approach applied to the theoretical explanation of the IAEA safeguards is used to explain the effectiveness of the self-authentication notion. The deterrence effect on the operator's falsification is shown as a compromise with the profit and the penalty and this concern makes the deterrence effect one of explanations for the self-authentication. The last study on SM is the uncertainty analysis to optimize the safeguards measures with the tradeoff relation between the safeguards performance due to measurement error and the economical consideration as increasing the throughput in the advanced reprocessing process. Both the harsh circumstances with the residual minor actinide (MA) and FPs and the increase of measurement uncertainty due to the large throughput support more NDA installment than DA with considering the initial and running cost of those measures.

On the other hand, for the purpose of quantitative application of SM to the IAEA safeguards, the validity of the SM data taken from the unauthenticated tank is investigated in terms of the detection probability (DP) at the authenticated tank. The self-authentication based on the mass conservation of authenticated solution among those tanks is investigated by the detection capability for the D-diversion and is discussed in the same way for the MUF-diversion. Although the quantitative SM application is capable of showing high DP for abrupt falsification, it is understood that the small and protracted falsification is difficult to detect due to the systematic error. In order to investigate the DP in the distribution of two random variables, D and MUF, the correlation between D- and MUF-diversions was investigated in the traditional approach to evaluate the D- and MUF-diversions. However, it is understood that in the small and protracted diversion the distribution of D cannot be assumed as a Gaussian, so that the operator's strategy is considered using the game model. In this regards, the game theoretical approach needs to be pursued to explain the two-dimensional probability distribution of the proliferation risk analysis.

The probabilistic risk methodologies in safeguards and security have been developing and the inherent difficulties due to intentional acts are still challenges. However, the Markov model, the game method, and other mathematical methods could be applicable to the decision problems in safeguards as well as security. Integrating the PSA in safety with the risk assessment techniques in safeguards and security would have a potential to fascinate with the younger generation, and the comprehensive 3S regulation based on the quantitative risk discussion should be transparent and persuasive for a reasonable approach in the mandatory 3S implementation.

References

[1] T. Arai and K. Naito, "The new nexus, 3Ss: safeguards, safety, security, and 3s-based infrastructure development for the peaceful uses of nuclear energy," *Journal of Nuclear Materials Management*, vol. 37, no. 4, pp. 6–10, 2009.

[2] M. Stein, M. Morichi, L. Van Den Durpel et al., "Safety, security, and safeguards by design—an industrial approach," in *Proceedings of the Global Conference*, Paris, France, September 2009.

[3] M. Suzuki, Y. Izumi, T. Kimoto, Y. Naoi, T. Inoue, and B. Hoffheins, "Investigating 3S synergies to support infrastructure development and risk-informed methodologies for 3S by design," in *Proceedings of the IAEA Safeguards Symposium*, IAEA-CN-184/64, 2010.

[4] IAEA Safeguards Glossary 2001 Edition, *International Nuclear Verification Series No. 3*, IAEA, Vienna, Austria, 2002.

[5] T. Bjornard, M. Schanfein, D. Hebditch et al., "Improving the safeguardability of nuclear facilities," in *Proceedings of the INMM 50th Annual Meeting*, 2009.

[6] J. Howell, M. Ehinger, and T. Burr, *Process Monitoring for Safeguards*, LA-UR-07-7305, 2007.

[7] T. Burr, L. Wangen, and M. Mullen, *Authentication of Reprocessing Plant Safeguards Data through Correlation Analysis*, LA-12923-MS, ISPO-374, 1995.

[8] Engineering Safety Aspects of the Protection of Nuclear Power Plants against Sabotage, *IAEA Nuclear Security Series No. 4, Technical Guidance*, IAEA, Vienna, Austria, 2007.

[9] "Sandia National Laboratories Security Risk Assessment Methodologies," http://www.sandia.gov/ram/RAM-CI.html.

[10] E. Kardes and R. Hall, "Survey of literature on strategic decision making in the presence of adversaries," CREATE Report, 2005.

[11] R. Avenhaus and M. J. Canty, "Formal models for NPT safeguards," *Journal of Nuclear Materials Management*, vol. 35, no. 4, pp. 69–76, 2007.

[12] S. V. Mladineo, C. T. Olinger, R. S. Denning et al., *Guidelines for the Performance of Nonproliferation Assessments*, PNNL-14294, 2003.

[13] M. Suzuki, T. Burr, and J. Howell, "Risk-informed approach for safety, safeguards, and security (3S) by design," in *Proceedings of the 19th International Conference on Nuclear Engineering (ICONE '11)*, ICONE19-43154, Chiba, Japan, May 2011.

[14] M. Suzuki and S. Demuth, "Proliferation risk assessment for large reprocessing facilities with simulation and modeling," in *Proceedings of the Global Conference*, Paper 399247, Chiba, Japan, December 2011.

[15] M. Yue, L. Y. Cheng, and R. A. Bari, "A Markov model approach to proliferation-resistance assessment of nuclear energy systems," *Nuclear Technology*, vol. 162, no. 1, pp. 26–44, 2008.

[16] R. Avenhaus and M. J. Canty, "Playing for time: a sequential inspection game," *European Journal of Operational Research*, vol. 167, no. 2, pp. 475–492, 2005.

[17] R. Avenhaus and M. Canty, *Compliance Quantified: An Introduction to Data Verification*, Cambridge University Press, Cambridge, UK, 1996.

[18] M. Suzuki and T. Burr, "Self-authentication of solution monitoring data for large reprocessing facilities," in *Proceedings of the 2nd Japan-IAEA Workshop on Advanced Safeguards for Future Nuclear Fuel Cycles*, Tokai, Japan, November 2009.

[19] J. E. Stewart, N. Ensslin, T. L. Cremers et al., *Measurement and Accounting of the Minor Actinides Produced in Nuclear Power Reactors*, LA-13054-MS, 1996.

[20] M. M. Pickrell and K. Budlong-Sylvester, *Safeguards Alteratives for a UREX+ Facility NA-NE Joint Fuel Cycle Facility Design Project Technology Denonstration to Enhance the Safeguards of a UREX+ Facility*, LA-UR-06-1075, 2005.

[21] H. J. Zimmermann, "Fuzzy programming and linear programming with several objective functions," *Fuzzy Sets and Systems*, vol. 1, no. 1, pp. 45–55, 1978.

[22] P. Silvennoinen, T. Vieno, and J. Vira, "Multigoal fuel cycle optimization including nonproliferation objectives," *Nuclear Technology*, vol. 48, no. 1, pp. 34–42, 1980.

[23] M. Suzuki and H. Ihara, "Development of safeguards system simulator composed of multi-functional cores," *Journal of Power and Energy Systems*, vol. 2, no. 2, pp. 899–907, 2008.